June 2003

Advanced Fuel Cycle Initiative

January – March 2003
Quarterly Report – Volume I

SAND2003-2060P

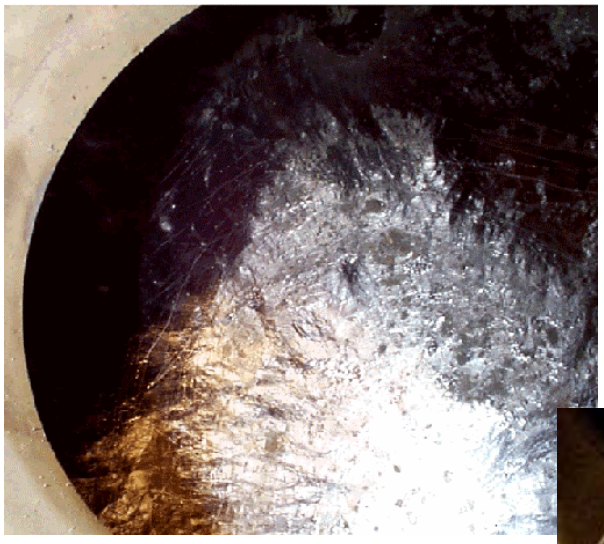

Transmutation Engineering:
Surface of liquid lead-bismuth with oxides

Solid oxides removed from the liquid metal surface.

Argonne National Laboratory, Brookhaven National Laboratory, Burns & Roe, Enterprises, Inc.
General Atomics, Idaho National Engineering & Environmental Laboratory
Idaho Accelerator Center, Lawrence Livermore National Laboratory
Los Alamos National Laboratory, Oak Ridge National Laboratory
Sandia National Laboratories, University of Nevada, University of Michigan
University of California, University of Texas
University Research Alliance, Westinghouse Savannah River Company

Sandia is a multiprogram laboratory operated by Sandia Corporation, a Lockheed Martin Company, for the United States Department of Energy's National Nuclear Security Administration under contract DE-AC04-94AL85000

Advanced Fuel Cycle Initiative Quarterly Report Volume I

January – March 2003

Approval

Signature on File

_____ Date _____

John Kelly

AFCI Program Manager

This page intentionally left blank

Table of Contents

Acronyms and Symbols

AAA Advanced Accelerator Applications
AC Accelerating cavities
ACP Advanced Crystallization Process
ACRR Annular Core Research Reactor
ADS Accelerator-Driven System
ADTF Accelerator-Driven Test Facility
ADMAB Accelerator-Driven Minor Actinide Burner
AES Advanced Energy Systems (formerly Northrup-Grumman Corp.)
AET Ability Engineering Technology
AFCI Advanced Fuel Cycle Initiative
AFM Atomic Force Microscopy
A-h Ampere-Hour
AHA Acetohydroxamic acid
ALWR Advanced Light-Water Reactor
Am Americium
AMUSE Argonne Model for Universal Solvent Extraction, the generic TRUEX model expanded to include UREX and PUREX processing
ANL Argonne National Laboratory (Chicago)
ANL-W Argonne National Laboratory-West (Idaho Falls)
ANRC Amarillo National Research Center
ANS American Nuclear Society
ANSYS structural analysis modeling code
ANTT Advanced Nuclear Transformation Technology
appm atomic parts per million
APT Accelerator Production of Tritium
ASME American Society of Mechanical Engineers
ATR Advanced Test Reactor (INEEL)
ATW Accelerator Transmutation of Waste
Ba Barium
BCM Beam-Current Monitor
BCP Baseline Change Proposal
BCP Buffered Chemical Polishing
Be Beryllium
Beta (β) Ratio to the speed of light
Bi Bismuth
BISTRO Two-Dimensional Discrete Ordinates Code
BNFL British Nuclear Fuels, Ltd
BNL Brookhaven National Laboratory
BOF Balance of Facility
BOL Beginning of Life
BOP Balance of Plant
BOR-60 Sodium-Cooled Fast Reactor (Dmitrovgrad, Russia)
BPM Beam-Position Monitor
BSE backscattered electron (images)
BWR Boiling Water Reactor

CCDTL Coupled-Cavity Drift-Tube Linac
CCL Coupled-Cavity Linac
Ce Cerium
CEA Commissariat à l'Energie Atomique (France)
CEM Cascade Exciton Model code (Model-based Monte-Carlo particle transport code)
CERCA Compagnie Pour L'Etude Et La Realisation De Combustibles Atomiques
cercer Ceramic-Ceramic
cermet Ceramic-Metal
CFD Computational Fluid Dynamics
CINDER90 Computer Code
CLWR Commercial Light-Water Reactor
Cm Curium
CMPO Neutral Extractant
CMR Chemistry and Metallurgy Research (facility at LANL)
CONCERT COmbined Neutron Center for European Research and Technology
Cr Chromium
Cs Cesium
Cu Copper
CVD Chemical Vapor Deposition
cw Continuous Wave (100% duty factor)
DACS Data Acquisition and Control System
DAS Data Acquisition System
DBTT Ductile-To-Brittle Transition Temperature
DCR Design Change Request
DDN Design Data Need
DELTA Development of Liquid Metal Technologies and Applications
DIAMEX Aqueous Solvent Extraction Process for TRU Recovery
DOE Department of Energy
dpa Displacements per Atom
EAM Embedded Atom Method
EBR Experimental Breeder Reactor
ED&D Engineering Development and Demonstration
EDS Energy Dispersive Spectrometry
EFPD Effective Full-Power Day
EFTTRA-T4 Radiation Test Sponsored by the European Union
EIS Electrochemical Impedance Spectroscopy
EIS Environmental Impact Statement
EMT Electrometallurgical Treatment
ENDF Evaluated Nuclear Data File – Evaluations that can be used in MCNPX for more accurate predictions of fission, criticality, transport, and radiation damage
EOI End of Irradiation
EOL End of Life
EPICS Experimental Physics and Industrial Control System
ERANOS Computer modeling code
ERC External Review Committee
ES&H Environmental, Safety, and Health

ESAP Experimental Safety Assurance Package
ESS European Spallation Source
ESSAB Energy System Acquisition Advisory Board (DOE)
Eu Europium
FBBRF Fast Breeder Blanket Research Facility
FC Fuel Cycle
FCF Fuel Conditioning Facility
FCOPT Fuel Cycle Optimization
FDWG Fuel Development Working Group
FDD Facility Design Description
FD&S Fill and Drain System
F&OR Functional and Operational Requirement
Fe Iron
FFTF Fast Flux Test Facility
F/M Feretic/Martinistic
FMF Fuel Manufacturing Facility
FNFB Fast Neutron Flux Booster
FODO Focus-Drift-Defocus-Drift
FPY Full-Power Year
FWHM Full Width Half Maximum
FZJ Forschungs Zentrum Jülich (German Laboratory)
FZK Forschungs Zentrum Karlsruhe (German Laboratory)
GEM Gas Expansion Module
GEN IV Generation IV
g/L Grams per Liter
GA General Atomics Inc.
GFR Gas-cooled Fast Reactor
GIF Generation IV International Forum
GNASH Nuclear Reaction Code
gpm gallons per minute
GSI Gesellschaft für Schwerionenforschung (Darmstadt, Germany)
GT-MHR Gas Turbine Modular Helium Reactor
H Hydrogen
HAN Hydroxylamine
HCP Hazard Control Plan
He Helium
HEBT High-Energy Beam Transport
HEU Highly enriched uranium
Hf Hafnium
HFEF Hot Fuel Examination Facility
HFIR High Flux Isotope Reactor (ORNL)
HFR High Flux Reactor (Petten, Netherlands)
Hg Mercury
HIP Hot Isostatic Process (for bonding materials)
HLW High-Level Waste
HM Heavy metal

HPRF High-Power Radio Frequency
HRS Heat Removal System
HS/WS Halo-Scraper/Wire-Scanner (diagnostic device)
HX Heat exchanger
I&C Instrumentation and Control
IAC Idaho Accelerator Center
IAEA International Atomic Energy Association (Vienna, Austria)
ICP-MS Inductively Coupled Plasma-Mass Spectrometry
ICS Integrated Control System
IFMIF International Fusion Materials Irradiation Facility
IFR Integral Fast Reactor
IHX Intermediate Heat Exchanger
IMS Information Management System
INEEL Idaho National Engineering and Environmental Laboratory
I-NERI International Nuclear Energy Research Initiative
IPBT In-Pile Beam Tube
IPPE Institute of Physics and Power Engineering, Obninsk, Russia.
ISABEL Physics Modeling Code
ISTC International Science and Technology Centre (Moscow)
ITER International Thermonuclear Experimental Reactor
ITU Institute for Transuranium Elements (Karlsruhe, Germany)
JAERI Japan Atomic Energy Research Institute
JCNNM Johnson Controls Northern New Mexico
JLAB Jefferson Laboratory (VA)
K Potassium
KAERI Korean Atomic Energy Research Institute
KEK National Laboratory for High-Energy Physics (Tsukuba, Japan)
keV Kiloelectron Volt
kW kilowatt
LA150n Los Alamos generated nuclear data library, extending up to 150 MeV
LAHET Los Alamos High-Energy Transport
LANL Los Alamos National Laboratory
LANSCE Los Alamos Neutron Science Center
LBE Lead-bismuth eutectic
LBHM Low- Hot Model
L/d Length-to-diameter ratio
LFR Lead-Cooled Fast Reactor
L/hr Liter per hour
LEBT Low-Energy Beam Transport
LEDA Low-Energy Demonstration Accelerator
LHGR linear heat generation rate
LINAC A computer code based on PARMILA that has been modified to include CCDTL and SCRF elliptical cavities as options
LLFP Long-lived fission product
LLNL Lawrence Livermore National Laboratory
LLRF Low-level radio frequency

LME Liquid-metal embrittlement
LMR Liquid-metal reactor
LTA Lead Test Assembly
LUA Lead Use Assembly
LWR Light-water reactor
M Molar
MA Minor actinide
mb Millibarr
MCA Multi-criteria analysis
mCi Millicurie
MCNP Monte Carlo N-Particle Transport Code
MCNPX Merged code—Los Alamos High-Energy Transport (LAHET) and Monte Carlo N-Particle Codes (MCNP)
MCWO MCNP Coupling With ORIGEN2 (burnup calculation code)
MDD Modified Direct Denitration
MEAM Modified Embedded Atom Method
MEGAPIE Megawatt Pilot Experiment
MFM Magnetic Flow Meter
MIT Massachusetts Institute of Technology
mL Milliliter
Mo Molybdenum
MOTA Materials Open Test Assembly
MOX Mixed oxide fuel
mR Millirad (a measure of radiation)
MSR Molten Salt Reactor
MT Metric Ton
MTL Materials Test Loop
MUSE CEA-Cadarache Zero-Power Subcritical Experiments
MW Megawatt
MWD/T Megawatt Days per Ton (standard unit for burnup)
MWth Megawatt thermal
MYRRHA Multipurpose hYbrid Research Reactor for High-Tech Applications
N Nickel or nitride
Na Sodium
Ni Nickel
Np Neptunium
n/p Neutrons per proton
NDA Nondestructive analyses
NE DOE Office of Nuclear Energy, Science, and Technology
NEA Nuclear Energy Agency (Paris)
NEPA National Environmental Protection Agency
NERAC Nuclear Energy Research Advisory Committee
NERI Nuclear Energy Research Initiative
NFC Nuclear Fuel Cycle
NFF Nonfertile Fuel
NRC Nuclear Regulatory Commission

NTD National Technical Director
O&M Operations and Maintenance
OCRWM Office of Civilian Radioactive Waste Management
OECD-NEA Organization for Economic Cooperation and Development-Nuclear Energy Agency (Paris)
OIL Open-Issue List
ORIGEN A computer code system for calculating the buildup, decay, and processing of radioactive materials
ORNL Oak Ridge National Laboratory
P&ID Piping and Instrumentation Diagram
P&T Partitioning and transmutation
PACS Personnel Access Control System
PARMTEQM RFQ simulation code
PAS Positron-Annihilation Spectorscopy
Pb Lead
PCM Pulse Control Modulation
Pd Paladium
PFD Process Flow Diagram
PHA Preliminary Hazards Assessment
PHENIX Fast Spectrum Reactor in France
PIE Post-irradiation examination
PNNL Pacific Northwest National Laboratory
POP Proof of Performance, Proof of Principle
PRAD Proton Radiography
PRISM Power Reactor Innovative Small Module
PSAR Preliminary Safety Analysis Report
PSS Personnel Safety System
PSI Paul Scherrer Institute (Switzerland)
Pu Plutonium
PUREX Plutonium-Uranium Extraction
PWR Pressurized Water Reactor
PYRO Pyrochemical process
Q Quality factor
QA Quality Assurance
QAC Quick ATW Costing
QC Quality Control
R Rad (a measure of radiation)
R&D Research and Development
RAMI Reliability, Availability, Maintainability, and Inspectability
RBS Rutherford Backscattering Spectrometry
RCCS Resonance-Control Cooling System
RERTR Reduced Enrichment for Research and Test Reactors program
RF Radio Frequency
RFM Readiness for Manufacturing
RFQ Radio-Frequency Quadrupole
RG Reactor Grade

RIA Rare Isotope Accelerator
RIAR Russian Institute of Atomic Reactors
rms root mean square
RRR Residual Resistance Ratio
RSICC Radiation Safety Information Computational Center
RTD Surface Temperature Detector
RTH Royal Institute of Technology (Stockholm, Sweden)
Ru Ruthenium
SAA Systems Approaches Analysis
SANEX Aqueous Solvent Extraction Process for Am and Cm Recovery
SAR Safety Analysis Report
SC Superconducting
SCK•CEN Studiecentrum Voor Kernenergie Centre D'Etude De L'Energie Nucleaire
SCM Subcritical Multiplier
SCRF Superconducting RF
SCWR Supercritical Water-Cooled Reactor
SDD System Design Description
SEM Scanning Electron Microscopy
SFR Sodium-Cooled Fast Reactor
SFT Stacking-Fault Tetrahedral
SFTF Spent Fuel Treatment Facility
SHR shutdown heat-removal
SINQ Spallation Neutron Source at Paul Scherrer Institute (Switzerland)
SNF Spent Nuclear Fuel
SNL Sandia National Laboratories
SRS Savannah River Site
SRTC Savannah River Technology Center
STAYSL A computer code to analyze results of activation foil measurements
STAYSL2 A computer code to analyze results of activation foil measurements in both a proton and neutron flux
Star-CD Computational fluid dynamics code
STP Standard Temperature and Pressure
STIP Spallation Target Irradiation Program (at PSI)
STIP Spallation Target Irradiation Program
Ta Tantalum
TAC Technical Advisory Committee
T/B Target / Blanket
TBP Tri-*n*-butyl Phosphate or Tributylphosphate
Tc Technitium
TEM Transmission Electron Microscopy
TESLA International Collaboration on a TeV Superconducting Linear Accelerator
TGA Thermal Gravimetric Analysis
Ti Titanium
TiN Titanium Nitride
TJNAF Thomas Jefferson National Accelerator Facility
TMA Thermo-Mechanical Analyzer

TMT Target and Materials Test Station
T/p Tritons (nucleii of tritium atoms) per Proton
TRAC Transient Reactor Analysis Code
TRACE 3-D Interactive computer code that calculates the envelopes of a bunched beam through a user-defined transport system
TREACS TReat Experiment for ACcelerator-driven Systems
TREAT Transient Reactor Test Facility
TRISO Tri-isotropic, referring to a multi-layered fuel-particle coating consisting of pyrolytic carbon and silicon carbide
TRADE TRIGA Accelerator Driven Experiment
TRIGA Small Reactor Type
TRISPAL Refers to the French APT Program
TRL Technical Readiness Level
TRU Transuranics (americium, curium, neptunium, and plutonium)
TRUEX Aqueous solvent extraction process for TRU recovery
U Uranium
UFP University Fellowship Program
UNLV University of Nevada Las Vegas
UPP University Participation Program
UREX Uranium Extraction (an aqueous partitioning process)
URA University Research Alliance
URP University Research Program
USQD Unreviewed Safety Question Determination
V Vanadium
VHTR Very-High Temperature Reactor
VPS Vapor Plasma Spray
VARIANT Three-Dimensional Nodal Transport Code
W Tungsten
WBS Work Breakdown Structure
WEDM Wire Electro-Discharge Machining
WG Weapons Grade
WNR Weapons Neutron Research (facility at LANL)
WPPT Working Party on Partitioning and Transmutation
WSRC Westinghouse Savannah River Company
Xe Xenon
XRD X-ray Diffraction
Y Yttrium
ZPPR Zero Power Physics Reactor
Zr Zirconium
ZrC Zirconium Carbide
ZrN Zirconium Nitride

1 INTRODUCTION

The mission of the Advanced Fuel Cycle Initiative (AFCI) is to develop and implement spent fuel treatment and transmutation technologies in order to improve the efficiency of the proposed repository and reduce the cost of geologic disposal for the United States. The AFCI is closely coupled with the Generation IV Nuclear Energy Systems Program (Generation IV), which seeks to deploy a new generation of nuclear power plants by 2030 to provide a transmutation capability. Together, these two programs enable an expanded role for nuclear power as a sustainable energy resource that will address long-term U.S. energy security, environmental, and economic concerns. The AFCI also provides for an effective transition from the current once-through nuclear fuel cycle to a future sustainable fuel cycle. Such a closed nuclear fuel cycle could provide a number of benefits, including:

- Reducing the cost of geologic disposal of commercial spent nuclear fuel,
- Recovering the energy value from commercial spent nuclear fuel,
- Reducing the inventories of civilian plutonium in the U.S.,
- Reducing the toxicity of high-level nuclear waste requiring geologic disposal, and
- Eliminating or significantly delaying the technical need for a second geologic repository in the U.S.

Key to the mission of the AFCI is development and demonstration of technologies that can be employed in a number of facilities that will need to be constructed. The first of these is a light water reactor (LWR) Spent Fuel Treatment (SFT) facility that would begin operation in FY 2015 to process the spent fuel from both the existing and newly constructed advanced LWR systems. It can be sized to treat fuel at a rate equal to the current spent nuclear fuel discharge rate. In this facility, cesium and strontium will be extracted and managed separately. Minor actinides will be stored for transmutation in future systems. Slightly enriched uranium, plutonium, neptunium, and possibly other minor actinides will be recycled into LWRs through fabrication of a proliferation-resistant fuel in a facility that will begin operation by
FY 2018. Most existing and newly constructed LWRs are expected to utilize proliferation-resistant fuel to the maximum degree possible for their operational lifetimes.

Processing of LWR spent nuclear fuel in the U.S. could offer significant advantages over direct disposal. Separation of the uranium, which constitutes more than 95% of spent nuclear fuel, results in a dramatic decrease in the volume of material bound for geologic disposal. Separate management of cesium and strontium significantly decreases the short-term heat load in the repository and removal of the minor actinides decreases the long-term heat load. Together, these effects could result in substantial decreases in the number of waste packages that must be disposed. Recycling of plutonium into a proliferation-resistant fuel would also slow the growth of the U.S. civilian inventories of plutonium.

Fully closing the nuclear fuel cycle requires introduction of one or more fast-spectrum systems found among the Generation IV systems and possibly an Accelerator-Driven System (ADS) to provide a transmutation capability. A preliminary determination will be made by FY 2007 as to whether an ADS will be required to supplement the transmutation capability provided by Generation IV fast reactors. In a fast reactor system, unburned plutonium and minor actinides from the LWR SFT facility could be consumed, helping to close the nuclear fuel cycle. The

small quantity of waste that would be eventually disposed under this approach would have dramatically reduced toxicity and long-term heat load when compared to the existing inventory of spent nuclear fuel. The AFCI will develop the nuclear fuel for a range of Generation IV fast reactor systems and help guide the selection of the fast reactor to be used for transmutation. In order to support performance testing of these systems and a decision on their deployment by FY 2030, engineering-scale demonstrations of prototypic candidate Generation IV fast reactor fuels will be performed by FY 2022.

Implementing a closed nuclear fuel cycle could significantly reduce the cost of geologic disposal of spent nuclear fuel. A preliminary analysis has shown that the implementation of AFCI technologies could reduce the cost of the first geologic repository by approximately $5 billion. These savings result from decreasing the number of waste packages and drip shields, as well as from reduced operational costs. With full implementation of the AFCI, a second repository and its associated $50 billion cost either would not be needed or would be delayed significantly. The AFCI could provide other economic benefits as well. It has been estimated that recycling the LWR fuel into proliferation-resistant fuel could produce gross revenue of $12 billion between 2018 and 2040. Overall, the AFCI could result in a net savings of between $35 and $50 billion between 2010 and 2040.

The AFCI could provide substantial intangible benefits in addition to these projected cost savings. The closed nuclear fuel cycle is essential to enabling an increased role for nuclear power in the future, thus enhancing our energy security. Nuclear energy can also address energy security concerns by decreasing the need for oil imports. Nuclear energy can serve a critical role in addressing environmental concerns by providing large-scale power generation without carbon emissions and clean hydrogen for transportation and other applications. The energy value contained in the spent nuclear fuel currently stored in this country is equivalent to over 6 billion barrels of oil, or about two full years of U.S. oil imports. The reduction of civilian plutonium inventories in the U.S. would reduce the associated physical protection and material control and accounting requirements, in addition to reducing the proliferation risk associated with these materials.

This report is Volume I of the January through March FY03 Technical Quarterly Report for the Advanced Fuel Cycle Initiative. Volume I covers research activities for the Fuels Development, Transmutation, Systems Analysis, University Programs, and Technical Integration elements. Volume II will cover the Separations element of the AFCI. For more information on the contents of this report, please contact the following people:

- Fuels Development – Kemal Pasamehmetoglu, LANL, (505) 667-8893, kop@lanl.gov
- Transmutation – Mike Cappiello, LANL, (505) 665-6408, mcappiello@lanl.gov
- Systems Analysis – Ralph Bennett, INEEL, (208) 526-7708, rcb@inel.gov
- Idaho Accelerator Center – Frank Harmon, (208) 282-5875, harmon@physics.isu.edu
- UNLV Programs – Tony Hechanova, UNLV, (702) 895-1457, hechanova@unlv.edu
- Fellowship Program – Cathy Dixon, URA, (806) 376-5533, dixon@uraweb.org
- Technical Integration – John Kelly, SNL, (505) 844-8993, jekelly@sandia.gov

2 FUELS DEVELOPMENT

The AFCI fuels development effort will provide proliferation-resistant fuels for use in advanced fuel cycles for both our current light water reactors (LWRs) or advanced light-water reactors (ALWR) (Series One) and for the next generation of nuclear power and transmutation systems (Series Two).

Series One focuses on developing LWR recycle fuels. The objective is to develop proliferation-resistant plutonium (Pu) and uranium oxide (UO_2) fuels with additional contaminants for use in LWRs. This fuel is referred to as proliferation-resistant LWR fuel. The Series One fuels and separations technology will provide the means to significantly reduce the quantity of high-level waste (HLW) materials that must be stored in the repository. Additional irradiation in the LWRs will reduce the plutonium inventory in the spent fuel.

Series Two will develop advanced fuels for use in both Generation IV power systems and in transmutation systems that can be deployed by 2030. Series Two fuels and separations will be designed to maximize transmutation performance and significantly reduce the toxicity, long term decay heat in the repository, and longevity of materials stored in the repository. Depending on the fuel cycle deployment scenarios, Series Two fuel development addresses fertile-free fuels (accelerator-driven systems and fast reactors with inhomogeneous cores), low-fertile fuels (fast-reactors with low conversion ratios), fertile-rich fuels with high-burnup (for Generation IV reactors after achieving an equilibrium fuel-cycle, including thermal and high-conversion ratio fast reactors).

Detailed descriptions of the scope, short and long-term objectives, goals, and schedules for the AFCI fuel development program are provided in the AFCI Program Plan and the reader is referred to this document for additional background information. General questions regarding the fuel development program should be addressed to the National Technical Director (NTD) Kemal Pasamehmetoglu at kop@lanl.gov.

The FY03 quarterly progress for the fuels development activities during the second quarter (January 1st through March 31st 2003) is presented in this section for the following technical categories of activities:

- Integration of Fuel Development Activities,
- Series One Fuels Design, Specifications and Analyses,
- Series One Fuel Fabrication,
- Series One ATR Irradiation Experiments,
- Series Two Fuel Design Specification and Analyses,
- Series Two Nitride Fuel Development,
- Series Two Metallic Fuel Development,
- Series Two TRISO Fuel Development,
- Series Two Advanced Fuel Forms,
- Series Two ATR Irradiation,

- Series Two FUTURIX Irradiation, and
- ATR Fast Flux Booster Design.

2.1 Integration of the Fuel Development Activities

The AFCI fuel development is a national effort with participation by multiple institutions, lead by a National Technical Director (NTD). The NTD's responsibility is to implement the five-year program plan, which includes integrating the efforts over the various institutions, interfacing with the DOE fuels manager and the AFCI Technical Integrator, and interfacing with the other elements of the AFCI (Systems, Separations, and Transmutation).

2.1.1 Integration Objectives

The FY03 objectives for the Integration activities performed by the NTD are as follows:

- Coordinate and provide technical leadership to all fuels development activities within the AFCI program, including the international collaboration activities;
- Provide fuels input to the 5-year program plan prepared and maintained by the Technical Integrator and update as requested;
- Coordinate and compile the fuels section of the monthly and quarterly reports;
- Coordinate the planning and work-package development for the fuels activities for FY03 and FY04;
- Participate in international collaboration development activities in support of DOE staff (specifically, establish an international agreement with Switzerland on advanced dispersion fuels);
- Participate in program-wide meetings and, as necessary, working group meetings of other program elements (Systems, Separations, Transmutation, Generation IV) to ensure timely flow of technical information within the program;
- Provide technical and programmatic presentations on behalf of the AFCI program in internal and external review meetings;
- Form a fuel development working group (FDWG), chair the working group meetings, and publish the meeting minutes within a month following the meetings;
- Provide assistance to DOE-NE AFCI and fuel managers in resolving technical issues as they emerge within the program.

2.1.2 Integration Highlights

The following are the major highlights of the Integration activities:

- Two meetings of the FDWG were held and the meeting minutes were published.
- An Integration meeting was held with the Commissariat a l'Energie Atomique (CEA) fuels team (French) in Washington D.C. on January 14 and 15, 2003, at which a detailed work plan was developed for FUTURIX.

2.1.3 Integration Activities Summary

In the area of Integration, the major second quarter activities are:

- Fuel Development Working Group (FDWG) meetings,
- AFCI Semi-Annual Program Review, and
- DOE-CEA collaboration technical exchange meeting.

For additional information on these activities, contact Kemal Pasamehmetoglu at kop@lanl.gov.

FDWG Meetings. The first meeting was run in conjunction with the AFCI semi-annual technical review on January 24, 2003, in Albuquerque, NM. The meeting was scheduled for 3 hours, which resulted in a limited set of discussion topics. The highlights of the meeting are provided below:

- The charter of the working group (distributed to all members prior to the meeting) was agreed on to guide the fuel research under AFCI.
- In general, the latest work-packages (WPs) were in agreement with the program plan. In the case of Argonne-West, some scope was removed from the WPs to be consistent with the Program Plan. However, the scope was reduced without impacting the Advanced Test Reactor (ATR) testing in direct support of FUTURIX.
- Assignments were made for addressing the FDWG milestones for research fuel testing requirements and five-year detailed research plan.

Additional details can be found in the meeting minutes.

The second FDWG meeting was held in Salt Lake City, UT, on February 26-27, 2003. The one-and-a half-day format allowed for an overall review of the program status. The meeting agenda is provided in Table 2.1.1. Details of the discussions and the presentations can be found in the meeting minutes. Highlights from the meeting are:

- An outline was agreed on and writing assignments were made for the Detailed Five-Year Fuel Development Plans for Series One and Series Two.
- An outline was agreed on for preparation of the irradiation Test Plans. We strongly recommended that DOE publish the AFCI procedures for Test Plan Preparation and Approval and Document Management System. This will guide the expensive series of tests that are being planned and prepared.
- It was agreed that the ATR core internal change-out (CIC) schedule does not need to be delayed so long as the AFC-1 (e&f) tests are inserted in October as planned. A delay in the CIC would negatively impact the Very-High Temperature Reactor (VHTR fuel-testing program.

Table 2.1.1 – Topics for the 2nd FDWG Meeting

WEDNESDAY, FEBRUARY 26th, 2003	
Discussion topic	**Lead**
WP Status and FY03 Budget, Scope & Schedule Overview	Savage/Pasamehmetoglu
LWR Fuel testing requirement for development (test prior to LTA)	Chidester/Cowell
ATR modification needed for LWR-2 test (schedule & scope)	Ambrosek
Series One Analysis Plans and TRANSURANUS	Cowell
Implementation Scenario/Industrial Interviews	Sheetz
Series One Detailed Development Plan	Pasamehmetoglu
Series Two: selection criteria, testing needs, special tests, analyses	Chidester/ Crawford
Status of ATR-1 (a-d) experiments, test plan, cask transport and receipt issues	Ambrosek/Hayes
AFC-1 E&D Test description	Hayes
Status of metallic fuel development (thermal analyses results)	Meyer/Hayes
Status of Nitride fuel development (emphasis on process improvements, sintering aid, etc..)	Margevicius/ McClellan
Update on FUTURIX Collaboration	Hayes
THURSDAY, FEBRUARY 27th, 2003	
Discussion topic	**Lead**
Update on VHTGR fuel development needs	Southworth
Update on TRISO fuel development (emphasis on integration of AFCI and GEN IV needs)	Williams/ McEachern
Series Two Detailed Development Plan	Pasamehmetoglu
DOE questions to FDWG & Open Discussions	Pasamehmetoglu

- Low-fertile nitride fuel compositions for AFC-1 (e) and FUTURIX tests will be finalized by LANL and forwarded to INEEL and ANL-W, respectively, by COB on March 4th, 2003. Metallic fuel compositions for the same tests proposed by ANL-W were reviewed and agreed on.
- We reviewed the VHTR fuel development program. The program requires $104 M in the next 10 years and more than $10 M in FY04. The VHTR program assumes that this amount will be included in the AFCI FY04 budget.
- Next meeting will be held in Idaho Falls, Idaho, on May 21st (full day) and May 22nd (morning), with the expectation that it will coincide with the first week of the ATR-1 (a – d) experiments.
- It was agreed that, before pursuing the gas-cooled deep-burn reactor concept proposed by GA further, the deep-burn capability must be assessed using a ZrC coated fuel.

Semi-Annual Technical Review meeting. The AFCI semi-annual technical review meeting was held in Albuquerque, NM, on January 22 and 23, 2003. All elements of the fuels development program were discussed by ANL, INEEL, LANL, and ORNL staff, followed by a fuels development program overview presented by the NTD.

DOE-CEA Collaboration Technical Exchange Meeting. The semi-annual technical exchange meeting was held in Washington, D.C., on January 15 and 16, 2003. The fuels teams from both sides were well represented. Additional details about the meeting are provided in Section 4.1.2.

2.2 Series One Fuels Design, Specifications and Analyses

The fuel requirements are being developed in close coordination with the National Technical Director for System Analysis on implementation scenarios, system point designs for LWRs/ALWRs, and licensability studies. Industry and NRC interactions, which are essential in developing the requirements, will be conducted under this activity. A Nuclear Energy Research Advisory Committee (NERAC) Advanced Nuclear Transformation Technology (ANTT) Blue Ribbon Panel will make recommendations on the fuel proliferation resistance requirements, which will also be incorporated into the fuel design and specifications.

In addition, analyses of LWR/ALWR cores establish required operating conditions for the proliferation-resistant fuel. Fuel pellet specifications and requirements flow down from these analyses. Parametric analyses of irradiated fuel performance guides the development of irradiation test matrices. The results of all fuel tests are used to validate phenomenology in the fuel model. This activity will provide the final fuel pellet design specifications, a data package that documents fuel performance, and experimentally validated fuel performance models. In the long term, the validated models developed by this activity will become the tools for performing fuel safety analyses required by the licensing process.

The major milestone for this activity is the completion of the fuel specifications and final performance data package by the end of FY 2007. Interim milestones include:

Develop initial set of fuel specifications.	FY 2003
Develop testing requirements and specifications.	FY 2004
Prepare initial LWR licensing and operational requirements.	FY 2004
Initiate fuel performance modeling and validation.	FY 2004
Develop interim set of fuel specifications to be used for loop tests in ATR (LWR-2).	FY 2005
Complete fuel safety modeling.	FY 2006

2.2.1 Series One Fuels Design, Specifications and Analyses Objective and Scope

This activity consists of defining the fuel specifications, which include performance modeling and data validation. This activity leads to final fuel design specifications by FY 2007 to support fuel technology selection. Derivation of the licensability requirements (based on the associated systems studies and interactions with private industry and NRC) is a part of this activity.

In FY 2003, the LWR Fuel Design and Specifications Activity will emphasize the preparation of the detailed fuel development plan, initiation of the modeling and analyses activities, and establishing the proper internal and external interfaces required for future fuel licensing and use.

The major FY 2003 milestones include:

- Complete initial revision of five-year Series One fuel development plan, including functions and requirements, pellet specifications, and testing requirements.
- Procure TRANSURANUS code (a Belgian U/Pu MOX fuel performance model) and make the necessary modifications.

- Perform initial analysis of fuel irradiation performance.
- Complete parametric studies that assist identification of objectives for the irradiation test program.
- Develop an initial implementation plan for Series One transmutation.

2.2.2 Series One Fuels Design, Specifications, and Analyses Highlights

During the continuing resolution, the second quarter progress in this activity was slow and after the actual budget was published a large fraction of the work-scope was deleted.

- A white paper, "Evaluation of Initial Market for MOX from Recycled Commercial Spent Nuclear Fuel" was drafted.
- The tasks associated with TRANSURANUS code and fuel performance modeling were postponed until FY04.
- The licensability study performed under the Systems analysis also was postponed until FY04, which will impact the completeness of the implementation plan.

2.2.3 Series One Fuels Design, Specifications and Analyses Technical Summary

The major activities in this quarter were the Westinghouse Savannah River Company (WSRC) activities on the mixed oxide fuel (MOX) deployment plan and meetings with the Vogtle Nuclear Power station outage managers. For additional information on this topic, please contact Steve Sheetz at steve.sheetz@srs.gov.

The activities toward development of a Series One MOX deployment plan, including issuing draft outlines for the plan and the strategy for its development, continued. WSRC staff met with outage management at Vogtle Nuclear Power Station to discuss use of MOX and its impact on plant operations. While using MOX could make receipt and handling of fresh fuel more time consuming, once the assemblies are staged, there will be no impact on the length of time the reactor will be off-line for refueling. A trip report was issued on the meeting. A white paper, "Evaluation of Initial Market for MOX from Recycled Commercial Spent Nuclear Fuel," was drafted and issued for internal review. It reviews the use of MOX in the suggested baseline class of commercial reactors and discusses the amounts of plutonium required, challenges to the program, and recommendations.

WSRC staff also continued to interface with the Separations Deployment Activity Team to promote integration and consistency between the Fuels and Separations deployment plans. A presentation was made to the Separations Working Group on a potential market for MOX.

2.3 Series One Fuel Fabrication

Using small-scale fabrication equipment in the LANL TA-55 facility, the test fuels will be characterized, fabricated, and supplied to the ATR for irradiation testing. The first two years focus on developing and confirming modifications to commercial fabrication processes so that the fuel can meet fuel design specifications. From 2005 to 2007, the activity will focus on optimization of the fabrication process to define process specifications by 2007, supply of fuel from irradiation testing and supporting design requirements for the LTA, and fuel fabrication plant preconceptual design activities.

The major milestone for this activity is completion of the final fuel fabrication process definition by the end of FY 2007. Interim milestones include:

- Supply fuel pellets, characterization data, and test capsules for the initial irradiation tests in ATR (initial part of LWR-1).
- Supply fuel pellets, characterization data, and test capsules for the remaining LWR-1 tests in ATR.
- Supply fuel pellets, characterization data, and test capsules for LWR-2 loop tests to be performed in an ATR pressurized loop.
- Supply fuel pellets, characterization data, and test capsules for transient tests (safety tests).

2.3.1 Series One Fuel Fabrication Objectives and Scope

In FY 2003, the Fuel Fabrication activities focus on process development and fabrication of (U, Pu, Np) oxide fuel pellets for irradiation testing in the ATR (LWR-1). The fuel composition will vary but will be focused on a nominal 5% Pu with very small amounts of Np and potentially some amount of a depletable neutron absorber. Oxide feed powders will be acquired and the process testing will include varying the blending, milling, pressing, and sintering (temperature, time, and atmospheric) parameters. Process development will include key property measurements and initial modeling of material behavior.

Samples of the fabricated pellets will be measured for U, Pu, and Np assay, impurities, and all other pertinent parameters. The pellets will be prepared for shipment from LANL to INEEL, where they will be loaded into fuel pins and assembled into capsules for irradiation in the ATR. After all samples have been measured, a data package will be assembled to document the condition of the fuel batches. Pellet samples will also be prepared for other potential irradiation tests.

The major FY 2003 milestones for the Fuel Fabrication activity include:

- Acquisition of the oxide feed powders for process development and for test fuel in the ATR experiments,
- Demonstration of (U, Pu, Np,) oxide fuel,
- Completion of the ATR fuel pellet fabrication, and
- Completion of the oxygen diffusion model.

2.3.2 Series One Fuel Fabrication Highlights

The following are the major second quarter highlights for Series One fuel fabrication:

- A draft experimental plan for LWR-1 has been written and is being reviewed and revised.
- Modifications have been made to a furnace to allow for sintering of MOX fuel.
- The model of defect chemistry and oxygen diffusion in CeO(2-x) was completed and a journal article is being written. The model will be extended to include the UO(2+-x) and PuO(2-x) compounds.
- A computer code for binary phase diagram simulations was integrated in a MathConnex project and is ready to be used to calculate phase diagrams in actinide-based oxides and nitrides.

2.3.3 Series One Fuel Fabrication Technical Summary

Technical summaries for the following two activities are provided below:

- Fuel fabrication
- Fuel modeling

Fuel Fabrication. A meeting was held at INEEL to discuss the details of the upcoming LWR-1 irradiation experiment. Personnel from LANL, INEEL, and ANL-W were in attendance. At that meeting, it was agreed that the overall experiment would use much of the design work generated from the MOX irradiation experiment sponsored by DOE MD in 1996-8. Conceptually, there will be three compositions with three burn-up levels. The compositions will be: 1) 5% weapons grade (WG) Pu in depleted U (a duplication of the MD MOX composition); 2) ~7.5% reactor grade (RG) Pu in DU; and 3) ~7.5% RG Pu with 4000 ppm Np. The targeted burn-up levels would be 5, 25, and 50 GWd/t; however, the exact irradiation schedule is being evaluated. It also was agreed that LANL would draft the experimental plan and circulate it to INEEL for review.

In order to sinter MOX, two modifications to a furnace in PF-4 had to be made. A HEPA filter on the exhaust gas has been replaced and a step-down gas regulator must be installed. This regulator is a custom-made model; the order was placed, and delivery of the regulator is expected during the second week in April.

For additional details, please contact Bob Margevicius at margevicius@lanl.gov.

Fuel Modeling. For SOFC modeling, a critical point is to understand the oxygen diffusion in non-stoichiometric oxides. While, for restricted non-stoichiometric range, some information can be extracted from the available ionic and electronic conductivity measurements, modeling over an extended domain is much more complicated. Our numerical results show that a good agreement with the available experimental data for oxygen diffusivity in non-stoichiometric ceria is obtained only if all defects containing oxygen are taken into consideration. In the present study, we have incorporated V^*_O, V^{**}_O, $(CeV_O)^*$, and $(CeV_O)^x$. The oxygen diffusion was found to be thermally activated, with the activation energy being in the range 1.8 – 2.3 eV. We used for the reported results 2.1 eV, consistent with the value derived from Steele and Floyd

experiments,[1] without taking the dependence on composition (x) into consideration. A good agreement with experimental data over a restricted range of compositions can also be achieved in the same range by using x dependent activation energies. However, without incorporating an appropriate factor for modulation, such relations will fail in describing the observed very sharp increase of the oxygen diffusion coefficient, close to full stoichiometry (x ≅ 0).

Our results showed that the oxygen diffusivity at a given temperature, T, and as a function of composition (x) (or different oxygen pressures P_{O2}), is well described by:

$$D_{Oxygen}(x,T) = D_0(T)\sum C_n x_n^2 \qquad (1)$$

where E_a= 2.1 eV, $D_O(T) = [1.1\times10^8 k_B/e]\exp(-E_a/k_BT)$ cm^2/s, and x_n are the reduced concentrations of V^{**}_O, V^{*}_O, $(CeV_O)^*$, $(CeV_O)^x$ species, respectively. The coefficients C_n are given in Table 2.3.1.

Table 2.3.1 – Coefficients of the diffusivity polynomial expansion (Eq. 1).

C_1	C_2	C_3	C_4
95	1.3	5.3	0.45

Using Eq. (1), the changes in the oxygen diffusivity were computed for different compositions and temperatures. The concentrations of x_n species in Eq. (1) were calculated with our MathCad code, which implements a statistical-thermodynamic approach devised by Ling[2]. The results are plotted against x for different temperatures (°C) in Fig. 2.3.1. Also, experimental points calculated with data from Steele and Floyd were plotted for comparison. This figure also includes the calculated electronic diffusivities.

By inspecting the contribution of various terms in Eq. (1), we observe that, very close to the stoichiometric compound (x ≅ 0), the leading term is $C_1x_1^2$, representing the contribution due to double-charged oxygen V^{**}_O vacancies. This is not a surprise because, in this range, V^{**}_O vacancies are the dominating defect. Due to coulombian interaction, the reaction enthalpies for the production of V^{**}_O and V^{*}_O vacancies are increased (i.e. if t = 1100 C and V^{**}_O, from 5eV corresponding to x = 0, to 6.7 eV corresponding to x = 0.4). This means that it is less likely to form double and single charged oxygen vacancies. However, in the same range, the V^{*}_O concentration increases and $C_2x_2^2$ starts dominating in Eq. (1). Between x = 0.05 and x=0.015, the terms contributing in Eq. (1) are $C_2x_2^2$ and $C_4x_4^2$ $(CeV_O)^x$. When entering the deep nonstoichiometry region, (x>0.15), $C_4x_4^2$ clearly become the leading terms. The x values are slightly modified by the temperature, but the conclusion is the same. According to this picture, it seems therefore that single-charged $(CeV_O)^*$ complexes play practically no role in oxygen diffusion.

1 B. C. H. Steele and J. M. Floyd, Proceedings of the British Ceramic Society, 19, 55 (1971).
2 S. Ling, Phys. Rev. 49, 864 (1994).

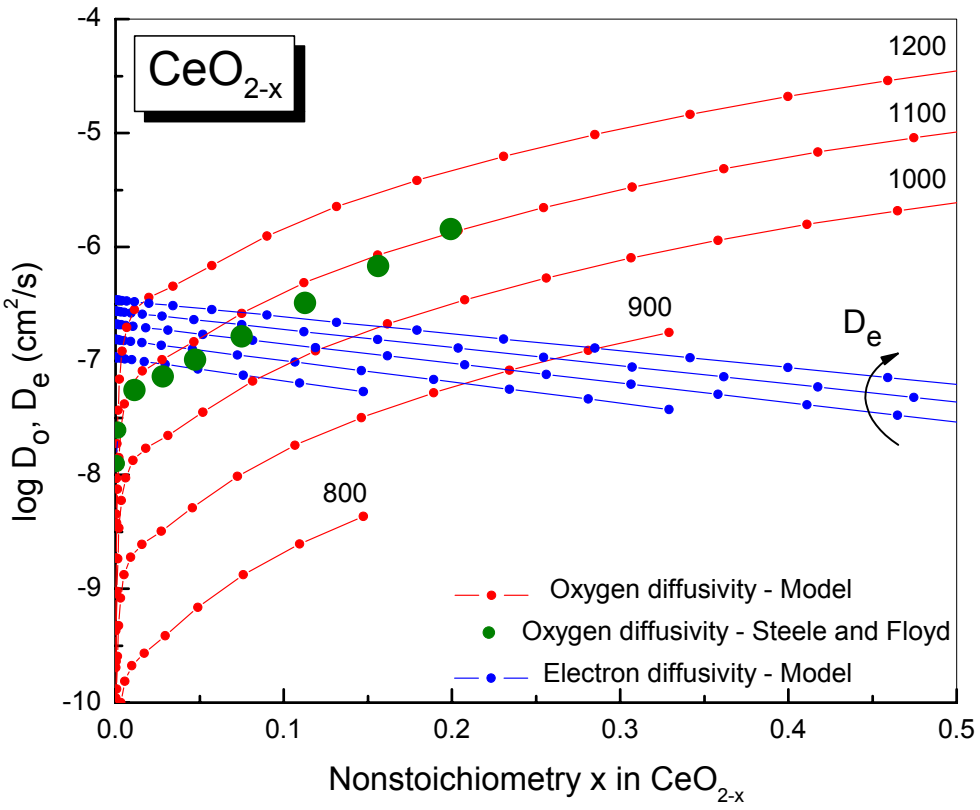

Fig. 2.3.1 – Oxygen diffusivity in non-stoichiometric ceria and electron diffusivity as functions of composition (x) and temperature: red points – oxygen diffusivity (model), blue points – electron diffusivity (model), green points – oxygen diffusivity calculated with experimental data from Steele and Floyd [1]. The temperature is indicated in °C.

For further details, please contact Marius Stan at mastan@lanl.gov.

2.4 Series One ATR Irradiation Experiments

The first test for Series One fuel is an accelerated burnup irradiation of clad and unclad (U, Pu, Np) oxide fuel pellets and wafers. The primary motivation of these tests is to determine the degree to which the existing MOX fuel performance database is applicable to (U, Pu, Np) oxide fuels. Fuel prototype samples, termed "rodlets," will be irradiated in the LWR-1 test to assess fuel behavior and fuel/cladding interactions, including formation of a rim effect. Tests of wafer-sized samples in easily accessible irradiation positions as part of a series of materials characterization tests will allow more detailed assessment of densification, recrystallization, and modification of the fuel ceramic. Test irradiations will be simulated on the proliferation-resistant fuel performance code, and model-data comparisons will be used to modify and validate the performance codes. These tests are planned to be performed in ATR (and High Flux Isotope Reactor (HFIR) if needed) from the third quarter in FY 2004 through the end of FY 2007.

The performance of prototypic fuel rods in prototypical neutron flux and coolant conditions will be assessed in the LWR-2 irradiation test series. The irradiation tests will focus on confirming behavior of the reference fuel and will be designed to fine tune fuel parameters such as stoichiometry, density, etc. The testing will include tests to demonstrate full lifetime performance and provide supporting licensing and performance data for lead test assembly (LTA) testing. This test series will be performed in the ATR using a pressurized water test loop. The LWR-2 and ATR test loop design, fabrication, insertion, and irradiation activities will take place between FY 2006 and FY 2013.

Additional tests may be planned as the results of the initial irradiation tests (LWR-1) are reviewed and the licensing requirements are developed. In addition, the international database on MOX and similar fuels will be reviewed to determine additional testing requirements. Currently, the primary test facility is envisioned to be the ATR. Additional tests may be performed in test stations of HFIR as necessary.

An additional key fuel performance and safety test will be transient testing of an irradiated fuel rodlet from the LWR-1 test in the Annular Core Research Reactor (ACRR). The purpose of this scoping test will be to supplement information on ramp testing in (U, Pu) oxide fuel that will allow the NRC to determine whether more expensive, more rigorous transient testing of proliferation-resistant fuel will be necessary for licensing.

The Post-irradiation examination (PIE) tasks of examining the samples from the initial first LWR-1 irradiation tests will begin late in FY 2004. More detailed PIE tests will be performed on fuel retrieved from the LWR-1 and LWR-2 transient tests and will continue until the end of FY 2007. However, large-scale PIE work will not begin until the fuel in LWR-1 is irradiated at least for a year and thus is not expected to begin until FY 2006. The hot-cells at ANL-W, INEEL and LANL will be the primary PIE locations, but other hot-cells (e.g. at ORNL) may be used if necessary.

2.4.1 Series One ATR Irradiation Experiments Objective and Scope

In FY 2003, the main task for Fuel Irradiation is LWR-1 testing in ATR. The design test plan and safety analyses for LWR-1 tests will be completed in FY 2003 to prepare for irradiation testing in ATR in the beginning of FY 2004. In addition, the fuel pellets fabricated at LANL will

be used in the fabrication of the fuel pins and irradiation capsule. The FY03 scope also includes the pre-conceptual design for the loop test (LWR-2).

2.4.2 Series One ATR Irradiation Experiments Highlights

There are no highlights because the activities did not start until late in the second quarter.

2.4.3 Series One ATR Irradiation Experiments Technical Summary

These tasks were delayed during the second quarter. However, funding was received in late March and activities have been initiated. For information on these activities, please contact Richard Ambrosek at rga@inel.gov.

2.5 Series Two Fuel Design Specification and Analyses

The Series Two fuels development effort will provide advanced transmutation fuels for Generation IV fast reactor systems that will be deployed by 2030. During the first five years, the Series Two effort is structured to provide fabrication and irradiation test information for a range of promising advanced fuels to support a transmutation technology decision in 2007. After key transmutation and Generation IV technology decisions have been made, Series Two will focus on fuels development to support the selected concepts and technology. The transmutation requirements will be developed through an iterative process throughout the first five years of assessment. The feasibility of meeting these requirements and resulting fuels requirements will also be assessed.

Studies supporting this initiative and the Generation IV Program have previously identified several advanced fuel types that have the potential to meet performance requirements for transmutation and future power systems. Oxide, nitride and metal-based fuels support fast spectrum sodium- or lead-cooled systems for power and transmutation. Advanced tri-isotopic (TRISO) fuels support the development of very high temperature gas systems for power, hydrogen, and potentially epithermal transmutation applications. A range of other advanced fuel types (e.g., cermet, dispersion, etc.) are being considered for gas-cooled fast reactors.

The Series Two fuel requirements and the Series Two Fuel Development Plan will continue to be revised and updated as new data is obtained. This activity will benefit from technical progress made by international partners in transmutation fuels and materials.

Five-year milestones include:

- Develop Series Two fuel requirements and planning and alternative testing options.
- Integrate Generation IV fuel development efforts within the Series Two Fuel Development Plan.
- Provide fuels data to transmutation technology selection studies.

2.5.1 Series Two Fuel Design, Specifications and Analyses Objective and Scope

This activity involves evaluating various fuel concepts within the framework of transmutation objectives. Detailed development plans for each fuel concept and testing requirements until the technology selection also covered by this activity.

The major FY 2003 objectives for Generation IV Transmutation Fuels are as follows:

- Evaluate alternative options for curium-bearing fuels.
- Conduct Fuels and Materials Modeling Workshop.
- Revise Series Two fuels functions and requirements.
- Revise the Five-Year Fuel Development Plan.
- Revise the International Series Two Fuels Handbook.
- Conduct initial safety assessment on low-conversion ratio fast reactors.

2.5.2 Series Two Fuel Design, Specifications and Analyses Highlights

The following are the major highlights for the low-conversion ratio fast reactor safety analyses:

- Work continued on the examination of reactivity coefficient predictions for the low-conversion ratio fast reactor systems; the high leakage configurations pose difficulties for conventional physics methods.
- Reports from CEA regarding the fast burner reactor CAPRA project were reviewed.

2.5.3 Series Two Fuel Design, Specifications and Analyses Technical summary

Work continued on the examination of reactivity coefficient predictions for the low-conversion ratio fast reactor systems; the high leakage configurations pose difficulties for conventional physics methods. A complete set of transport theory reactivity coefficients was generated for the four fast reactor designs developed in the FY02 study with conversion ratios (CR) ranging from 0.5 to 0.0. For the bounding cases, the finite difference diffusion theory results are compared to VARIANT nodal variational transport results using P_5 spherical harmonics expansion in Table 2.5.1. Very large variations in the sodium void worth are observed for the high leakage CR=0.0 configuration with the diffusion result at -$6 and the transport results at $0.7. An independent Monte Carlo model was also performed with the VIM code; the void worth result of $3.58±0.05 for the CR=0.47 core agreed well with the transport results; however, for the CR=0.0 core, the VIM result of –$1.06±0.07 does not agree well with either solution.

Table 2.5.1 – Comparison of Diffusion and Transport Theory Reactivity Coefficients

Whole-Core Reactivity Coefficient	CR=0.47 Configuration		CR=0.00 Configuration	
	Diffusion	Transport	Diffusion	Transport
Delayed Neutron Fraction	0.0032		0.0023	
Sodium Void ($)	**2.21**	**3.68**	**-6.19**	**0.70**
Sodium Density (cents/K)	0.07	0.09	-0.08	0.01
Radial Expansion Coefficient (cents/K)	-0.35	-0.32	-0.58	-0.54
Axial Expansion (cents/K) (fuel)	-0.13	-0.13	-0.22	-0.23
Voided GEM Worth ($)	-0.68	-0.35	-1.50	-0.80

Significant variations are also observed for the gas expansion module (GEM) reactivity worth with the transport results roughly ½ the negative reactivity of the diffusion results. For both cores, the diffusion and transport theory geometric expansion results are similar.

Trade studies indicated that the void worth differences observed in Table 2.5.1 arises from voiding of the above-core gas plenum/axial reflector region. A refined multigroup cross section generation procedure was developed to provide a more rigorous treatment of the neutron energy spectrum in the upper axial zone. With these corrected group constants, the CR=0.47 void worth

predictions are $3.49 for diffusion theory and $4.19 for transport theory, with the diffusion results now in excellent agreement with the VIM solution. Thus, this approach is promising for improving the diffusion theory evaluations that are utilized to generate the detailed spatial reactivity profiles for safety analysis. However, transport effects will be more severe in higher leakage configurations (e.g., at CR=0), which should also be investigated.

Low conversion ratio design options using compact fast reactor core geometry (as compared to the high leakage configurations employed in FY02) were explored; such designs would have economic benefits associated with reduced core radii. By reducing the fuel volume fraction, burner core designs with conversion ratios ranging from 0.5 to 0.0 were developed. The resulting performance and key reactivity coefficients are summarized in Table 2.5.2. The compact design uses a reduced core volume that results in a peak linear power that is significantly higher (>400 W/cm) than the FY02 approach (~300 W/cm). The reduced core volume also increases the reactivity loss rate; this has been compensated for by reducing the cycle length from one year to six months. As expected, the sodium void worth and radial expansion coefficient are adversely impacted (as compared to the pancaked configuration results, Table 2.5.1) because of the reduced core leakage.

Table 2.5.2 – Compact Configuration Performance and Reactivity Coefficients

Performance Parameter	Core Size A	Core Size B	Core Size C	Core Size D
TRU Conversion Ratio	**0.49**	**0.35**	**0.24**	**0.00**
Peak Linear Power (W/cm)	417	430	449	516
Burnup Reactivity Loss ($ over **six month cycle**)	2.6	3.5	4.3	6.1
Delayed Neutron Fraction	0.0031	0.0029	0.0028	0.0024
Sodium Void ($)	5.80	5.21	4.29	-1.99
Doppler Coefficient (cents/K)	-0.08	-0.07	-0.06	-0.01
Radial Expansion Coefficient (cents/K)	-0.29	-0.33	-0.36	-0.44
Axial Expansion (cents/K) (fuel alone)	-0.24	-0.28	-0.30	-0.38

The FY02 simplified safety analysis model was modified to accommodate the compact core configuration. The increased core height required changes in the above core and control rod driveline modeling; the balance-of-plant model was retained. Loss-of-flow, transient-overpower, and loss-of-heat-sink transients without scram were evaluated for the four compact core designs shown in Table 2.5.2. Qualitatively, the results obtained are similar to those obtained for the "pancaked" configuration in FY02. However, the margins to coolant boiling and fuel melting are significantly smaller. In the loss-of-flow transient, peak fuel temperatures range between 50 and 60° K higher as the conversion ratio varies between 0.5 and 0. They are between 60° and 100° K higher in the transient overpower cases and between 40° and 45° K higher in the loss-of-heat-sink transients. Peak coolant outlet temperatures are between 120° and 135° K higher for the loss-of-flow case, between 10° and 20° K higher for the transient-overpower case, and between 65° and 80° K higher in the case of the loss-of-heat-sink transient.

Also this quarter, reports from CEA regarding the fast burner reactor CAPRA project were reviewed. In order to reduce the burnup swing in their fast burner reactor, they implemented subcycles in which they swapped relatively few assemblies. At (BOC), they loaded the core with poisoning assemblies and, at 6 months, they removed these assemblies and replaced them with dilution assembles (boron-11 or simply steel reflectors) and continued in the new configuration for another 6 months. Such an approach does not appear to be very practicable and we are instead investigating operating a shortened (6 month) cycle with a compact configuration with many fewer assemblies than described above.

For further information on this topic, please contact Bob Hill at bobhill@anl.gov.

2.6 Series Two Nitride Fuel Development

Nitride fuel is one of the fuel forms that are being pursued for transmutation applications. Such fuel types can be used in the sodium or lead alloy cooled fast reactors and accelerator driven systems (ADSs). The development of nitride fuels to support Generation IV and higher actinide transmutation presents many technical challenges. These fuels must: be capable of high burnup to minimize the number of recycles required; be compatible with low-loss separations processing; be easily fabricated in a remote environment; and behave in a benign manner during core steady-state and off-normal events. Because the Generation IV/transmutation system architecture has not yet been defined, the five-year fuel development program concentrates on developing a technology base common to most applications.

For fast reactors, the fuel composition of interest includes fertile materials mixed with plutonium and minor actinides. However, for potential heterogeneous core design scenarios, fertile-free fuels are also of interest. If ADSs are chosen in conjunction with fast reactors to achieve the transmutation goals, fertile-free fuels are of primary interest.

2.6.1 Series Two Nitride Fuel Development Objective and Scope

The FY03 objectives for the nitride fuel development cover process improvements in parallel with fuel pellet fabrication and characterization for ATR irradiation. Specific activities include:

- Continue to investigate enhanced nitride synthesis, blending, pressing, and sintering techniques;
- Develop process parameters to fabricate actinide fuel with DU as a diluent;
- Characterize fertile-free and fertile nitride test batches for physical and chemical composition and property measurements; and
- Fabricate cylindrical pellets from each composition for the ATR fertile actinide nitride irradiation test. Ship completed fuel pellets to ANL for loading into test fuel capsules.

2.6.2 Series Two Nitride Fuel Development Highlights

The following are the major highlights for the nitride fuel development during the second quarter of FY03:

- Feedstock materials have been acquired for the upcoming fabrication effort.
- Initial experiments on alternate fabrication routes for the actinide nitrides have demonstrated success.
- Methods for evaluating the extent of pellet cracking (endcapping) have been explored.
- Nanoindentation hardness and modulus measurements continue to be performed on heavy ion irradiated ZrN to provide an indication of the changes of these extrinsic and intrinsic properties. Hardness of ZrN continues to increase with implantation of up to 2E16 Xe @ 450 keV (80 dpa peak) while the modulus is substantially unchanged within the error of the measurement.

- In the effort to minimize americium (Am) volatilization during fuel processing, the nitride pressing parameters continue to be optimized and the sintering aid study has been restarted. The mill/cold-press//sinter process has been improved for ZrN processing enabling a >5% increase in green and corresponding sintered densities. This process enhancement must still be transferred to TA-55 and verified for the (TRU)N-ZrN fuels.
- The role of preferred crystallographic orientation of grains (texture) with respect to the anisotropy of mechanical properties in the mononitride fuel materials continues to be examined. Previously, significant texture was measured in sintered ZrN pellets. Further measurements of fracture toughness anisotropy have revealed variations from sample to sample; however, a qualitative trend is present. Measurement of texture on green ZrN pellets has been carried out and it was found to be similar to the as-sintered textures.
- Long-term QM calculations of UN/ZrN solid solutions have been the exclusive focus throughout this period. A series of different UN/ZrN compositions (stoichiometries) have been simulated and current results show that structure volumes and energies do not follow a simple rule of mixtures (non-ideal behavior). It is not yet clear whether this is a consequence of the limitations of the calculations or indicative of behavior in this system.
- First principles calculations of the electronic structure of Am predicted the energy-versus-volume functions for several possible crystal structures. The results will allow for the optimization of the Modified Embedded Atom parameters, with impact on the modeling of thermo-mechanical properties of Am and AmN.

2.6.3 Series Two Nitride Fuel Development Technical Summary

Second quarter progress for the nitride fuel development is reported for the following sub-tasks:

- Nitride pellet fabrication,
- Assessment of radiation tolerance of nitride,
- Thermomechanical characterization,
- Quantum mechanical simulations of actinide nitrides, and
- Atomistic modeling of americium using Ab initio and semi-empirical potentials.

Nitride Pellet Fabrication. Feedstock materials for the upcoming AFC-1E irradiations in the ATR—the low-fertile nitride compositions—have been identified and acquired. Four compositions, listed in Table 2.6.1 below, with two compositions at two positions in the reactor, have been agreed upon. All compositions include 50 % (molar) of uranium. The ratio of depleted to highly-enriched uranium is still being calculated. The primary FUTURIX composition is targeted for insertion into the PHENIX reactor in FY06. Two positions in the ATR, a position in the centerline of the fuel column giving a relatively high burn-up and one at the end giving a relatively low burn-up, will be used to give two levels of burn-up. A secondary FUTURIX composition containing no Np will also be assessed in a similar fashion. Two other compositions will be evaluated, one that is analogous to one of the ANL metal fuel compositions, and a model system. The targeted compositions are shown in Table 2.6.1.

Table 2.6.1 – Targeted compositions for ATR irradiation

Nominal Composition	Description
$(U_{0.5}Pu_{0.25}Am_{0.15}Np_{0.1})N$	Primary FUTURIX Composition, low burn-up position
$(U_{0.5}Pu_{0.25}Am_{0.15}Np_{0.1})N$	Primary FUTURIX Composition, high burn-up position
$(U_{0.5}Pu_{0.25}Am_{0.25})N$	Secondary FUTURIX Composition, low burn-up position
$(U_{0.5}Pu_{0.25}Am_{0.25})N$	Secondary FUTURIX Composition, high burn-up position
$(U_{0.5}Pu_{0.4}Am_{0.1})N$	Approximate match to metal fuel
$(U_{0.5}Pu_{0.5})N$-30ZrN	Model system

One issue that was raised during the fabrication efforts of AFC-1A and –1C was internal pellet cracking. This could be a result of a number of factors, including a heterogeneous mixture of the nitrides and pellet pressing conditions. To address the first issue, an alternative means of nitride fabrication is being explored. The baseline fabrication route has the nitrides being formed as pure nitrides (i.e., pure PuN is formed from the oxide, pure AmN is formed, etc.) and the correct ratio of actinide and zirconium nitride is mixed and reacted to form the mixed nitride. The alternate method has the reaction occurring in the oxide phase, and then the mixed oxide is reacted to nitride. Initial results demonstrate that very little Am loss is measured and that the nitride phase has formed. The other issue being addressed is changing the pellet processing parameters to reduce cracking. Those initial results show no cracking.

For additional information on nitride pellet fabrication, please contact Bob Margevicius at margevicius@lanl.gov.

Assessment of Radiation Tolerance of Nitrides. Heavy ion implantation has been used to determine the effects of radiation on the ZrN inert matrix fuel. Xenon (Xe) was chosen for its mass, ease of implantation, its abundance as a fission product, and its known swelling effects in other fuel forms. As a heavy ion, it produces considerable damage to crystal structure yet has little effect on the chemistry. It is considered dissolved in the structure until it is expelled into a void, pore, grain boundary, or any growing bubble.

Samples are irradiated at liquid nitrogen temperature to "freeze in" defects as they are produced. An accelerating voltage commonly used is 300 keV, which causes heavy damage and a high dose within relatively short times. It is also a standard to which many irradiated materials can be compared/contrasted. Fluences up to $5x10^{16}$ Xe/cm^2 have been used, which gives about 200 displacements per atom (DPA) and 12 atomic % Xe in a very limited cross sectional area. This quantity of damage and implanted atoms places tremendous strain on the crystal and microstructure of any material. Many materials amorphize at this level of damage, yet ZrN has yet to show this effect.

In the past, doses up to $5x10^{15}$ Xe/cm^2 have shown microstructure changes such as polygonization, grain refinement, microtwins, and bubble formation. Amorphization and

swelling were not observed. Fluences from 1 to 5 times 10^{16} Xe/cm^2 have produced the same microstructural effects. These all had the same high dose rate of about $1x10^{16}$ Xe/(cm^2 hour).

Presently, in contrast to these past experiments, the dose rate has been reduced. This was done primarily for the nanoindentation experiment in which higher implant energy required a lower dose rate. With a greatly reduced dose rate of about 10^{16} Xe/(cm^2 14 hours), completely different microstructure changes have been observed under cross-sectional TEM. At 80 dpa, no grain refinement, twins, or bubbles were observed, yet amorphization is again absent. Figures 2.6.1 & 2.6.2 show the distinct difference.

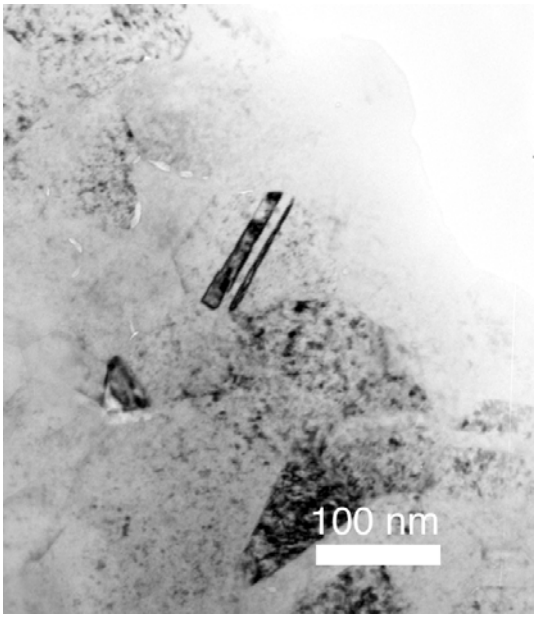

Fig. 2.6.1 – No distinct layer of damage, only small grains, twins, and voids can be observed $5x10^{16}$ Xe/cm^2 into @300 keV

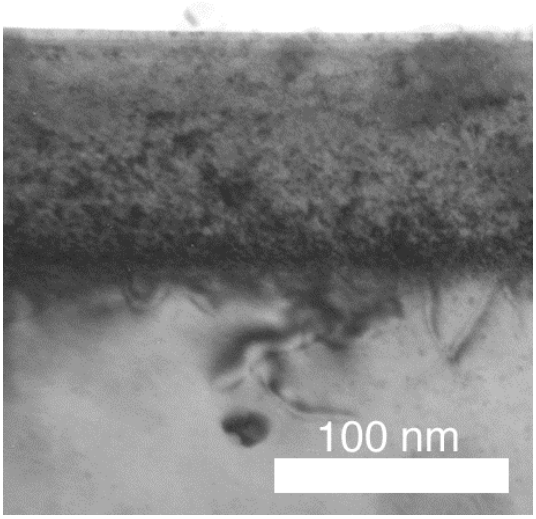

Fig. 2.6.2 – Damage layer clearly seen with low dose rate $2x10^{16}$ Xe/cm^2 into @450 keV

With the possibility of the dose rate having such a large effect, further studies are underway. It is currently surmised that the rate of damage may be balanced by the rate of recovery and that point defects are mobile enough to take up the added stress. At high dose rates, the damage produces stresses that can not be reduced by mobile point defects and thus the polygonization and other effects may occur.

Physical properties, such as hardness and stiffness (modulus) are typically changed by radiation damage. Using the nanoindentation technique, these properties have been measured with respect to increasing fluence on ZrN irradiated with Xe.

Nanoindentation introduces a very small broad-tipped, three-sided pyramidal indenter that pushes into the surface of the material. The applied load is correlated with the movement of the indenter into the material giving a value of the resistance to deformation, or hardness. The indenter, as it is moved into the material, is oscillated up and down slightly, and this measures the material's stiffness. Because the indenter is very small, only a very small depth of about 200 nm is sampled. This technique gives the hardness and modulus at different depths as the indenter penetrates and is ideal for the depths of implantation of Xe.

Hardness is an extrinsic property of a material and is the resistance to deformation. Young's modulus is an intrinsic property and is a measure of stiffness or the elasticity of a material. Point defects produced during irradiation, such as vacancies or interstitials, inhibit dislocation movement due to lattice strains and thus increase hardness. These defects have little effect on the atomic bonds and thus the modulus.

Because the implantation of any ion produces a skewed Gaussian distribution of both the ion and the damage profile, different Xe fluences and energies were used to sum to the flattest profile with depth. The energies were 70, 200, and 450 keV, and the fluences were 0.25, 0.5, and 2 times 10^x Xe/cm^2, where x is the magnitude chosen. Samples were implanted at liguid nitrogen (LN_2) temperature at a rate of about 10^{16} Xe/(cm^2 14 hours). Figures 2.6.3 & 2.6.4 show the TRIM-predicted damage-produced vacancy profile and Xe distribution with depth.

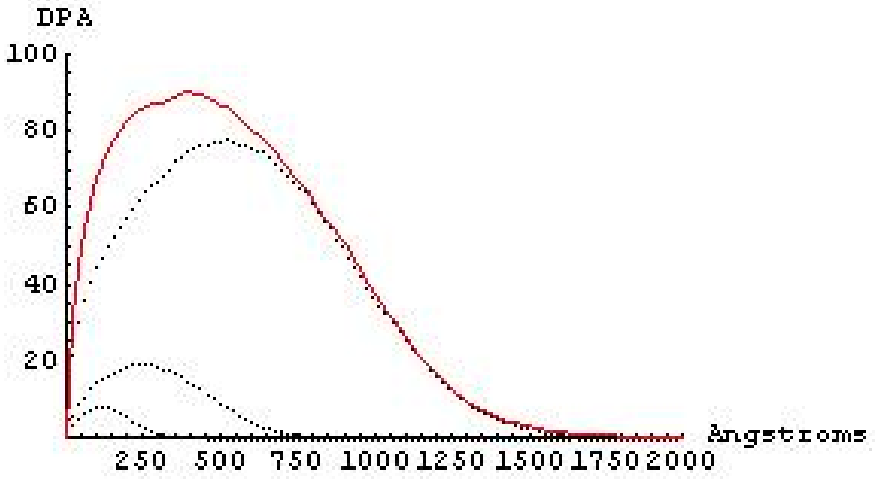

Fig. 2.6.3 – Plot shows the sum (red line) of the vacancy distribution formed by displacement damage (Xe into ZrN, 0.25x10^{16} @ 70 keV, 0.5x10^{16} @200 keV, & 2x10^{16} @ 450 keV)

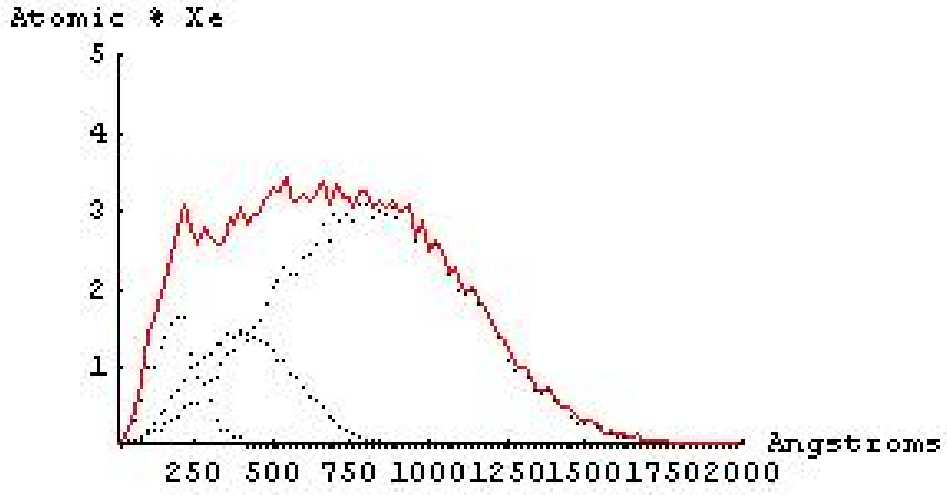

Fig. 2.6.4 – Plot shows the sum (red line) of the Xe distribution (Xe into ZrN, 0.25x1016 @ 70 keV, 0.5x1016 @200 keV, & 2x1016 @ 450 keV)

Nanoindentation penetrates to a greater depth than the peak damage. Due to effects of the surface and initial penetration errors, a function is generated with regression to calculate the peak hardness and reduce these errors. As the tip pushes deeper, it pushes past more of the damage and into more of the undamaged substrate below. The hardness decreases as it is measured as a sum of the two in relation to depth. Figure 2.6.5 shows typical hardness raw data.

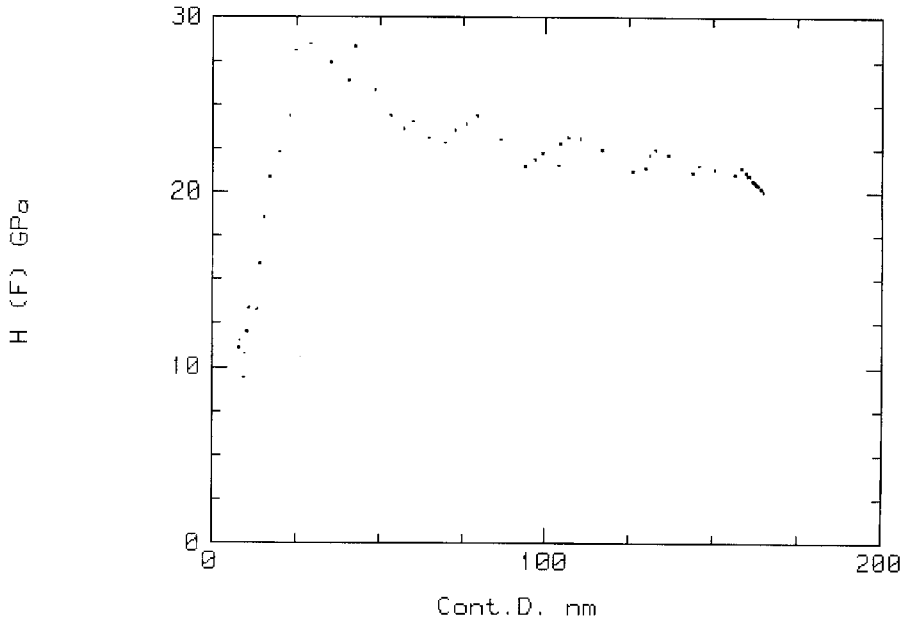

Fig.2.6.5 – Typical nanoindentation hardness data

Results show the hardness to increase slightly at a lower fluence of 10^{14} Xe/cm^2 (about 0.8 dpa) but increase dramatically at higher fluence. The trend follows a logarithmic curve with implantation as the defect production begins to saturate. Hardness was increased by about 20% at

the highest fluence (10^{16} Xe/cm^2, about 80 DPA). The modulus, however, did not show significant change. Within statistical error, the modulus measured was approximately the same as the published value for HIPed ZrN, as shown in Figs 2.6.6a and 2.6.6b. These results correlate with TEM images showing high point defect concentration but no amorphization.

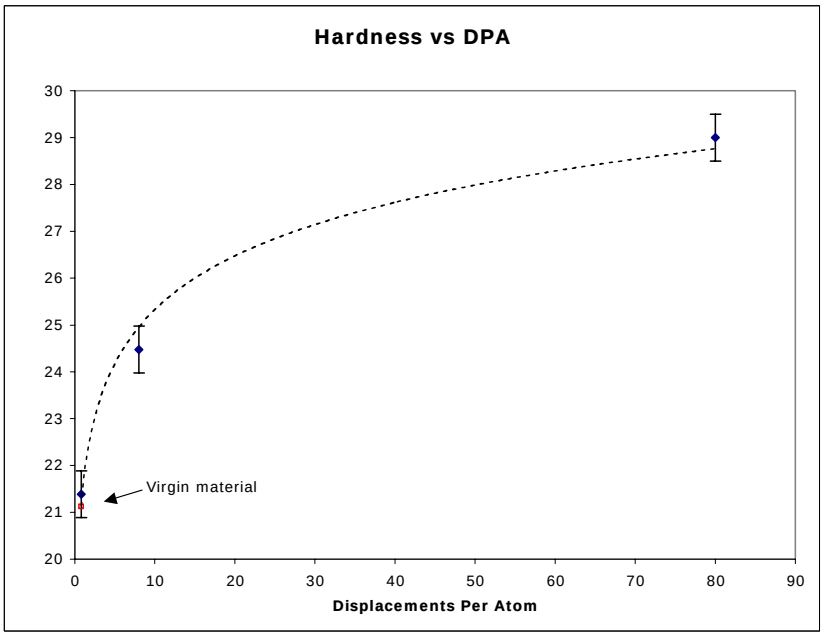

(a)

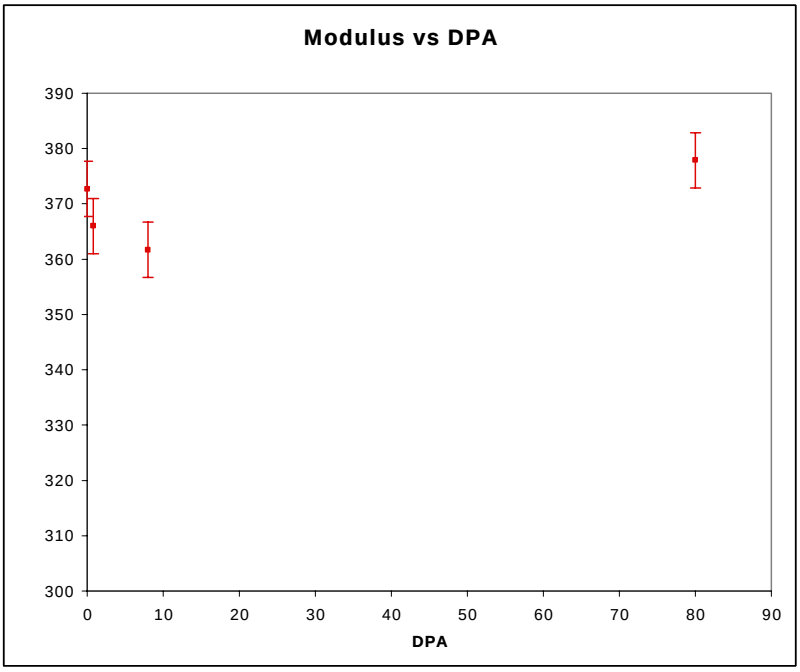

(b)

Fig. 2.6.6 – Hardness and modulus measurements as a function of dpa

For additional information on this topic, please contact Gerald Egeland at jegeland@lanl.gov.

Thermomechanical Characterization. Crystallographic Texture Development and Effect of Heat Treatment on Anisotropy of Mechanical Properties of Sintered ZrN Pellets are studied at Arizona State University (ASU). For additional information on this topic, please contact Pedro Peralta at pperalta@asu.edu.

To understand changes in directional variations of properties resulting from processing, evolution of crystallographic texture was studied in green and sintered ZrN pellets. In addition, the variation of mechanical properties with respect to characteristic sample directions was studied and measured in sintered ZrN before and after heat treatment to evaluate the effects that post-processing treatment may have on the deformation and fracture mechanisms that can control the structural stability of fuels during transmutation. The results presented here build on the initial assessment on anisotropy of the mechanical properties previously reported, with emphasis on texture characterization of green pellets as well as Vickers hardness (Hv) variations and fracture toughness (K_{Ic}) of both sintered and heat-treated samples. The texture analysis of the green material revealed a well-defined fiber texture in the specimens. This texture has two components: a {200} component with an intensity of 3.4 times the intensity of a random distribution (m.r.d) and a {111} component with an intensity of 2.6 m.r.d. These values are quite similar to the textures measured from sintered samples, indicating that most of the texture is produced during powder compaction rather than during sintering. The hardness tests were carried out on planes perpendicular to the principal directions defined by the texture, radial and longitudinal, and fracture toughness was also evaluated on these planes. This was carried out for sintered samples without heat treatment to gather more measurements and improve the statistics of the study reported previously. Samples were also heat treated in pure nitrogen to study the effect of heat treatment on the anisotropy of mechanical properties. Indentation testing revealed that average hardness values did not change significantly from one plane to another for both untreated and treated samples; however, meaningful variations were observed between different pellets. The fracture toughness, on the other hand, showed more significant changes, and the trend observed before (i.e., radial planes being tougher than longitudinal ones) has been confirmed. Scanning electron microscopy study of the fracture surfaces indicates that the fraction of cleavage facets is higher in heat-treated specimens, which points to an increase in the strength of interfaces and grain boundaries as a result of the heat treatment. However, further studies in monolithic ZrN are needed to pinpoint the exact mechanisms leading to these results.

Cylindrical ZrN pellets, 12 mm in diameter and approximately 12 mm in height, were sintered at LANL using an improved process. Samples for texture, metallographic characterization, and microhardness testing were cut from these pellets using wire electro-discharge machining (WEDM). These samples were first polished with SiC paper (600, 800 and 1200 grit) and then finished with 1 μm diamond paste. The samples for texture analysis were disks perpendicular to the axis of the pellets, which were also used to obtain the hardness on the longitudinal plane. Slices parallel to the longitudinal direction were also cut to obtain hardness values on the radial plane. Samples for fracture toughness were also cut using WEDM in the form of micro-beams with height and thickness of approximately 1 mm and lengths of about 6-7 mm. The axes of some of these beams were cut parallel to the axis of the cylinder (longitudinal fracture plane) whereas another set of beams had their lengths cut parallel to the radial direction (radial fracture plane). Notches with lengths of approximately one half of the height were also made using WEDM. The surfaces of these beams were polished with SiC paper up to 1200 grit. Some of the

samples for hardness and fracture toughness were heat treated at 800 °C for 24 hours under a pure nitrogen atmosphere. In addition, samples for texture analysis were cut from a green pellet using a thin diamond blade. The green pellets fractured easily during cutting; however, a piece large enough for texture characterization was obtained and mounted in epoxy to keep it from breaking any more.

Texture analysis was carried out in a Rigaku RU200 rotating anode X-ray diffractometer equipped with a pole figure goniometer. The diffractometer was operated at 50 kV and 100 mA with a 0.5° slit. Data collection was carried out at 5° intervals between 0° and 75° tilt angle and full rotations for the twist angle. Hardness testing was carried out in a standard microhardness testing apparatus using a Vickers indenter (four-sided pyramidal diamond tip) with a load of 500 grs. Five indents were made per sample, in order to obtain average values of the hardness. Fracture toughness testing was performed using a screw-driven loading stage under displacement control following the procedures specified by the standard ASTM E-399. The load resulting in fracture was measured using a 500 lb load cell. Microstructural characterization, hardness determination and fractographic observations were carried using optical microscopy and scanning electron microscopy.

The raw pole figures collected for the texture characterization of green (not yet sintered) material are shown in Fig. 2.6.7.

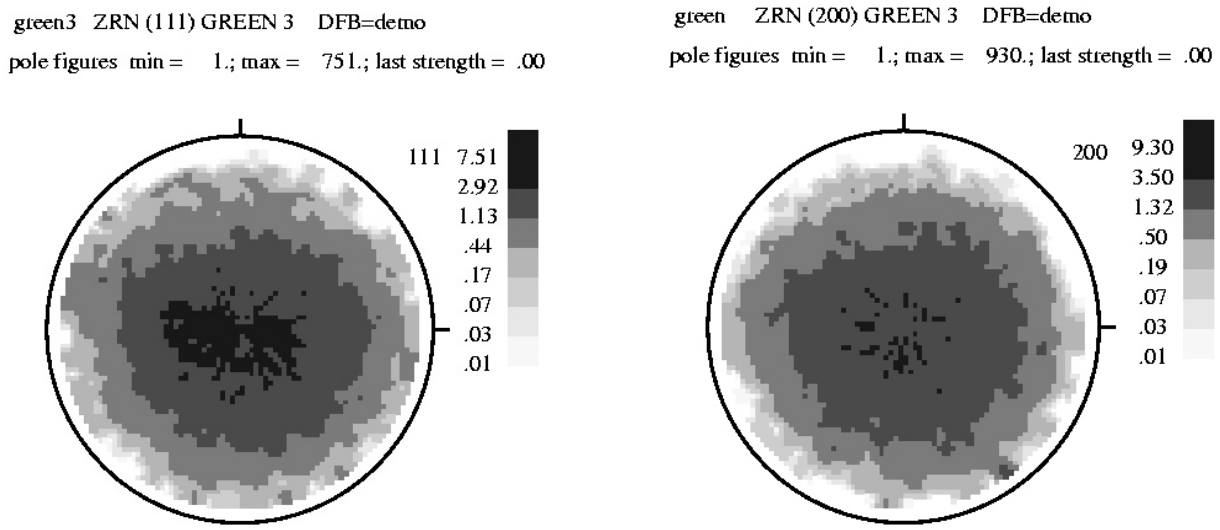

Fig. 2.6.7 – (a) {111} pole figure; (b) {200} pole figure. The axis of the cylindrical pellets corresponds to the center (axis 3)

It is evident from these pole figures that the sample has a clear {200}-{111}fiber texture, as was the case for the sintered material. Further analysis was carried out to extract the strength of the texture components as multiples of the intensity of a random sample. The refined pole figures are shown in Figs. 2.6.8 and 2.6.9.

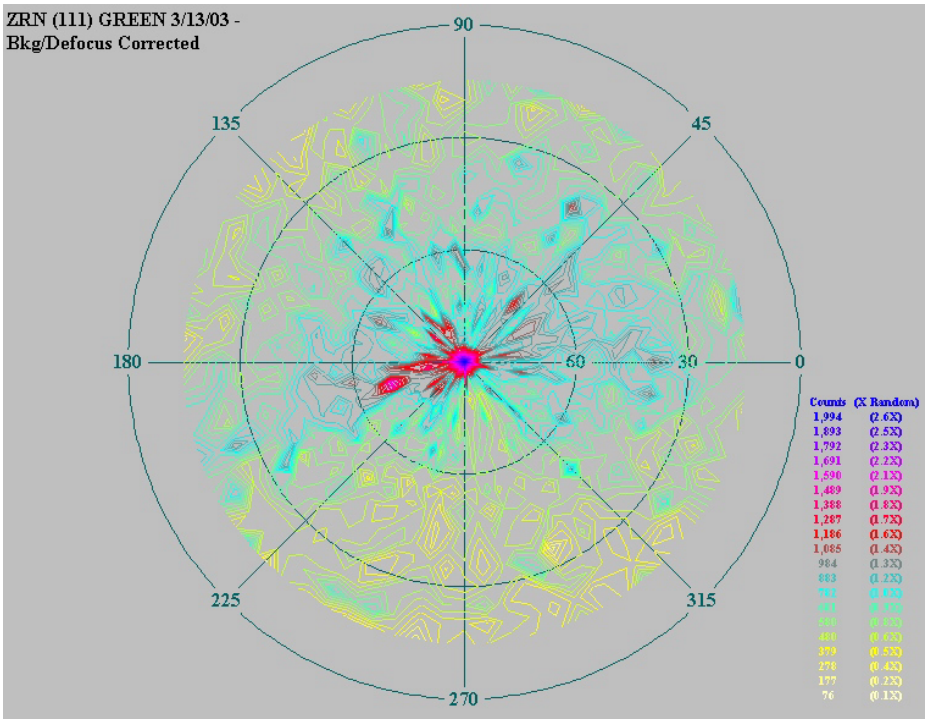

Fig. 2.6.8 – Refined {111} pole figure after background subtraction and defocusing correction.

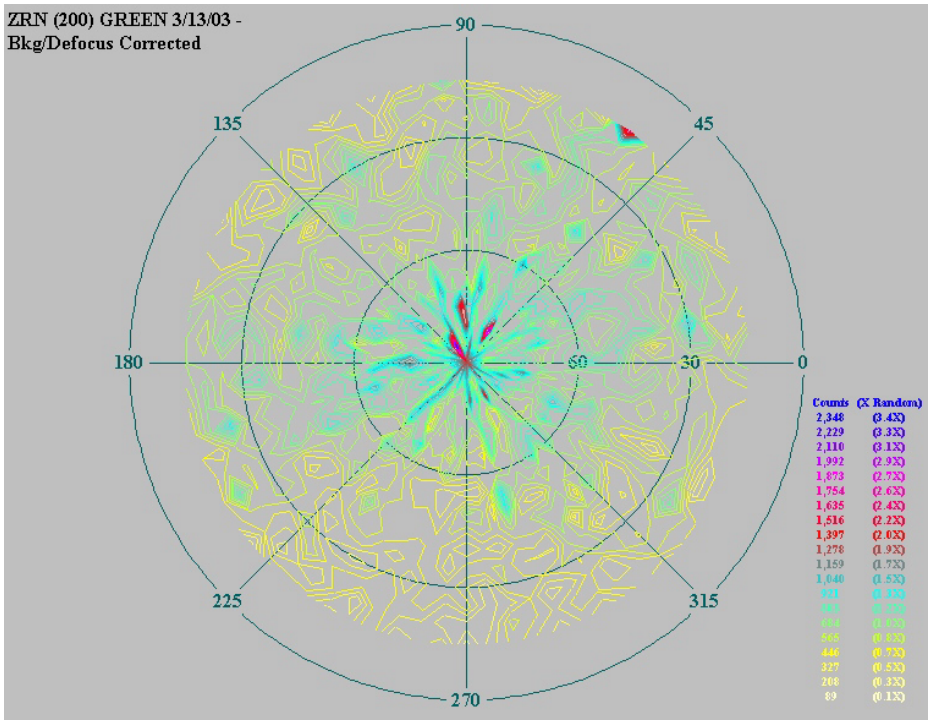

Fig.2.6.9 – Refined {200} pole figure after background subtraction and defocusing correction.

Note that the maximum intensity in the two pole figures corresponds to the center, which is the direction parallel to the axis of the cylindrical pellets, and that the maximum intensity of the {200} figure is about 3.4, m.r.d whereas the maximum intensity of the {111} pole figure is 2.4 m.r.d. The {200} texture is somewhat weaker than that measured for the sintered specimen,

which was about 4.0 m.r.d., suggesting that the {200} texture component may have evolved and strengthened during sintering. The strength of the {111} texture component in the green specimen is quite similar to that of the sintered specimen, which was 2.5. The difference between the two is too small to speculate regarding a sintering effect on strengthening this texture component. Fiber textures with {200}-{111} components are common in cubic metals, particularly after recrystallization.[3] [4] However, ZrN has the rock salt structure and the mechanisms by which texture develops in ceramics are not that well understood.[3] Two or three mechanisms may be responsible for the development of this texture. The first mechanism is particle rotation during powder compaction. This mechanism could play a significant role if the powder particles used to prepare the material have facets due to cleavage or can cleave easily during compression. Once the cleavage facets are present, the compression will tend to align the crystallographic facets perpendicular to the applied stress (i.e., the compression direction). No references regarding the existence of cleavage planes in ZrN were located in a preliminary survey of the literature. Scanning electron microscopy of green samples will be carried out to look at individual particles and look for facets. The presence of a fiber texture in the green specimens seems to add some support for this mechanism because it is one of the few that can produce texture without plastic deformation or recrystallization.

Another mechanism is inelastic deformation during sintering. It is well known that (in metals) compressive deformation tends to produce texture components parallel to the vector normal to the slip plane of the active dislocations (i.e., {111} in FCC and {110} in BCC). Ionic materials with the rock salt structure tend to slip on {110} planes, whereas rock salt materials with more covalent bonding tend to slip on either {110} or {100}.[5] The slip behavior of ZrN does not seem to be well characterized, a thorough literature search did not result in any published results in this regard. The strengthening of the {200} texture component in the sintered material as compared to the texture of the green sample seems to suggest that ZrN may slip on {100} planes, given that compression textures align themselves normal to the slip plane. Finally, recrystallization can occur during sintering. Recrystallization textures result from the preferred crystallographic orientation of grains nucleating during the recrystallization process. This phenomenon is not well understood in metals and this is even more the case for ceramics due to the large number of parameters involved. [3] This may play a role in the texture development in this material because large grains are observed in sintered samples.

Further analysis of the texture will be carried out using Preferred Orientation Package, Los Alamos (popLA) to look at the distribution of orientations on lateral directions. Inverse pole figures will be generated via harmonic analysis of the measured pole figures. This work is currently in progress. However, it is expected that the results will be similar, except that the strength and definition of the fiber texture will be lower for the green samples. The main symmetry of the cases is, therefore, expected to be similar. The anisotropy of the mechanical properties resulting from this crystallographic texture in the sintered material was explored further as a function of testing plane and heat treatment. The results of this effort are discussed in the next section.

---

[3] Kocks, U.F., C.N. Tomé, and H.-R. Wenk, *Texture and Anisotropy*. 1998, Cambridge: Cambridge University Press.

[4] Llanes, L., et al., Effect of Grain Size and Annealing Texture on the Cyclic Response and the Substructure Evolution of Polycrystalline Copper. Acta metall. mater., 1993. 41(9): p. 2667-2679.

[5] Nabarro, F.R.N., *Theory of Crystal Dislocations*. 1987, New York: Dover Publications, Inc.

The results from the micro-hardness testing for the sintered material with and without heat treatment for both longitudinal and radial indentation planes are shown in Fig. 2.6.10.

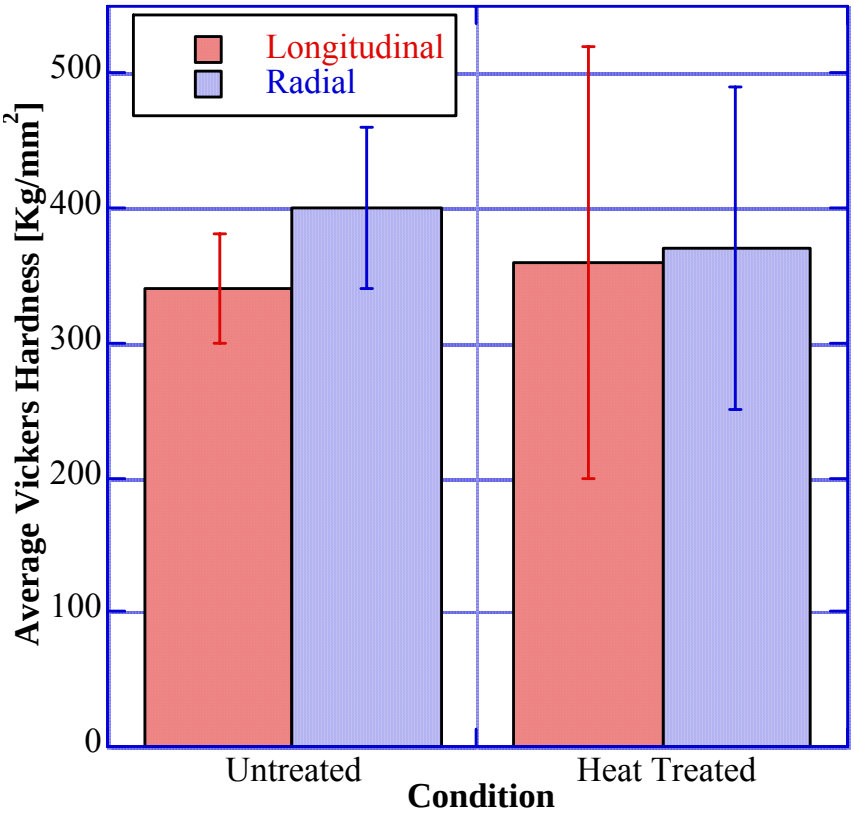

Fig.2.6.10 – Vickers hardness as a function of heat treatment and indentation plane.

Note that the average value of hardness was very similar for both indentation planes, as indicated by the preliminary analysis reported previously. A small anisotropy can be seen, with the average hardness on the longitudinal plane being slightly lower than for the radial plane. This difference goes away with the heat treatment; the average for the two cases is quite similar. Note that the average hardness did not increase significantly with heat treatment; however, the error bar is significantly longer for the heat treated specimens, indicating that hardness can be either much higher or much lower than the average as compared to the untreated specimens. This means that large increases in hardness are possible, but the uniformity of the resulting material is not optimum. Note that the Vickers hardness of monolithic ZrN has been reported to be between 13 and 16 GPa (1300 to 1600 Kg/mm^2)[6], whereas the average value obtained here is approximately 340 Kg/mm^2, about four times lower. As discussed in previous reports, hardness is controlled by porosity, the distribution of which does not seem to be affected significantly by the existence of a preferred crystallographic texture. The fracture toughness, on the other hand, is more likely to be affected by the texture because the strength of particles along the crack path will certainly depend on the orientation. This is discussed in the next section.

[6] From NIST ceramic database: http://www.ceramics.nist.gov/srd/scd/Z00220.htm#M6P1

The fracture toughness measured on the two principal material directions showed the same trend it had been found previously (i.e., a higher fracture toughness on the radial plane); however, the difference between the two planes was about 25% for untreated specimens and approximately 42% for heat-treated samples. Results are shown in Fig. 2.6.11.

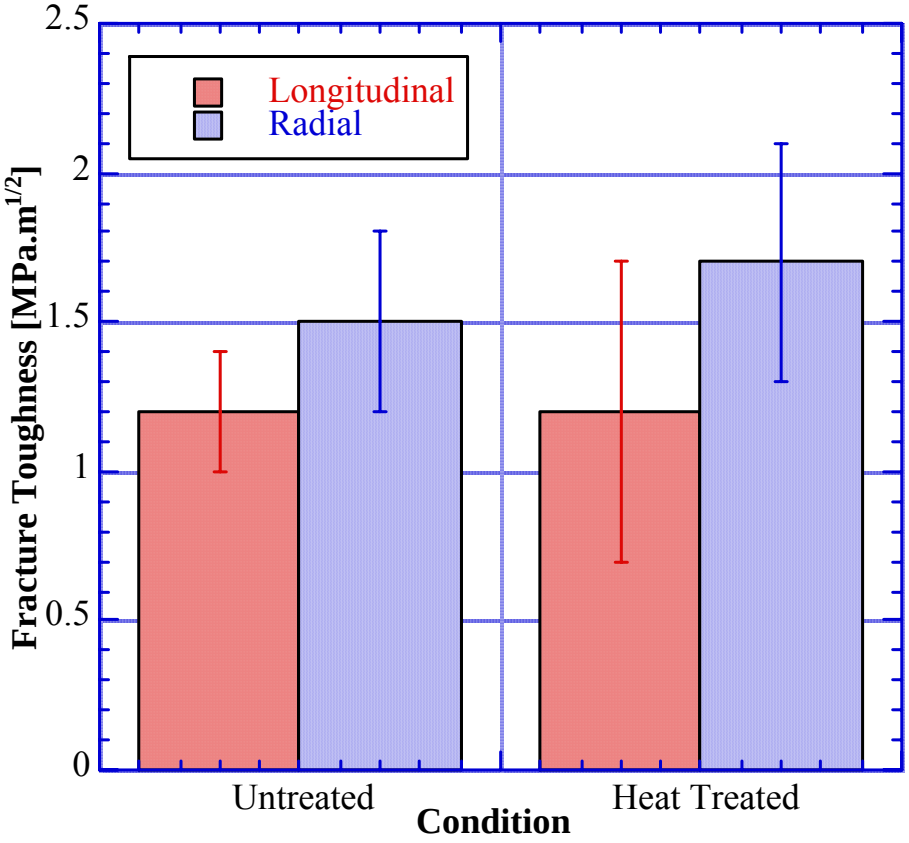

Fig. 2.6.11 – Fracture toughness as a function of heat treatment and fracture plane.

The heat treatment had a clear tendency to increase the average toughness on the radial plane, while leaving the average toughness on the longitudinal plane mostly unchanged. Note that the error bar for heat-treated specimens is higher, indicating that higher toughness values are possible, if better material uniformity is achieved. The fracture surfaces of the broken specimens were examined using Scanning Electron Microscopy (SEM) to try to elucidate the reasons for the higher toughness values in the heat-treated specimens. Fracture surfaces for both fracture planes in heat-treated samples are shown in Fig.2.6.12.

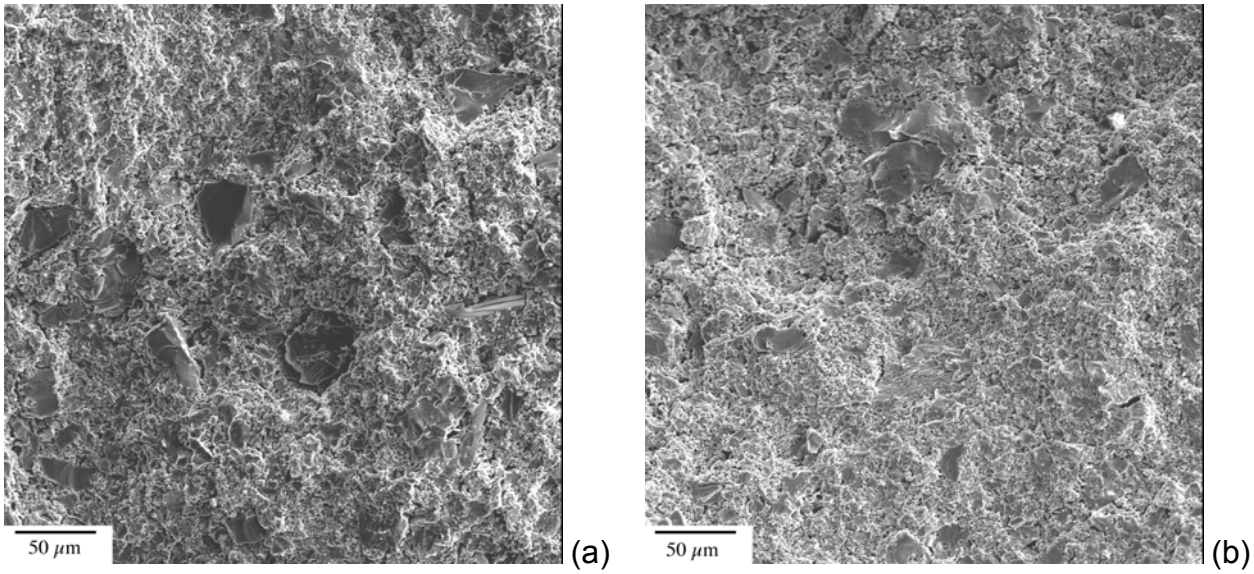

Fig. 2.6.12 – Typical fracture surfaces for heat treated samples. (a) radial plane; (b) longitudinal plane.

Note from Fig. 2.6.12 that the fraction of cleavage facets is larger for fractures on the radial plane than on the longitudinal plane, indicating that cracks on that plane must go through a larger number of particles in order to propagate. This explains the higher value of fracture toughness on the radial plane because cleavage of particles must offer higher resistance to crack propagation than cracking of the porous matrix surrounding the particle, particularly considering that the fracture toughness of monolithic ZrN is much higher than the average values measured here for the porous material[7]. Further comparisons were carried out with the fracture surface of an untreated sample broken on the radial plane, which is shown in Fig. 2.6.13.

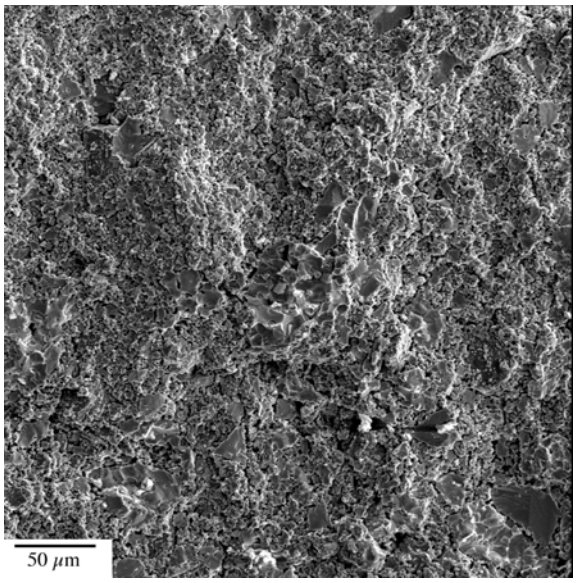

Fig. 2.6.13 – Fracture surface of an untreated specimen broken on the radial plane.

[7] Note that the value of toughness for monolithic ZrN is between 5 and 7 MPa.m$^{1/2}$ according to the NIST database.

A direct comparison of the fracture surface shown in Fig.2.6.13 and that presented in Fig. 2.6.12a makes it very evident that the number of cleavage facets increases substantially after the heat treatment (the fracture surfaces shown come from samples made from the same pellet). Therefore, the crack is somehow forced to travel more through the particles rather than through the porous matrix after the heat treatment, resulting in an increase of the fracture toughness. This also indicates that the effect of the heat treatment is to strengthen the interfaces between the particles and the porous matrix as well as the matrix itself because the cracks can no longer deviate when they run into a large particle (i.e., it takes less energy to go through the particles than to deviate and break through the interfaces or the porous matrix). A refinement of the processing leading to this effect could result in meaningful improvements to the structural reliability of this material while keeping the same porous microstructure.

The study of crystallographic texture and mechanical behavior anisotropy of sintered ZrN pellets leads to the following conclusions:

- A well-defined fiber texture with components along {200} and {111} was found in the green samples and it was similar, but weaker, than the texture measured in sintered samples.
- The {200} component of texture becomes stronger during sintering, indicating that inelastic deformation and recrystallization may play a role in texture development for this material.
- Assessment of the Vickers hardness of ZrN samples with and without heat treatment indicates that there is only a small amount of anisotropy on this variable for longitudinal and radial indentation planes. Again, this is likely to be due to the fact that the porosity controls the hardness of the material.
- There is a significant difference between the fracture toughness on radial and longitudinal planes that increases with the heat treatment.
- Fractography indicates that crack-path changes are responsible for the increase in fracture toughness after the heat treatment. Higher values of fracture toughness are associated with a larger fraction of cleavage facets on the fracture surface.
- More information on the mechanical properties of monolithic ZrN is needed in order to fully understand the mechanical behavior of the sintered material.

Quantum Mechanical Simulations of Actinide Nitrides. The quantum mechanical simulations are performed at the Imperial College, London, under LANL contract. For additional information, please contact Robin Grimes at r.grimes@ic.ac.uk. We have predicted lattice parameters for a range of nitride materials using spin-polarized quantum mechanical simulations. The comparison with experimental values is in Table 2.6.2 and Fig. 2.6.14. Excellent agreement is apparent for ZrN and TiN, and the agreement for actinides and DyN is satisfactory. There are two reasons for this disparity in results. First, the spin-polarized calculations are computationally more difficult and, consequently, we still need to investigate convergence more closely. Second, certainly for the actinides, the (GGA) simulations conducted here essentially ignore spin orbit coupling. Its inclusion will slightly modify selected ion-ion interactions and thereby the total volume of the unit cells. Comparison of these calculations with more complete quantum mechanical simulations would therefore be of interest.

Table 2.6.2 – Lattice Parameter and Mulliken population for various nitrides.

Material	Expt. Lattice Parameter (Å)	Predicted Lattice Parameter (Å)	Mulliken Population (e)	Ionic Radii (Å)[8,9]
CmN [10]	5.027	4.94	0.84	0.97
PuN [11]	4.905	4.99	0.73	1.0
UN [12]	4.89	4.96	0.76	1.025
DyN [13]	4.89	4.81	0.81	0.912
ZrN [14]	4.585	4.61	0.87	0.83
TiN [15]	4.238	4.25	0.79	0.67

Although the agreement for actinides and DyN is less satisfactory, as shown in Fig. 2.6.14, it does predict a non-monotonic increase in lattice parameter with ionic radii as observed experimentally.

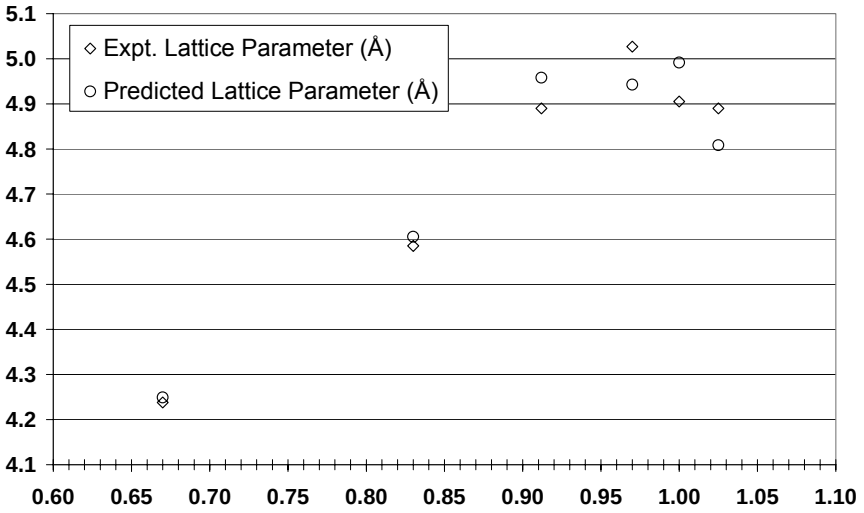

Fig. 2.6.14 – Trend of experimental and predicted lattice parameter with 3+ cation radii.

We have predicted the Young's modulus and Poisson's ratio for each of the actinide nitrides (see Table 2.6.3). The aim of these calculations is to provide data that may be useful when

[8] R.D. Shannon, *Acta. Cryst. A* 32 pp752-767 (1976).
[9] Alexandre *et al.*, *J. Mater. Sci.*, vol. 28, pp2385-2390 (1993).
[10] Y. Akimoto, *Journal of Inorganic and Nuclear Chemistry* **29** pp2650-2652 (1967).
[11] W.H. Zachariasen, *Acta Crystallographica* **2** pp388-390 (1949).
[12] H. Hollek, E. Smailos and F. Thuemmler, *Journal of Nuclear Materials* **32** pp281-289 (1969).
[13] P. Ettmayer, J. Waldhart and A. Vendl; Monatshefte fuer Chemie **110** pp1109-1112 (1979).
[14] N. Schoenberg, *Acta Chemica Scandinavica* **8** pp213-220 (1954).
[15] A.N. Christensen, *Acta Chemica Scandinavica Series A* **29** pp56-568 (1975).

considering the mechanical properties of a composite nitride – nitride fuel form (analogous to MOX fuels in oxide technology). In this regard, probably the most important parameter of those investigated is the Young's modulus. For high strength it can be beneficial to have one of the phases with a higher Young's modulus. Interestingly the values in Table 4.7 suggest that TiN may have a significantly higher Young's modulus and as such, even a small percent addition of TiN may improve strength performance at high temperatures although Young's modulus for all these materials is already high. Certainly there is nothing from these data that suggests a problem. However, differences in the thermal expansion coefficients should also be considered in future work.

Table 2.6.3 – Predicted Young's Modulus and Poisson's ration for selected nitrides (from quantum mechanics).

Material	Expt. Lattice Parameter (Å)	Young's Modulus (Gpa)	Poisson's Ratio
CmN	5.027[2]	368	0.175
PuN	4.905[3]	359	0.201
ZrN	4.585[6]	378(380)	0.203(256)
TiN	4.238[7]	492	0.184

Experimental results in brackets for comparison.[9]

We have also predicted the bulk and shear moduli for these nitrides. These results are presented in Table 2.6.4. Significantly, no great differences are apparent between the actinides and the diluent ZrN.

Table 2.6.4 – Predicted elastic constant matrix, bulk and shear modulus for selected nitrides (from quantum mechanics). Note $B = 1/3(C_{11}-C_{12})$; $S_1 = 1/2(C_{11}-C_{12})$; $S_1 = C_{44}$.

Material	Expt. Lattice Parameter (Å)	C_{11} (Gpa)	C_{12} (Gpa)	C_{44} (Gpa)	Bulk Modulus (Gpa)	Shear Modulus (Gpa)
CmN	5.027[3]	397	109	84	205	144
PuN	4.905[1]	399	100	98	200	149
ZrN	4.585[4]	422	107	84	212(260)	157
TiN	4.238[5]	536	121	177	259(318)	207

Experimental results in brackets for comparison [9,16]

Quantum mechanical simulations of UN-ZrN solid solutions are computationally demanding. In particular, the number of ions within the simulation repeat cells will be limited. Consequently

[16] Kim *et al.*, *J.Phys.* **72** pp1805-1811 (1992).

we can report results derived using $Zr_{31}UN_{32}$, $Zr_{15}UN_{16}$, Zr_7UN_8 and Zr_3UN_4 unit cells. These correspond to stoichiometries of: $Zr_{0.96875}U_{0.03125}N$, $Zr_{0.9375}U_{0.0625}N$, $Zr_{0.875}U_{0.125}N$ and $Zr_{0.75}U_{0.25}N$.

In a true solid solution, the distribution of Zr and U ions will exhibit no long-range order. Therefore, we must consider how useful an approximation using a fixed unit cell really is. First we consider the lattice parameters for these specific example solid solution unit cells (see Fig. 2.6.15). Interestingly, the lattice parameters for the solid solutions are all lower than the ideal mixing line.

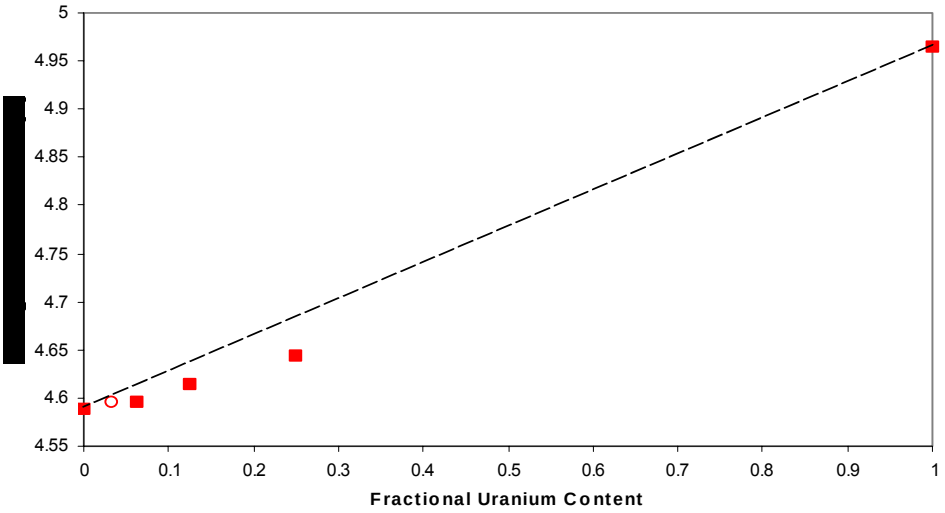

Fig. 2.6.15 – Lattice parameter of UN-ZrN solid solutions as a function of uranium content.

Second, we consider the internal energy for solution, E_S, corresponding to each stoichiometry, relative again to the end members (see Fig. 2.6.15).

$$E_S(Zr_nU_mN) = \left(E_{Zr_nU_mN} - nE_{ZrN} - mE_{UN}\right)/(n+m)$$

where E_{ZrN} etc. are the lattice energies of the various components.

As can be seen in Figure 2.6.16, the solution energy initially increases with U content increase but the energy corresponding to $Zr_{0.75}U_{0.25}N$ shows no further increase (the value for $Zr_{0.96875}U_{0.03125}N$ corresponds to a medium convergence rather than fine and is presently being repeated). During the next month, we intend to analyze these results and determine to what extent we can use the values to define a true concentration-dependent solution energy for use in thermodynamic simulations.

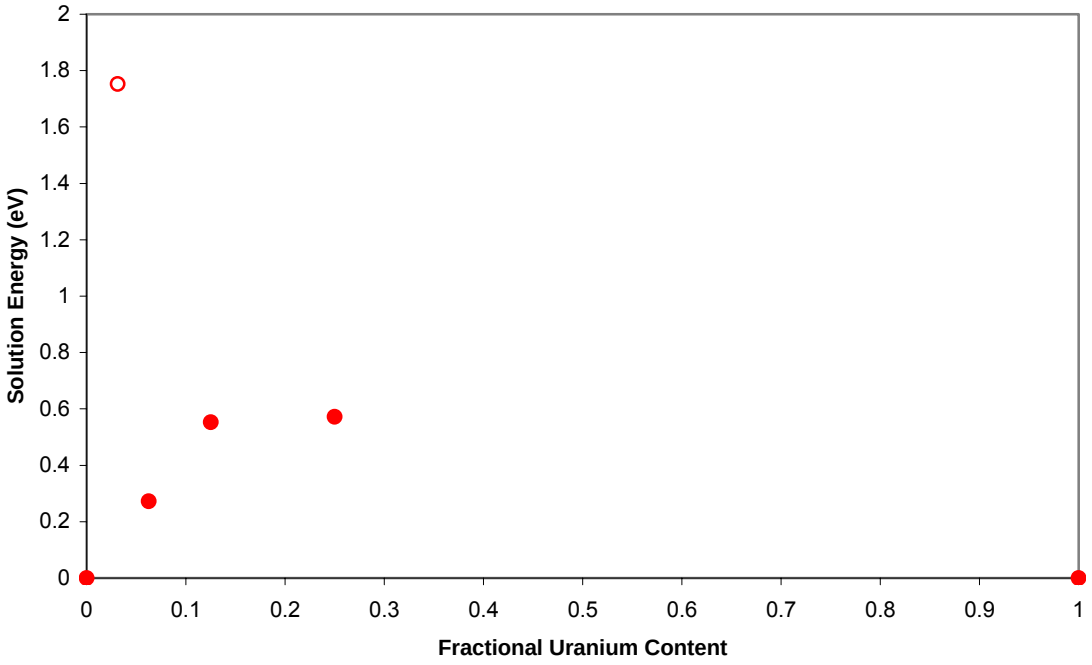

Fig. 2.6.16 – Solution energy (eV) of UN into the diluent ZrN.

We have also calculated the incorporation energy for Xe into a range of nitride materials – from CmN to TiN. In these lattice structures, we have considered three possible trap sites; isolated cation and nitrogen vacancies and the neutral di-vacancy (which is composed of one cation and one nitrogen vacancy). This is analogous to previous work done by Grimes and Caltow[17] on fission product accommodation on UO_2. Results are given in Table 2.6.5. Incorporation energies assume that the trap site is available for the fission product to occupy. As such, it is not surprising that, for all materials studied, the di-vacancy trap is energetically favored because this trap site provides the largest lattice space for Xe, which is a large atom.

[17] R.W. Grimes and C.R.A. Catlow, *Phil. Trans. R. Soc. Lond. A,* 335, 609 (1991).

Table 2.6.5 – Predicted incorporation and equilibrium solution energies for selected nitrides (from energy minimization).

		Incorporation energy at pre existing site (eV)			Solution energy in equilibrium (eV)		
Material	Lattice Parameter (Å)	Cation vacancy	Nitrogen vacancy	Di vacancy trap	Cation vacancy	Nitrogen vacancy	Di vacancy trap
CmN	5.027[2]	2.35	0.87	0.70	11.15	9.66	12.63
UN	4.98[3]	2.40	0.92	0.74	9.75	8.27	11.14
ZrN	4.585[4]	3.99	1.70	1.41	11.61	9.32	12.52
TiN	4.238[5]	5.49	2.53	2.13	13.26	10.31	13.65
NpN	4.897[1]	2.37	0.90	0.72	10.13	8.65	11.55
PuN	4.905[1]	2.41	0.91	0.74	10.28	8.78	11.70
DyN	4.89[2]	2.98	1.16	0.94	12.14	10.32	13.47

As the concentration of fission products increases, there are no longer sufficient intrinsic trap sites for the fission product ions to occupy. Because we have previously shown that the intrinsic defect concentrations will be very low in these materials, this will be the situation after a very short time. Thus, the fission product will occupy a trap site that must be formed specifically through the majority defect process, which for these materials is the Schottky reaction. We have therefore also calculated the internal energy for solution, which incorporates the trap formation. These are also presented in Table 2.6.5. Interestingly we now observe that the di-vacancy is no longer the favorable trap site but, in all cases, it is the nitrogen vacancy. Nevertheless, the solution energies are high, indicating that solution of Xe is a very unfavorable process thermodynamically. Nevertheless, Xe may still be trapped due to a large kinetic barrier to migration (i.e. a high migration activation energy). It is now clear that actinide nitride materials generally provide lower isolated solution site energies than the diluent ZrN (with the possible exception of CmN).

Atomistic Modeling of Americium Using Ab Initio and Semi-Empirical Potentials. The elemental actinide metals exhibit several fascinating features connected to their electronic structure and they are among the most complex and least understood elements in nature.[18] The understanding of the basic electronic properties of the actinides and Am in particular is a serious challenge. In view of their potential for use in the next generation nuclear fuels, a fundamental understanding is necessary.

A major problem, especially for Am and the heavier actinides, is the limited amount of reliable experimental data. There is a paucity of even the basic data on defect formation and migration

[18] A. J. Freeman, G. H. Landers (Eds.), "Handbook on the Physics and Chemistry of the Actinides", North-Hollands, Amsterdam, 1984. {\it Challenges in Plutonium Science}, Los Alamos Sci., 26, 91 (2000).

energetics and phase stability of Am / Am-N systems that are of interest to this project. With the advancement of computer technology, modeling and simulation have emerged as an indispensable tool to bridge this gap in our experimental understanding. Pure theoretical considerations based on state-of-the-art ab initio electronic structure calculations are therefore most desirable. However, these calculations are computationally intensive and allow only a few hundreds of atoms in a system. On the other hand, semi-empirical many-body interatomic potentials such as the molecular embedded atom method (MEAM), based on the density functional theory, allow us to handle large systems with millions of atoms.[19] This is a powerful enhancement of the classical embedded atom method (EAM) and allows us to handle directional forces, important in actinides.[20] Furthermore, in order to extend a potential to model alloys such as Am-N, it would be convenient to describe the atomic interactions of the multitude of alloying elements using a common formalism.

Our ultimate goal for the Year 2003 is to develop a MEAM model for the Am-N system and compute the phase diagram for this system using the developed MEAM model. To achieve this, we first need to develop a MEAM model for pure Am. This requires a sufficiently large database of properties of a pure Am system. Because reliable experimental values of Am properties are lacking, we first used *ab initio* calculations to generate a database of many equilibrium properties of pure Am. This dataset will then be used to determine a reliable MEAM model for Am. Next, using the same approach, we will determine a MEAM model for the Am-N system.

As mentioned earlier, pure theoretical considerations based on state-of-the-art *ab initio* electronic structure calculations are very desirable. This is a difficult task due to the strong 5-f electron correlation in the actinides, especially the later actinides such as Am, where the 5-f electrons are believed to be localized. In the present study, we have incorporated the 5-f localization in Am via spin-exchange modeling, which, despite its unphysical long-range magnetic ordering, can be seen as an approximation describing the main features of energetics such as bulk modulus and equilibrium volume. In order to impose the exchange split and localization, an external magnetic field was applied. However, during the refining of the MEAM potential, we realized that this applied field led to a small shift in the total energy that was slightly different for the different structures. This did not affect properties like the elastic constants and equilibrium volumes, but it did make the comparison in total energy between the different crystal symmetries uncertain.

During the last quarter we corrected this systemic problem and the erroneous data was recalculated. This quarter we refined the MEAM model for Am using these corrected properties. Table-2.6.6 shows some of the properties of pure Am predicted by our model. Calculations of other properties of pure Am, first principles calculations of Am-N system, development of Am-N MEAM, and determining its phase diagram will be done during the remainder of this year.

For additional information on this topic, please contact Anders M. Niklasson at amn@lanl.gov.

[19] M.I. Baskes, Phys. Rev. B. 46, 2727 (1992); B-J. Lee and M.I. Baskes, Phys. Rev. B 62, 8564 (2000).
[20] M.I. Baskes, Phys. Rev. B, 62, 15532 (2000).

Table2.6.6 – Predicted properties of Am using MEAM. E_{vF} is vacancy formation energy, E_s is surface energy, and E_{IF} is interstitial formation energy.

Property	BCC	FCC	HCP
E_{VF}	1.36 eV	1.86 eV	1.87 eV
(100) E_S	--	2.29 J/m^2	--
(110) E_S	--	2.15 J/m^2	--
(111) E_S	--	1.50 J/m^2	--
(100) Dumbbell E_{IF}	--	1.62 eV	--
Octahedral E_{IF}	--	1.52 eV	--
Thermal Expansion	--	6.59e-6 /K	--

2.7 Series Two Metallic Fuel Development

The objective of the Metallic Fuel Development activities is to establish a metal alloy fuel option for transmutation in a Series-Two-type fast spectrum reactor or ADS. The metal fuel development activities involve fabrication and fabrication process development, characterization, and modeling. Non-fertile and Low-U compositions are being addressed, per the direction of the larger program.

Fabrication activities described in the five-year plan address two primary needs for the AFCI and Generation IV programs: (1) development of fabrication processes that can be deployed for large-scale transmutation fuel manufacturing, and (2) fabrication of specimens suitable for irradiation testing, characterization, and property measurement.

Characterization activities are intended to gather a working knowledge of the metal fuel alloy, and include studies of phase equilibria and melting temperatures, fuel/cladding interdiffusion behavior, and measurement of thermophysical properties.

Modeling activities will develop models and codes that predict fuel properties and behavior and collect property information into the AFCI Fuels Handbook.

2.7.1 Metallic Fuel Development Objective and Scope

Initial efforts, including those in FY 2003, are concentrated on providing small samples of metal fuels with well-characterized microstructures for irradiation testing. Experience gained in fabricating small samples will provide a basis for developing large-scale fuel manufacturing processes in subsequent years.

FY 2003 activities are narrowly focused on obtaining the information necessary for safety analysis of the AFC-1 and FUTURIX irradiation experiments. Specific objectives and milestones for FY 2003 are to complete fabrication of metallic fuel slugs (fertile and non-fertile fuel).

2.7.2 Metallic Fuel Development Highlights

The following are the major highlights of the fuel development activities:

- Test castings were performed on low fertile fuel composition U-35Pu-30Zr to verify the suitability of the arc-casting process for uranium-bearing transmutation fuels. Specimens suitable for examination and irradiation were produced.
- The guiding document for low-fertile metallic fuel fabrication "Fuel Test Specimen Specification for the AFC-1F Low-Fertile Fuel Capsule Irradiation in the ATR" (W7520-0527-ES-00) was written and submitted to the AFC NTD and DOE-HQ. This document details the composition, configuration, and acceptance criteria for metallic fuel specimens to be irradiated in the AFC-1F experiment capsule in the ATR.
- The Final Report on the microstructure analysis and phase equilibria of as-cast AFC1(b,d) samples was completed and submitted, fulfilling the March 17, 2003, deliverable of WBS 1.22.25.01.

- Two presentations on AFC1 (b, d) fuel characterization were given at the (TMS) annual meeting in March and one presentation on AFC1 (b, d) fuel characterization was given both at the AFCI FDWG meeting in February and the AFCI semi-annual technical review in January.
- Two (2) baseline background experiments, three (3) standard reference material experiments and nine (9) fuel sample experiments were performed with the thermo-mechanical analyzer (TMA). These preliminary results were compared with the previous DTA/DSC results. Phase equilibria were identified and no evidence of melting was observed except for a ternary Np sample, which gave inconclusive evidence and resulted in the removal of the composition from the AFC1 experiment.
- Six (6) diffusion couple samples were prepped for fuel-cladding chemical interaction (fcci) studies by grinding, squaring, polishing and interface binding with nine (9) 422 stainless-steel cladding samples (also ground, squared and polished).
- Six (6) diffusion couple fcci samples were heat treated, four (4) at 850ºC for 100 hours and 2 at 650ºC for 50 hours. These samples were subsequently prepped (cut, ground and polished) for and subjected to SEM investigation. SEM study showed 850ºC heat treatment resulted in complete diffusion of Fe/Cr throughout the fuel. The 650ºC heat treatment showed minimal diffusion, perhaps up to 10-20 microns of Fe/Cr in the fuel. The SEM study revealed no evidence of melting (contrary to apparent TMA studies on the ternary Np sample). The SEM study showed that the ternary Np sample, which came from the same casting sample as was used in the TMA study mentioned above, contained significant amounts of copper (Cu). These important observations resulted in a re-evaluation (which is ongoing) of the apparent ternary Np fuel melting behavior.
- A surrogate low-fertile metallic fuel casting of composition U-35Pu-30Zr (wt%) employing depleted uranium was performed. Samples from this casting will be sectioned for microstructure, phase and thermal analyses.

2.7.3 Metallic Fuel Development Technical Summary

The metallic fuel development is primarily performed at ANL-W. For additional information the readers are referred to Mitch Meyer at mitchell.meyer@anl.gov.

Test castings were completed on low fertile fuel composition U-35Pu-30Zr. Specimens suitable for examination and irradiation were produced, providing verification that the arc-casting method is suitable for fabrication of metallic low-fertile fuel specimens.

The TMA in the Fuel Manufacturing Facility (FMF) was brought online and tested. For this, two baseline background experiments and three standard reference material experiments were conducted. Nine fuel sample TMA experiments were performed: MA005TM1, MA005TM2, MB007TM1, MB007TM2, MB010TM1, MC017TM1, MD020TM1, ME027TM1, ME027TM2 (one or more experiments on each of the five compositions). Preliminary analysis on the results produced inconclusive evidence as to the melting behavior of the Pu-10Np-40Zr composition. This resulted in a decision to pull the composition from reactor testing. Due to the high sensitivity of the TMA instrument to the sample form, all of the samples were returned to the Analytical Laboratory for better preparation, which included stabilizing the saw blade used to cut samples from the as-cast fuel slug pins as well as squaring and polishing the samples. Because it

was discovered from the SEM studies that the MB007 cast contained significant amounts of copper, another 1 cm TMA sample (MB009TMA2) was cut and prepped from the MB009HTA1 cast sample. All these samples are awaiting transfer to the FMF for study.

Preliminary analysis results from the thermal analysis experiments are shown in Figs. 2.7.1 through 2.7.11 for the compositions Pu-40Zr (ME027, Figs.2.7.1 and 2.7.2), Pu-10Np-40Zr (MB007, Figs. 2.7.3, 2.7.4; MB010, Fig. 2.7.5), Pu-12Am-40Zr (MC017, Figs. 2.7.6 and 2.7.7), Pu-10Am-10Np-40Zr (MD020, Figs. 2.7.8 and 2.7.9) and Pu-60Zr (MA005, Figs. 2.7.10 and 2.7.11). The DTA experimental results from those samples that did not completely oxidize in earlier experiments are included for comparison. It can be seen that there is generally good correlation between the DTA/DSC and the TMA results. In Fig. 2.7.1, the contraction of the lattice during the β (fcc) to ε (bcc) transition in Pu-40Zr is clearly observed. The sample, after two heat treatments to 925ºC, is shown in Fig. 2.7.2. The sample shape is unchanged from the original shape, yet shows decidedly why the samples were returned for better experiment preparation, considering the sensitivity of the instrument.

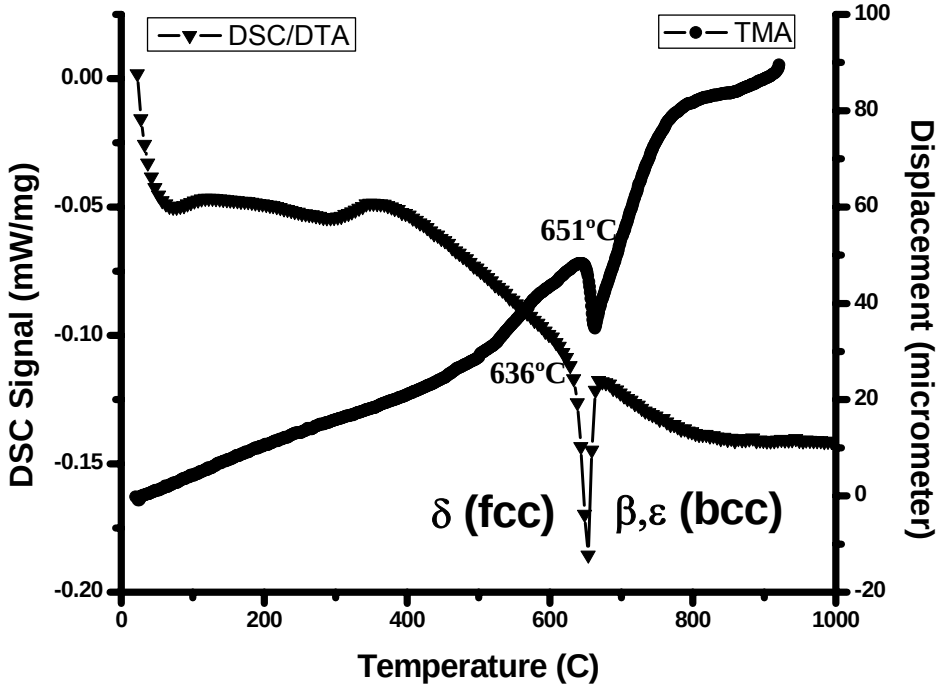

Fig. 2.7.1 – Thermal analysis heating plots for Pu-40Zr as-cast alloy.

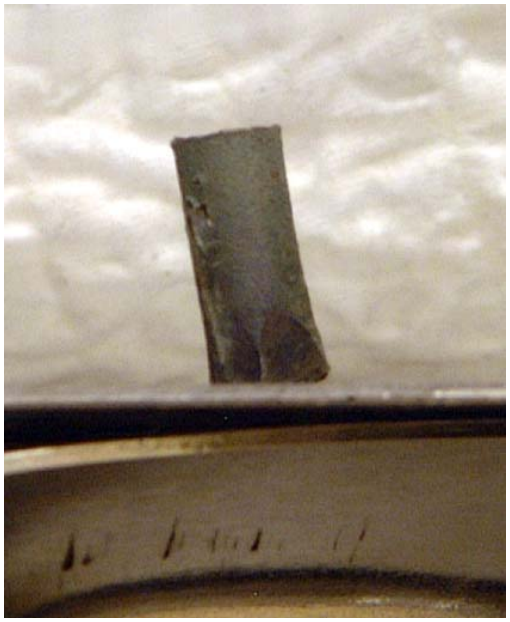

Fig. 2.7.2 – Pu-40Zr TMA sample following two heat treatments to 925ºC. Shape is unchanged from original.

Figure 2.7.3 shows the TMA plot from the initial heating run on the as-cast Pu-10Np-40Zr alloy that had been inadvertently contaminated with copper. X-ray diffraction had shown the (uncontaminated) as-cast alloy to consist of an fcc phase and an MZr_2 phase. Most prominent to be observed is the transition to a larger positive expansion coefficient at about 746ºC, which may correspond to the formation of a bcc structure. Other minor features possibly corresponding to phase transitions related to the fcc phase and the MZr_2 phase can be identified but are too weak for positive identification. A fresh sample is being prepared for additional analysis. The DTA/DSC sample completely oxidized during data collection and is not shown.

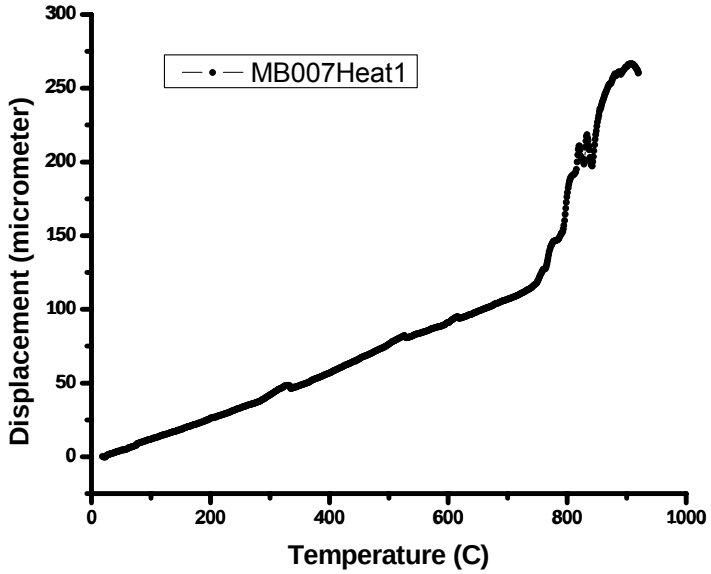

Fig. 2.7.3 – TMA heating curve for Pu-10Np-40Zr (contaminated with copper).

Figure 2.7.4 shows the TMA sample after heat treatment to 925ºC. Compared to all other TMA samples, this sample exhibits some drastic change in shape and, for this reason, the Pu-10Np-40Zr composition was excluded from irradiation testing. SEM studies showed this casting sample to have contained significant amounts of copper. Figure 2.7.5 shows a picture of a post TMA heated sample that was cut from a Pu-10Np-40Zr casting that was not inadvertently contaminated with copper from fusion with the arc-melter hearth. Although the sample is only about one quarter the size of the typical TMA samples and the signals obtained are too weak to draw conclusions from, it is clear to see in Fig. 2.7.5 that no change in shape occurred. Despite this, and because the copper contamination issue was not yet realized, the conservative decision to pull the ternary Pu-Np-Zr composition from the ATR experiment was made. Fresh samples have been prepared to confirm that this ternary phase does not exhibit melting behavior at reactor temperatures.

Fig.2.7.4 – Pu-10Np-40Zr TMA sample following two heat treatments to 925ºC. Sample was cut from a cast that had significant contamination with copper.

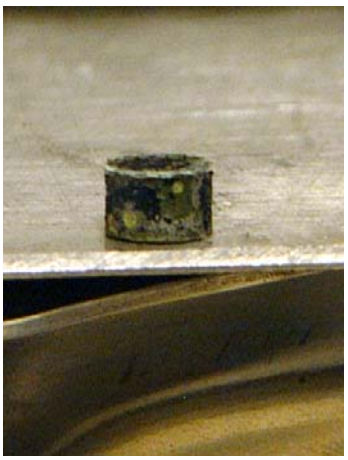

Fig. 2.7.5 – Post heating picture of a 0.25 cm Pu-10Np-40Zr TMA sample from a cast that did not have copper contamination.

Figure2.7.6 shows the thermal analysis heating curves for the Pu-12Am-40Zr as-cast alloy. The room temperature alloy was shown to consist of only the fcc phase (δ-Pu stabilized structure) and its transition to a bcc phase is clearly observed at about 710ºC, which is about 70ºC higher than the Pu-40Zr binary system. Figure 2.7.7 shows the TMA sample after heat treatment to 925ºC. No change in shape or dimension from the fresh cut sample is observed.

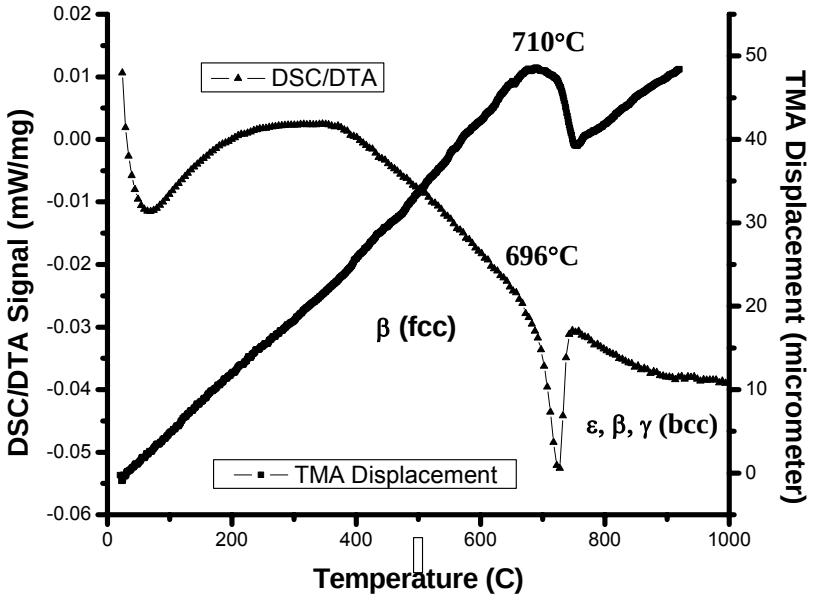

Fig. 2.7.6 – Thermal analysis heating plots for Pu-12Am-40Zr as-cast alloy

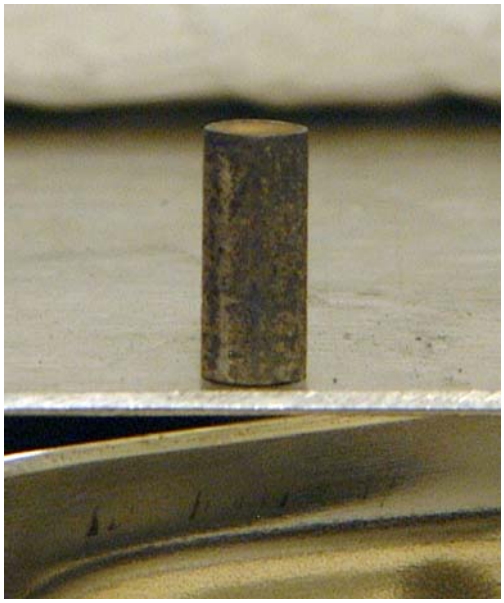

Fig. 2.7.7 – Pu-12Am-40Zr TMA sample after heat treatment to 925ºC.

Figure 2.7.8 reproduces the thermal analysis heating curves for the quaternary Pu-10Np-10Am-40Zr as-cast alloy that XRD analysis showed was composed of an fcc phase and an MZr_2 phase. A transition at 510ºC-540ºC related to the MZr2 phase is observed (most prominently in the DTA/DSC experiment). The DTA/DSC curve shows a second broad feature at about 611ºC, which in the TMA may result from two transitions at 592ºC and 643ºC. The former could relate to the MZr_2 phase and the latter the fcc phase and the formation of a bcc phase. The picture in Fig. 2.7.9 shows that the heat treatment to 925ºC did not alter the shape or dimension of the quaternary composition TMA sample.

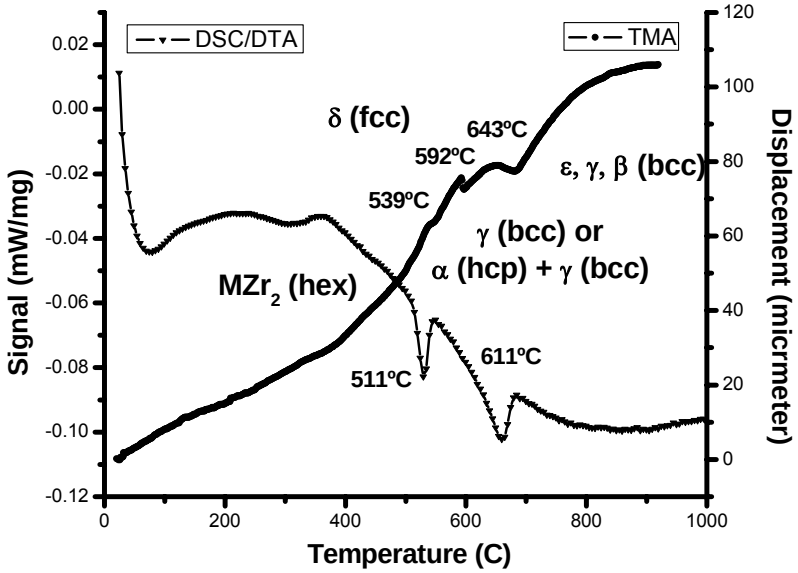

Fig.2.7.8 – Thermal analysis heating plots for Pu-10Np-10Am-40Zr as-cast alloy.

Fig. 2.7.9 – Pu-10Am-10Np-40Zr TMA sample after heat treatment to 925ºC.

Finally, Fig. 2.7.10 shows the thermal analysis plots for the Pu-60Zr as-cast alloy. The thermal behavior can be accounted for mostly from the published phase diagrams except for the prominent transition at 533ºC, which may be an artifact of a thermal gradient in the furnace. The heat treatment did not affect the appearance of the TMA sample (Fig. 2.7.11). Further and repeated analyses are continuing on these samples to more fully understand the thermal characteristics of these alloys.

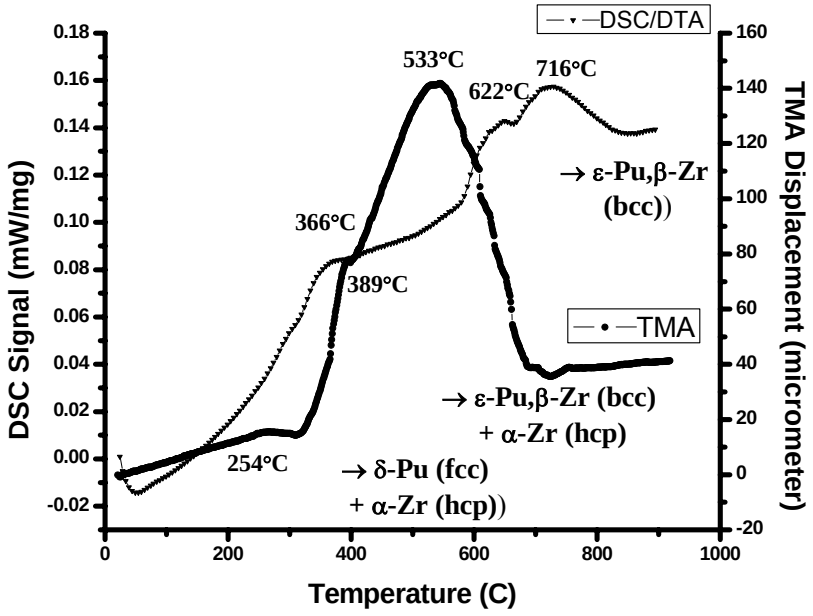

Fig. 2.7.10 – Thermal analysis heating plots for Pu-60Zr as-cast alloy.

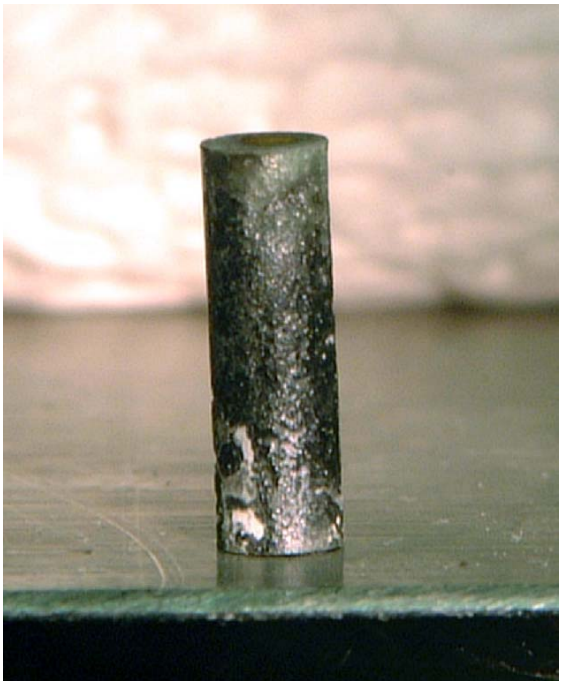

Fig. 2.7.11 – Pu-60Zr TMA sample following heat treatment to 925ºC.

The representative preliminary results from the fuel-cladding chemical interaction (fcci) studies are shown in Figs. 2.7.12 and 2.7.13.

Figure2.7.12 shows the SEM backscattered electron image of a Pu-40Zr sample coupled to 422 stainless steel that has been heated to 862ºC for 100 hours. This temperature represents the approximate maximum nominal centerline fuel temperature. As can be seen, deposits of iron from the steel can be observed throughout the fuel sample. Such a result at this temperature is not unexpected and has been seen in fcci studies in EBRII fuels.

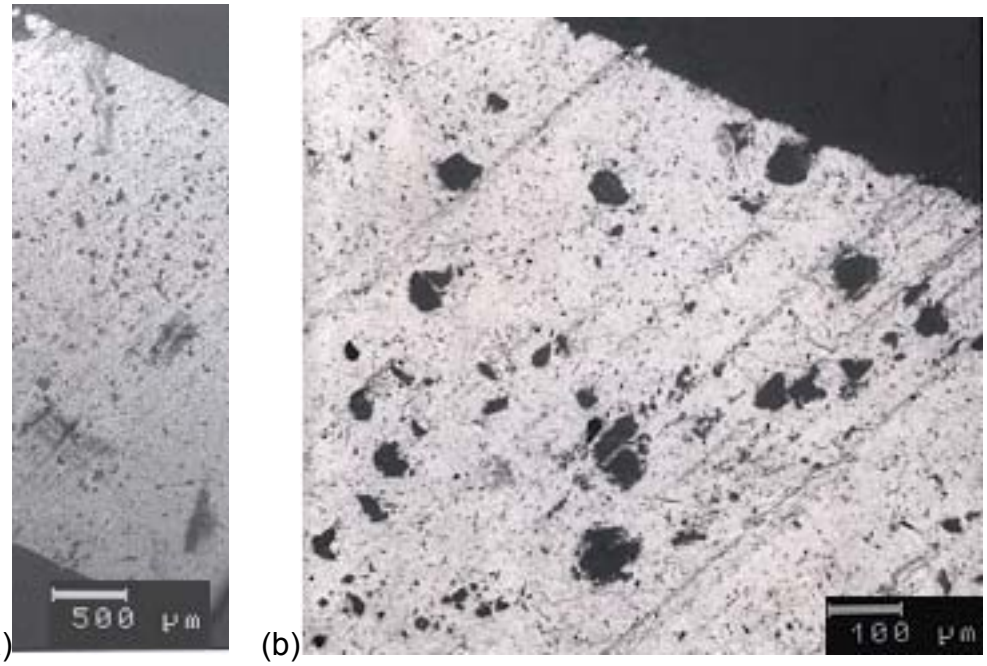

Fig. 2.7.12 – Backscattered electron micrographs of the Pu-40Zr/steel couple annealed at 862˚C for 100 hours. The dark-contrast area is the steel and the brighter-contrast area is the fuel. Dark-contrast, globular phases were observed throughout the fuel as shown in (a) and (b). Some porosity is present in the fuel. Identical phases were observed in the Pu-40Zr-10Np-10Am/steel and Pu-40Zr-12Am/steel diffusion couples annealed at the same temperature and length of time. (b) is a higher magnification image of the Pu-60Zr/steel interface. EDS analysis of the globular phases showed that they were mostly Fe-rich. Some of the phases were Zr-rich. No actinides were observed in these phases.

Figure 2.7.13 shows a representative SEM micrograph of a Pu-60Zr/422 stainless-steel interface heated to 650ºC for 50 hours. This temperature represents the maximum fuel cladding temperature and is the temperature of interest for the ATR experiment. Minimal interaction is observed with iron deposits found only within 10-20 microns of the diffusion couple interface. These deposits are similar in composition to those found in the 850ºC annealed samples.

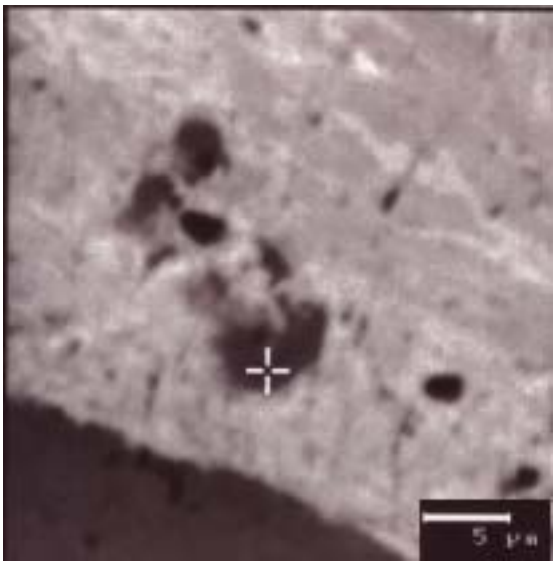

Fig. 2.7.13 – Backscattered electron micrograph of the MA003 Pu-60Zr/steel couple annealed at 650˚C for 50 hours. The steel is the darker region at the bottom, and the brighter region is the fuel. Fe-rich phases were observed around 10 microns into the fuel. An Fe-rich phase is marked in the figure; this phase did not contain any Pu. Some of the darker areas in the fuel are pores.

2.8 Series Two TRISO Fuel Development

Advanced TRISO fuels can be used in gas-cooled systems. They are of interest for deep burn applications, especially for fuels containing plutonium. Inclusion of minor actinides in this fuel type may also have practical transmutation implications if used in gas-cooled epithermal or fast reactors, which are being considered as part of the transmutation strategy in Series Two. TRISO fuel particles are also of interest for the Very High Temperature Gas-Cooled reactors (VHTGR).

Zirconium carbide-based coating systems have the potential for operation at higher temperatures and for more effective retention of silver and palladium fission products. These characteristics make ZrC of interest to both the VHTR and to transmutation fuels with Pu and other transuranic elements in the kernel. Titanium nitride coating systems have potential application to gas-cooled fast-spectrum reactors, and may have applications to the VHTR and transmutation systems. Advanced kernel chemistries such as oxycarbides and carbides offer potential performance advantages while high-density nitride and oxide kernel formulations are of interest to fast spectrum gas–cooled reactors. Irradiation testing of advanced TRISO fuels will provide scoping evaluations of the irradiated performance of advanced coating/kernel uranium fuels with testing for fission product release at temperatures above 1600˚C in existing fuel testing apparati. Advanced coated particles will be fabricated, compacted, and shipped to INEEL for irradiation in ATR (AFC-2). TRISO-coated particles with kernels containing Pu and Np, and no U, are of interest for fast-spectrum, gas-cooled reactors and for deep-burn transmutation designs of thermal gas-cooled reactors. Such coated particles have never been fabricated nor characterized and may require dimensional modifications to the kernel, the buffer layer, and the coating layers for optimal performance. This series of activities would establish kernel fabrication and coating equipment in a plutonium glovebox facility, develop and demonstrate the chemistry of the gelation process for Pu/Np kernel fabrication, design and fabricate Pu/Np fuel (with either advanced or standard coatings systems), and perform out-of-core characterization and testing of the fuel by 2007.

The major milestone is to develop a performance package by FY 2007 to support the technology selection. Intermediate milestones include:

Start the Pu kernel development.	FY 2005
Start the fuel irradiation tests.	FY 2005
Perform out-of-core characterization and testing of fuel (AFC-2)	FY 2007

2.8.1 Series Two TRISO Fuel Development Objective and Scope

In FY 2003, development of kernel fabrication and advanced coating technologies will continue. As part of the kernel fabrication task, uranium oxide kernel fabrication will be performed in support of research tasks on advanced coating and advanced characterization methods. The evaluation and testing of the advanced kernel fabrication methods include (a) microwave methods that eliminate the use of solvents, and (b) materials to produce oxy-carbide, carbide and nitride kernels for evaluation as candidates for Generation IV reactors.

For coating technologies, this activity includes completion of a coating laboratory at ORNL, and fabrication of uranium oxide particles for use as a reference fuel for quality control (QC) and

characterization studies. These particles will also be used for defining reference coating conditions for dense kernels. The FY 2003 scope also includes the installation of auxiliary equipment and development of process techniques for applying advanced coating zirconium carbide titanium nitride (ZrC, TiN) in existing labs with existing coatings.

The above fabrication tasks are performed primarily by ORNL. In addition, General Atomics (GA) will support the TRISO fuel work by preparing a test specifications document for the initial irradiation of coated TRISO fuels and developing ZrC coatings. GA will continue the technology transfer for fuel design and fabrication to ORNL.

The major FY 2003 milestones include:

- Fabrication of 1 kg of UO_2 kernels,
- Fabrication of 100 g of UO_2 particles with reference coating,
- Fabrication of coated particles with advanced coating system,
- Design methods, analyses and test specifications for the TRISO fuel,
- Fabrication of advanced oxycarbide, carbide and nitride kernels,
- Characterization for Series Two advanced coatings, and
- Formulation of an accident evaluation model.

2.8.2 Series Two TRISO Fuel Development Highlights

The following are the major second-quarter highlights for the Series Two TRISO fuel development activities:

- TRISO fuel development and the VHTR fuel program were reviewed during the 2nd FDWG meeting through three presentations provided by ORNL, GA, and INEEL.
- Because of the reduced AFCI budget, the TRISO fuel research performed under AFCI was delayed until FY04.

2.8.3 Series Two TRISO Fuel Development Technical Summary

There are no detailed technical highlights in the second quarter. This section will be removed from the 3rd and 4th quarterly reports in FY03.

2.9 Series Two Advanced Fuel Forms

Fuel forms will be assessed and feasibility studies will be conducted for the most promising candidates. Dispersion fuels of several metallic and ceramic matrix materials and a few solid solution materials will be evaluated. The goal is to narrow the list of candidates to two and perform initial scoping studies by the end of FY 2003.

Subsequent efforts will be focused on a few selected forms and will require some initial scoping tests. Special tests may be designed and fuel samples may be included in the AFC-1 through AFC-5 test series discussed previously. The development of advanced fuel concepts will be performed in collaboration with international partners. U.S. efforts in selected fuel forms will likely complement and supplement similar international efforts in order to maximize the benefits of mutual research and reduce the development time period.

As Generation IV fuel development needs are defined, they will be developed within the framework for this activity.

The major milestones for this activity include:

Develop advanced fuels testing plan.	FY 2004
Identify and develop (to the point of proof-of-principle) high-risk but large payback innovative fuel concepts.	FY 2007

2.9.1 Series Two Advanced Fuel Form Development Objectives and Scope

Work under this activity includes an assessment of innovative fuel forms, which hold the potential for increased efficiency and reduced overall cost in processing, transmutation, and recovery.

For the case of micro-structured fuels, a more detailed assessment will be performed. This task will investigate fuels manufactured to contain micron-sized fissile material structures (e.g., spheres or cylinders) spaced uniformly in matrix materials. Such structures will allow most fission product fragments to escape from the fissile material and come to rest in the matrix material. After a period of irradiation, separation of the fissile material from the matrix containing the embedded fission products will allow an efficient partitioning of the bulk of the fissile material from the fission products. The fissile material can then be reused by incorporating it into new micro-structured fuel. Efficient separation of the fissile materials from the fission products using this technology could greatly reduce costs for an advanced fuel cycle as compared to aqueous or pyrochemical separation methods.

2.9.2 Series Two Advanced Fuel Form Development Highlights

In the second quarter work on micro-structured fuel development continued while DOE's patent application is pending.

2.9.3 Series Two Advanced Fuel Form Development Technical Summary

Due to the pursuit of a DOE patent on this work, technical disclosure will be unavailable. Any inquiries on this topic must be directed to Gordon Jarvinen at gjarvinen@lanl.gov or Ken Chidester at kchidester@lanl.gov.

2.10 Series Two ATR Irradiation Experiments

With the exception of TRISO fuel (which has applications in deep burn epithermal gas cooled reactors), all other Series Two transmutation fuel types are developed for fast-spectrum systems. At present, the U.S. emphasis is on metal and nitride fuels that are either fertile-free or with low-fertile content. Because there is no fast-spectrum irradiation capability in the U.S., initial screening tests for these fuels will be performed in thermal reactors (ATR). Such thermal spectrum irradiation will provide some initial data for fuel behavior and is also a pre-requisite for subsequent fast-spectrum irradiation.

2.10.1 Series Two ATR Irradiation Experiments Objectives and Scope

Tests of metal and nitride fuels (in ATR) are required in order to assess fuel performance. Series Two fuels for Generation IV transmutation applications will be subject to high burnup irradiation testing to assess their transmutation potential. Developing a database of irradiation behavior is therefore the key component of the near–term fuel development program. Irradiation performance data will be combined with physical, thermal, and chemical property data to develop models leading to better understanding of the complex behaviors of these fuels.

The AFC-1 test series will include samples of metal and nitride fuels containing plutonium, americium, and neptunium. Uranium contents in the test fuels will reflect the range of uranium contents being considered for different transmutation scenarios. This initial series of screening tests will provide initial fuel behavior information and identify potential life-limiting phenomena to be addressed with further design and performance assessment. The Series Two tests are expected to continue through FY 2007 as additional fuel design parameters and compositions and notable performance phenomena are evaluated. It is likely that some of the AFC-1 test capsules will be irradiated to provide irradiated test samples for later safety-related transient testing. The specific FY03 milestones are given below:

Complete fabrication of fuel capsules for AFC-1 (a-d) tests (non-fertile metallic and nitride fuel).	March 2003
Initiate AFC-1 irradiation test in ATR.	April 2003
Complete fabrication of fuel capsules for AFC-1 (e-f) tests (fertile metallic and nitride fuel).	September 2003
Complete safety documentation and approval for the AFC-1 (e&f) tests	September 2003

2.10.2 Series Two ATR Irradiation Experiments Highlights

The following are the major highlights for the Series Two ATR irradiation experiments:

- All required QA inspections and tests for metallic fueled rodlets were completed early this quarter.
- Review of LANL's QA plan for AFC-1A and AFC-1C nitride pellet fabrication was completed.

- Nitride fuel pellets were loaded into cladding tubes, however, many of the pellets were broken on receipt at ANL-W. After encapsulation into rodlet specimens, many more pellets broke during routine handling for inspection and radiography. The cause of these fractures appears to be defects introduced during fuel fabrication.
- The cadmium basket drawing for the Advanced Test Reactor Critical (ATRC) facility was approved and released by INEEL. The eight cadmium baskets needed for ATRC physics testing were fabricated by ANL-W.
- The Post-Irradiation Examination Plan for AFC-1 (A-D) was issued by ANL-W.
- Draft AFC-1E&F Experiment Description was issued for evaluation by ANL-W.
- All necessary approvals were received and paperwork was prepared for the ATRC tests by INEEL to start on April 7, 2003.
- Approval of the Environmental Checklist for the AFC-1 EFT baskets was obtained in March by INEEL, along with an approved, identified waste stream for the un-irradiated and irradiated cadmium baskets.
- A drawing for the AFC-1 experiment storage grid in the ATR canal was completed and approved with fabrication to begin in early April. Transportation will be accomplished in a single shipment of all six test assemblies. The assemblies will be loaded in the ATR Canal and sent directly to ANL-W using the GE-2000 cask.

2.10.3 Series Two ATR Irradiation Experiments Technical summary

The technical summary for the Series Two fuel irradiation experiments activities in the first quarter are provided for the following sub-tasks:

- Nitride Fuel Rodlets,
- Cadmium Basket Fabrication,
- AFC-1 A-D Experiment Description,
- The Post- Irradiation Examination (PIE) Plan,
- AFC-1 (E-F) Irradiation Tests of Low-Fertile Fuels,
- ATRC Tests, and
- Analyses and documentation.

Nitride Fuel Rodlets. Nitride fuel pellets supplied by LANL were encapsulated into HT-9 clad rodlets. The rodlets were shipped to ANL-W in welded steel tubes with retaining springs. On opening the welded steel shipping containers, several pellets were broken with features of the break characteristic of end-capping defects introduced during pellet fabrication. Two photographs of typical and extreme breakage of the pellets are shown in Fig.2.10.1.

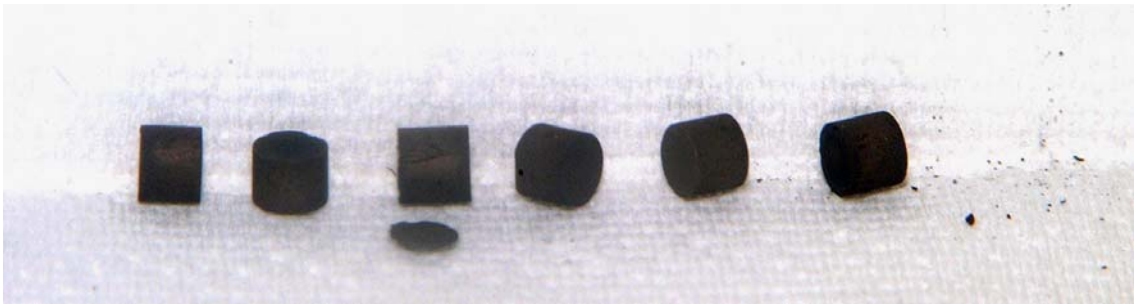

(a)

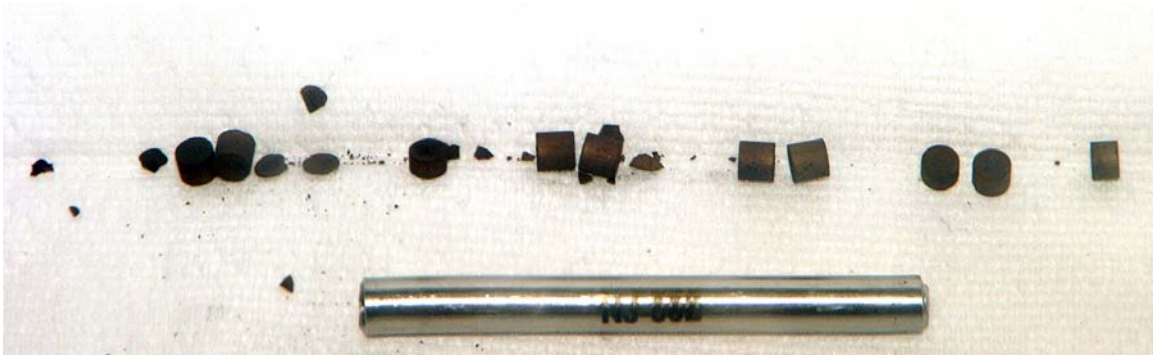

(b)

Fig. 2.10.1 – Photographs of broken nitride fuel pellets after removal from shipping package. (a) Pellets from container NN001 (Pu0.5,Am0.5)N-36ZrN. (b) Pellets from container NJ002 (Pu0.8, Am0.2)N-36ZrN.

After consultation with R. Margevicius and K. McClellan (LANL), these pellets were replaced with archive material where possible. Top end plugs were welded onto the rodlets. During top end plug weld radiography at the Fuel Manufacturing Facility (FMF), it was noted that fuel debris and other defects were visible in several rodlet radiographs. Because these radiographs were focused on only the top rodlet weld, not all of the pellets were visible; however, more than one-half of the pellets visible on the radiographs were broken, chipped, cracked, or contained internal end-cap defects. Typical radiographic images are shown in Fig. 2.10.2.

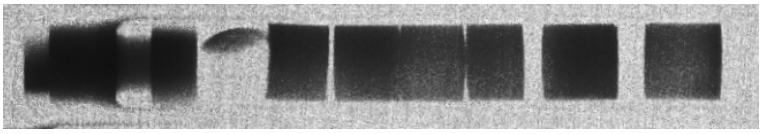

(a)

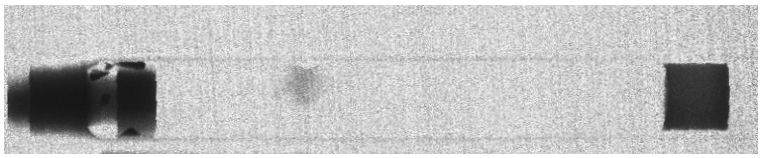

(b)

Fig.2.10.2 – X-ray radiographic images of broken pellets inside welded cladding tubes. (a) Rodlet NM-2AA ((Pu0.5,Am0.25,Np0.25)N-36ZrN) showing manifestation of end-cap defect as separation of pellet. (b) Rodlet NJ-2AB ((Pu0.8,Am0.2)N-36ZrN) showing debris in upper left hand corner of top end plug area.

Additional follow-up radiographic examination was performed focusing on the fuel pellets. Due to the high gamma field from the fuel specimens with high Am content, radiographic details on all of the pellets are not visible. A summary of the types and number of defects are given in Fig. 2.10.3 and Table 2.10.1, respectively. Some pellets show more than one defect, such as capping on both ends. Rodlets in which debris is present always contain a 'dish-out' type defect in which the end-cap has disintegrated or a loose 'chip' of material. Radiography parameters will be refined to allow imaging of the remaining high-Am pellets.

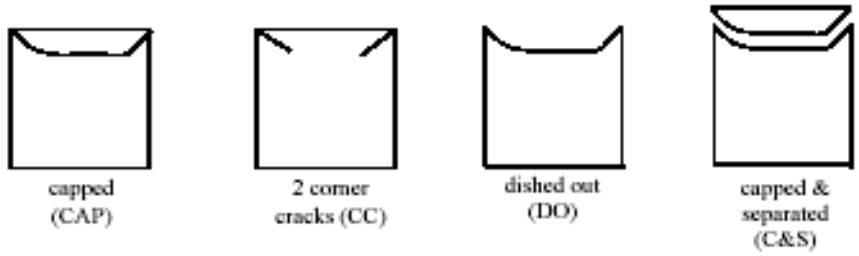

Fig.2.10.3 – Major categories of defects visible in radiographic images of clad nitride pellets. Not shown are chips, which are manifested as material missing on corners.

Table 2.10.1. Number of each class of defect present in nitride fuel pellets*

Defect Type	Rodlet							
	NJ-2AA	NJ-2AB	NK-1AA	NK-2AA	NL-1AA	NL-2AA	NM-1AA	NM-2AA
none	7	2	1	4	1	-	2	3
CAP	-	4	9	7	1	1	2	2
CC	1	1	-	-	3	2	4	1
DO	3	1	-	1	-	-	1	4
C&S	-	-	7	-	-	-	1	1
CHIP	1	-	1	1	-	1	2	1
debris	yes	yes	yes	no	no	no	yes	yes
Nominal Comp	(Pu0.8,Am0.2)N-36ZrN		(Pu0.5,Np0.5)N-36ZrN		PuN-36ZrN		(Pu0.5,Am0.25,Np0.25)N-36ZrN	
Total	12	7	12	12	5	4	10	9

*Note: some pellets contain multiple defects. In thee cases, total defects tabulated are greater than number of pellets.

For additional information on this topic, please contact Steve Hayes at steven.hayes@anl.gov.

Cadmium Basket Fabrication. The initial concept for hardening the neutron spectrum was to use a basket design based on borated aluminum. The plan was to extrude tubes of borated aluminum to the required inside/outside diameter from billets prepared to specification.

Initial extrusion attempts proved unsuccessful because the borated aluminum billet was harder and more brittle than expected, which caused the specially-devised extrusion mandrel to break. Accordingly, the plan was modified to extrude the billets into rods of specified outside diameter for the basket and then drill the rods. Due to pre-cutting of the aluminum billet to a size needed to produce the required extruded tube length, the extruded rods were shorter. Thus, aluminum extensions had to be welded to the borated aluminum rod to meet the required length. Drilling a test piece of borated aluminum rod with a special bit yielded the desired results, however test welds to secure the aluminum extensions to the borated aluminum rods were unsuccessful.

Test welding of the 6092 borated aluminum (annealed and non-annealed) tubes to 6061-T6 aluminum tubes was performed using the GTAW process with different amperage & voltage values, purge values, different filler materials, and other techniques. Due to the materials' inability to flow and its extreme brittleness and porosity, the joints were not able to meet the mechanical strength or soundness requirements of the RDT-F6-2. This test demonstrated that welding of this particular material is not feasible. Consequently, drilling of the borated aluminum rods was discontinued and all basket fabrication efforts were shifted to the cadmium blanket design.

The full extent of fabrication difficulties with borated aluminum were not foreseen in the early stages of the project. As difficulties were encountered, it became clear that it would be necessary to reschedule reactor insertion to May while data could be developed and the alternative cadmium basket design could be fabricated.

Initial design efforts for the cadmium basket commenced in January and were based on preliminary thermal and physics analyses performed by INEEL. Fabrication costs and schedules were obtained from ANL-W. To qualify ANL-W as an INEEL-approved fabricator/vendor, the ANL-W Quality Assurance Program was reviewed and approved. Accordingly, a contract for fabrication of the ATRC baskets was prepared and approved with a scheduled release date in the first week of March.

The first cadmium basket was successfully fabricated by the ANL-W machine shop approximately one week ahead of schedule, demonstrating feasibility for production of the revised basket design. INEEL established a contract with ANL-W to produce 8 cadmium baskets for use in the ATRC reactivity measurements; these baskets were fabricated and awaiting pick-up by INEEL staff at the close of the quarter. Preparations then began for fabrication of baskets needed for the actual experiments that will be inserted into the ATR in May.

An outstanding issue relative to the selection of the cadmium baskets for production is the waste disposition path of the irradiated baskets, which will be mixed hazardous waste. INEEL has been investigating disposal of the irradiated baskets at EnviroCare in Utah; but initial calculations indicate that a storage period of possibly several years (perhaps even longer) to allow for the decay of Cd-113m might be required to meet the EnviroCare waste acceptance criteria. Discussions were initiated with the management of ANL's Radioactive Scrap and Waste Facility (RSWF), a facility permitted to store mixed hazardous waste, regarding the possibility of storing the irradiated cadmium baskets there. Such an approach seems sensible because the baskets will likely need to go to ANL-W along with the fueled capsules in order for the cadmium depletion to be determined by analytical chemistry to validate the INEEL's rodlet power calculations during irradiation.

For additional information on this topic, please contact Steve Hayes at steven.hayes@anl.gov or Richard Ambrosek rga@inel.gov.

AFC-1 A-D Experiment Description. The AFC-1A, -1B, -1C & -1D Final Experiment Description and Design & Data Package (Rev. 2) were issued. The revision included two major changes: 1) the fuel rodlet powers used in the thermal analyses were changed to reflect the values that will result from using the cadmium rather than the borated-aluminum baskets (though the final decision on basket selection has not been made, the cadmium baskets have been designated the reference by the INEEL), and 2) the Pu-10Np-40Zr composition (previously Rodlet 5) was removed from both the AFC-1B and -1D experiments. Recent thermal analysis experiments give indications that a liquid phase may form in the Pu-10Np-40Zr alloy at temperatures below 900°C. Because 900°C is the steady-state temperature limit for the metallic fuels in the AFC-1B and -1D tests, and the safety case was developed under the assumptions of no fuel melting up to that limit, the Pu-10Np-40Zr composition had to be eliminated. This alloy was being tested only to obtain fundamental alloy irradiation performance information, specifically attempting to separate effects due to Am and Np, and it is not a composition of interest as a real transmutation fuel. The Pu-10Am-10Np-40Zr alloy gave no indications of liquid phase formation up to 900°C in similar thermal analysis experiments and will remain in the test matrix. With the elimination of Rodlet 5 from AFC-1B and -1D, the Pu-60Zr fuel in Rodlet 6 was moved to the Rodlet 5 position and Rodlet 6 will be replaced with a non-fueled dummy rodlet. The revised test matrix is shown in Table 2.10.2.

For additional information on this topic, please contact Steve Hayes at steven.hayes@anl.gov or Richard Ambrosek rga@inel.gov.

Table 2.10.2 – Revised AFC-1A, -1B, -1C & -1D Test Matrix.

Rodlet	Fuel Test Matrix	
	AFC-1A & -1C	**AFC-1B & -1D**
1	$(Pu_{0.20},Am_{0.80})N$-36ZrN	Pu-12Am-40Zr
2	$(Pu_{0.80},Am_{0.20})N$-36ZrN	Pu-10Am-10Np-40Zr
3	$(Pu_{0.50},Np_{0.50})N$-36ZrN	Pu-40Zr
4	PuN-36ZrN	Pu-12Am-40Zr
5	$(Pu_{0.50},Am_{0.25},Np_{0.25})N$-36ZrN	Pu-60Zr
6	$(Pu_{0.50},Am_{0.50})N$-36ZrN	DUMMY

The Post- Irradiation Examination (PIE) Plan. The PIE plan for AFC-1 (A-D) issued in January was presented to the AFCI Fuel Development Working Group in February and a consensus was reached on the plan as presented. The working group and the DOE fuels manager were briefed on the delay in the receipt of the AFC-1A and -1B capsules at HFEF that will be caused by deferring this year's funding and workscope for hot cell preparation for the first-time receipt of the GE-2000 cask; this delay was acknowledged but, because no impact to the FUTURIX schedule will result from the delay, it is deemed acceptable.

ANL-W completed the evaluation of LANL AFCI Fuel Development Quality Assurance Program. The initial findings and status of the evaluation were reported in two ANL memoranda during the first quarter. In these memoranda, ANL provided detailed comments and specific suggestions for the resolution of the deficiencies. The final conclusions of the evaluation were issued in an ANL Inter-Laboratory Memorandum to D. Crawford, ANL-W AFCI Program Management Representative, and distributed to the LANL technical staff, National Technical Director for AFCI Fuel Development, and DOE-HQ manager. Based on the review, ANL-W determined that LANL is an approved supplier of nitride fuel and that pellets fabricated according to the reviewed procedures should satisfy all requirements specified in ANL-W Document W7520-0473-ES-01, Fuel Test Specification for the ATW-1A-ATW-1D Capsule Irradiations in the ATR.

For additional information on this topic, please contact Steve Hayes at steven.hayes@anl.gov.

AFC-1(E-F) Irradiation Tests of Low-Fertile Fuels. The Draft Experiment Description of AFC-1E and AFC-1F was completed and distributed in March. The experiment description incorporated the results of the initial physics calculations. The experiments may be further revised based on technical and programmatic input.

The fuel compositions and positions of the nitride fueled rodlets in AFC-1E and of the metallic fueled rodlets in AFC-1F are shown in Table 2.10.3. Note that the metallic alloy compositions are expressed in weight percentage, and the nitride fuel compositions are expressed in mole percentage for transuranic content and in weight percentage for the zirconium-nitride content.

Table 2.10.3 – AFC-1E and -1F Fuel Test Matrix.

Rodlet	Fuel Test Matrix	
	AFC-1E	**AFC-1F †**
1	PuN-36ZrN	U-29Pu-4Am-2Np-30Zr
2	$(U_{0.5},Pu_{0.25},Am_{0.25})N$ *	U-34Pu-4Am-2Np-20Zr
3	$(U_{0.5},Pu_{0.4},Am_{0.1})N$-30ZrN	U-25Pu-3Am-2Np-40Zr
4	$(U_{0.5},Pu_{0.25},Am_{0.15},Np_{0.10})N$	U-29Pu-4Am-2Np-30Zr
5	$(U_{0.5},Pu_{0.25},Am_{0.25})N$	U-28Pu-7Am-30Zr
6	$(U_{0.5},Pu_{0.5})N$-30ZrN	U-25Pu-3Am-2Np-40Zr

†Alloy composition expressed in weight percent.
*Homogeneous nitride with same composition as Rodlet 5, but nitride formed from oxide solid solution.

The compositions were selected to accomplish two objectives: 1) Provide the requisite irradiation performance data on the fuel compositions that are proposed for irradiation in the FUTURIX experiment, and 2) Investigate effects of variable materials parameters within the range of design values. The fertile, actinide-bearing compositions of AFC-1E an AFC-1F have all been designed with a uranium-to-transuranic (i.e., plutonium, neptunium, and americium) ratio of 1:1. This

ratio ensures that the neutronic characteristics of the fuels are consistent with stable operation in a reactor system. At this constant U-TRU ratio, the higher actinide content is varied to test compositions predicted for different transmutation deployment scenarios. The zirconium content is considered an alloying parameter in the low-fertile nitride and metallic fuels. In the non-fertile compositions, zirconium was added as a diluent, which is not necessary in the fertile fuels. In the low-fertile nitride fuels, zirconium is added to provide a direct comparison with analogous non-fertile nitride compositions. Zirconium is varied in the metallic fuels to investigate the dependence of material properties and irradiation stability.

Four metal fuel compositions were identified for irradiation testing in the AFC-1F Experiment. The compositions are U-29Pu-4Am-2Np-30Zr, U-25Pu-3Am-2Np-40Zr, U-34Pu-4Am-2Np-20Zr, and U-28Pu-7Am-30Zr. A meeting was held at INEEL on March 20, 2003, to discuss the AFC-1E low-fertile, nitride fuel compositions. In attendance were S. Hayes and B. Hilton (ANL), R. Margevicius and M. James (LANL), and R. Ambrosek, G. Chang, and D. Utterbeck (INEEL). Five nitride fuel compositions were agreed upon. The compositions are PuN-36ZrN, $(U_{0.5},Pu_{0.4},Am_{0.1})$N-30ZrN, $(U_{0.5},Pu_{0.25}, Am_{0.15}, Np_{0.10})$N, $(U_{0.5},Pu_{0.5})$N-30ZrN, and $(U_{0.5},Pu_{0.25},Am_{0.25})$N.

The AFC-1 (E-F) experiments will use the same irradiation test assembly design as the AFC-1(A-D) experiments. The irradiation test assembly consists of the experiment basket and the capsule assembly, which contains six rodlet assemblies stacked vertically. The experiment basket of the test assembly is designed to interface the capsule assembly with the ATR and to act as a thermal neutron flux filter. The current basket design is an aluminum sheathed cadmium tube. The aluminum sheath accommodates a cadmium tube thickness between 0.021 and 0.045 in. For the AFC-1E and -1F experiments, it is proposed that the Cd thickness be the same as for the AFC-1A, -1B, -1C and -1D experiments design, which is 0.045 in. The decrease in the thermal neutron flux will have a commensurate reduction in the linear power, which is necessary to satisfy the experiment design conditions.

The design objective for these experiments is to have a peak linear heat generation rate (LHGR) of 30.0 kW/m; however the LHGR limit for the nitride experiment AFC-1E is set higher at 35.0 kW/m because of its higher melting temperature. The LHGR for each rodlet will be calculated by INEEL using MCNP Coupling With ORIGEN2 (MCWO) burnup calculation code. The uranium enrichment will be selected to achieve the LHGR design objective. The AFC-1E experiment will have the same enrichment in all fuel compositions to facilitate the nitride pellet fabrication schedule. The AFC-1F experiment will have varying enrichments in the different metallic fuel compositions to achieve similar peak linear powers. The duplicate rodlet compositions are designed with the same enrichment and are located at different axial positions in the reactor core to provide irradiation performance data at different LHGRs, fission density (burnup), and temperature.

Preliminary enrichment values for AFC-1E and AFC-1F were estimated based on the linear powers of AFC-1(A-D) and the total fissile atom density as a scaling parameter. Initial physics calculations were performed for the AFC-1E and AFC-1F fuel compositions (G. S. Chang Memorandum, March 27, 2003). Based on these results, the enrichment of the nitride fuel is proposed to be 65% U-235 for all rodlets. The physics calculations indicated the preliminary enrichments of the metallic fuels were acceptable except for AFC-1F Rodlet 2, which will be increased from 33% to 55%. The proposed enrichment values for the metallic fuels are 78 wt% for Rodlets 1 and 4, 55 wt% for Rodlet 2, and 93 wt% for Rodlets 3, 5, and 6. Results of the next

physics calculations will be reported in the second quarterly report. The final enrichment values will be determined based on these results.

For additional information on this topic, please contact Steve Hayes at steven.hayes@anl.gov.

ATRC Tests. Because the geometry of the ATRC facility is different than that of the actual geometry of the ATR flux trap in which the experiment will be inserted, special test baskets had to be designed. They were designed to be fully representative of the actual baskets used for irradiation but were configured for full sacrificial testing in the ATRC facility.

ANL-W successfully fabricated four ATRC baskets with a .045-inch cadmium blanket enclosed in an aluminum sleeve to represent beginning of life (BOL), and four ATRC baskets with a .020-inch cadmium blanket, over the center 12 inches of the core region, enclosed in an aluminum sleeve to represent cadmium depletion.

All necessary approvals were received and all paperwork was prepared for the ATRC test to commence on April 7, 2003. ATRC reactivity measurements will be performed on a two- and four-basket BOL configuration, and on a four-basket depleted configuration. Azimuthal and axial profile measurements on the four-depleted-basket configuration will also be performed to support the Core Safety Assurance Package. All data received from the ATRC measurements will be documented in the AFC-1 Experiment Safety Assurance Package (ESAP).

For additional information on this topic, please contact Richard Ambrosek rga@inel.gov.

Analyses and Documentation. Temperature reactivity coefficient analyses for variants on the AFCI experiment assembly were performed. Analyses were also completed to predict the reactivity change associated with insertion of the AFC-1 experiments. Results indicate that four AFC-1 assemblies are comparable in reactivity to LSA cobalt configuration. Thus, LSA cobalt will be used as a backup test if needed.

It was concluded that the AFC-1 (E&F) irradiations would meet the required burnup prior to CIC if the current insertion schedule were maintained. Hence no delay in CIC is required and will not be perused by the project.

Thermal/hydraulics analysis was 95% complete at the end of the second quarter. Figures 2.8.4 and 2.8.5 show models created to analyze temperature distribution in the capsule wall and cadmium sleeve.

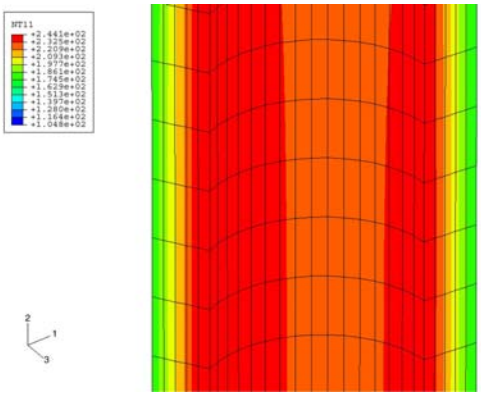

Fig. 2.8.4 – Temperature Distribution in ATW-1 Capsule

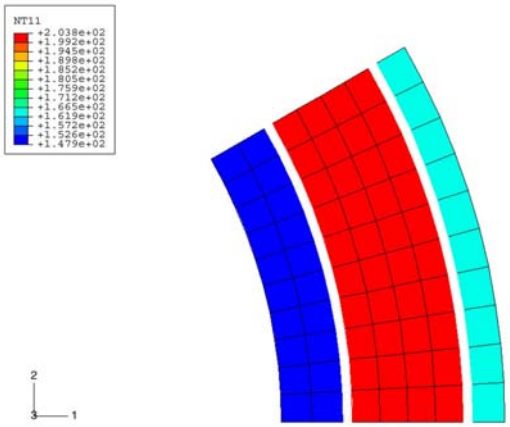

Fig. 2.8.5 – Temperature Distribution in Cadmium Sleeve.

The INEEL received updated experiment fuel compositions for the AFC1 A-D experiments. Physics analysis of the test assemblies and their associated cadmium "thermal neutron filter" in the TRA east flux trap positions was performed using the updated data. Five variants of transuranic containing zirconium-based alloy fuels (AFC1-B and D) and six plutonium-zirconium nitride based fuels (AFC1-A and C) containing Am and Np were analyzed. Tables 2.10.4 and 2.10.5 provide the updated results of the linear heat generation rate (LHGR) and actinide depletion rates in the east flux trap following one and two typical irradiation cycles (50 EFPDs per cycle), respectively, with lobe powers of 18 MW (NW), 18 MW (NE), 23 MW (C), 25 MW (SW), and 25 MW (SE).

Table 2.10.4 – Updated linear fission heat rate and burnup distribution of the proposed AFC-1 fuel in the east flux trap position at the end of 50 EFPDs of irradiation

ID		Liner heat rate	Fission heat rate	^{239}Pu depletion (atom%)	Heavy metals depletion	Am depletion
		(w/cm)	(w/g)		(atom%)	(atom%)
AFC-1B	Rodlet 1	169.4	139.53	2.87%	1.39%	6.12%
(Metal)	Rodlet 2	162.65	133.95	3.10%	1.34%	6.22%
	Rodlet 3	270.28	227.4	3.60%	2.04%	8.04%
	Rodlet 4	194.7	170.38	3.53%	1.73%	7.00%
	Rodlet 5	116.76	173.97	4.37%	2.40%	0.00%
	Dummy	0	0	0.00%	0.00%	0.00%
AFC-1D	Rodlet 1	136.55	115.75	2.38%	1.14%	5.19%
(Metal)	Rodlet 2	153.74	131.78	3.19%	1.39%	6.06%
	Rodlet 3	236.09	202.23	3.25%	1.81%	8.64%
	Rodlet 4	184.46	157.49	3.15%	1.56%	6.37%
	Rodlet 5	151.77	153.3	3.75%	2.07%	0.00%
	Dummy	0	0	0.00%	0.00%	0.00%
AFC-1A	Rodlet 1	45.61	49.37	2.84%	0.90%	4.05%
(Nitride)	Rodlet 2	127.39	124.5	2.93%	1.49%	6.76%
	Rodlet 3	152.33	141.09	3.87%	1.54%	8.64%
	Rodlet 4	257.64	226.22	3.98%	2.39%	11.27%
	Rodlet 5	151.25	146.93	3.95%	1.80%	9.84%
	Rodlet 6	97.55	100.31	2.61%	1.21%	5.92%
AFC-1C	Rodlet 1	57.7	55.97	3.22%	0.98%	4.92%
(Nitride)	Rodlet 2	195.06	142.69	3.42%	1.73%	7.27%
	Rodlet 3	184.43	150.14	4.18%	1.67%	9.71%
	Rodlet 4	282.38	224.82	3.70%	2.28%	11.12%
	Rodlet 5	174.05	150.57	3.98%	1.87%	9.93%
	Rodlet 6	157.8	145.79	3.66%	1.67%	6.68%

Table 2.10.5 – Updated linear fission heat rate and burnup distribution of the proposed AFC-1 fuel at the East flux trap position at the end of 100 EFPDs irradiation.

ID		Liner heat rate	Fission heat rate	^{239}Pu depletion (atom%)	Heavy metals depletion	Am depletion
		(w/cm)	(w/g)		(atom%)	(atom%)
AFC-1B	Rodlet 1	177.64	147.56	5.80%	2.80%	12.06%
(Metal)	Rodlet 2	173.7	144.24	6.36%	2.75%	12.40%
	Rodlet 3	294.74	251.23	7.36%	4.25%	14.52%
	Rodlet 4	224.51	198.49	7.00%	3.46%	13.81%
	Rodlet 5	138.04	207.71	8.84%	4.91%	0.00%
	Dummy	0	0	0.00%	0.00%	0.00%
AFC-1D	Rodlet 1	138.92	118.59	4.83%	2.33%	10.31%
(Metal)	Rodlet 2	162.17	140.12	6.30%	2.71%	11.97%
	Rodlet 3	250.38	216.97	6.58%	3.72%	15.55%
	Rodlet 4	195.28	168.28	6.31%	3.12%	12.62%
	Rodlet 5	157.87	160.86	7.60%	4.29%	0.00%
	Dummy	0	0	0.00%	0.00%	0.00%
AFC-1A	Rodlet 1	47.07	51.14	5.60%	1.64%	7.92%
(Nitride)	Rodlet 2	135.61	133.51	5.94%	2.99%	13.34%
	Rodlet 3	159.17	148.62	7.80%	3.08%	15.60%
	Rodlet 4	270.33	240.38	7.94%	4.79%	20.09%
	Rodlet 5	162.14	158.84	7.98%	3.62%	19.04%
	Rodlet 6	105.38	109.07	5.30%	2.41%	11.89%
AFC-1C	Rodlet 1	60.92	59.36	6.48%	1.87%	9.69%
(Nitride)	Rodlet 2	207.59	153.14	6.84%	3.46%	14.48%
	Rodlet 3	204.66	168.03	8.37%	3.30%	17.26%
	Rodlet 4	313.44	252.75	7.64%	4.76%	19.78%
	Rodlet 5	200.49	174.98	8.11%	3.79%	19.30%
	Rodlet 6	174.9	163.11	7.49%	3.35%	13.35%

Calculations on total heat rate distributions for the AFC-1 test train in the east flux-trap position were also performed. The heat rate analyses consist of the neutron heat rate calculations and combined neutron / photon heat rate calculations for the prompt gamma heating. The detailed total heat rate distributions are provided for the thermal analysis.

The physics analysis was performed using the computer code MCNP currently being used for evaluation of experimental programs in the ATR. This is a general Monte Carlo n-particle code written at Los Alamos National Laboratory. This version has been verified at INEEL by benchmarking calculated flux magnitudes with measured flux levels for several experiments and in several test positions of the INEEL Advanced Test Reactor (ATR) core. The code and the ATR core model have also been benchmarked for heat rate evaluations by comparing measured to predicted temperatures in the ATR experiments.

There are four major tallies used in the MCNP model calculation process. The first tally in the model computes the neutron flux (particles/cm^2) averaged over the target cells. The second tally calculates the cell average fission reaction rate. The third tally calculates the neutron energy and the fourth tally calculates prompt gamma deposition (MeV/g) averaged over the target cells. It also includes the capture gamma and inelastic gamma energy depositions in the test assembly. A conservative approximation for delayed gamma heating = 20% of the prompt gamma heating is included in the total heat rates.

The following tally normalization factor was used with the total core power corresponding to E-lobe power (21.8 MW) to convert the MCNP tallies to heat rates in w/g. Heat rate normalization factor = (fission neutron / fission) x (fission /MeV) x (w per MW)

$$= (2.42) \times (1/194) \times 1.0X10^6$$

$$= 12470 \text{ per core MW.}$$

All the MCNP-calculated fission and total heat rate distributions were based on the beginning of cycle condition without fuel depletion, which is conservative for the thermal analyses.

The results of the physics analysis provided the test assembly volume average neutron/fission and prompt gamma heat rate distribution data in the AFC-1 tests, at BOL, at the end of 50 EFPDs irradiation, and at the end of 100 EFPDs irradiation. Calculations were found to meet all experiment requirements.

Stress analysis to support the Experiment Safety Assurance Package (ESAP) was completed and submitted for review. Following verification of all thermal/hydraulics, physics and stress analyses, data will be incorporated into the ESAP and distributed for project personnel to review. The plan is to complete project corrections and modifications by the end of April and circulate for TRA review and approval in early May.

For additional information on this topic, please contact Richard Ambrosek at rga@inel.gov.

2.11 Series Two FUTURIX Irradiation

FUTURIX is the international name of the irradiation test designated as AFC-3 in the AFCI 5-Year Program Plan. It is a collaborative irradiation experiment with the French CEA, with significant participation by the Institute for Transuranium Elements (ITU). This experiment will test 10-cm-long experimental fuel pins in the Phénix fast-spectrum reactor located in France. The US program will provide fuels for four of the experimental fuel pins. Plutonium, neptunium, and americium transmutation fuels will be fabricated in the US and transported to ITU for encapsulation in standard Phénix cladding. Reactor insertion of this experiment is scheduled to occur in April 2006. The experiment is scheduled for two irradiation cycles (240 effective full-power days (EFPDs) before the shutdown of the Phénix reactor and should achieve heavy metal burnups in the range of 5-10 at.%, with americium transmutation as high as 20 at.%. The irradiated fuels will be shipped back to the US for post-irradiation examination (PIE) and separations testing.

2.11.1 Series Two FUTURIX Irradiation Objective and Scope

The FY03 efforts are primarily focused on providing technical data to CEA about the fuels that are being fabricated in the U.S. Part of the technical data will be a compiled Transmutation Fuels Handbook with oxide fuel input from CEA. The second revision of the International handbook will be published at the end of FY03. Also, the fabrication process qualification and quality control reviews will be performed at U.S. sites.

2.11.2 Series Two FUTURIX Irradiation Highlights

The following are the major highlights for the FUTURIX Irradiation in the first quarter of FY03:

- Final input to the FUTURIX-FTA Presentation Report was provided to CEA for the nitride and metallic fuels to be included in the FUTURIX fuels test in the Phénix reactor.
- The document “Fuel Research and Development Plan for Metal Fuel to be irradiated in the FUTURIX-FTA Experiment in Phénix” (W7520-0524-ES-00) was submitted to the AFC Fuels NTD, DOE-HQ and transmitted to the CEA. This document details the testing and characterization necessary to provide the French authority with a basis for insertion of metallic fuel specimens in the Phénix reactor.

2.11.3 Series Two FUTURIX Irradiation Technical Summary

For additional information on the status of the FUTURIX collaboration please contact Steve Hayes at steven.hayes@anl.gov.

ANL and LANL fuels staff members participated in the DOE/CEA Coordination Meeting held in Washington, DC, in January. A half-day breakout session was held between CEA, ANL and LANL fuels staff members to discuss the status of the FUTURIX irradiation test collaboration.

The following are the highlights of the agreements:

- It is recognized that additional collaboration opportunities exist, especially in the area of Series One fuels, but these discussions are deferred to a later meeting when the contents of the U.S. Series One fuel are better defined.

- It is agreed that, once the contract is signed, FUTURIX will be managed as a project. A steering committee will be formed and the project will be base-lined under a project control system. Subsequently, a project team will be formed with specific roles and responsibilities.
- Both sides agreed that, to successfully run FUTURIX, frequent meetings among the technical people are needed, which will require international travel. Such meetings will take place in facilities where fuel development and characterization activities are taking place. At a minimum, quarterly interactions are necessary, especially as we get closer to the reactor insertion. An initial travel schedule for calendar year 2003 is developed and included in the agreements document.
- U.S. will provide up to 120 g of americium oxide (AmO_2) to CEA to be used in the oxide fuel development as an in-kind contribution. Depending upon the purity of the americium, a smaller amount may be adequate and shipment in two separate batches also is acceptable. The cost of shipping 120 g of AmO_2 is approximately $150K. Detailed estimates for various shipping strategies are being evaluated.

CEA announced that the Phénix power cycle we had previously identified for the insertion of the FUTURIX test has been delayed from December 2005 to April 2006. A detailed schedule for deliverables associated with the FUTURIX experiment was tentatively developed by the participants consistent with the new insertion date and the delay of more than one year on any significant work on the experiment due to the fact that DOE has not yet secured funding for the CEA work. The funding delay has resulted in the Presentation Report, expected to be complete and issued before the end of FY-02, to remain incomplete. The new target for submitting the Presentation Report, which formally proposes the experiment to the Phénix reactor operator, is April 2003. Inputs to the key deliverables for the US participants are shown in Table 2.11.1 below.

Table 2.11.1 – Key US Deliverables for the FUTURIX Fuels Experiment.

US Deliverable	Date
Presentation Report	February 2003
Technical Report	April 2004
Test Fuel R&D Report	June 2004
Fabrication Control Plan and Fuel Specification	September 2004
Receipt of US test fuels at ITU	July 2005
Fabrication Report	August 2005
Safety Report	August 2005

The pressing deliverable for the US program is our input to the Safety Report, which must include the PIE results from the AFC-1A, -1B, -1E and -1F non-fertile and low-fertile fuel experiments to 8% burnup in the Advanced Test Reactor.

The proposed fuels for the US test pins, two metallic fuel pins and two nitride fuel pins, were discussed at length. The initial test matrix proposed last year under the Advanced Accelerator

Applications program included only non-fertile fuels. With the new objectives of the AFCI introduced this year, it is desirable to modify the test matrix to include one non-fertile and one low-fertile composition for both the metallic and nitride fuels. CEA agreed with the proposed change in the test matrix.

Preparation of the input to the Presentation Report for the US test fuels was completed and submitted to the CEA for inclusion in the full package that will be issued to the Phénix operations staff in April. The proposed compositions for the US fuels are: U-29Pu-4Am-2Np-30Zr and Pu-12Am-40Zr metallic fuels, and $(U_{0.50},Pu_{0.25},Am_{0.15},Np_{0.10})N$ and $(Pu_{0.50},Am_{0.50})N$-30ZrN nitride fuels. Also required for the Presentation Report was an overview of the safety issues that are foreseen relative to acceptance of the proposed experiment for irradiation in the Phénix fast reactor; these have been identified as:

1. No thermal conductivity data exists for any of the proposed metallic alloy or nitride fuel compositions. These data must be obtained experimentally.
2. Metallic fuel is known to chemically interact (FCCI) with stainless-steel cladding during high temperature irradiation. This phenomenon is exacerbated as Pu content increases, but mitigated as the Zr content increases. The proposed alloys incorporate more Pu and more Zr alloys in the current FCCI database, so this issue must be addressed.
3. The phase diagrams for the proposed metallic alloy fuels are unknown. Solidus temperatures must be determined and the resulting thermal margin during irradiation and anticipated transients must be evaluated.
4. Nitride fuels are known to exhibit decomposition at a temperature that is lower than the congruent melting temperature. The temperature at which this occurs must be determined and the resulting thermal margin during irradiation and anticipated transients must be evaluated.
5. Mixed nitride fuels are known to exhibit pellet fragmentation at temperatures in excess of 1600°C.

2.12 ATR Fast-Flux Booster Design

Earlier studies have shown that fast-spectrum transmutation is most effective to meet the transmutation objectives of reducing the minor actinide inventories in spent nuclear fuel. Therefore, it is important that fast-spectrum test capabilities are readily available for the fuel developers as the proof-of-principle experiments continue and transition into proof-of-performance testing with a more prototypic neutron spectrum. Unfortunately, all fast reactors in the U.S. are shut down and fast-spectrum irradiation capabilities are currently available only outside the U.S. Conducting experiments overseas will be slow and expensive. Therefore, the U.S. must develop some small-scale, fast-spectrum irradiation capabilities in this country. A leading option at this time is the installation of a fast-neutron flux booster (FNFB) in the ATR.

The five-year milestones include:

Complete fuel specifications.	FY 2004
Complete preliminary design.	FY 2004
Complete final design.	FY 2005
Complete fabrication, assembly, and installation.	FY 2005
Begin operation.	FY 2006

2.12.1 ATR Fast-Flux Booster Design Objectives and Scope

An initial project will be to design, fabricate, and install an FNFB ATR. The FNFB will convert thermal neutrons in the flux trap into fast neutrons and create an environment representative of the fast-flux spectrum in a fast reactor. The FNFB would boost the fast flux in the ATR South flux trap by a factor between 2 and 3, produce a fast flux greater than 6.0×10^{14} n/cm^2-sec, and have a volume large enough to accommodate the fuel test samples. In FY 2003, INEEL will define the requirements, begin developing the specifications for the FNFB fuel, and complete the pre-conceptual design and the conceptual design.

2.12.2 ATR Fast-Flux Booster Design Highlights

Because of the reduced AFCI budget, the start of this activity is delayed until FY04.

2.12.3 ATR Fast-Flux Booster Design Technical summary

This activity is postponed until FY04 and this section will no longer be included in the subsequent FY03 quarterlies.

3 TRANSMUTATION ENGINEERING

3.1 Introduction

The top-level objective for Transmutation Engineering is to develop the engineering basis for the transmutation of minor actinides (MAs) and long-lived fission products (LLFPs) so that informed decisions can be made in the next five years concerning transmutation technologies and a path forward can be developed for implementation. In support of that objective, Proof-of-principle information is being developed in areas not supported in the fuels, separations, Generation IV research, or other DOE-NE research programs. In the near-term, five-year period, transmutation engineering activities are focused in the areas of physics, nuclear data and codes, coolants and corrosion, structural materials, and accelerator-based transmutation. Subsequent to the decision on transmutation technology and a successful proof-of-principle phase, engineering development and demonstration will be performed to provide proof-of-performance in preparation for deployment of a transmuter technology.

In the next five years, information provided by transmutation engineering and other advanced fuel-cycle activities will provide support for key decisions. This support can be summarized as follows:

Transmutation Engineering Physics will provide nuclear cross-section data in the thermal, epithermal, and fast-neutron spectra. This data will allow the accurate prediction of transmutation rates and reduce calculation uncertainties. Coefficients of reactivity will be obtained in all three spectra to support licensing and safety analyses. Analysis codes will be developed, validated, and benchmarked so that design calculations can be made with confidence.

Transmutation Engineering Materials activities will provide detailed information on the degradation of structural materials in a fast-neutron spectrum and mixed-particle environment (neutrons and protons). Material limits will be established that help determine the level of burnup that can be obtained and, therefore, the effectiveness of the various options. Coolant technology for critical reactor and accelerator-driven systems will be developed that supports the selection of technology options.

Transmutation Engineering Activities in Accelerator-Driven Systems will provide necessary information on the physics of coupling an accelerator to a subcritical system and the operation and start-up of such systems. In addition, the target technology necessary to drive these systems will be developed to support the technology decisions.

3.2 Transmutation Physics (Series Two)

3.2.1 Transmutation Physics Objectives and Scope

Transmutation engineering physics will provide nuclear cross-section data in the thermal, epithermal, and fast-neutron spectra. This data will allow the accurate prediction of transmutation rates and reduce calculation uncertainties. Coefficients of reactivity will be obtained in all three spectra to support licensing and safety analyses. Analysis codes will be developed, validated, and benchmarked so that design calculations can be made with confidence. The major objective of high-energy physics activities is to improve and maintain the computer codes used in the analyses of transmutation systems. As part of the improvement, the nuclear data accuracy is reevaluated to match desired objectives.

Implementation of part of the physics FY03 scope is to analyze the results of irradiations performed in the French fast reactor (PHENIX) of PROFIL-2 (irradiation of actinides) and TRAPU (irradiation of mixed-oxides) to gather information on the transmutation rates and associated cross sections of such isotopes. Time-dependant calculations are carried out to perform the analysis and evaluate the discrepancy between experimental and computational results.

Codes and associated libraries for thermal and fast reactor as well whole-core codes need to be upgraded for new types of fuels and reflectors to be used for different types of advanced fuel cycle strategies involving MOX, gas-cooled reactors, and liquid metal-cooled systems with presence of minor actinides and/or fertile-free compositions.

3.2.2 Transmutation Physics Highlights

- The re-analysis of the PROFIL-1 experiment with a new approach (i.e. using an R-Z model) has been completed and results found to be consistent with the results obtained during previous analyses.
- The analysis of the PROFIL-2 experimental data with JEF2.2, ENDF/B.V and ENDF/B.VI, was completed and the report "Analysis of *PROFIL Irradiation Experiments for Cross Section Validation"* was written, satisfying an AFCI Level-3 milestone on schedule.
- The MC^2-2 code was updated, allowing the stored broad-group structure to be processed when the ultra fine-group structure (ufg) was increased. Another update was made, allowing modification of the in-group P_1 scattering matrix to take into account the correction.
- Several trial versions of a vacuum-node treatment were implemented in a nodal framework to test feasibility with the VARIANT methodology. Preliminary analysis shows that the first-order spherical-harmonics formulation is producing stable and accurate vacuum-node response matrices for P_9 and higher-order angular approximations.
- Belgonucleaire announced that with the addition of CEA and COGEMA, they are now ready to open the program. The MALIBU Technical Program Meeting has been set for June 26-27, 2003, in Brussels.

- MALIBU participation funding was cut significantly but will allow some participation in FY03. ORNL will participate in upcoming meetings, start analysis and modeling, and begin contract negotiations.

3.2.3 Transmutation Physics Technical Summary

Analysis of Integral Experiments for Cross-Section Validation & Cross-Section Evaluations

PROFIL Analysis. The effectiveness of the new PROFIL analysis approach using a R-Z model has been tested by comparing calculated/experimental (C/E) values obtained for PROFIL-1. Cross sections for minor actinides, coming from ECCO calculations in a 33-group energy structure and relative to the inner fuel zone of an R-Z model of the PHENIX reactor provided by the French colleagues, have been condensed into one-group cross sections (in order to be used in the time-dependent calculations) using the actual fluxes calculated with the ERANOS/BISTRO code at the real position (R,Z) of each pure isotope sample. A generally good agreement between C/E values obtained with the new method and those obtained during the previous PROFIL-1 analysis (in which reaction rates had been corrected on the Fundamental Mode), has been found (see Table 3.2.1).

Table 3.2.1. Calculated/Experimental Values in the PROFIL-1 Experiment (JEF2.2 Data)

Data Type	Old Method	New Method
σ_{capt} U-235	0.95	0.95
σ_{capt} U-238	0.98	0.99
σ_{capt}Pu-238	0.98	0.98
σ_{capt}Pu-239	0.99	0.99
σ_{capt}Pu-240	1.14	1.12
σ_{capt}Pu-241	1.24	1.26

C/E values relative to PROFIL-2 analysis are summarized in Table 3.2.2. Generally, good agreement is found between PROFIL-1 and PROFIL-2 results as was expected. The PROFIL-2 results have confirmed that, while C/E values for the uranium isotopes are nearly similar when using both JEF2 and ENDF/B data, the latter library (in both its versions ENDF/B-V and ENDF/B-VI) performs slightly better for the capture cross sections of ^{240}Pu, ^{241}Pu and ^{242}Pu. Important discrepancies between experimental values and calculation results have been underlined also by the PROFIL-2 analysis, particularly for the capture cross sections of ^{238}Pu and ^{240}Pu when using ENDF/B and JEF2.2 data, respectively, as well as for the (n,2n) cross section of ^{239}Pu when using the three sets of nuclear data files. C/E values obtained with JEF2.2 data for both experiments are also consistent with values calculated by CEA in a previous study. Notice the excellent results obtained for the capture cross section of ^{237}Np, particularly using ENDF/B-V data.

Table 3.2.2. C/E Values Relative to the PROFIL-2 Experiment Using JEF2.2, ENDF/B-V and ENDF/B-VI Data

Data Type	C/E[(a)]			A-priori Uncertainty[(b)]
	JEF2.2	ENDF/B-V	ENDF/B-VI	
σ_{capt} U-235	0.97 ± 1.7 %	1.01 ± 1.7 %	0.98 ± 1.7 %	3.3 %
σ_{capt} U-238	1.01 ± 2.3 %	1.04 ± 2.3 %	1.02 ± 2.3 %	1.6 %
σ_{capt} Pu-238	1.05 ± 4.0 %	1.45 ± 4.0 %	1.97 ± 4.0 %	13.8 %
σ_{capt} Pu-239	0.96 ± 3.0 %	0.98 ± 3.0 %	0.96 ± 3.0 %	5.7 %
$\sigma_{n,2n}$ Pu-239	0.58 ± 15.0 %	0.53 ± 15.0 %	0.56 ± 15.0 %	15.5 %
σ_{capt} Pu-240	1.16 ± 2.2 %	1.09 ± 2.2 %	1.02 ± 2.2 %	11.9 %
σ_{capt} Np-237	0.95 ± 3.6 %	0.98 ± 3.6 %	0.91 ± 3.6 %	6.4 %
σ_{capt} Am-241	1.07 ± 1.7 %	0.94 ± 1.7 %	0.90 ± 1.7 %	17.0 %

(a) C/Es are in absolute values, while the experimental uncertainties are relative and given in percent
(b) No energy correlation

CROSS SECTION EVALUATIONS

ENDF Formatting of High-Energy Evaluations. We have improved our ENDF formatting tools to encompass our new high-energy actinide evaluations. Codes developed previously were inadequate to treat the particular case of fissioning nuclei, and therefore needed various improvements. The newly developed codes are now documented (written in both Perl and Fortran95) in a report entitled "ENDF Formatting of High-Energy Actinide Evaluations." This report is a step-by-step description of the merging of old, low-energy ENDF files with new, high-energy information.

New Evaluations on n+^{237}Np and n+^{241}Am. Our work on ^{237}Np continued, and we made significant progress on re-evaluating the fission cross section. The reduction of Lisowski's fission data was finalized, and the new cross sections are consistent with our evaluation. We have incorporated these changes into an ENDF file and have performed integral data testing in LANL fast-critical assemblies by comparing the ^{237}Np/^{235}U fission ratio in Jezebel, Godiva, Jezebel-23, and Bigten & Flattop. Experiment and theory agree to within 2-3%.

We are improving the ^{241}Am ENDF evaluation to provide better AFCI calculations of criticality and transmutation using new recently published measurements. The (n,2n) cross section in the existing ENDF file is considered to be approximately 50% too small due to the fact that the evaluation was made before any experimental data existed. Recently, two new measurements (Russia, and Livermore) have been published. We are undertaking a multistage Hauser-Feshbach analysis of n+ ^{241}Am reactions to reevaluate this nucleus. We are also working on the (n,g) reaction to provide information on the splitting of the capture cross section to ^{242}Am ground and meta-stable states.

Helium and Hydrogen Production Cross-Section Measurements. Hydrogen and helium are produced when energetic neutrons interact with materials, and these gases can lead to significant changes in materials properties such as embrittlement and swelling. Such effects have been seen in fission reactors and a significant effort has been made for the development of fusion reactors in which the effects are expected to be greater because of the higher neutron energy. For AFCI,

new structural materials are proposed, and the amount of gas production must be known to assess the properties of these materials under radiation damage.

During this reporting period, we followed up on the production measurements of the first quarter, completed calibration efforts, analyzed data to yield preliminary results, proceeded with maintenance activities, and prepared for the next beam cycle to begin in the summer of 2003.

Helium and hydrogen gases are produced initially as energetic protons, deuterons, and alpha particles from nuclear reactions. When these charged particles slow down and stop (with ranges of mm to cm), they acquire electrons from the material and become hydrogen (protons and deuterons) or helium (alpha particles). Our method is to measure the protons, deuterons, and alpha particles that escape from thin foils, as illustrated in Fig. 3.2.1.

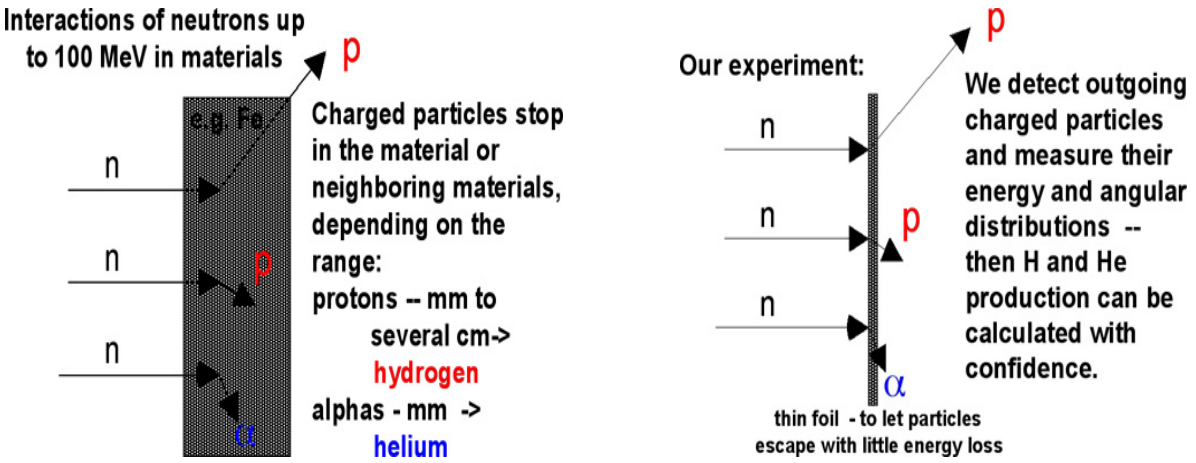

Fig.3.2.1. Interactions of neutrons with materials produce charged particles that stop either in the material or in neighboring materials. In our experiment, we use a thin foil of the material so that the charged particles can escape and be detected.

We measure the charged particles with detector systems at four angles concurrently. Then we can move the detector systems to investigate a new set of angles. Each detector system consists of 2 or 3 detectors in coincidence and arranged so that the charged particles pass through the first detector and stop in the second or third. We do this in order to identify the protons, deuterons, alpha particles, and the small numbers of tritons and ^{3}He.

Data-taking for the most recent operation of the LANSCE/WNR neutron source was completed this quarter. Some beam at low intensity was available in January 2003, and we used that time for calibration runs. Following beam shutdown for a 6-month maintenance period at the LANSCE accelerator, we further calibrated the detectors with an alpha-particle source. Then upgrades to our experimental apparatus could begin with improvements to the vacuum system and data transmission from the experimental area to the data-acquisition room. The vacuum system upgrade was completed and the cabling improvements are in progress.

Data analysis is progressing. A new software program is being developed to speed the analysis and to have the analysis system compatible with the new data-acquisition hardware and software to be installed before the next running period.

New results for helium production on the two most abundant nickel isotopes have been obtained and are shown in Figs. 3.2.2 and 3.2.3. Data up to 50 MeV were obtained previously[1] and the

present information is a slight update of that work. The results from 50–100 MeV are new, and show that the helium production cross-section stays rather constant in this energy range.

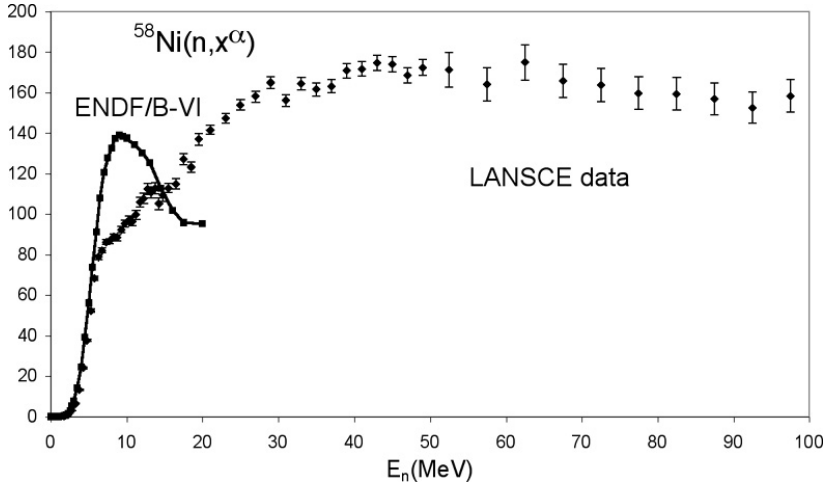

Fig. 3.2.2. Helium production from neutron bombardment of 58Ni. The data below 50 MeV are slight revisions of our previous work.1 The data from 50–100 MeV are new.

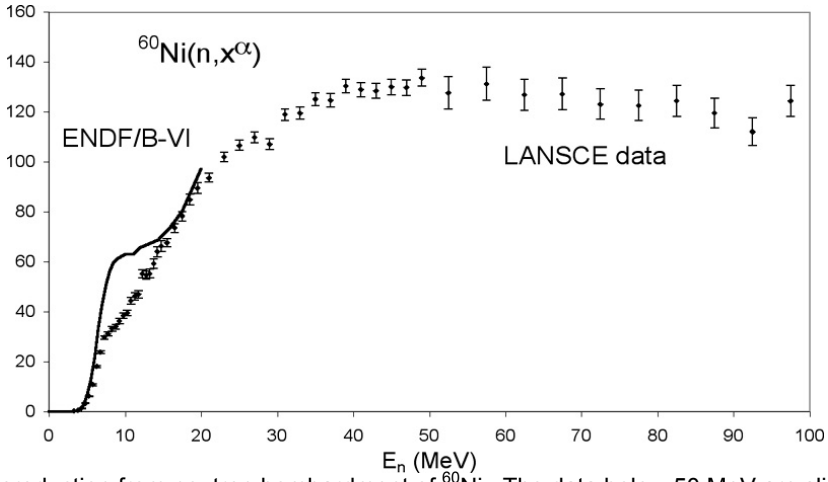

Fig. 3.2.3. Helium production from neutron bombardment of ^{60}Ni. The data below 50 MeV are slight revisions of our previous work.[21] The data from 50–100 MeV are new.

Minor Actinide Cross-Section Measurements. Contact has been made with researchers at Khlopin Radium Institute (KRI) in Russia to investigate the possibility of having this institute fabricate the actinide foil samples needed for our experiments. We have also been in contact with LANL's C Division concerning their ability to manufacture the foil samples. A cost estimate from C Division is due shortly.

A proposal was submitted to the LANSCE Nuclear Program Advisory Committee requesting beam time in late summer on the "DANCE" instrument at the Lujan Center for making a measurement of the ^{237}Np capture cross section.

[21] R. C. Haight, F. B. Bateman, S. M. Sterbenz, S. M. Grimes, O. A. Wasson, P. Maier-Komor and H. Vonach, "An Update on (n,charged particle) Research at WNR," Proc. International Workshop on Nuclear Data, Del Mar, California, December, 1995. Fusion Engineering and Design **37**, 73-77 (1977).

CODE DEVELOPMENT

Fuel Cycle Method The MC^2-2 code was updated so that the stored broad-group structure would be processed when the ultra-fine-group structure (ufg) was increased by ETOE2-2 from 2000 ufg to 18000 ufg. The convergence between the ufg boundaries and the broad group boundaries were relaxed. The reason for testing the 18000 ufg structure was to verify that MC2-2 code correctly energy shields the resonance-like structure of the elastic scattering cross sections for the structural isotopes above the resolved resonance region. In the future, we may regenerate the MC^2-2 library for ENDF/B-V1 data with this fine ufg structure.

The MC^2-2 code was updated to allow the in-group P_1 scattering matrix (written in an ISOTXS format) to be modified on user option. This is intended to fix an inconsistency in the P_N approximation of MC^2-2. The P_1 scattering matrix can now be correctly used in transport of whole-core calculation codes.

The most recent form of the vacuum-node treatment using the first order spherical harmonics formulation was implemented into MathCAD. Preliminary analysis shows that the method is producing stable and accurate vacuum-node response matrices for P_9 and higher-order angular approximations that can be coupled with the existing angular trial functions used in VARIANT. Of course, this does not reach the preferred goal of obtaining response matrices that give good solutions for P_1 through P_5 calculations. This is, however, a giant leap forward in progress over what we have achieved in the past.

Efforts continued to derive a more straightforward formalism to describe our approach in anticipation of reducing the computational burden imposed by the method by using an even-parity expansion rather than a full-parity expansion from the beginning.

MCNPX. MCNPX version 2.5.c was released for testing to the AFCI sponsors. This version of the code contains the results of three AFCI milestones met on or before their scheduled due dates. We integrated the IntaNuclear Cascade-Liege (INCL) of Cugnon and ABLA evaporation model of Schmidt into MCNPX, involving a full upgrade of the new routines to Fortran90. The code was previously implemented into the LAHET Code system, and we preserved the external user interfaces designed for that work. Internal interfaces were changed to be compatible with the MCNPX architecture. We also switched the INCL random number generator to the MCNPX standard. We enabled the exponential transform for neutral particles in the model region; and we enabled the mesh-based weight window generator for neutral particles in the model region.

Additional features in MCNPX 2.5.c include: enabling the use of neutron physics models below 20 MeV to enhance the results of the 'mix and match' problem. Before mix and match was implemented, model cross sections were set to zero below 20 MeV because it was assumed that evaluated data libraries would be available below that energy. Preliminary results look good because the total evaluated cross sections are fairly flat like the models, although we can not pick up the low energy nuclear structure with an INC model. We enabled labeling of lattice 'ijk' elements. The user no longer has to figure out the indicing offline, which tends to be a complicated process very prone to error. Error estimates were added to fission multiplicity tallies. Message Passing Interface (MPI) multiprocessing is now available, in addition to the previously implemented Parallel Virtual machine (PVM) capability.

MCNPX Classes. We held an MCNPX beginners' class in Orlando, Florida from Feb 24-28th. Sixteen students attended, including UNLV AFCI collaborators.

Publications. Four publications were released, three of which have been submitted to the upcoming ANS Accelerator Applications Embedded Topical Meeting, to be held in San Diego, CA, June 1-5, 2003.[22]

MALIBU Program Support (ORNL). The MALIBU (Radiochemical analysis of MOX And LEU Fuels Irradiated to High Burnup) program is a project organized by Belgonucleaire (BN) to perform detailed analysis of high-burnup MOX and UOX fuel to provide experimental data on the isotopic inventory of high burnup fuel for code validation.

In February 2003, CEA and COGEMA became participating members of the MALIBU program. With these additions, the program now has the minimum number of participants and the official start of the program was announced by BN. The date of the first MALIBU Technical Program meeting has been set for June 26-27 at BN Headquarters in Brussels, Belgium. This meeting will provide an opportunity for the participants to discuss the program, providing direction to BN. In addition, representatives from the analytical laboratories will make presentations and a visit to the SCK·CEN laboratory will be arranged. During the meeting, the important topic of contracting will also be discussed.

In March 2003, the ORNL FY03 budget for this activity had been set. Based on budgeting decisions and the potential flexibility of the MALIBU program, the FY03 budget was significantly reduced. The impact of this budget reduction is that only minimal support will be available this year, but the funding is sufficient to attend the Technical Program Meeting, start of the modeling effort (to a lesser extent than previously planned), and contract negotiations.

The payment to BN that was planned for this fiscal year (FY03) has been postponed to FY04 and FY05. This topic has been discussed with BN and, to date, they have been very accommodating to meet our funding conditions. The topic will be discussed further with BN at the June meeting, but certainly a contract can not be placed until FY04 funding is obtained. The FY03 work package and the FY04 and FY05 funding profile have been revised to provide for our full participation in the program.

---

[22] J. S. Hendricks, G. W. McKinney, L. S. Waters, Franz X. Gallmeier, "MCNPX Advances for Accelerator Applications," Los Alamos National Laboratory Report LA-UR-03-0075, submitted to ANS Accelerator Applications Embedded Topical Meeting, San Diego, CA, June 1-5, 2003.
J. S. Hendricks, G. W. McKinney, L. S. Waters, "New MCNPX Capabilities for Nuclear Applications," Los Alamos National Laboratory Report LA-UR-03-0076, submitted to ANS Meeting, San Diego, CA, June 1-5, 2003.
J. S. Hendricks, M. T. Swinhoe, S. J. Tobin, D. R. Mayo, "Neutron Multiplicity Counting for Nuclear Safeguards with MCNPX," Los Alamos National Laboratory Report LA-UR-03-0456, submitted to ANS Meeting, San Diego, CA, June 1-5, 2003.
J. S. Hendricks, "MCNPX Model/Table Comparison," LA report submitted to sponsors as LA-UR-0564 (January 2003), finalized as an LA report LA-14030 (March 2003).

3.3 Structural Materials

3.3.1 Structural Materials Objective and Scope

The objective of the materials program is to qualify the structural materials of interest to a high-flux and high-fluence irradiation environment with high-energy particles relevant to fast-spectrum transmutation. We intend to determine the effect of high-energy proton and neutron irradiation on the mechanical properties of structural and target materials.

Mechanical test specimens of prototypic target and structural materials irradiated at moderate temperatures (250ºC-350ºC) will be tested at prototypic fast-spectrum transmuter test temperatures (400ºC-600ºC). Specimens are and will be available from irradiations at the 560-MeV accelerator (SINQ) at moderate temperatures (250ºC-350ºC) at PSI from STIP I and STIP II this year. Materials include Mod9Cr-1Mo (T-91), SS-316L, HT-9, EP-823, tungsten, and tantalum (Ta). Mechanical tests include shear punch tests, tensile tests, microhardness tests, and bend tests.

Our scope also includes maintaining and updating the Materials Handbook with relevant data. In addition to updating the existing data for high-temperature properties, chapters on HT-9, EP-823 and tantalum will be added to the handbook. We hope to obtain and include legacy material samples that were irradiated to high dose in the Fast Flux Test Facility (FFTF).

Transmutation efficiency is directly related to the material lifetime limits caused by radiation damage. This is true for both the ADS and fast reactor (GEN IV) options for transmutation. It is impossible to test materials for all possible spectra. Thus, modeling is essential to fill in the details for an informed technology decision in 5 years. The FY03 scope for radiation damage modeling of structural materials includes:

- Developing potentials for Fe-H and Fe-He interactions;
- Performing calculations for helium-bubble formation and energy reactions of PKA; and
- Benchmarking code calculations with microstructural observations of helium-bubble formation at different proton irradiation temperatures.

3.3.2 Structural Materials Highlights

- Three-point bend tests were performed on SS-316L and Mod 9Cr-1Mo on control specimens at room temperature, 250ºC, and 500ºC.
- Three-point bend tests were also performed on irradiated SS-316L and Mod 9Cr-1Mo at room temperature. Specimens were irradiated in rod form in the STIP I irradiation at PSI at 350ºC.
- Materials Handbook: A first draft of the Ta handbook chapter was reviewed.
- Rad Modeling: First principles calculations of pure Fe and He systems were completed.
- Rad Modeling: First principles calculations of energy-volume relations in Fe-He impurity system were completed.
- Rad Modeling: First-principles calculations for determining Fe-He cross-interactions were completed.

3.3.3 Structural Materials Technical Summary

LANL Hot-Cell Work. In support of determining the effect of high-energy proton and neutron irradiation on the mechanical properties of structural and target materials at prototypic AFCI irradiation temperatures, irradiated specimens were subjected to three-point bending tests. Specimens of SS-316L and Mod-9Cr-1Mo were irradiated in the STIP I irradiation at 225ºC–300ºC. Specimens were irradiated in rod form to a maximum dose of 9.8 dpa.

To obtain mechanical properties in three-point bending, specimens were sliced from the rods in the hot cells to obtain rectangular specimens with the dimensions of 2mm x 8mm x 0.25 mm. The surfaces of these specimens were ground with 800-grit paper before testing. The initial properties measured at room temperature are shown in Fig. 3.3.1. This figure shows the calculated stress and strain in the outer fiber of the three-point bend specimens. This clearly shows the strong effect of irradiation in increasing the stress at which bending occurred by more than a factor of two. No cracking was observed in the surface of these bend specimens. This work is continuing and three-point bend testing at 250ºC and 500ºC will be finished at the end of April.

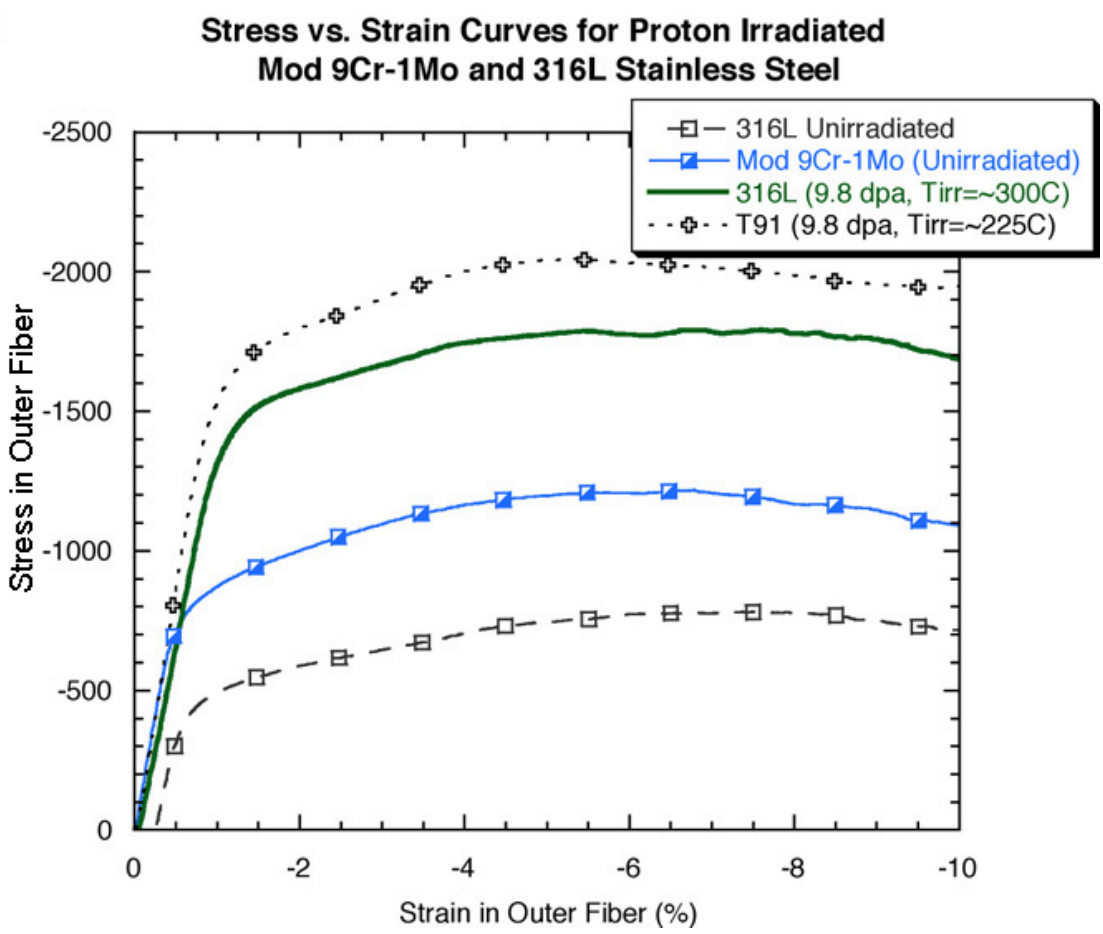

Fig. 3.3.1. Plots of Stress vs. Strain for the outer fiber of three-point bend specimens before and after irradiation in a high-energy proton beam.

Inventory of Ferritic/Martensitic Materials Irradiated in FFTF. Compilation of the ferritic/martensitic (f/m) specimen data left over from FFTF-MOTA (Materials Open Test Assembly) irradiations is just getting underway. The MOTA irradiations took place between 1983 and 1992. F/M specimens were irradiated to doses as high as 225 dpa at temperatures as high as 750°C. Tensile specimens, TEM specimens, charpy specimens, compact tension specimens, and other less common specimens were irradiated. Many of the specimens were never examined or tested.

The preliminary compilation of the f/m specimen inventory shows that a very large number of pressurized tubes were irradiated and measured, but the data were never published. These data are to be compiled, analyzed, and published. Other preliminary examinations of inventory records indicate that a large number of TEM specimens may also be present. Tensile specimens, compact-tension specimens, and charpy specimens are also present. Materials include, but may not be limited to, several different heats of HT-9, several heats of 9Cr-1Mo, and two heats of an oxide dispersion strengthened Fe-14Cr alloy.

MATERIALS HANDBOOK

Materials Handbook Revision 4. The Materials Handbook Coordinator visited LANL in January to discuss plans for Materials Handbook activities for the remainder of the fiscal year. The major activities agreed on are incorporations of chapters on tantalum and HT-9 12Cr-MoWV steel into Revision 4 of the handbook.

The first draft of the chapter on tantalum was received from the European Spallation Source (ESS) Project at FZJ (Germany). A second draft was prepared after a thorough review by the handbook coordinator. The chapter is now ready to be issued for general review.

A preliminary draft of a chapter on HT-9 steel was prepared last year by ANL and given an early review. During this report period, effort has been expended to extract additional information and data for HT-9 from the open literature for incorporation into the chapter. In particular, new compilations of data have been prepared for tensile properties (yield and tensile strengths plus uniform and total elongations), ductile-to-brittle transition temperature (DBTT), and fracture toughness. Both irradiated and non-irradiated materials are included in these compilations.

Redrafting of the chapter on HT-9 is in progress. Sections on material biography, chemistry, and specifications have been completed as well as all sections relating to physical and elastic properties.

Reports for Inclusion in Materials Handbook. Two reports were written on the irradiation creep, swelling, and embrittlement of three Russian ferritic/martensitic stainless steels irradiated in the BN-350 fast reactor to rather high neutron exposures. The steels were EP-450, developed for use in sodium-cooled reactors, and EP-852 and EP-823, developed for compatibility with Pb-Bi coolants. The first report addressed EP-450 and EP-823 at irradiation temperatures between 390ºC and 520ºC, and the second report presented results on EP-450 and EP-852 at 305ºC–335ºC. At ~300ºC, the steel was observed to be very brittle after irradiation to high neutron exposure (~60) dpa.

The approach used in these comparative irradiation series was to perform side-by-side irradiations of the Pb-Bi compatible steels with EP-450, for which the irradiation database is much more extensive. As a class, the three steels are shown to be very similar in behavior,

exhibiting swelling at temperatures below 420ºC, precipitation-induced densification throughout the temperature range studied, and thermally-assisted creep above ~500ºC. In general, the creep coefficients measured are about one-half those of austenitic steels, in agreement with earlier experiments on HT-9 and European f/m steels.

RADIATION DAMAGE MODELING OF STRUCTURAL MATERIALS

Introduction

It is well known that reactor materials undergo radiation damage from the impingement of neutrons and protons emitted from the nuclear reactions. While there have been many successful efforts in modeling this process, the interactions and the damage induced by H and He—the main gaseous by-products of the nuclear reactions—on the underlying materials (usually ferritic steels) are still unclear. Because of elevated H and He production from damage due to high-energy irradiation, the team needs to urgently expand the materials' properties database. A major problem is the limited amount of reliable experimental data. There is a paucity of even the basic experimental data on defect formation and migration energetics and phase stability of H-Fe/Fe-He systems that are of interest to this project. It is important to keep in mind that the laboratory experiments (irradiations) are often cost-prohibitive.

With the advancement of computer technology, modeling and simulation have emerged as an indispensable tool to bridge gaps in our experimental understanding. Theoretical approaches based on state-of-the-art *ab initio* electronic-structure calculations are therefore most desirable. However, these calculations are computationally intensive and allow only a few hundreds of atoms in a system. On the other hand, semi-empirical, many-body, inter-atomic potentials such as the molecular embedded atom method (MEAM), based on the density-functional theory, allow us to handle large systems with millions of atoms [1]. This is a powerful enhancement of the classical embedded atom method (EAM) and allows us to handle directional forces, important in ferritic materials [2]. Furthermore, in order to extend a potential to model alloys such as He inclusions in ferritic steels, it would be convenient to describe the atomic interactions of the multitude of alloying elements using a common formalism. Thus, for our modeling work, we will develop inter-atomic interactions based on the MEAM model.

Our ultimate goal for FY03 is to develop a reliable MEAM model for Fe-He systems in order to understand the effect of He on the properties of Fe. Using this potential we will investigate the phase stability, defect energetics, defect mobility, and mechanical properties of the Fe-H systems using a combination of molecular dynamics and thermo-chemical calculations. The ultimate goal is to use MEAM to investigate effect of radiation dose, defect microstructure, and gas inclusions on macroscopic materials properties. To achieve this, we first need a sufficiently large database of properties of the Fe-He systems. Because reliable experimental values of properties are lacking, we first used *ab initio* calculations to generate a database of many equilibrium properties. This dataset will then be used to determine a reliable MEAM model of He-Fe systems.

First Principles Modeling of Fe-He. In this quarter we used state-of-the-art *ab initio* electronic structure calculations to compute equilibrium properties of Fe-He systems. These properties are shown in Fig. 3.3.2 and summarized in Tables 3.3.1 and 3.3.2. These properties, in conjunction with known experimental properties of Fe, were used to develop a MEAM model. Currently, we are refining the model.

Table 3.3.1. Properties of Fe-He Rocksalt Structure Computed Using *ab initio* Calculations

Property	BCC
Cohesive Energy	3.06 eV
Lattice Constant	4.14 Angstroms
Bulk Modulus	66.3 GPa
C_{44}	-20.2 GPa
$(C_{11}-C_{12})/2$	-108.4 GPa

Table 3.3.2. Properties of FCC He Structure Computed Using *ab initio* Calculations

Property	BCC
Cohesive Energy	0.032 eV
Lattice Constant	4.1 Angstroms
Bulk Modulus	1.57 GPa

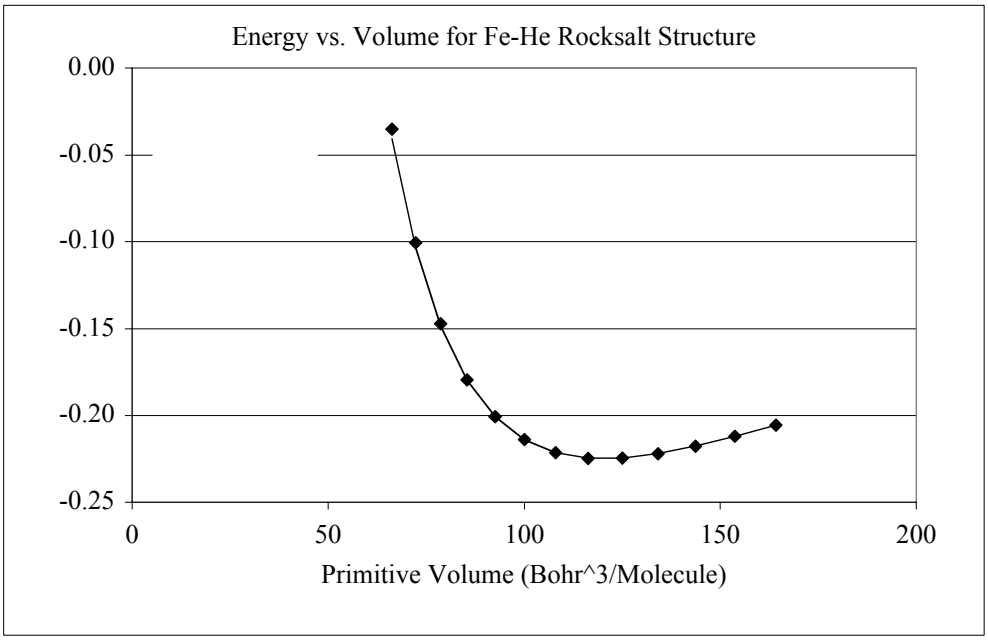

Fig. 3.3.2. *Ab initio* calculations of Fe-He rocksalt structure. These calculations give us the equilibrium volume and cohesive energies and are used to develop MEAM model.

Energies of Recoils in Pure Fe. The recoil-energy spectrum of Primary Knock-On Atoms (PKAs) was computed for a pure Fe material bombarded by 800-MeV protons. Computation on the recoils was accomplished using MCNPX. The recoil information from MCNPX was extracted from the HISTP file. The results of the computation are shown in Fig 3.3.3.

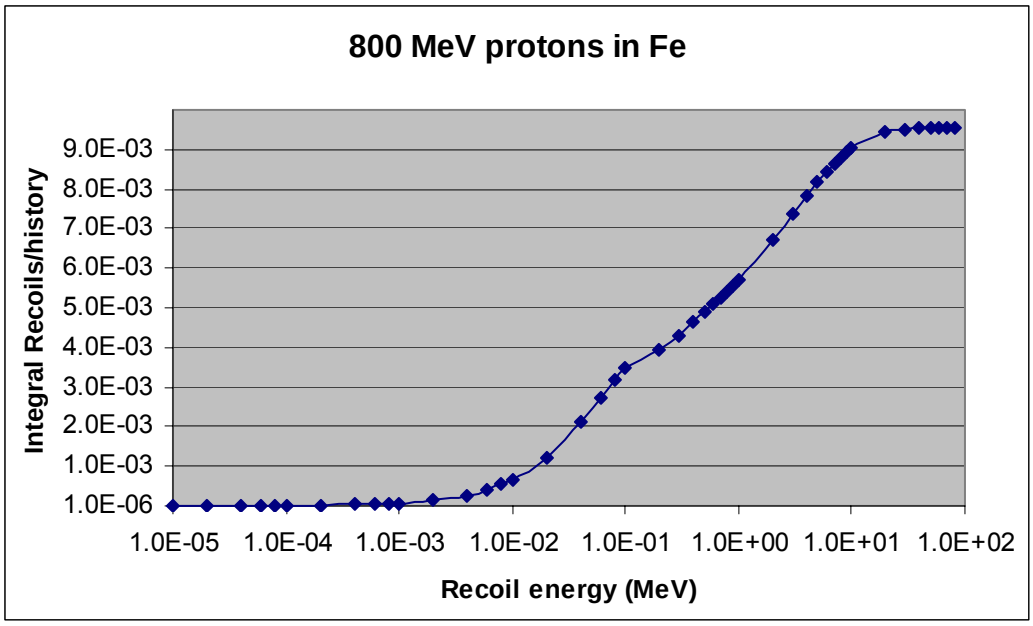

Fig. 3.3.3. Integrated recoil spectrum on 800-MeV protons on Fe.

The results indicate that the average recoil energy is greater than 3 MeV. These results are intended to feed into the evolution of damage cascades in molecular dynamics modeling. These results are consistent with previous computations of spallation recoil-energy spectra.

3.4 Coolant Technology

3.4.1 Coolant Technology Objectives and Scope

The major objective of lead-bismuth eutectic (LBE) research activities is to develop a fundamental understanding of LBE performance parameters and measurement techniques when used as a nuclear coolant, with primary emphasis on spallation-target applications. Specific activities include continued oxygen sensor development and calibration, corrosion modeling for transients, and transient reactor analysis code (TRAC) modeling of DELTA Loop thermal hydraulics.

3.4.2 Coolant Technology Highlights

- The oxygen-sensor assemblies were modified to provide sufficient force on the graphite gasket seals, and subsequently tested in a pressurized chamber. Three of the modified assemblies were installed in the DELTA Loop.
- The DELTA Loop was operated at 450^{o}C (or higher) for >120 hours, including unattended overnight runs. All oxygen sensors showed consistent readings and good agreement to the theoretically predicted temperature coefficient; there was good stability after repeated thermal transients.
- Oxygen sensors indicated excessive amounts of oxide present in the DELTA Loop due to many hours of operation without hydrogen cleaning. The melt tank was opened up and manual scooping of the oxide from the melt surface was performed.
- LBE Technology: We completed the design of the new oxygen sensor and high-temperature materials test stand.
- We started modeling of the oxidation kinetics of structural materials in oxygen-controlled LBE.
- We updated the DELTA Loop TRAC model to track trace species of oxygen and iron solutes and performed a pre-test natural-circulation calculation for DELTA.
- We hosted a group of KAPL researchers at LANL and presented the status and development plan for LBE nuclear coolant technology.

3.4.3 Coolant Technology Technical Summary

DELTA LOOP OPERATIONS

Initial Operations. Initially, oxygen sensors leaked during runs in preparation for loop conditioning. Also, lead-bismuth penetrated the seal between the ceramic element of the sensor and its stainless-steel retaining ring. We examined the sensor design and determined that the sealant was inadequate and the sensor body did not provide sufficient force to compress a gasket to maintain the seal. The sensor body was quickly redesigned to provide proper loads on the sealing surface. Graph-lock and tantalum were proposed as the gasket material (Graph-lock is a laminated graphite gasket material made by Garlock Company). This material was used elsewhere on the loop and performed well. Tantalum is a relatively soft metal that can withstand

high temperatures. Other proposed sealing methods were Helicoflex seals by Garlock and high temperature sealants and glues. Figure 3.4.1 shows the ceramic sensor element with the gasket on it and the stainless-steel sheath with the seating ring that must seal against the ceramic.

Fig. 3.4.1. Ceramic oxygen sensor element with a Graph-lock gasket and the stainless steel sheath with the seating ring.

We tested Graph-lock and tantalum gaskets in the new sensor design under necessary compressive loads. A special test vessel was constructed in which the sensors were tested under pressures up to 170 psig at up to 450°C (see Fig. 3.4.2).

The assembled oxygen sensors are shown in Fig. 3.4.3. The two parts of the sensor are screwed together until the load needed at the gasket between the ceramic element and its steel seating-ring is achieved. Three oxygen sensors were replaced in the loop and operations commenced to test them. All four sensors, including the one that functioned properly and was not replaced, had good readings consistent with the theoretical predictions.

We conducted over twenty tests with various gaskets, internal spring designs and test conditions. The conclusion was that the immediate available solution for the oxygen-sensor sealing problem is a graphite gasket with a seating load of about 200 lbs. The tantalum gaskets did not hold the helium pressure even when the calculated sealing load was applied. However, tantalum will be investigated further as it might provide a better long-term solution.

The loop was operated up to 450ºC for >120 hours after the sensors were installed, including unattended overnight runs. The sensor readings stayed consistent.

Fig. 3.4.2. Pressure test vessel for oxygen sensor seal tests.

Fig. 3.4.3. Assembled oxygen sensors.

The oxygen sensors showed that the LBE in the loop was saturated with oxygen and contained a significant amount of oxides. We started the liquid metal cleaning process but the oxides continued to replenish the oxygen content of the liquid metal. To accelerate the cleaning process, we manually cleaned the solid oxides from the liquid metal. Because this operation involved opening the large melt tank with the liquid metal inside, a special Hazard Control Plan was written. An industrial hygienist observed the operation and took air samples. The workers wore respirators. A picture of the surface of the liquid lead-bismuth with visible solid oxides can be seen in Fig. 3.4.4. A bucket with the slug removed is shown in Fig. 3.4.5.

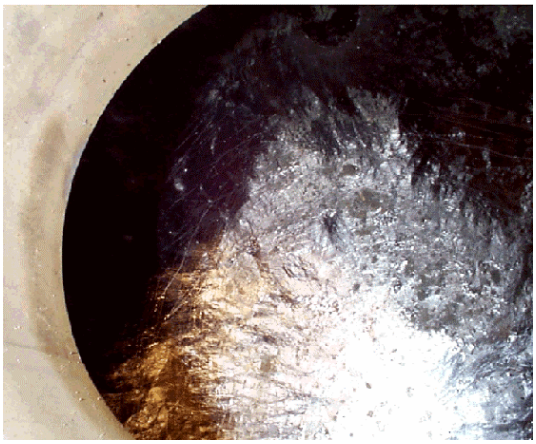

Fig. 3.4.4. Surface of the liquid lead-bismuth with the oxides.

Fig. 3.4.5. Solid oxides removed from the liquid metal surface.

The H/He cleaning-gas mixture was injected into lead-bismuth for >20 hours. The first long-term operation with the gas injection, however, showed that the liquid metal flow reduced significantly over just several hours. We suspected that the normal loop flow path allowed the entrapped gas to be released on volume expansion of the recuperator, creating a bubble of gas that caused a "plug" in the piping and reduced the flow of the liquid. We reconfigured the loop to bypass both the recuperator and the heat exchanger and made the highest point in the flow the expansion tank, through which the gas could escape from the free surface and be vented using the loop gas system. This solution worked very well; and, along with manual oxide removal, it allowed us to significantly reduce the amount of oxygen in the liquid metal. All of the oxygen sensors showed change in the oxygen content, as can be seen in Figs. 3.4.6 and 3.4.7.

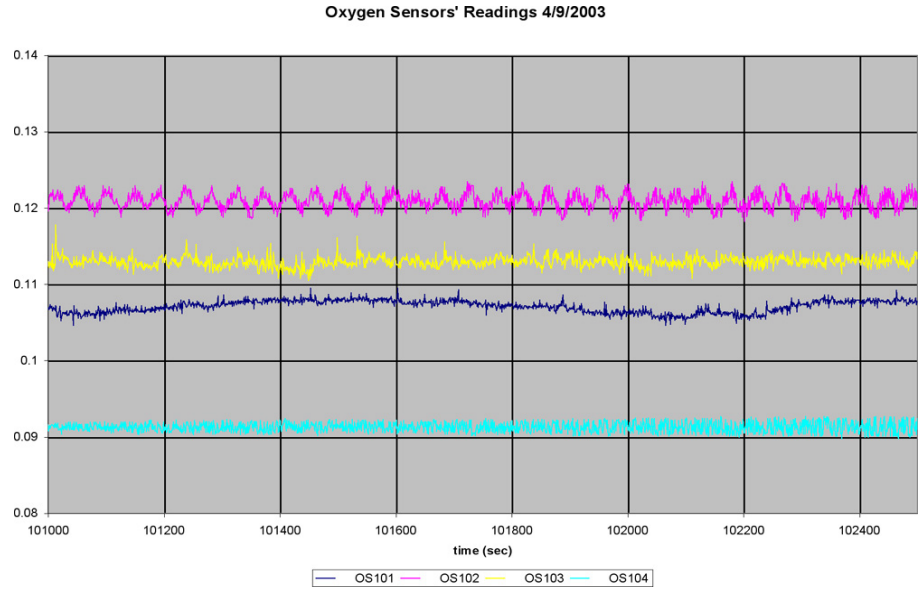

Fig. 3.4.6. Oxygen sensors readings before cleaning.

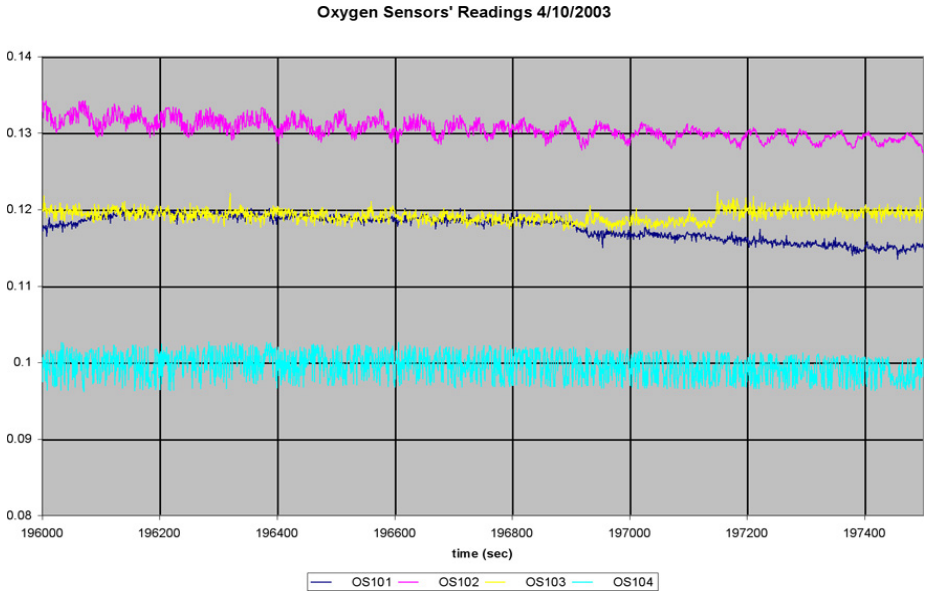

Fig. 3.4.7. Oxygen sensors readings after cleaning.

The material samples are loaded in the holder and will be installed as soon as the liquid metal content is reduced to nominal. The oxygen sensors should read between 0.2–0.24 volts (currently 0.12 volt on average). If regular cleaning by hydrogen gas injection takes a long time we may have to consider using solid materials serving as "getters" of oxygen in the liquid metal in the melt tank to reduce oxygen content manually.

LBE TECHNOLOGY DEVELOPMENT

Oxygen Sensor Development and Calibration. In order to improve oxygen sensor test capability in range, simultaneity, and accuracy, add higher-temperature-materials test capability, and improve safety, a new test stand was designed. The stand, shown in Fig.3.4.8, consists of a ceramic crucible that functions as an LBE/Pb container, an induction heater, a motorized ceramic stirrer, and a stainless-steel containment vessel with multiple sensor ports and gas lines. This stand will allow us to screen materials for LBE compatibility at temperatures of up to 800ºC.

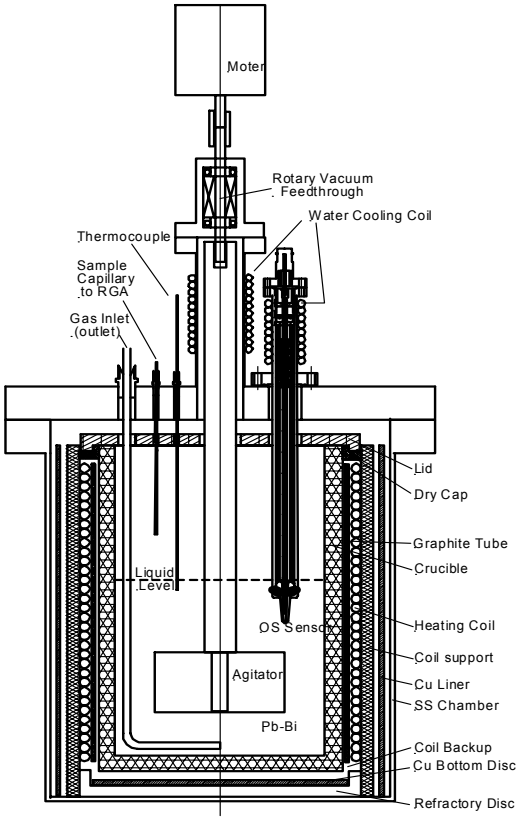

Fig. 3.4.8. Cross-sectioned view of the test stand design

Corrosion Model. To benchmark the performance of our kinetic corrosion model, we calculated the corrosion/precipitation profile for the pure lead natural convection loop (fig. 3.4.9) set up by Sannier & Santarini.[23] In the experiment, the samples were installed in the highest temperate leg. The authors found that the corrosion depth for steel 10 CD 9-10 is between 75-110 μm after 3000 hours and for Z 10 CD Nb V 92 steel is between 25-40 μm after 2800 hours. The present model

[23] Journal of Nuclear Materials, 107(1982), 196

predicts an iron corrosion depth between 40-70 μm after 3000 hours. The deviations are probably due to experimental uncertainties and alloy composition effects.

The current model has improvements over the sectioned model by Sannier & Santarini because it removes some non-independent assumptions (e.g., a constant thickness for the mass diffusion boundary layer).

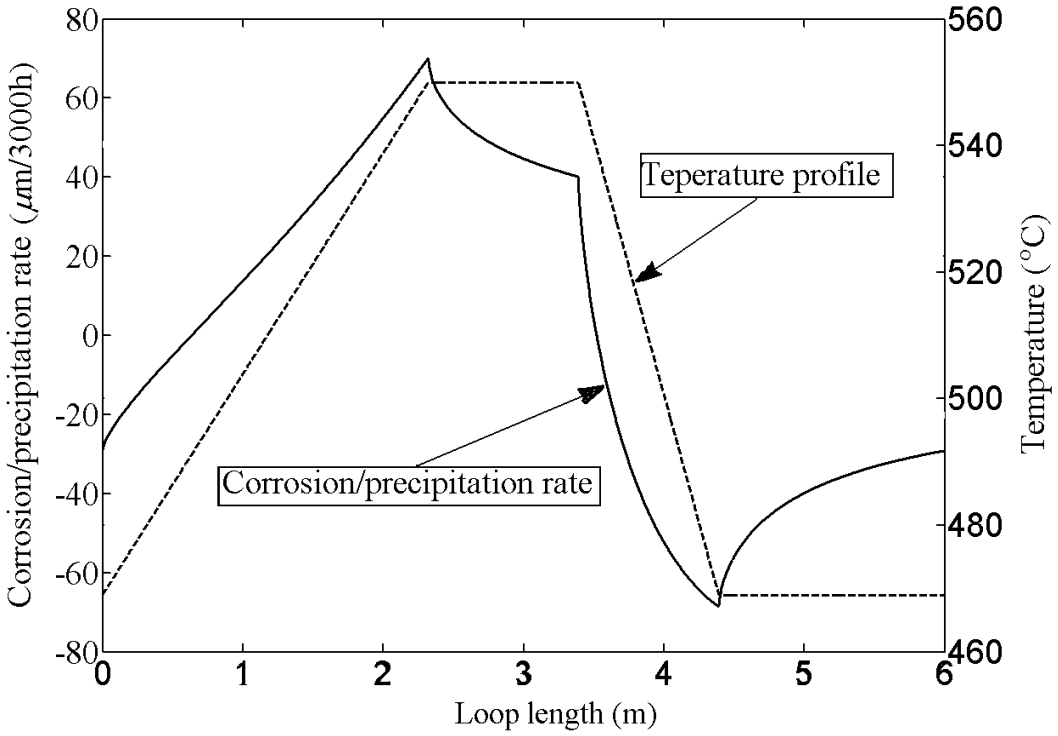

Fig. 3.4.9. Calculated corrosion/precipitation rate for a pure lead loop with its temperature profile.

Oxide-Growth Modeling. We initiated a study on surface-oxide growth in LBE systems. An oxide-growth model has been developed for a pure-metal case. It is assumed that the depth of the oxide layer growth and the consumption depth of the metal obey the parabolic law and can be written as: $X = 2\gamma_1 (D_O^{ox} t)^{1/2}$, $Y = 2\gamma_2 (D_O^{ox} t)^{1/2}$. We are studying the parametric dependence of the growth constants γ_1 and γ_2. Some results are shown in the following figures (figs. 3.4.10 – 3.4.13). This model will be used to study the oxide growth on iron, chromium and metal alloys.

Notation:

γ_1	Liquid metal corrosion constant.
γ_2	Oxide growth constant.
N_O^b	Mole fraction of the oxygen in the bulk LBE.
N_O^{III}	Mole fraction of the oxygen at the LBE-oxide surface.
N_B^{III}	Mole fraction of the metal B at the LBE-oxide surface.
υ	Stoichiometry of oxygen and metal B in the oxide BO_υ
D_O^{LBE}	Diffusion coefficient of oxygen in LBE.
D_O^{Ox}	Diffusion coefficient of oxygen in the oxide.

D_B^{LBE}	Diffusion coefficient of the metal in LBE.
m, V, ρ	Gramme-molecular weight, the atom/molecular volume and the density.
u_1	$=V_B/V_{BO_\upsilon}$
u_2	$=m_B/m_{LBE}$
β_1	$=(D_O^{ox}/D_O^{LBE})^{1/2}$
β_2	$=(D_O^{Ox}/D_B^{LBE})^{1/2}$

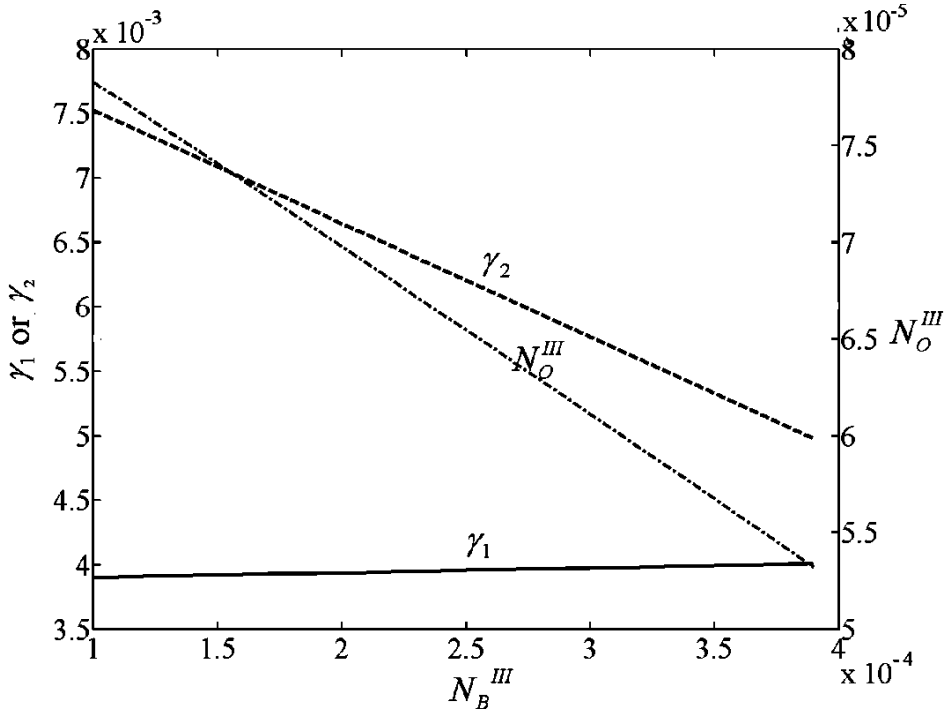

Fig. 3.4.10. Effects of N_B^{III} on γ_1, γ_2 and N_O^{III} for $\beta_1 = 0.1$, $\beta_2 = 0.1$, $u_1 = 0.46$, $u_2 = 0.78$, $\upsilon = 4/3$ and $N_O^b = 10^{-3}$.

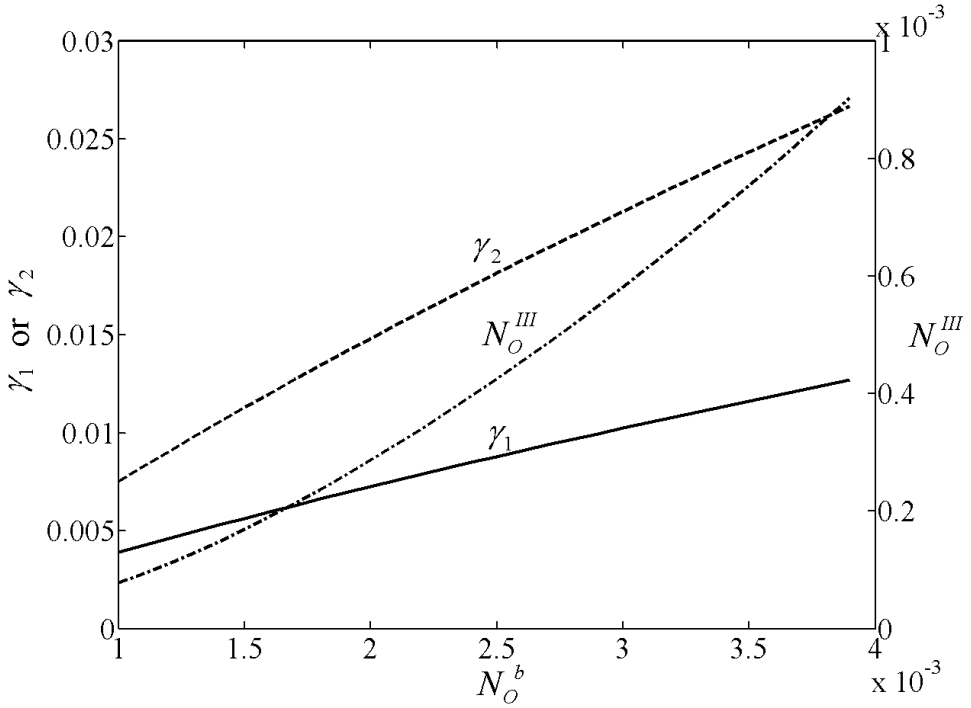

Fig. 3.4.11. Effects of $N_O{}^b$ on γ_1, γ_2 and $N_O{}^{III}$ for $\beta_1 = 0.1$, $\beta_2 = 0.1$, $u_1 = 0.46$, $u_2 = 0.78$, $\upsilon = 4/3$ and $N_B{}^{III} = 10^{-4}$.

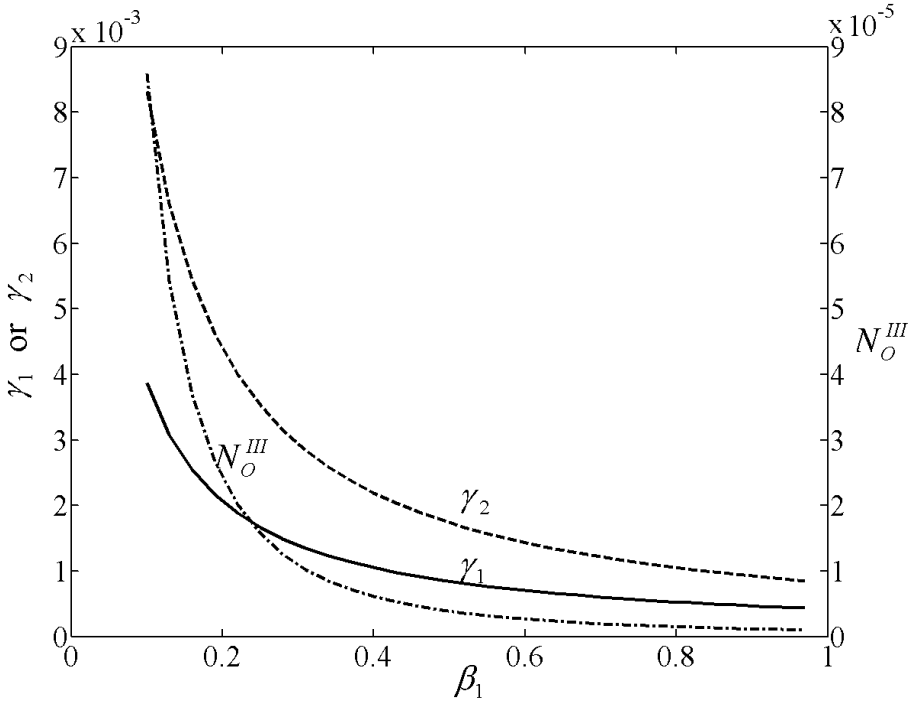

Fig. 3.4.12. Effects of β_1 on γ_1, γ_2 and $N_O{}^{III}$ for $\beta_2 = 1.0$, $u_1 = 0.46$, $u_2 = 0.78$, $\upsilon = 4/3$, $N_B{}^{III} = 10^{-4}$ and $N_O{}^b = 10^{-3}$.

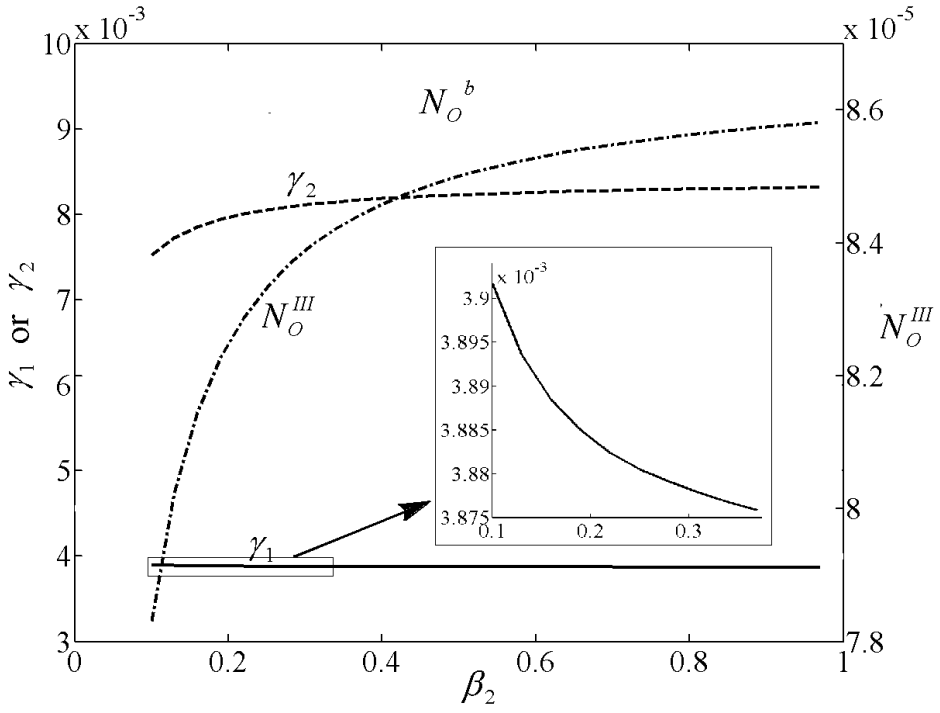

Fig. 3.4.13. Effects of β_2 on γ_1, γ_2 and $N_O{}^{III}$ for $\beta_1 = 0.1$, $u_1 = 0.46$, $u_2 = 0.78$, $\upsilon = 4/3$, $N_B{}^{III} = 10^{-4}$ and $N_O{}^b = 10^{-3}$.

TRAC Modeling. The DELTA Loop TRAC model was updated to track trace species of oxygen and iron solutes. The TRAC code was updated to provide a smoother heat-transfer calculation in the LBE intermediate coolant channel, which together with the adjacent heat structure components in the DELTA Loop model were re-noded back to the original nodding, and the steady state was recalculated. The TRAC code was corrected for errors in the plotting of the trace species elements.

Two pretest prediction calculations were performed. For the first pretest calculation, the DELTA Loop model was modified to simulate a test run for which the heater section outlet temperature was 500°C and the heat exchanger outlet temperature was 400°C. The TRAC calculation showed that these conditions could be met with a heater power input of 54.76 kW and a pump mass flow of 16.2 kg/s.

The second pretest prediction calculation was a natural-convection test run. Starting from the flow conditions of the 500°C/400°C calculation, we determined what the natural convection-flow conditions would be for the case in which the pump is bypassed, the heater section power is maintained at a power of 54.76 kW, and the heat exchanger heat-removal rate is controlled to maintain the heat exchanger outlet temperature at 400°C (673° K). The flow is assumed to still pass through the recuperator tube side. The TRAC calculation showed that a natural convection mass flow of 2.63 kg/s could be maintained. This corresponds to a flow velocity of 0.468 m/s through the test section. Calculated results for both pretest calculations are shown in Table 3.4.1.

Table 3.4.1. Calculated Results for DELTA Loop TRAC Model Pretest Calculations

Calculated Parameter	500°C/400°C Test Case	Natural Convection Flow Test Case
Heater section power	54.76 kW	54.76 kW
Pump total mass flow	16.2 kg/s (25.1 gpm)	N/A
Test section mass flow	11.26 kg/s (17.65 gpm)	2.63 kg/s (4.13 gpm)
Test section flow velocity	2 m/s	0.468 m/s
Sump tank temperature	670.4 K (397.2°C)	N/A
Recuperator shell-side inlet temperature	668.4 K (395.2°C)	N/A
Recuperator shell-side outlet temperature	741.7 K (468.5°C)	N/A
Recuperator shell-side ΔT (T_{out} - T_{in})	73.3°C	N/A
Heater section inlet temperature	740.1 K (467.0°C)	664.9 K (391.8°C)
Heater section outlet temperature	773.5 K (500.4°C)	808.1 K (535.0°C)
Heater section ΔT (T_{out} - T_{in})	33.4°C	143.2°C
Recuperator tube-side inlet temperature	771.1 K (498.0°C)	797.4 K (524.3°C)
Recuperator tube-side outlet temperature	697.0 K (423.8°C)	793.2 K (520.0°C)
Recuperator tube-side ΔT (T_{out} - T_{in})	-74.1°C	-4.3°C
Heat exchanger inlet temperature	696.6 K (423.4°C)	791.1 K (518.0°C)
Heat exchanger outlet temperature	673.0 K (399.9°C)	672.0 K (498.8°C)
Heat exchanger ΔT (T_{out} - T_{in})	-23.6°C	-119.1°C
Heat exchanger heat removal rate	37.48 kW	44.23 kW
Piping external heat losses	17.28 kW	10.53 kW
Secondary side water mass flow	1.42 kg/s (22.5 gpm)	1.42 kg/s (22.5 gpm)
Secondary side water inlet temperature	295 K (21.8°C)	295 K (21.8°C)
Secondary side water outlet temperature	301.3 K (28.1°C)	302.4 K (29.3°C)
Secondary side water ΔT (T_{out} - T_{in})	6.3°C	7.4°C

Technical Papers. The following papers have been accepted and/or submitted for publication in archival journals and conference proceedings:

"Parametric Study of a Corrosion Model Applied to Lead-Bismuth Flow Systems," by J. Zhang and N. Li, accepted for publication in *Journal of Nuclear Materials*.

"Improved Application of Local Models to Steel Corrosion in Lead-Bismuth Loops," by J. Zhang and N. Li, accepted for publication in *Nuclear Technology*.

"Analytical Solution on the Transient Corrosion and Precipitation in Closed Loop Flow System," by J. Zhang and N. Li, submitted to *Corrosion*.

"Oxygen Sensor Calibration for LBE Coolant Chemistry Control," by N. Li, W. Hang and T. Darling, and "Modeling Corrosion in Oxygen Controlled LBE Systems," by N. Li and J. Zhang, published in the Proceedings of ICONE-11 (4/2003), Tokyo, Japan.

"A TRAC Model of the Los Alamos National Laboratory DELTA Loop Facility," by J. Lime et al., and "A Kinetic Model on Corrosion/Precipitation in Lead-Bismuth Eutectic Flow Loop," by J. Zhang, N. Li and C. Chao, submitted for the proceedings of AccApp'03 (6/2003), San Diego, CA.

UNIVERSITY RESEARCH

University of Illinois, Urbana-Champaign. We extended the contracts with the University of Michigan for irradiation of materials with pre-implanted hydrogen, and with University of Illinois, Urbana-Champaign, for corrosion probe development for an LBE system (Phase II).

University of Florida. The University of Florida (UF) and the University of Michigan (UM) are collaborating in an effort to assess the effects of irradiation on the oxidation of structural steels ("The Influence of Radiation on Passivating High Temperature Oxides"). Specifically, irradiation exposures have been planned and will be conducted at UM's ion-beam facility. Two irradiations will be conducted with the focus on the HT-9 stainless steel. The samples will be irradiated with a 3.2 MeV proton ion beam at an irradiation temperature of 360ºC to a dose of one dpa. A 35–40-μm thick damage layer forms as the result of irradiation with the selected beam energy and irradiation temperature. The samples are 20 mm x 4 mm x 1.5 mm (flat bars), which are compatible with UM's existing irradiation stage. Irradiated samples will be analyzed by electron microscopy and other physical measurements at UF. Irradiations are currently awaiting the completion of machining of specimens.

Oxidation studies have been modified to include a non-isothermal component. Irradiated specimens will be oxidized in air and will first be heated non-isothermally at 8ºC/min (480ºC/hr) then isothermally heated for 48 hours at 300ºC, 400ºC, 500ºC, and 600ºC. These samples are divided in to two groups. Group A includes samples that are first irradiated then oxidized following the procedure mentioned above, while Group B includes samples first oxidized following the same procedure then irradiated. The non-irradiated specimens will be divided into two groups depending on the selected oxidation process. Group C1 will follow the oxidation procedure mentioned above, while group C2 will be subjected only to the isothermal part.

Initial thermal gravimetric analyses (TGA) on two SS-316L and three HT-9 stainless-steel samples were performed. All samples were polished to 600 grit on both sides of the flat bar and oxidized in lab air. The HT-9 samples were isothermally oxidized at 500ºC for 12 hours and 600ºC for 48 hours. One of the SS-316L samples was isothermally oxidized at 800ºC for 45 hours. The second SS-316L sample was non-isothermally heated at 10ºC/min to 800ºC then held at this temperature for 6 hours. All the samples were physically inspected and no surface oxidation was observed. The data obtained from the TGA were unexpected and deviate from expected oxidation behavior.

3.5 Accelerator-Driven Systems (ADSs)

3.5.1 Accelerator Driven Systems Objectives and Scope

To simulate the physics and dynamic behavior of Accelerator-Driven Systems (ADSs) and to support their design, coupling experiments must be performed. Work is being carried out on the MUSE experimental program at the MASURCA zero power facility at the Cadarache French Research Center, and on TRADE, the proposed experiment of ADS dynamic behavior simulation, to be run at the water-moderated TRIGA reactor of the Italian Casaccia Research Center. The MUSE program is a series of experiments carried out at CEA (since 1995) to study the neutronics of ADS. One scope of the work consists of providing high quality experimental data by assisting CEA in conducting critical and subcritical experiments of the MUSE-4 configuration. We also assist in coordinating the TRADE experiment for experimental techniques development and for neutronic design in support of experimental planning.

International support and collaboration is a strong part of the ADS research conducted under transmutation science, and a major collaborator is CEA in France. However, this collaboration is defined at the basic research level, and there are no tasks specifically conducted or funded in support of CEA's efforts. Some tasks are specifically funded in support of the MEGAPIE Project at Paul Scherrer Institute (PSI) in Switzerland.

3.5.2 Accelerator Driven Systems Highlights

MUSE Highlights:

- The first technical committee meeting of the MUSE experimenters was held at Cadarache and a new schedule was proposed.
- Experiments have begun at Cadarache using the GENEPI accelerator on the first subcritical configuration (SC0, about –500 pcm) of the MUSE4 program. Dynamic measurements have commenced.
- ^{235}U-fission radial traverses (EW and NS) of the MUSE4 critical configuration have been calculated and compared against experimental results, with all traverses showing good agreement with calculations in the margin of the measurement uncertainty.
- For validation purposes, the methodology for taking spectrum transient reflector effects (used for the MUSE4 analysis) was applied to the analysis of the Purdue University Fast Breeder Blanket Research Program, generally showing no energy group effect.
- Investigation of reflector effects of configurations similar to the MUSE experimental setting continued using macrocell calculations for the cross-section generation. Results indicate a large improvement compared to standard methodology.

TRADE Highlights

- A TRADE technical coordination meeting was held in Karlsruhe in January, resulting in agreement (after technical discussions) on the major characteristics of the TRADE target.
- The report on the first experimental campaign of Phase IA of the TRADE program was drafted.

- The TRIGA reactor core to be used for TRADE has been analyzed using the DIF3D and MCNP codes in hexagonal geometry. Different configurations were considered and compared with the previous MCNP calculations using the real TRIGA reactor geometry, and reaction rates distributions using the VARIANT code were generated.

International Collaboration Highlights:

- For the Organization For Economic Co-Operation And Development / Working Party on Partitioning and Transmutation (OECD/WPPT), LANL staff drafted the Introduction, and the Functions and Requirements chapters for the state-of-the-art report on Accelerator Utilization and Reliability for Transmutation. LANL staff also developed an outline for the accelerator sections of the report.
- LANL staff attended the Accelerator Utilization and Reliability Subgroup (AURS) and WPPT meetings in Paris, where writing assignments for the above-mentioned report were made, and where working-group charters for LBE Technology and Accelerator Reliability were completed and memberships were established.

MEGAPIE Highlights:

- A second target detailed design review (DDR2) was held because not enough documentation was available to complete the first review. Review of target drawings and available documentation, in advance of "Readiness For Manufacturing" (RFM) was the major activity of this quarter.
- The Heat Removal System (HRS) was also a major focus. A detailed final review of design and documentation was conducted and completed. Procurements and manufacturing are under way.
- Construction of the Integral Test Stand structure was completed.
- The cover gas system operation strategy is being reviewed and refined. Options of continuous venting and periodic venting are being evaluated.
- DOE contributions for this reporting period included:
    - Continued development on the TRAC model, which now includes an oil coolant side and a full secondary heat exchanger;
    - Participation in the HRS readiness review process;
    - Preparation of the absorber tests;
    - Initiation of a reliability study, starting with preliminary assessments of high-risk components such as the window, pump, guide tube, and heat exchanger;
    - Experiments on Oil/LBE interaction completed, with results indicating no adverse effects;
    - Participation in the target design review process; and
    - Analysis of the flange on the upper part of the guide tube—a unique, custom part in which different materials and components are joined.

3.5.3 Accelerator-Driven Systems Technical Summary

MUSE (ANL)

Problems with the GENEPI ion source filaments were corrected with the installation of new hardware. Beam tests were performed with satisfactory results, allowing measurements in the SC0 configuration (about –500 pcm) with a tritium target to begin. Because the intensity is so much greater with the DT source relative to DD, we are having some problems with unplanned shutdowns. This is primarily due to exceeding the allowed doubling time in the reactor due to rapid rises in GENEPI output. The control system of GENEPI is being modified to alleviate this problem.

The first technical program committee meeting was held in January at Cadarache. Participants from CEA, SCK/CEN, ISN Grenoble, Delft University, CIEMAT, PSI, and ANL attended, representing the major experimentalists. Detailed planning for the SC0 phase was completed, as was some planning for the SC2 phase.

During March, the transition was made from the SC0 configuration (-80 pcm) to the SC2 configuration (-3000 pcm nominal). This configuration will be studied until mid-July, with the great majority of experiments using the tritium target. About 1 week of dynamic measurements with the deuterium target will be performed at the end of the SC2 phase. At this time, it appears that there will not be enough time to perform measurements in the SC3 (-5000 pcm) configuration with the deuterium target; however, there are still plans to study an SC3/lead configuration in late fall.

Many dynamic and static data have been taken and stored during these phases of MUSE. There is a manpower problem, which is creating a delay in preparing the data for distribution outside. The californium traverses in the reference configuration will be released very shortly, followed by the reaction rate traverses. In spite of these delays, the experimental team has jointly drafted a lengthy paper for *Nuclear Science and Engineering* describing the early static and dynamic measurements.

Analysis Activity. ^{235}U-fission radial traverses (EW and NS) of the MUSE4 critical configuration (1115 cells) have been calculated. In Fig. 3.5.1, comparison with experiment results are shown for the NS (North-South) radial traverse. All the traverses show good agreement with calculations with the margin of the measurement uncertainty. For the NS traverse, a 2.5-cm translation is suspected. A good agreement between calculation and experiment is found also in proximity to the reflector. In the case of the NS traverse, this agreement decreases because of the proximity to the void region.

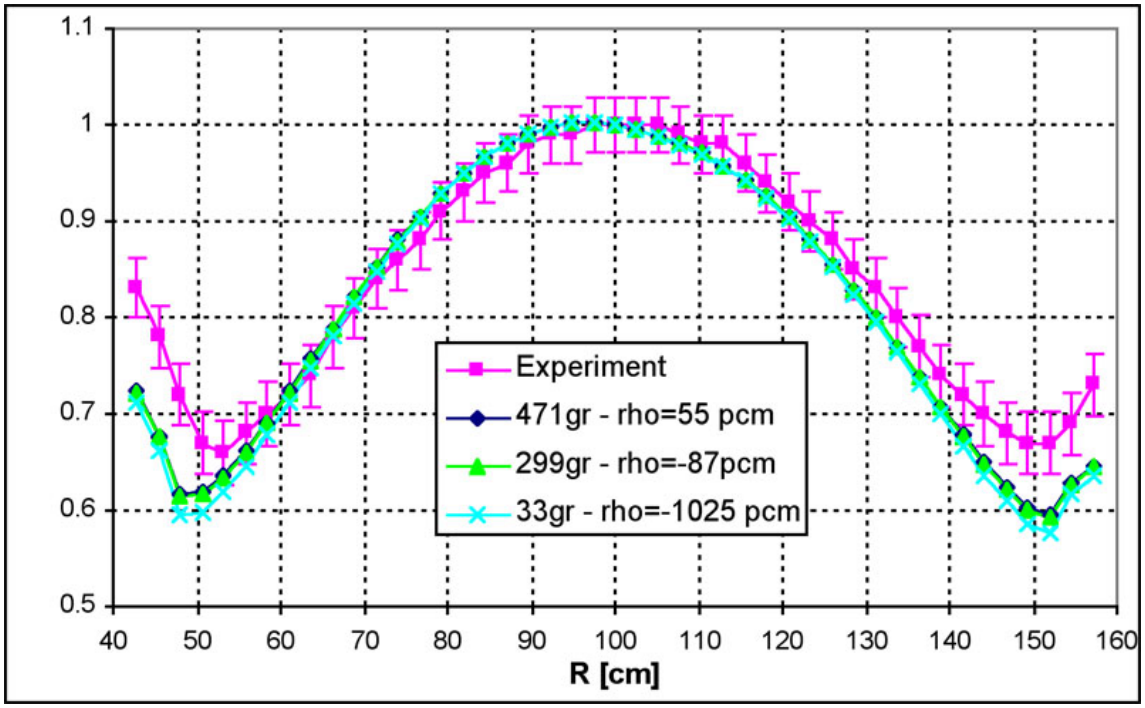

Fig. 3.5.1. MUSE4 REF – ^{235}U Radial Traverse NS

In the frame of the analysis of the effects at the core/reflector interface (mainly related to the reaction rate distribution), we have investigated the experimental results of the Purdue University Fast Breeder Blanket Research Program.

This experimental program was devised to measure integral neutron capture and fission rates and differential neutron spectra in the blanket region of the Fast Breeder Blanket Research Facility (FBBRF), a source-driven facility designed to simulate the transport of neutrons and gamma rays in a fast reactor blanket. Three blanket loadings were investigated during the measurements, for which the blanket was fueled with natural UO_2 rods with a pellet diameter of 13.9 mm.

The measured reaction rates were compared with the reaction rates obtained with a typical 2-D transport calculation using the ERANOS code system. The cross sections were processed with the ECCO code using the JEF2.2 data library. In order to study the impact of the number of energy groups on the calculated values, different group structures (33, 299 and 471 groups) were generated via condensations from a preliminary fine-step-cell calculation (1968 groups).

Contrary to the case of having a reflector around the core, we found that the reaction-rate distributions do not seem to be affected by the energy group numbers.

Calculations vs. experiment results compared quite well for all traverses. In particular, the agreement was excellent for all actinides fission rates. For some distributions, such as ^{197}Au and ^{186}W capture rates, discrepancies of some significance were observed inside the blanket region.

To define a standard calculational procedure that takes into account the transitional effects at the core-reflector interface in a fast reactor, a simplified 1-D model was investigated with a core radius of 39 cm and a reflector thickness of 30 cm. We observed that the spectral effects were significant not only in the reflector, but also in the core. In particular, at high neutron energy, there is a transitional zone at the interface that extends from 10 cm inside the core to 10 cm in the

reflector. At low energy, the regions involved seem to increase on both sides of the core-reflector interface.

The effects observed will certainly have an impact on the reactivity values, besides flux and reaction-rate distributions. In particular, we evaluated the dependence of this impact on the energy group number used in the spatial calculation. The traverses of adjoint flux, the ^{235}U fission rate, ^{238}U fission and capture rate, ^{237}Np fission rate and the ^{239}Pu fission rate have been the object of the present analysis.

ECCO Calculations. For this purpose, the cross-sections were processed with ECCO in three different ways: a standard calculation, a standard macrocell calculation, and a revised macrocell calculation. The standard ECCO calculation refers to a procedure that provides the cross sections for the core and the reflector regions separately, which are assumed as infinite media. A macrocell ECCO option allows a more rigorous coupled core-reflector calculation, for which cross sections are processed for both regions by weighting with the corresponding fluxes calculated for them (in this way, spatial effects at the core/reflector interface are properly accounted for during the processing of cross sections). Finally, the revised macrocell ECCO calculation makes proper use of the currents when needed (i.e., currents are used for condensation of higher moments of the cross sections).

Looking at the results of reactivity, adjoint flux, and reaction rate traverses obtained with different numbers of groups, we observed approximately the same effects with both the standard ECCO calculation and the standard ECCO macrocell procedure. For the reaction rate distributions, the most significant effects were found on the ^{235}U fission rate, ^{238}U capture rate, and ^{239}Pu fission rate traverses.

TRADE

Coordination. Several topics were presented, discussed, and agreed on at the January TRADE technical coordination meeting held in Karlsruhe, including the following:

1. The material of the TRADE target should be Ta, with forced-convection cooling to evacuate the power deposited by the proton beam, now upgraded to ~140 MeV.
2. Studies show a cost increase estimate of 10-15% to upgrade the accelerator to E=140 MeV, i=2mA.
3. Natural vs. forced convection studies performed at CEA seem to indicate the need to demonstrate experiments at significant scale to assess the critical flux on the target surface (experiments have been proposed by FZK).
4. The full burn-up history of the TRIGA fuel was reconstructed by the TRIGA team and distributed.
5. The beam transport line was redesigned to accommodate a possible upgrade of the beam characteristics.
6. Neutronics calculations of the benchmark were completed by CEA and deemed satisfactory. A hexagonal model is being defined by ANL.
7. Finally, calculations performed at CERN indicate that the beam energy increase from 110 MeV to 140 MeV will result in a factor of ~2 increase in n/p.

Experimental Activity. The final report on Phase IA experiments performed at Casaccia in November 2002, was released for distribution to the partners.

The delays in signing the MOU have directly caused delays in procurement of equipment needed to perform the next phase of experiments. At present, it appears that detectors and electronics will not be available until this fall at the earliest. The schedule will slip accordingly.

Analysis Activity. Work continued on the deterministic model for the TRIGA reactor. The use of the hexagonal model to analyze the TRIGA reactor is dictated by the eventual necessity to perform calculations of the dynamic behavior of the core.

Detailed hexagonal TRIGA geometry was used in our calculation, with assumptions made for the small voids in the pins of the loop, source, and rabbit (they were incorporated in the density of the structure).

For the cross-section calculation, we used the WIMS-ANL code to generate group cross sections for different compositions of the reactor fuel pins and control rods in the axial direction. As a first step, nine groups were chosen. To preserve the total actual amount of water, we adjusted the density of water in the whole reflector, taking into account the voids in the tangential and radial channels. Also, an 'average' for all fuel elements was used in the calculation of the cross sections with the WIMS-ANL code.

To check our results, we constructed an MCNP deck (Model 2) using the same geometry as for the DIF3D model (Model 1). Once again, an average fuel composition was used. The difference between the two models (Models 1 and 2) involves the calculation method and the fact that the DIF3D model (Model 1) uses homogenized cross sections as calculated by WIMS.

Previously, an MCNP calculation in mixed hexagonal-real geometry (Model 3) was carried out. In this calculation, the core itself was modeled with hexagons and the reflector and water tank were left intact (not replaced with hexagons, represented by a cylindrical layer). The deficiency of this model is that seven rows of the core's hexagons can not be fitted into the core vessel radius. Therefore, supplementary fractions of water-filled hexagon rows were added. Detailed fuel composition differing from element to element was used.

Finally, the reference MCNP model (Model 4) contained the actual geometry, both for the core and the reflector, also using the detailed fuel composition.

We studied the adjustment of the materials densities in the reflector and the influence of the method of adjustment. Neutronics of the core suggested that density adjustment using a 'layer-by-layer' method, starting from the closest to the core materials, was appropriate. Voids were taken into account in the adjusted layer densities. Appropriate hexagonal geometry was used to represent the layers of water, graphite, and lead in the reflector. Table 3.5.1 shows the results for the core configurations in which the control rods were in the 'up' position.

Table 3.5.1. Complete Reactor Configuration Results

Model	DIF3D (diffusion, hexagonal) *Model 1*	MCNP hexagonal *Model 2*	MCNP (mixed) *Model 3*	MCNP (real) *Model 4*
Config. 'up'	1.081717	1.07976 ± 0.14%	1.05571 ± 0.10%	1.05463 ± 0.12%

Using this approach, the MCNP hexagonal model (Model 2) gives an overestimated result as compared to the MCNP calculation in mixed (Model 3) and real (Model 4) geometries. However, the corresponding DIF3D result for diffusion (Model 1) is reasonably close to the MCNP hexagonal model. This was expected because: 1) it was previously proven that there is no significant impact produced by the homogenization procedure in WIMS, and 2) there is a complete parity of the geometry of the system in both cases. Although it is seen that the DIF3D result and the MCNP hexagonal model result are coherent, they differ significantly from the MCNP real and mixed geometry results. The adjustment of water using the 'layer-by-layer' technique did not significantly affect the results of the calculations. Therefore, one concludes that there exists a geometry/homogenization affect in the reflector that accounts for the ~2400 pcm of error. This effect must be related mostly to the absence of the reflector cover in the DIF3D calculation and local channels void effects, which are not possible to model in DIF3D, as well as the impossibility to correctly represent the reflector's components by hexagon layers. We also mention that the results for Models 3 and 4 were based on the detailed fuel compositions while Models 1 and 2 are based on average fuel composition. Our estimation shows that this effect accounts for ~400 pcm to decrease the k_{eff} of Models 1 and 2.

Finally we note that we also used the DRAGON code to compare the cross sections obtained with WIMS. The cross sections from both codes give consistent results when used in DIF3D.

DOE Contribution to TRADE

TRAC Model. The DTHT coolant loop has been modeled and coupled to the LBE target loop. Thus, the physical model is basically complete but must be reviewed for accuracy and completeness. We still must validate the model for the main control feature, the 3-way valve on the DTHT loop that allows for bypassing the secondary heat exchanger during beam interruptions.

LBE/DTHT Interaction Experiments. Short-term (2 hour) LBE/DTHT interaction experiments were conducted last fall, indicating no measurable interactions or gas production from either DTHT-only or DTHT-LBE mixtures at 350ºC. During this quarter, a one-week test of the oil-LBE mixture was conducted, and some net pressure rise was observed presumably due to pyrolysis of the DTHT. Subsequently, another DTHT-only "control" experiment was conducted showing a similar pressure increase. A report has been written and presented at the MEGAPIE Technical Review Meeting.

International Science and Technology Centre (ISTC) Target Design Presentation. At the last MEGAPIE Technical Advisory Committee (TAC) meeting, it was suggested that MEGAPIE take more advantage of past experience in high power LBE target designs, particularly the target produced under the ISTC 559 program (LANL was heavily involved in the design of this target). To better inform the PSI of the details of this design, a comprehensive presentation was made at a target design meeting. All material presented had appeared in the public forum at some previous time, so no proprietary agreements were compromised. MEGAPIE constraints on space and the upward beam orientation, however, minimize the possibility of incorporating many of the design advantages of this earlier target.

HRS Readiness Preparations. We contributed to the Heat Removal System (HRS) documentation and design review process and attended meetings to resolve all open issues.

Reliability Study. A system-wide component and subsystem reliability study was initiated. The plan is to itemize each component and instrument, list all failure modes associated with that element of the system, and assign a reliability coefficient for each failure mode. The reliability of the element is then the product of all independent failure mode reliabilities. Manufacturers data and expert opinion, with related documentation and references, will be used to substantiate the reliability numbers. The goal is to document the status of the design from a reliability standpoint, to document efforts to improve reliability, and to emphasize the components and failure modes that are most likely to limit the life of the complete system. Failure modes and mitigations for most target components have already been determined and sent to experts and responsible persons for comment and edification.

Target Design Review. We participated in the MEGAPIE design review of documentation and drawings of the target subsystems, in preparation for "Readiness For Manufacturing" (RFM). We attended extensive meetings and detailed discussions to identify open issues to be addressed before RFM.

Flange Analysis. The target is centered on a complex coupling that joins the target guide tube to the outer container, the pump, and the heat exchanger. Three flanges seal the various parts to this coupling, and all of these flanges are custom designs using the Helicoflex O-ring-type seal. These were evaluated as far as possible and a written document describing these joints was prepared and sent to Helicoflex specialists for their assessment. A leak at this location after manufacture and assembly would be a serious setback to the project. American Society of Mechanical Engineers (ASME) code analysis seems to indicate that one flange may be too thin and a second flange joint, which seals five separate tubes, may require a flatness that will be difficult to achieve at the location (pump bottom). The final decision should be based on an assessment and specifications by the Helicoflex specialists. The potential issue of neutron-induced stress relaxation of bolts has been resolved; the radiation damage at this location is not sufficient to cause this problem.

MEGAPIE

Project Status and Activity

Target. A second Target Detailed Design Review (DDR2) was held in February; however, a constructive review was not possible due to lack of sufficient documentation. Most seriously absent was the stress-analysis documentation. MEGAPIE licensing requires that the target be approved by a "notified body" (pressure vessel authority) to ensure that the target was designed to appropriate standards. Further, ATEA (the contracted manufacturing company) notes that the drawings are insufficient for manufacture due to mistakes and omissions.

Following the DDR2 review, existing documentation was delivered and an extensive re-review has been underway. An Open-Issues List (OIL) is being generated and these issues are being resolved. The process is time-consuming, resulting in a delay of the RFM with ATEA. It is the goal of the design team to release some subassemblies in time for manufacturing to start in April.

Significant redesign of the upper part of the heat exchanger appears to have reduced the cyclical stresses, eliminating the risk of fatigue failure. Given the importance of this component and the fact that stresses are in some locations very near the allowable stresses, an independent assessment by a numerical stress analyst should be seriously considered.

Ancillary Systems. The Heat Removal System has been released for manufacturing and the major components have been ordered. Delivery is scheduled in December 2003, but this will be moved up if possible. QA, acceptance procedures, and documentation requirements have been established and accepted by all parties.

The Cover Gas System has been in a state of flux in the interest of designing the most reliable and safest system. Hydrogen absorbers have been removed from the design based on new production rates calculated by E. Pitcher. Currently, the project is evaluating the options of continuous venting vs. periodic venting to a decay tank at 1–2 month intervals. Absorbers and cold traps are being considered for mercury and iodine, and tests are being planned.

The Fill and Drain System (FD&S) was delayed while the issue of whether to drain after irradiation was decided. PSI has decided to freeze the target in place, rather than drain, in spite of strong objections by the TAC and some of the collaborating partners, including DOE. A formal document explaining this decision was promised at the PCG meeting held last October, but this document has not been seen. The next meeting with ENEA to restart the F&DS activity will be in April.

3.6 LANL-Sponsored University Programs

University support is an important part of the AFCI Program. In addition to the general university programs run by DOE-HQ, a number of universities are supported directly by programmatic funds to provide technical assistance to the AFCI Program. Universities that LANL supports include University of Michigan, UC-Berkeley, UT-Austin, North Carolina State University, University of Illinois at Urbana-Champaign, Georgia Institute of Technology, University of Florida, Imperial College of London, and Arizona State University.

University of California – Berkeley (UCB)

Scope: provide technical support to Systems Analyses and Transmutation Science teams via defined tasks, coordinated through the AFCI Program leads as follows:

- Benchmark the simple model for fuel-cycle analysis;
- Resolve the discrepancy with ANL on actinide built-up with cycles;
- Apply fuel-cycle analysis methods to compare design alternatives;
- Compare Na vs. LBE-cooled accelerator transmutation of waste (ATW);
- Assess ATW performance using molten salt and alternative (^{7}LiF-BeF_2);
- Assess ATW during approach to equilibrium using molten salt; and
- Perform optimization and analyses of a pebble-bed ATW system.

Highlights:

- UCB has identified seven research areas in which they are interested in contributing to the newly-organized AFCI Systems Studies program.
- The SCALE code package for transmutation calculations was installed and benchmarked against an NEA/OECD benchmark for Pu recycling in a pressurized water reactor (PWR). Results show good agreement, which increases confidence in SCALE for transmutation studies.
- An algorithm was written to correct a "bug" discovered in the MOCUP code regarding the branching ratio.
- We applied our simplified fuel-cycle analysis model to quantify the effect of the uncertainty in the Am-241-to-Am-242 branching ratio on the evolution of actinide concentration in an LBE-cooled transmuter.
- The evolution of the heavy metal inventory and composition in a typical LBE-cooled liquid-metal reactor (LMR) was established using UCB's multi-recycling simulation code, with a result showing that it will take ~20 cycles for the core to reach equilibrium composition.
- UCB developed an MCNP model for a full pebble for the analysis of pebble-bed transmuting reactors. The ability of MOCUP to perform depletion analysis for thousands of fuel kernels in a pebble was tested.

- UCB has proposed a methodology for quantifying the impact on the repository capacity of different transmutation options.
- Design of a reference finite-dimension molten-salt transmuting reactor continued, revealing two important results: 1) the total neutron leakage probability is small, consistent with previous assumptions, and 2) use of a graphite reflector flattens the radial-power density distribution across the core. To achieve optimal reflection, the intermediate heat exchanger should be displaced at least 60 cm from the core surface.

University of Michigan

Scope: provide technical support to Systems Analyses and Transmutation Science teams via defined tasks, coordinated through the AFCI Program leads as follows:

- Analyze coupled accelerator core dynamics with emphasis on k_{eff} predictions and control;
- Study LWR-based reactor transmutation for equilibrium cycles;
- Assess LBE slowing down spectrum and the associated cross sections;
- In collaboration with LANL, use proton irradiation to simulate spallation-neutron radiation damage in ADS to investigate the effect of higher gas production at significant doses, laying a foundation for a full-scale radiation campaign;
- Develop a detailed description of the irradiation campaign (temperatures, dose rates, doses, and He-implantation levels); and
- Conduct a single irradiation campaign (~240 hours of irradiation) on SS and T-91 at three dpa levels.

Highlights:

- We performed MC2-REBUS calculations to investigate the benefits of using a denatured thorium cycle in fast-spectrum reactors for transmuting Pu from LWR spent fuel.
- We established a PWR equilibrium cycle configuration using CASMO3-SIMULATE3 global calculations for typical UO_2 fuel to benchmark the corresponding CASMO3 assembly-level equilibrium cycle analysis.
- A plan was developed for the second irradiation of T-91 and HT-9, and material samples have been fabricated, machined and polished. Irradiation is scheduled for May 2003.
- For source-driven subcritical systems, a study is underway to formulate a functional definition of reactivity so that the deviation from criticality may be determined in various operating states.
- A physical interpretation of differences in the space-time behavior of the reactivity measured in different regions of a subcritical system has been obtained.

University of Texas – Austin

Scope: provide technical support to Systems Analyses and Transmutation Science teams via defined tasks, coordinated through the AFCI Program leads as follows:

- Model ADS to determine sensitivities to cross-section uncertainties;
- Develop a test plan and post-test analyses for cross-section measurements;

- Participate in cross-section measurements at LANSCE (Summer 2003);
- Incorporate time-dependence on the proliferation metrics development and analysis; and
- Develop the uncertainty-analysis methodology for the proliferation metrics, providing results to Systems Analyses.

Highlights:

- Visual coding using Visual Basic and the MS Visio software to create a user-friendly application for evaluating fuel cycles for proliferation-resistance assessments continued.
- Results for fuel-transmutation rates, fuel and structural-material isotopic compositions, decay heat, and radiation-damage rates to structural materials were generated using a full-core ADS simulation with MCNPX linked to ORIGEN. These results will be used in the future to analyze cross section values for LANL.

North Carolina State University (NCSU)

Scope: NCSU will calculate radiation damage (production of displacements, helium, hydrogen, and heavier transmutation products) and energy deposition in the target materials, containment structures, and entrance windows of the target assemblies (including Mark II and Mark III designs) for the SINQ spallation-neutron sources that are under design and development at the Paul Scherrer Institute (PSI). In addition, NCSU will examine less obvious (and less well studied) mechanisms for the transfer of energy to the irradiated materials and hence the production of displacements and will analyze the effects of the calculated radiation damage on mechanical and other property changes, assessing reasonable and safe lifetimes for radiation-damaged components.

Highlights:

- NCSU conducted a study of neutron flux and spectrum at SINQ Target 3 (target material, Zircalloy; coolant, heavy water) and SNS (target material, Hg; coolant, Hg) to compare radiation damage to materials at SINQ Target 5 (target material, Pb; coolant, heavy water).
- The transmutation yield of Si in the Al-alloy entrance windows of SINQ targets was calculated. Results indicate a production rate of about 0.01 at% Si per beam-on year, which is insignificant compared to the initial Si content.
- As part of the SINQ Target Irradiation Program (STIP III), MCNPX calculations were performed for transmutation-product yields in materials currently undergoing irradiation in SINQ Target 5 to assess the possible influence of transmutation products as impurities.

University of Illinois at Urbana-Champaign (UIUC)

Scope. UIUC will investigate impedance spectroscopy as a feasible method of measuring the effects and rates of LBE corrosion on structural materials. This impedance spectroscopy technique will use alternating electric currents of various frequencies to measure the electrical impedance of a surface corroded by lead-bismuth. They will collaborate with DELTA-Loop research members and construct a container/piping system to investigate those issues related to corrosion in high-temperature LBE. UIUC will construct an LBE loop (piping, pumps, thermocouples, heating elements, etc) at the Materials Research Laboratory (UIUC MRL), and

will conduct controlled experiments to take impedance spectroscopy measurements on corroding steel samples.

Highlights:

- Significant progress was made on the construction of the UIUC LBE corrosion facility (loop). We performed detailed design of cooling, gas, and thermal systems, and started fabrication of a ceramic (non-corroding) liner. We acquired the main components of the cooling and gas systems, purchased oxygen-sensing equipment, selected the metering system for gas delivery to control oxygen levels, acquired data-acquisition and instrument-control hardware and software for corrosion monitoring and control (assembled the computer system for controlling experiments), and acquired impedance spectroscopy hardware.
- We analytically modeled the impedance spectroscopy (IS) electrical circuitry to estimate experimental response for measuring oxide-coating growth *in situ* in LBE systems to optimize IS equipment.
- We reviewed current-impedance-measurement equipment to determine how best to reach the very high frequencies (>1 MHz) necessary to measure surface films.

University of Florida

Scope: measure effects of radiation damage on oxide coatings on structural materials in LBE-cooled systems to resolve critical corrosion issues. Collaborate with LANL to investigate issues related to coolant containment and coolant-induced corrosion of materials during irradiation in high-temperature liquid-metal systems by:

- Investigating the influence of radiation on the oxidation rate and the oxides formed on selected structural alloys, and
- Characterizing the oxide/substrate interface and the oxides formed after the irradiation process.

Highlights:

- We modeled and analyzed ions and beam parameters for irradiation studies.
- A calibration run for thermo-gravimetric analysis (TGA) was completed and specimens are being prepared. Baseline TGA, oxidation studies, and hydrothermal oxidation studies of HT-9 have begun.
- The ion beam facility at the University of Michigan was selected for irradiation of oxide layers on materials in LBE systems in relatively prototypical conditions. HT-9 samples have been machined, and irradiation on these samples will be conducted using a 3.2-MeV proton beam at 360ºC to a dose of one dpa.

University Projects Leader. Eighteen posters describing AFCI work-in-progress at various universities were presented at the AFCI Technical Review held in Albuquerque in January.

Several university contracts were extended (Michigan, Illinois, and NCSU). The Illinois contract was extended into Phase II to begin experiments on LBE corrosion studies, and a new PR was initiated for Michigan to begin a multi-year study of hydrogen and helium implantation in materials.

Collaborations continued for the University Consortium for Transmutation Research (UCTR) with UNLV, ISU, URA, and others, and plans were implemented for the April International Meeting on ADS System Technologies to be held at UNLV.

The LANL University Projects Leader, serving as Chair of the Technical Program Committee of the ANS AccApp'03, to be held June 1-5 in San Diego, completed the preliminary program with 175 papers (127 oral, 48 poster) and a diverse and distinguished plenary session followed by several special sessions. One of the oral sessions will be a memorial session on nuclear data in honor of Dr. Kazuo Shin of Kyoto University, whom we lost in an accident in 2001.

References

[1] M.I. Baskes, Phys. Rev. B. 46, 2727 (1992); B-J. Lee and M.I. Baskes, Phys. Rev. B 62, 8564 (2000).

[2] M.I. Baskes, Phys. Rev. B, 62, 15532 (2000).

4 SYSTEMS STUDIES AND ANALYSIS

4.1.1 Systems Studies and Analysis Scope and Objectives

Systems Analysis activity crosscuts the AFCI technical areas (Fuels, Separations, and Transmuters) and provides the tools and analyses to inform key decisions in the program. Systems Analysis also includes work related to the transmutation of radionuclides. The Systems Analysis activity is integrated between the Generation IV Program and the AFCI and coordinated with the Technical Integration function of each program. Currently the AFCI is focusing on Transmutation Systems Studies.

Transmutation Systems Studies provide a systematic analysis of the potential of existing and future reactor systems for transmuting transuranic elements and certain long-lived fission products. The first objective of transmutation systems studies is to develop a set of criteria for the candidate fuel cycle options. These criteria will allow an objective definition of the potential benefits of a candidate. The second objective of transmutation systems studies is to establish a systematic comparison between all candidate fuel cycle options available for transmuting key isotopes: each option will be evaluated for practicability, benefits and costs, useful implementation, and practical limits. The third objective of transmutation systems studies is to support detailed technical analyses of the most promising technologies to assess key feasibility issues and support their licensing case. For this fiscal year, the scope of work will include:

(1) Transmutation Criteria – Establish criteria for each operation in selected advanced nuclear transformation fuel cycles (e.g., recovery efficiency, decontamination factors, losses and their location in the flowsheet, waste form characteristics, plutonium/minor actinide burnup targets, etc.), taking into account: 1) technical feasibility, 2) cost/performance tradeoffs, 3) expected benefits, and 4) dynamic effects. These criteria will be integrated with detailed technology-specific criteria developed under the fuels and separations activities and iterated and refined in future years.

(2) Transmutation Options – The purpose of this task is to systematically assess transmutation system technology and implementation options. Results of previous transmutation systems studies will be synthesized and key programmatic systems inquiries will be answered. The primary activity for this year is a systematic analysis of PWR recycle strategies with a comprehensive review and assessment of extensive studies on multi-recycle, heterogeneous loadings (targets) and fuel (MOX, nonfertile, etc.) options.

(3) Transmutation Analyses – In this task, detailed fuel cycle analyses are performed to address key transmutation issues including reactor design and safety, fuel cycle impact of transmutation, and overall system performance. The main activity envisioned this year is to take a promising fuel cycle strategy (e.g., limited recycle of Pu+Np in a PWR) and develop a detailed system point design for Series One deployment. The more detailed assessment will illustrate the key reactor design and performance issues expected for Series One utilization and help identify key design constraints for Series One deployment. Work at ANL will focus on development of partial MOX loading scenarios to specify a preferred assembly design.

4.1.2 Systems Studies and Analysis Highlights

- To support the FY03 Report to Congress, a qualitative comparison matrix of reactor and advanced fuel cycle options was created. For the Generation-IV reactor concepts, safety, economics, and fuel utilization parameters were compared. Once-through, single and double tier transmutation, and thorium fuel cycle options were considered. Key repository performance impacts (e.g., volume, heat load, and dose) were rated. In addition, the fuel cycle and reactor facility requirements, life cycle costs, and repository savings were compared. Explanatory notes were provided for the specific attractiveness ratings. Similar materials were provided by the separations lead for comparison of spent fuel treatment technologies.
- ANL systems analysis personnel participated in the CEA/DOE Collaboration Meeting held in Washington D.C., January 14 and 15, 2003. Presentations were given on plutonium and TRU multi-recycling in PWRs and low conversion ratio fast burner reactor studies.
- Systems analysis experts also participated in the AFCI Semi-Annual Meeting held in Albuquerque during the week of January 20. Presentations were given on reactor-based transmutation studies, transmutation strategies for LWRs, and future plans.
- A Transmutation Systems Study Meeting was held at INEEL on February 4-5, 2003, to discuss short and long term activities under the following tasks: Transmutation Criteria, Transmutation Options, and Transmutation Analyses. The meeting was used to define and integrate the work scopes and responsibilities of each participating laboratory.
- A meeting of the Transmutation Criteria sub-group was held at ANL on March 24, 2003. Key questions requiring transmutation approach were discussed:
  - Should long-lived fission products be transmuted or converted to superior waste forms?
  - Is Pu+Np only to be burned in Series One reactors?
  - Is uranium disposable as Class C waste?
  - Is inert matrix fuel development required?
  - What fraction of Cs/Sr needs to be extracted from nuclear waste?
  - What fraction of minor actinides should be extracted from nuclear waste?
  - Is zero fission gas release during fuel processing achievable and reasonable?

  Participants were tasked to summarize and document the relevant issues and recommend specific transmutation criteria.
- Progress was made on the benchmark of the CEA COSI and NFCSim codes:
  - Completed the simulation of the benchmark scenario.
  - Transmitted the results to CEA for comparison.

- The criticality engine/ORIGEN2 burnup calculation driver was integrated into NFCSim, providing the capability to generate material balances for an arbitrary transient tier-1 scenario "on the fly."
- A detailed work plan for systemic inter-comparison of transmutation systems was developed. Both fast and thermal reactors using conventional and dedicated fuels will be considered. The work will summarize existing studies and quantify key physics parameters. A breakdown of the work between CEA and DOE for the ongoing collaboration was proposed.
- The behavior of Am-241 targets in a thermal spectrum was investigated in response to a DOE-NE inquiry. It was found that at typical PWR flux value, the Am-241 mass, by virtue of its high capture cross section, is reduced by about two orders of magnitude in about 10 years. The trend of the combined mass for Am-241, Pu-241, Np-237, and Cm-245 is quite similar, indicating a significant reduction of key daughter products (e.g., Np-237) that impact Yucca Mountain performance. However, it should be noted that significant increases in PWR uranium enrichment are required to meet the typical operational cycle length with such targets.
- A WIMS8 extended lattice (color-set) model has been developed for the analysis of partially loaded MOX cores of interest in the Series One System Point Design task. Preliminary qualification of this model is ongoing.
- A depletion benchmark problem for the CORAIL assembly using Pu+Np in MOX pins has been defined. This activity was performed with input from M. Todosow (BNL).
- The LWR lattice code (DRAGON) is being considered as an alternative to the proprietary WIMS8 code for LWR assembly design and fuel cycle analyses. This assessment involves the comparison of DRAGON results to those from WIMS8 and MCNP.
- Detailed isotopic vectors (actinides, fission products) were prepared for spent UO_2 and MOX (separated Pu) assemblies. Accurate data from WIMS8 fuel cycle analyses were blended with detailed ORIGEN2 isotopic vectors to provide data useful for repository impact analyses.
- Work packages were created for ANL contributions to Broad Systems Studies, Transmutation Systems Studies and Integrated Model Development, and Technology and Facility Assessment. The transmutation studies work includes deliverables on transmutation criteria, LWR recycle strategies, assembly design for the Series One system point design, Series One repository benefit analysis, and integrated safeguards for pyroprocessing.

4.1.3 Systems Studies and Analysis Technical Summary

Several key presentations regarding transmutation study results and fuel cycle strategy evaluations were prepared and given at the AFCI Semi-Annual Meeting. A comprehensive review of the FY02 reactor-based transmutation studies was presented. The fuel cycle impacts of deep burnup in PWRs using multi-recycle were summarized; and the fuel handling difficulties associated with transuranic (TRU) recycle were highlighted. Regarding fast reactor-based transmutation, the low conversion ratio fast reactor performance and safety results were

summarized. The key results of the long-lived fission product transmutation study (in both PWRs and fast reactors) were also summarized. A summary of transmutation schemes for LWRs, including an overview of international studies, was also given. Multi-recycle and once-through approaches were considered, using either homogeneous or target (dedicated) fuel forms. For multi-recycle, plutonium management is feasible and the homogeneous approach is preferred. The main consequence of multi-recycle is the build-up of minor actinides that must be transmuted to achieve the desired waste benefits. Finally, a presentation on future plans for transmutation systems studies was given. Based on gap analysis, needs for clear transmutation criteria, systematic assessment and comparison of the existing studies, and feasibility analyses (largely continuation of existing fuel cycle impact and system design studies) were identified.

A more focused plan for transmutation systems studies (as requested by the ANTT subcommittee) was developed. In particular, work tasks on transmutation criteria, transmutation options, and transmutation analyses were identified. The definition of criteria ranging from separations technology to reactor performance, to the integrated fuel cycle is required to both design and demonstrate the advanced fuel cycle system. The transmutation options area will systematically assess and synthesize the results of previous international studies. The transmutation analysis task includes the extension of previous work on multi-tier fuel cycle studies and fuel cycle impact evaluation. A Transmutation Systems Study Meeting was held at INEEL on February 4-5, 2003, to discuss short and long term activities. The meeting was used to define and integrate the work scopes and responsibilities; ANL, LANL, INEEL, BNL, SNL, ORNL, WSRC, PNNL, UC-Berkeley, and General Atomics (GA) participated in the meeting. Work packages were created. The transmutation systems studies work includes deliverables on transmutation criteria, LWR recycle strategies, assembly design for the Series One system point design, Series One repository benefit analysis, and integrated safeguards for pyroprocessing.

ANL systems analysis personnel participated in a CEA/DOE Collaboration Meeting. As part of the physics and systems studies working group, presentations were given on plutonium and TRU multi-recycling in PWRs, low conversion ratio fast burner reactor studies, and physics analyses of the MUSE and TRADE experiments. The desire to explore refined PWR assembly design to reduce the power peaking in the CORAIL multi-recycle concept was identified. A variety of outstanding discrepancies in the benchmark and experimental physics results were discussed. Commitments were made to provide additional PHENIX and TRAPU results in the near future; and the OSMOSE program for minor actinide measurements was highlighted.

TRANSMUTATION CRITERIA

A meeting of the Transmutation Criteria sub-group was held with participants from ANL, INEEL, LANL and PNNL. Key questions requiring transmutation approach were discussed:

- Should long-lived fission products (Tc-99 and I-129) be transmuted or converted to superior waste forms?
- Is Pu+Np only to be burned in Series 1 reactors?
- Is uranium disposable as Class C waste?
- Is inert matrix fuel development required?
- What fraction of Cs/Sr needs to be extracted from nuclear waste?
- What fraction of minor actinides should be extracted from nuclear waste?

- Is zero fission gas release during fuel processing achievable and reasonable?

Participants were tasked to summarize and document the relevant issues and recommend specific transmutation criteria.

Transmutation Options

A detailed work plan for systemic inter-comparison of transmutation systems was developed. Both fast and thermal reactors using conventional and dedicated fuels will be considered. The work will summarize existing studies and quantify key physics parameters. A breakdown of the work between CEA and DOE for the ongoing collaboration was proposed.

The behavior of Am-241 targets in a thermal spectrum was investigated in response to a DOE-NE inquiry. In Figure 4.1.1 is displayed the time evolution of the masses for Am-241, total heavy metal, Pu-238, and a combination of nuclides (Am-241, Pu-241, Np-237 and Cm-245), which is the key chain of concern for repository performance (Np-237/Am-241 production). The findings of the study can be summarized as follows:

- Am-241 is an absorber in the thermal spectrum; its fission-to-capture cross-section ratio is of the order of 0.01-0.02. The irradiation of the pure target, forms daughter products, of which Pu-238 is the most prominent.
- The French work targets destruction of the heavy metal (actinides and daughters), not just Am-241 transmutation. After 40 years of irradiation, 95% of the heavy metal is destroyed.
- By comparison, the Am-241 mass is reduced by about two orders of magnitude in about 10 years. The trend of the combined mass for Am-241, Pu-241, Np-237, and Cm-245 is quite similar (about 3% after 10 years). However, a decision would have to be made on the incineration or direct disposal of the daughter actinides.
- There will be a significant increase in the uranium enrichment required to meet the prescribed operational cycle length. This item was not evaluated as part of this study, but is confirmed by earlier French studies.

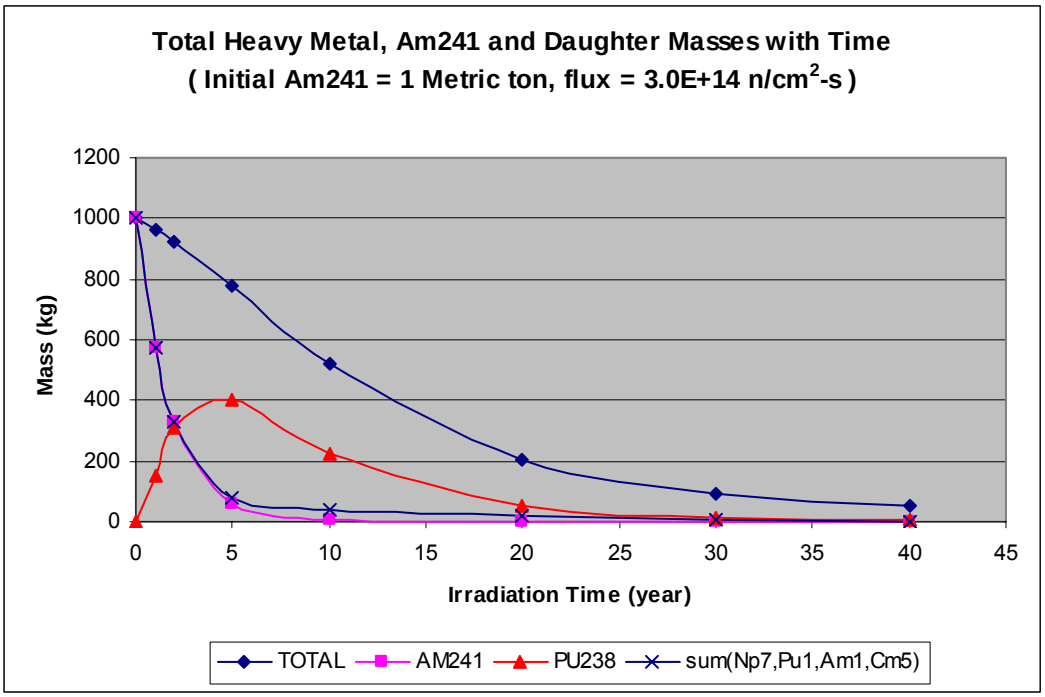

Figure 4.1.1. Evolution of Masses for Am-241 Target Irradiation

Transmutation Analyses

The main analysis activity for this year is to take a promising fuel cycle strategy (limited recycle of Pu+Np in a PWR) and develop a detailed system point design for Series One deployment. The more detailed assessment will illustrate the key reactor design and performance issues expected for Series One utilization and help identify key design constraints for Series One deployment. Work at ANL will focus on development of partial MOX loading scenarios to specify a preferred assembly design. The MOX assemblies will use heterogeneous fuel pin enrichments (Pu/HM) to limit localized power peaking at the MOX/UO_2 assembly interfaces. A 17x17 PWR assembly with typical design parameters for the fuel pin size, pitch, etc. was assumed with a MOX pin layout that was adopted from a French technical presentation; confirmation of the current application of this design was recently requested from the French CEA.

The mixed MOX/UO_2 lattice has been modeled using the WIMS8 code for depletion and power peaking analyses. The configuration shown in Figure 4.1.2 is used to model one-quarter of each assembly in the lattice (the solution area is enclosed by the dashed line). A specific power of 33.7 MW/MT is utilized in the WIMS8 calculation for the power normalization, based on a reactor loading of 193 assemblies and a total core power of 3,000 MWth.

A procedure was developed to perform efficient scoping calculations of a mixed MOX/UO_2 lattice to optimize the fuel pin loadings. A coarse depletion step length (15,000 MWd/MT) provides reasonable predictions of the reactivity letdown behavior for UO_2 and MOX assemblies. Given that a large number of design calculations is anticipated for optimization of the pin power distribution, a ½-symmetry along the southwest-northeast diagonal of the solution lattice is applied to provide a ~20% reduction in computation time, but this limits the flexibility

of the lattice model; the UO_2 assemblies in the northwest and southeast quadrants would be restricted to the same enrichment and burnup.

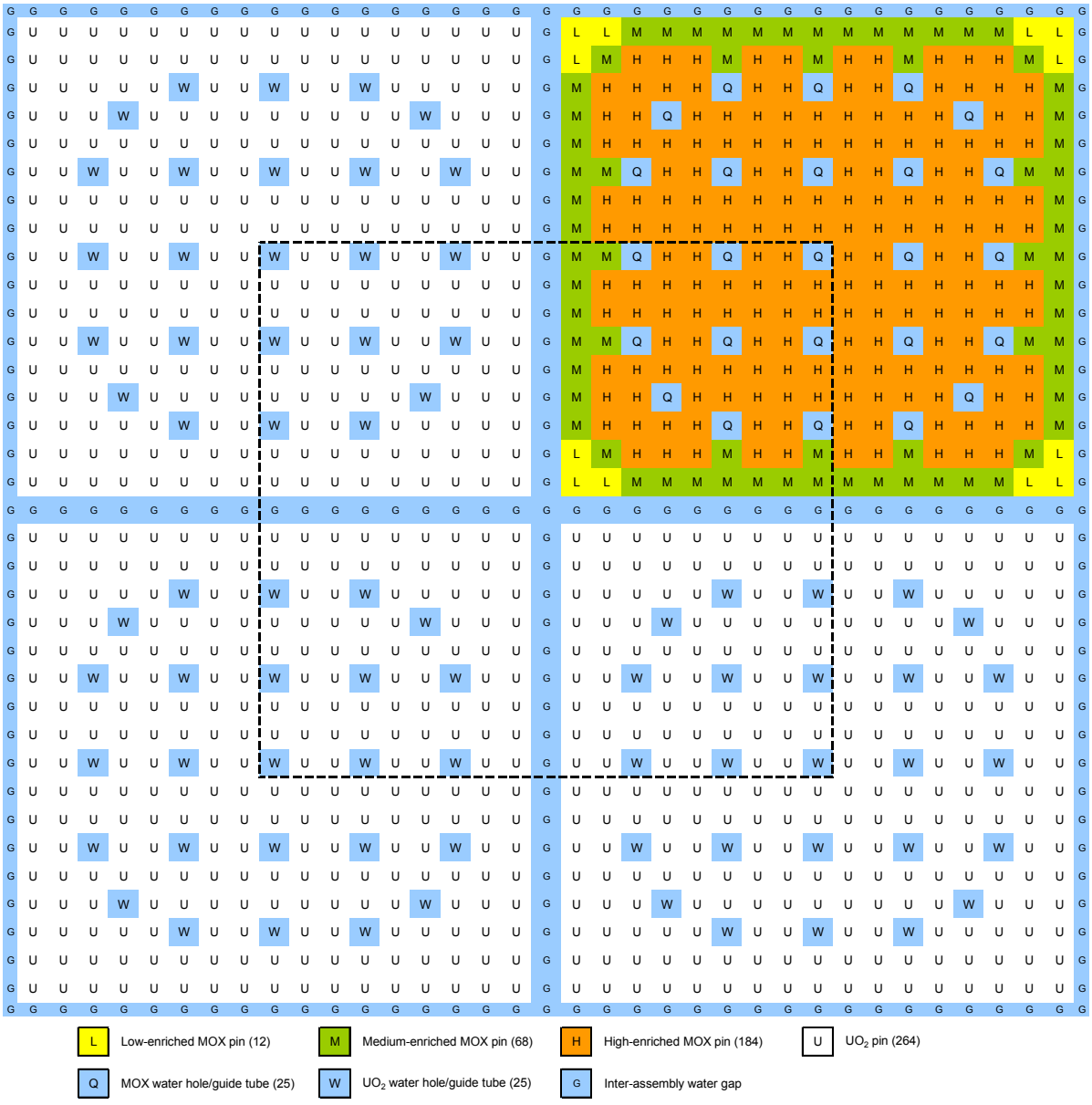

Figure 4.1.2. MOX/UO_2 Mixed Lattice used for System Point Design Scoping Calculations

Scoping calculations were also performed to assess the impact of the spectrum calculation solution parameters on computation time and accuracy. Calculations were performed for the mixed lattice shown in Figure 4.1.2 without the application of geometric symmetry. Reducing the number of azimuthal and polar angles or increasing the track separation reduces the computation time, but negatively impacts the accuracy of the solution, particularly the pin power distribution. For the cases considered, the rms difference of the power distribution relative to the reference solution increases to nearly 3%, while the largest pin power difference is nearly 9%.

Furthermore, the computed power distribution becomes more asymmetric as the solution parameters are coarsened. Differences of this sort will be magnified and become more important over the course of fuel pin depletion.

Based on these studies, the chosen solution scheme utilizes 3 azimuthal angles, a track separation of 0.3 cm, and a single polar angle. Full depletion of the mixed lattice with these parameters requires ~2 CPU-minutes, a five-fold reduction over the comparable problem solution with typical parameters. For a typical problem, the resulting eigenvalue error was 271 pcm, with pin power error of 1.3% (rms) and 4.1% peak. Of course, the final assembly design will be evaluated more rigorously.

Two spent fuel pins that were part of the former DOE Extended Burnup Demonstration have been slated for the *UREX+ aqueous processing demonstration* to be performed later this year. The pins were irradiated in the Big Rock Point boiling water reactor (BWR) and discharged in early 1982. An initial estimate of the isotopic content of the irradiated fuel pins is needed to determine shielding requirements and to prepare process flow sheets. Calculations were performed using the WIMS8 and ORIGEN2 codes to estimate the spent fuel characteristics and results were provided to the separations experts.

Detailed isotopic vectors (actinides, fission products) were prepared for spent UO_2 and MOX (separated Pu) assemblies to provide data useful for *repository impact analyses*. In previous work, techniques were developed to blend accurate data from WIMS8 fuel cycle analyses with detailed ORIGEN2 isotopic vectors. A systematic comparison of this technique to direct use of ORIGEN2 was conducted to evaluate the accuracy of alternative ORIGEN2 one-group data libraries and clarify the magnitude of resulting errors for MOX fuel options. The analysis shows that, while ORIGEN2 has a robust depletion chain that models over 1000 nuclides in spent fuel, the available one-group cross-section libraries must be used cautiously. Blending the WIMS8 and ORIGEN2 results provides a mechanism for exploiting the accurate depletion calculations in WIMS8 for a few key actinides and fission products while retaining the detailed nuclide chains available in ORIGEN2.

If *multi-recycle* of the Pu+Np is employed in LWRs, the heterogeneous assembly CORAIL concept is a promising option. This approach allows for mixing of the recycled MOX with "fresh" plutonium from the UO_2 pins of the same assembly. As part of the *DOE/CEA Collaboration* on transmutation systems studies, it was proposed to define a benchmark problem for the CORAIL assembly employing Pu+Np in the MOX pins. Thus, a problem has been defined to compare the neutronic properties of the CORAIL assembly at static and depletion states. Except for the composition of the MOX fuel (which now includes Np), the geometry and material data are identical to those of the FY02 CORAIL benchmark. Preliminary calculations were performed to set the fuel enrichment for an assembly discharge burnup of 45 GWD/t in a three-batch in-core fuel management scheme, assuming 3% neutron leakage. Benchmark static calculations for room temperature conditions were performed with the MCNP4C, WIMS8 and DRAGON codes. Comparisons of the k_∞ values obtained by the codes are provided in Table 4.1.1. The underprediction of the eigenvalue by WIMS8 relative to MCNP4C is consistent with previous results (-228 pcm for 8% Pu case).

Table 4.1.1. Comparison of Eigenvalues and Normalized Pin Power Distributions

Code	Neutron groups	Eigenvalue	rms of power difference (%)
MCNP4C	Continuous	1.27329 ± 0.00031 (ENDF/B-6)	± 0.61 [a)]
		1.27479 ± 0.00029 (ENDF/B-5)	-
WIMS8	6	1.271511	-
	28	1.270951	± 0.44 [b)]
	172	1.271594	-
a) Root mean square of the standard deviation of the MCNP4C normalized pin power. b) Root mean square difference compared to MCNP4C normalized pin power.			

The LWR lattice code DRAGON is being considered as an alternative to the proprietary WIMS8 code for LWR assembly design and fuel cycle analyses. Sensitivity calculations have been performed utilizing the CORAIL-Pu+Np benchmark problem. Comparisons of k_∞ and pin power distributions have been conducted. Various options of the collision probability method (CPM) and self-shielding modules have been evaluated using a 172-group library. Generally, the DRAGON code underestimates the eigenvalue by about 960 ~ 1470 pcm with default options of the CPM and self-shielding modules. However, these errors are significantly reduced by using the Livolant-Jeanpierre (LJ) modification option in the DRAGON self-shielding calculation; the differences become lower than 200 pcm (similar to the WIMS8 result).

The normalized pin powers of the WIMS8 calculation are close to the results of the MCNP4C calculation; the maximum error (1.2%) occurs at the interface of the MOX and UO_2 fuel pins. However, relatively higher differences are obtained in the comparison of the fission yield reaction rates produced by the DRAGON calculations. The maximum error is 2.6% and the RMS error is 0.86% in the EXCEL module calculation using isotropic tracking and a reflective boundary condition. Part of this discrepancy could be due to the different modeling of the water gap in the calculations. The water gap is integrated into the peripheral MOX fuel pins in the DRAGON calculations, while it is modeled explicitly in the MCNP4C and WIMS8 calculations.

Benchmarking of NFCSim with COSI

The ground rules for the benchmarking of the COSI and NFCSim codes are summarized as follows. The simulation period is from 2010 to 2050. There are two types of reactors: 24 UOX burners and 16 MOX burners. Each reactor generates 4250 MW of thermal power, 1510 MW of gross electric power, and 1450 MW net electric power. The MOX reactors are fueled with UOX and MOX, the latter accounts for only 30% of the core by weight. There is an initial (2010) inventory of 10560 tonnes of UOX and 1573 tonnes of MOX. Each reactor is taken down for two months every18 months to replace ¼ of the core. All fuel must be stored on site for 5 years, at which time it is moved to interim storage. Only the spent UOX fuel is reprocessed, and reprocessing takes a total of 2 years.

For NFCSim to operate properly, additional constraints were imposed by LANL. Transportation of nuclear materials between all processes takes 2 days. The chemical separation of Pu from spent UOX takes 18 months at an efficiency of 0.999, and the fabrication of MOX fuel takes 6

months, consistent with 2 years for reprocessing. Half of the UOX and MOX reactors are started in April of 1997; the remaining reactors are started 6 months later in October of 1997. Starting the reactors in 1997 ensures that the reactors have entered their equilibrium phase by the start of the simulation period. However, the UOX reactors settle into equilibrium 6 months before the MOX reactors. This difference in the time to achieve equilibrium results in 3 distinct outage periods, rather than the expected 2 distinct outage periods. All reactors are to be shut down by January 1, 2055. This constraint forces UOX reactors with an April start date to shut down in late August of 2054 and those UOX reactors with an October start date to shut down in early September of 2053. The MOX reactors with an April start date shut down in April of 2054 and those MOX reactors with an October start date shut down in April of 2053. The NFCSim simulation period is extended to 2080 to ensure stoppage of all activity.

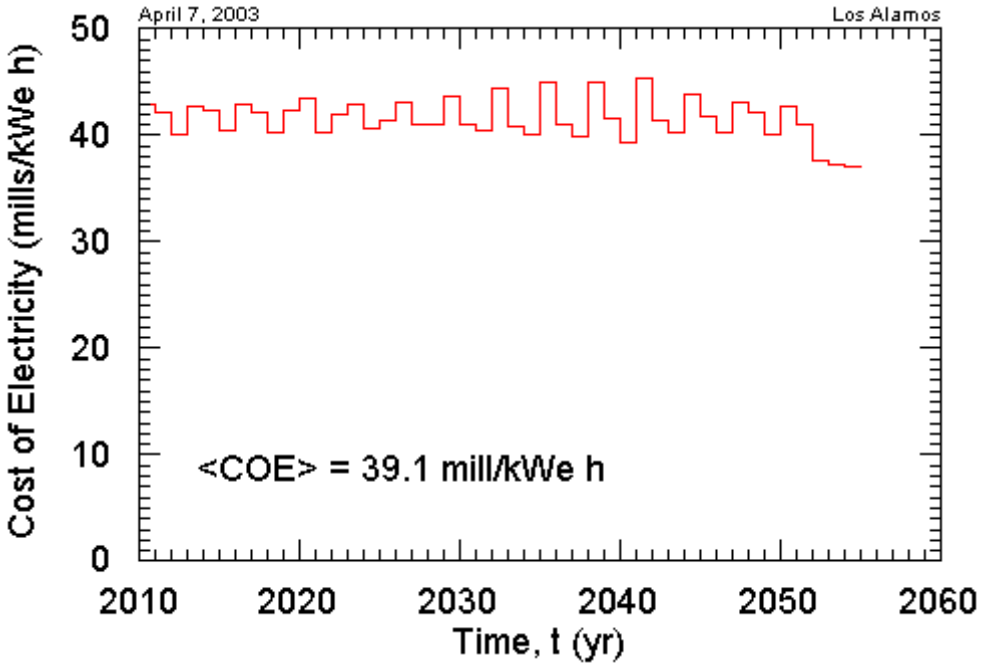

Figure 4.1.3. Cost of Electricity, Yearly Averages

The cost of electricity, shown in Fig. 4.1.3, displays an oscillatory behavior because both the annual charges, shown in Fig. 4.1.4, and the annual energy production, shown in Fig. 4.1.5, also display oscillatory behavior. The root cause of this oscillatory behavior is the reactor outages for refueling, shown in Fig. 4.1.6. The refueling periods of half of the UOX and MOX reactors overlap, as do the refueling periods of the remaining half of the UOX reactors. The refueling periods of the remaining half of the MOX reactors also overlap. These three distinct outages are clearly visible in Fig. 4.1.6b. This outage pattern results in a year-to-year variation in the annual energy production, as shown in Fig. 4.1.5. The annual reactor charges display only a small oscillation, as shown in Fig. 4.1.4b, because of leap year. The non-reactor charges, however, display large oscillations. These large oscillations result because these charges are incurred only as a result of discrete events associated with either discharging (i.e., storing spent fuel) or charging fuel (i.e., fabricating fuel).

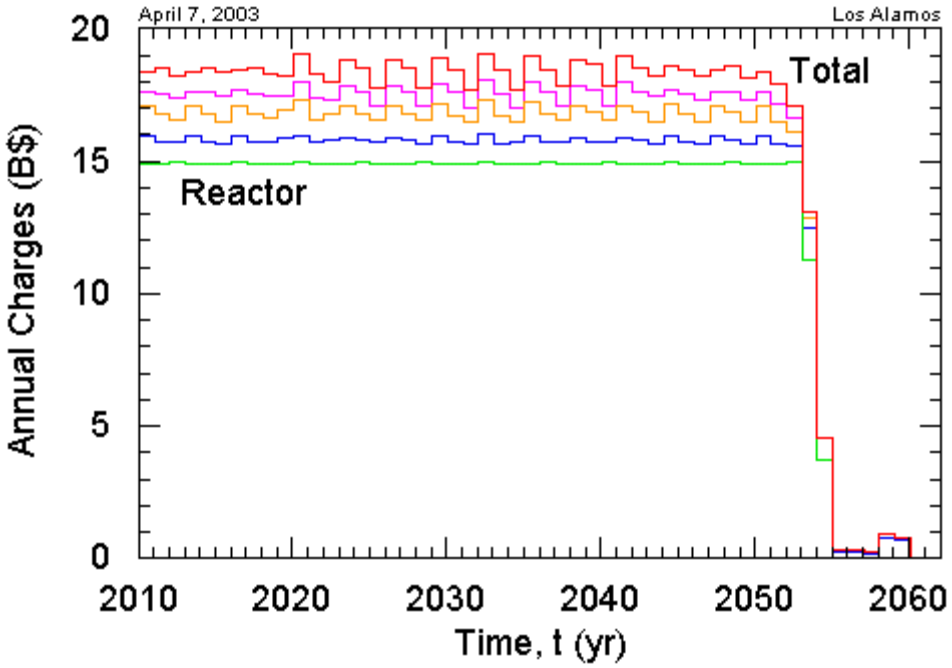

Figure 4.1.4a. Annual Charges

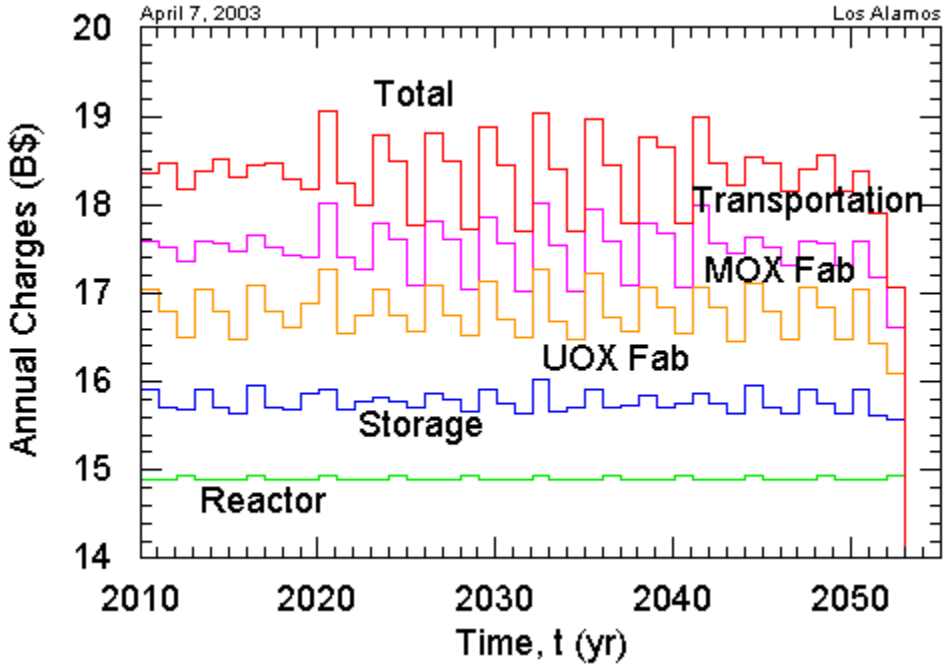

Figure 4.1.4b. Annual Charges

The non-reactor charges have been grouped into four categories: storage charges, UOX fab(rication) charges, MOX fab charges, and tranportation charges. The storage charges include charges for cooling storage, interim storage, depleted uranium storage, and storage of irradiated uranium, fission products, and high level waste (HLW) that result from the small inefficiency of separating Pu from spent UOX to make MOX fuel. The UOX fab charges include charges for

mining & milling, conversion, enrichment, and UOX fuel fabrication. The MOX fab charges include charges for separation and MOX fuel fabrication. The transportation charges are incurred for the transport of any nuclear material between any two facilities (*e.g.*, shipping uranium from mining & milling to conversion, shipping spent fuel from cooling storage to interim storage, or shipping plutonium from separations to MOX fuel fabrication).

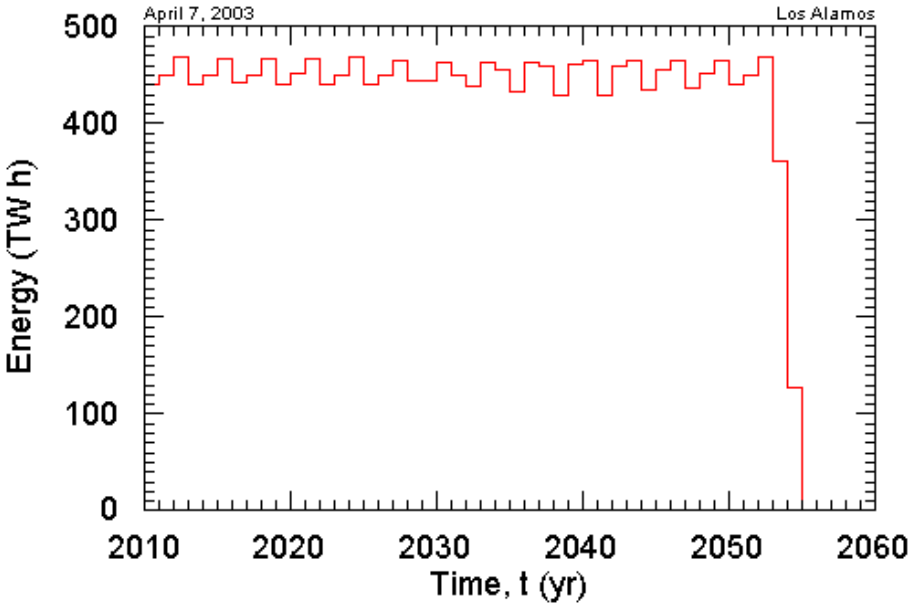

Figure 4.1.5. Annual Energy Production

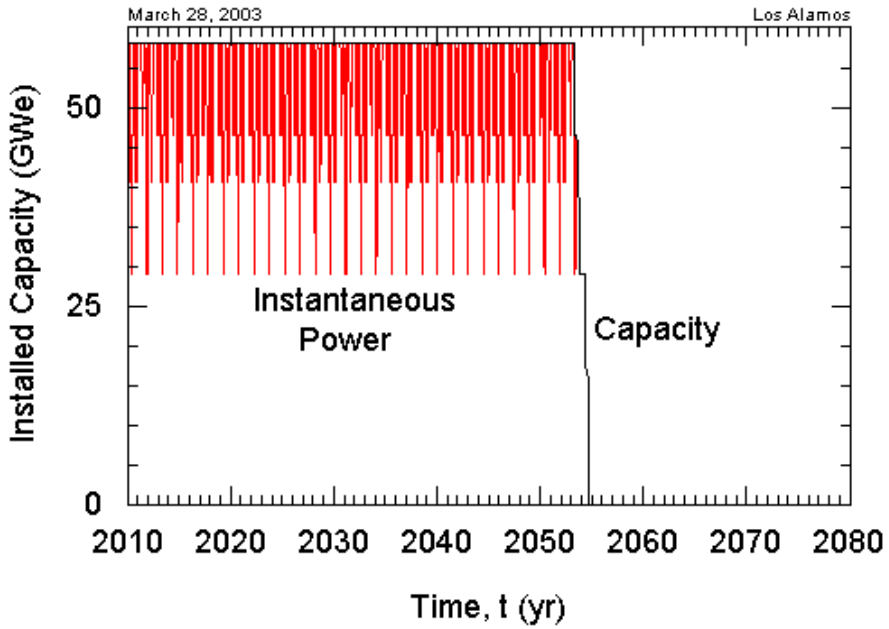

Figure 4.1.6a. Total Capacity and Instantaneous Power

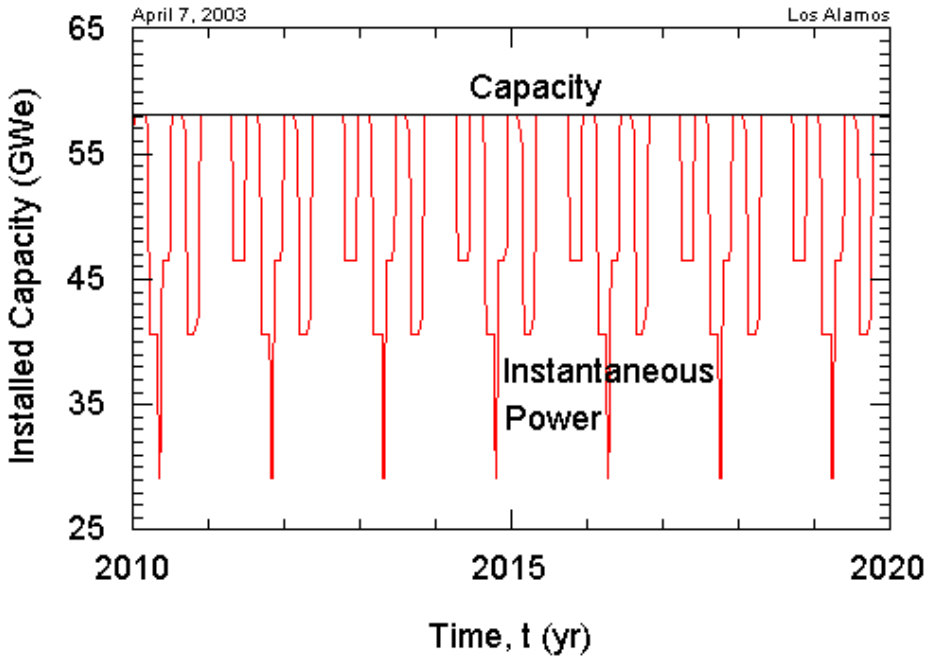

Figure 4.1.6b. Total Capacity and Instantaneous Power.

The ground rules specified just the amount of spent UOX at the beginning of the simulation period. The age distribution of this spent fuel was not specified as part of the benchmark. The age distribution of this spent fuel influences the age of the spent UOX entering the separations plant, as is shown in Fig. 4.1.7. Balancing a desire to minimize the impact on the simulation period and to minimize the time spent fabricating a distribution, an initial UOX inventory was split into three lots of equal mass having creation dates in 1992, 1995, and 1998. The spent UOX produced by the UOX reactors that come online in 1997 supplement this UOX inventory. The resulting initial age transient dissipates by 2014. The “saw tooth” behavior displayed by the age of the spent UOX entering the separations plant is a result of the discrete nature of the simulation. A group of UOX discharges of similar age fuel the MOX fabrication process until consumed, resulting in a linear increase in age until then. The next group of UOX discharges of similar age will be either 6 or 18 months younger than the previous group, resulting in a sharp decrease in age by either 6 or 18 months, respectively.

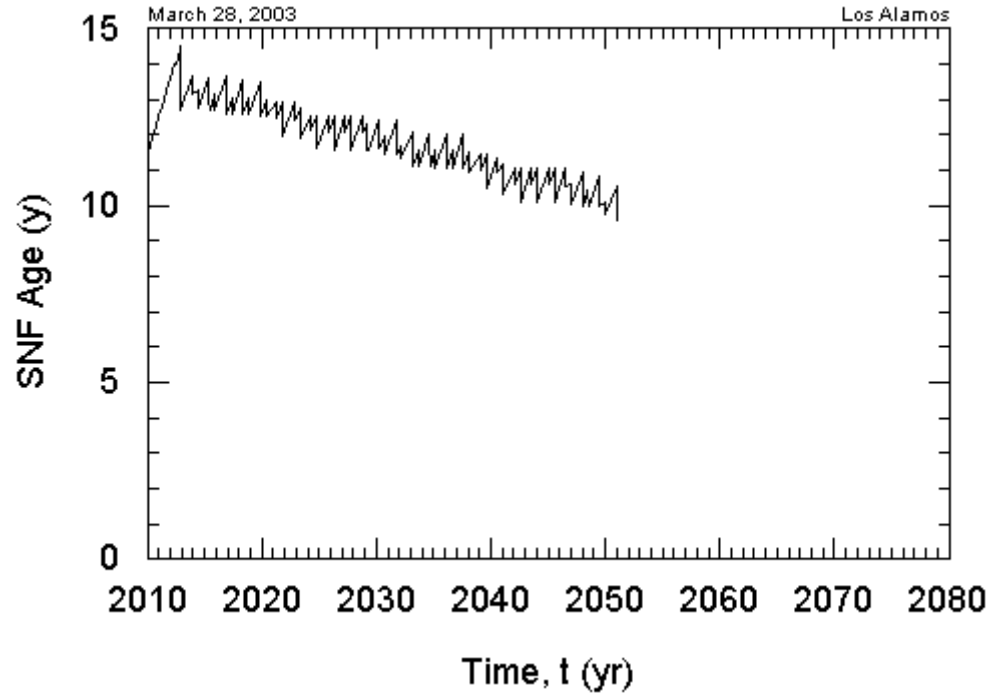

Figure 4.1.7. Age of Spent Fuel Entering Separations

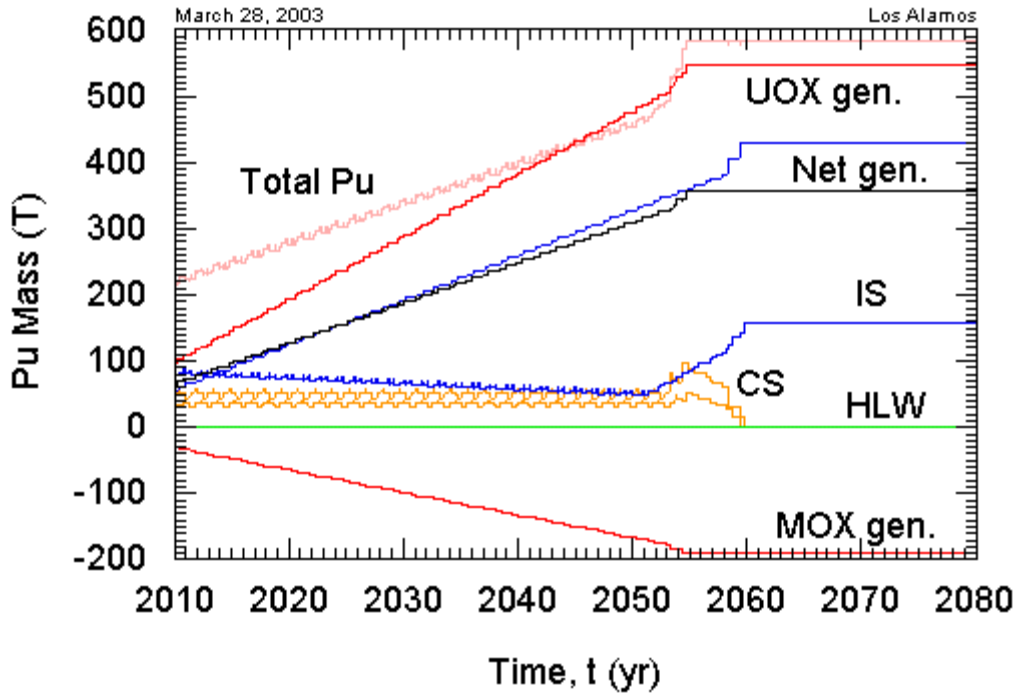

Figure 4.1.8. Discharged Plutonium by Location and Source

Plutonium is tracked in NFCSim by location and origin. Figure 4.1.8 displays plutonium inventory in cooling storage at UOX and MOX reactors (gold plots), in spent UOX fuel in interim storage from both UOX and MOX reactors (upper blue plot), in spent MOX fuel in

interim storage (lower blue plot), as well as plutonium sent to a HLW repository. The plutonium generated or consumed in UOX and MOX fuels is denoted by the red curves. The net plutonium generated is shown as a black curve. The total plutonium generated plus the initial inventory is also shown. The plutonium inventory in reactors is not shown.

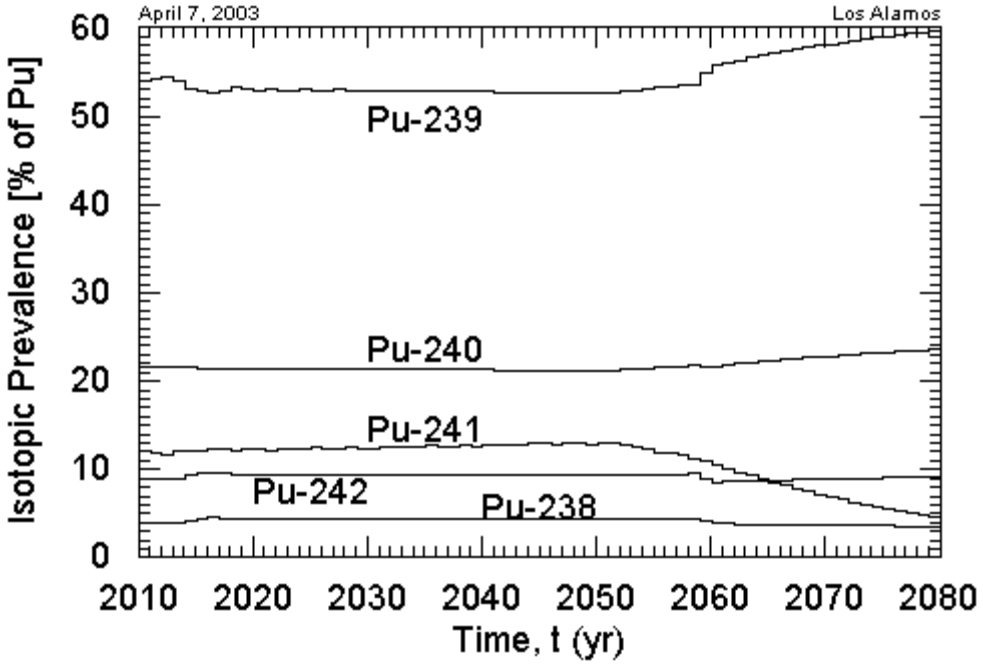

Figure 4.1.9. Averaged Isotopics of Pu in UOX SF Interim Storage

Plutonium isotopics, as well as those of other actinides from thorium through californium, are tracked. For instance, Figure 4.1.9 displays the composition of plutonium in UOX spent fuel residing in interim storage. Each fuel batch is unique; however for clarity, the average composition of all fuel currently present in interim storage is illustrated in these figures.

Because the benchmark scenario is quasi-steady-state – the size (see Fig. 4.1.10) and average age (see Fig. 4.1.7) of the UOX spent fuel stockpile is nearly constant, little evolution is seen in the isotopics of UOX-generated plutonium during the benchmark period of 2010-2050, as shown in Figure 4.1.9. Some features, however, require clarification. The perturbations from the steady-state composition that dwindle shortly after 2010 are a legacy of the reactors' startup transients. During startup, initial batch compositions and discharge burnups vary; hence plutonium isotopics at discharge also vary, favoring the greater Pu-239 prevalence characteristic of lower burnups. Because fuel remains in cooling storage for 5 years before passing to interim storage and becoming available for reprocessing, some of this transient fuel remains in interim storage in 2010.

A second perturbation appears shortly after 2050, when NFCSim decommissions the reactor fleet. The final discharges have been exposed to lower burnup, so a corresponding increase in Pu-239 prevalence is seen. After 2050, the average age of spent fuel in interim storage begins to increase as reprocessing has ceased, so the decay of Pu-241 becomes noticeable.

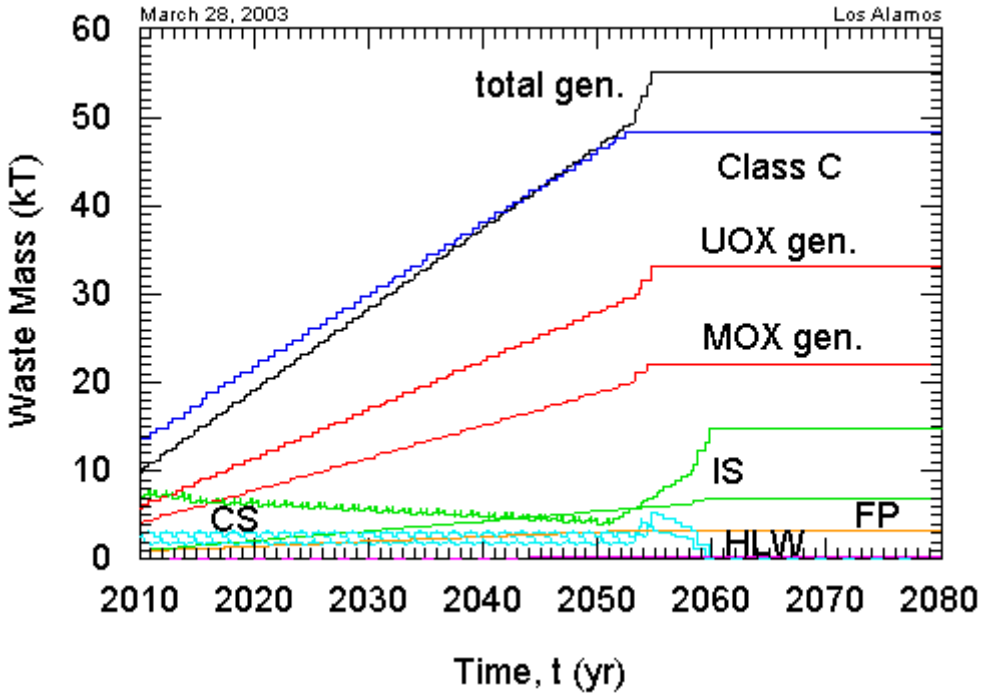

Figure 4.1.10. Total Spent Fuel / Waste Mass by Category and Location

An aggregated accounting of spent fuel and waste mass as a function of location is shown in Fig. 4.1.10. The red curves display the total spent fuel generated by the 24 UOX and 16 MOX reactors; the black curve is the sum of spent fuel discharged from all sources. For this benchmark, Class C waste consists exclusively of reprocessed uranium. It exceeds total spent fuel mass generated by the reactor fleet because the benchmark initial conditions require an amount of legacy spent fuel to be inserted into the nuclear economy and made available for reprocessing. The green curves describe UOX and MOX spent fuel in interim storage. The mass reduction in spent fuel due to reprocessing is determined by taking the difference between the black curve, which would be the spent fuel mass in the absence of reprocessing, and the sum of the green curves. A factor of 2.5 reduction in spent fuel mass is seen; this would be closer to a factor of 7 if the transient effect of several UOX discharges not being reprocessed due to the decommissioning of the entire fleet were not present. Separated fission products represent about 6% of spent fuel mass; it is assumed that they are stored separate from actinide HLW. Finally, the HLW category encompasses all other materials – minor actinides as well as product lost to the waste stream during reprocessing.

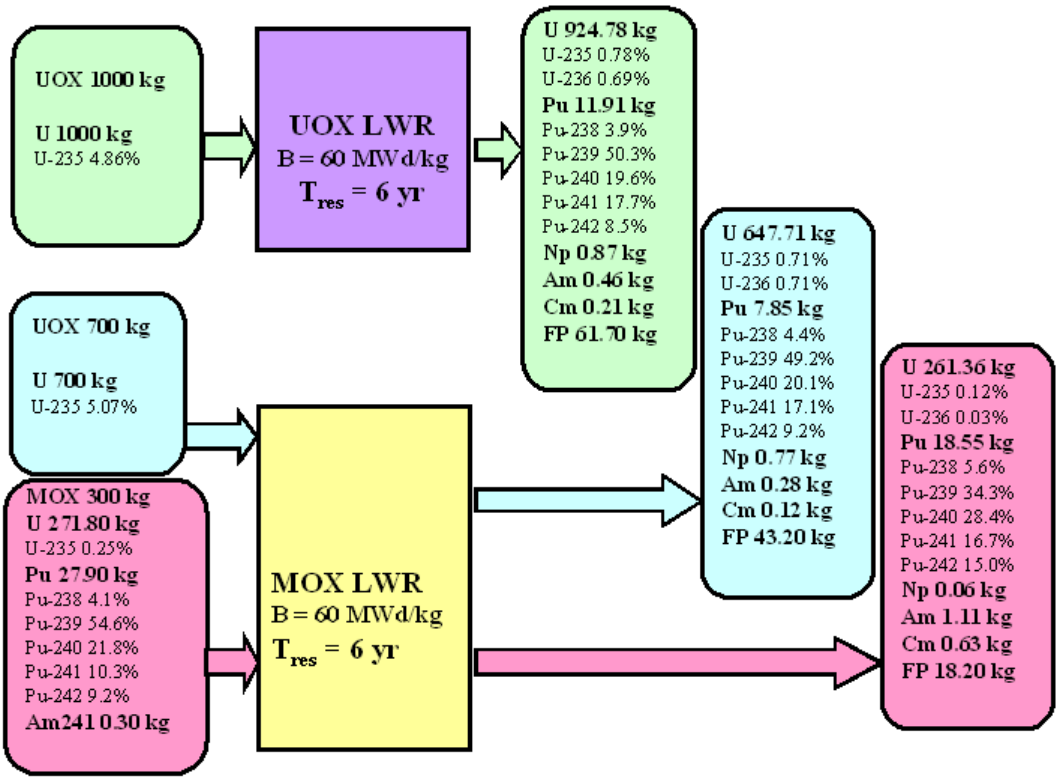

Figure 4.1.11. Criticality and Burnup Data for Equilibrium Fuel

A material balance for the two reactor types of the benchmark is shown in greater detail in Fig. 4.1.11. Criticality and burnup calculations were performed using NFCSim's ORIGENInterface capability. ORIGENInterface operates in transient and equilibrium fuel management regimes at the refueling batch level, derives reactor- and cycle-dependent initial fuel compositions and invokes ORIGEN2.x to do burnup calculations.

Note that UOX fuel for exclusively UOX burning reactors does not share the same burnup characteristics as UOX fuel present in MOX reactors. Spectral differences between these reactors, though not large, are significant to the extent that noticeable variations are observed. Perhaps the most obvious is the increased capture-to-fission ratio for U-235, which results in greater enrichment to obtain the desired initial reactivity surplus and leads to greater U-236 and Pu-238 buildup.

Development Of A Reprocessing Model In Support Of NFCSim

A reprocessing conceptual model has been prepared that includes capital cost for each unit operation (see Table 4.1.2) and separation factors for the primary species (see Table 4.1.3). Costs are based on the OECD/NEA 1993 study, escalated to the year 2002, based on the GDP factors of the Economic Report of the President, and aligned for the major processing activities (head-end, separations, conversion and waste management) according to those of Barnwell as published in ORNL/TM-12344, Methodology for Estimating Reprocessing Costs for Nuclear Fuels. The costs shown in Table 4.1.2 represent not only the equipment, but all infrastructure including the portion of the building required for the unit operation. The total capital cost of $10.6B shown in Table 4.1.2 is based on a typical PUREX plant; however, the unit operation costs are applicable to an Advanced Fuel Cycle reprocessing facility. Table 4.1.3 is only

partially complete at this time, but upon completion will provide input necessary to estimate product and waste compositions. The separation factors shown in Table 4.1.3 were gathered by conversations with the AFCI Separations Group and are intended to provide a reference to generate further dialogue leading to a complete table based on consensus. Additionally, the separation methods shown in Table 4.1.3 are intended as only a beginning point from which to achieve consensus.

Table 4.1.2. Unit operation capital costs for reprocessing

Unit Operation	$M/ Unit-Operation	Approximate number of operations for PUREX	Total Cost ($2002)
Head-End			
Receiving & storage	1135	1	1135
Shear	454	1	454
Dissolver	454	1	454
Centrifuge	113	1	113
Separations			
Solvent extraction (extract, partition or strip)	170	9	1532
Solvent extraction (scrub or diluent wash)	113	6	681
Packed column (Pu^{III+} oxidation)	57	2	114
Conversion			
Precipitator	113	1	113
Evaporator	113	1	113
Calcinator	227	2	454
Canning	227	2	454
Waste Management			
Evaporator	113	2	227
Aqueous distillation	227	2	454
Solvent distillation	227	1	227
Solvent wash (via SX)	113	1	113
$^{14}CO_2$ separation	567	1	567
Iodine separation	567	1	567
Inert gas separation (Kr & Xe)	567	1	567
Tritium separation	567	1	567
Packed column (NOx)	57	2	114
HEPA filter	113	2	227
HLW vitrification	851	1	851
LLW grouting	567	1	567
Total Facility			**10665**

Table 4.1.3. Separation factors for primary species

	Disso-lution	Iodine separation		UREX		Solvent extract	Precipitate		TRUEX	
	off-gas	liquid	gas	U extract	Tc extract	Pu&Np	Cs	Sr	Am extract	Cm extract
I	0.5	0.95	0.95							
U				0.995						
Tc				0.95	0.95					
Pu						0.99				
Np						0.99				
Cs							0.85			
Sr								0.85		
Am									0.95	
Cm										0.95

5 IDAHO ACCELERATOR CENTER (IAC)

5.1 Idaho Accelerator Center Scope

Idaho State University is a component of the national Advanced Fuel Cycle Initiative. Through this research project, which is centered in the Idaho Accelerator Center (IAC), research is conducted to support activities in the research programs of the AFCI: Transmutation Engineering, Separations, and Fuels. Most of our work is concentrated on Transmutation Engineering. In the two separate multifaceted research projects, support is provided for undergraduate and graduate students, and administration of the program, and provides infrastructure for conducting the research. The research includes the use of electron accelerators to produce photons and neutrons for use in experiments.

Experiments may include radiation damage to materials and/or cooling systems, investigations of neutron production and multiplication, reactor dynamics, and other topics that may be added as research needs are identified in the future. In addition, a new method for positron-annihilation spectroscopy (PAS) has been developed at IAC that allows stresses and defects to be measured in bulk materials. The application of this new PAS technique to AFCI nuclear materials problems (such as the examination of the zone of a weld between dissimilar materials) is under way. Both of these research and development activities are being conducted in collaboration with other AFCI member organizations.

5.1.1 Idaho Accelerator Center Technical Summary

Positron Annihilation for Materials Stress Analysis. This part of the program is the development of the IAC materials stress determination technology. These new techniques for PAS use highly penetrating gamma-rays to create positrons inside the material via pair production. Bremsstrahlung beams from small, pulsed electron Linacs (6 MeV) are used to bombard the materials to generate positrons, which annihilate with the material electrons emitting 511 keV radiation. PAS provides highly penetrating probes for material characterization and defect analysis in nuclear materials problems. In this quarter, we have used PAS measurements in bulk samples in a coordinated program with UNLV in order to compare PAS with traditional materials analysis techniques. Several different samples have been measured, and detailed comparison of these results with other techniques is underway (Fig. 5.1.1).

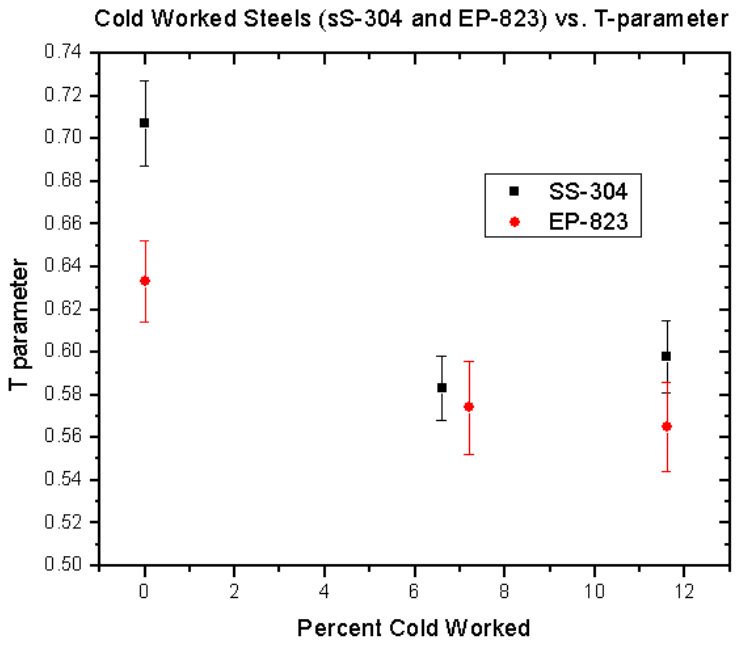

Fig. 5.1.1. An example of recent preliminary data on Cold-Worked Steel (SS-304)

Measurements were done in triplicate under identical conditions. Triplicate results were consistent; the averaged results are shown below. All error bars (uncertainty) are 1-sigma (Table 5.1.1).

Table 5.1.1. Averaged results on recent preliminary data on Cold-worked Steel

% Cold Worked	T-value*	Uncertainty
0.0%	0.707	+/- 0.020
6.7%	0.583	+/- 0.015
1.6%	0.598	+/- 0.017
*The T- value is a gamma spectrum line width parameter from the PAS measurement.		

To interpret this data, we note that there was a clear signal that repeated itself (three times) and the effect appears to saturate, suggesting either that the PAS effect of this kind of residual stress saturates, or perhaps, that the stress itself saturates as one increases the cold work. Without a series of cold-worked specimens between 0% and 6.7%, it is hard to speculate on how the PAS measurement will behave between these two numbers.

Accelerator-Driven Neutron Source. An electron-accelerator-driven neutron source for performing dynamic reactivity measurements in multiplying and non-multiplying assemblies is being set up and tested (Fig 5.1.2). The accelerator will provide a pulsed neutron fluence of ~10e11n/pulse and ~10e13n/sec time average fluence (Fig 5.1.3). Modifications on the IAC

building have been completed this quarter and the first accelerating section in this facility is delivering low-intensity beam.

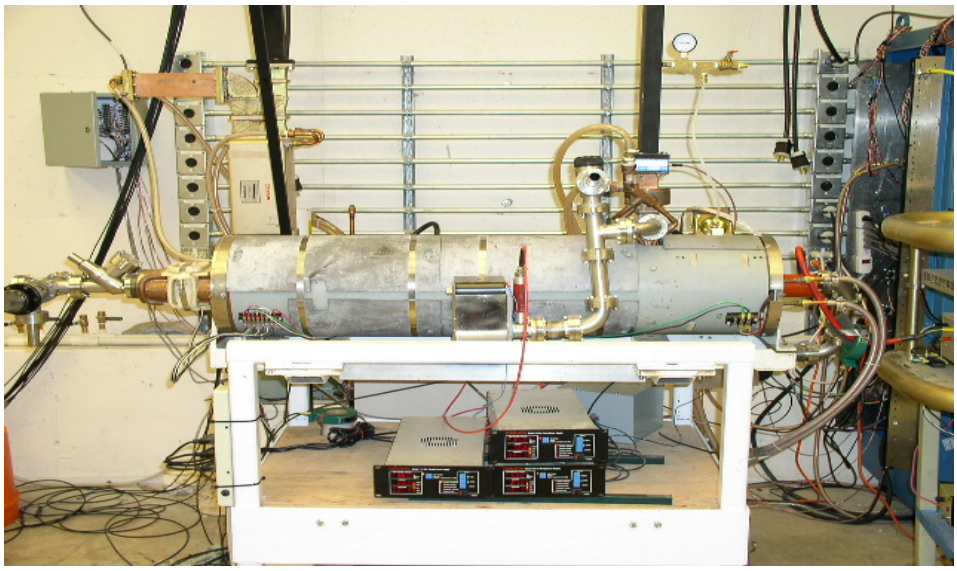

Fig. 5.1.2. First 20 MeV section of ANS undergoing RF conditioning

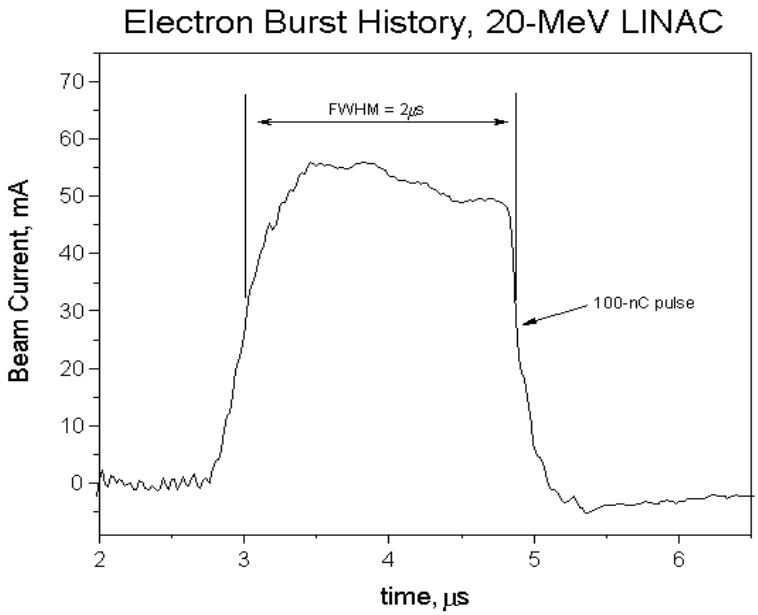

Fig. 5.1.3. Electron pulse from ANS; when operational, the energy will be selectable at 20 or 40MeV, the pulse width 5microseconds, and the peak current 100mA

Photo-neutron production calculations and benchmark experiments have been completed for a number of accelerator target configurations. The experiments were performed using the "20" electron linear accelerator at the Idaho Accelerator Center and the calculations were made using ACCEPT, PINP, MCNP, and MCNPX codes.

Calculations have begun on liquid lead and liquid LBE targets (Fig. 5.1.4 and 5.1.5) for use in radiation effects on oxygen sensors as part of collaboration with LANL in FY'03 (beginning in May '03). This target will be constructed in the summer of 2003 and will include an irradiation chamber to accommodate oxygen sensor units.

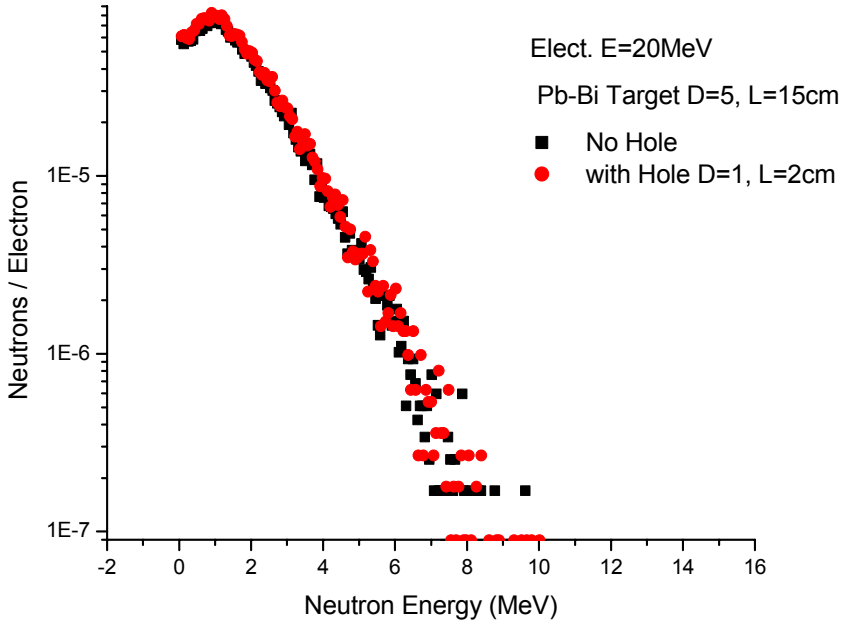

Fig. 5.1.4. Calculation of neutron energy distribution in a LBE target predicting the effect of a sample irradiation cavity (hole)

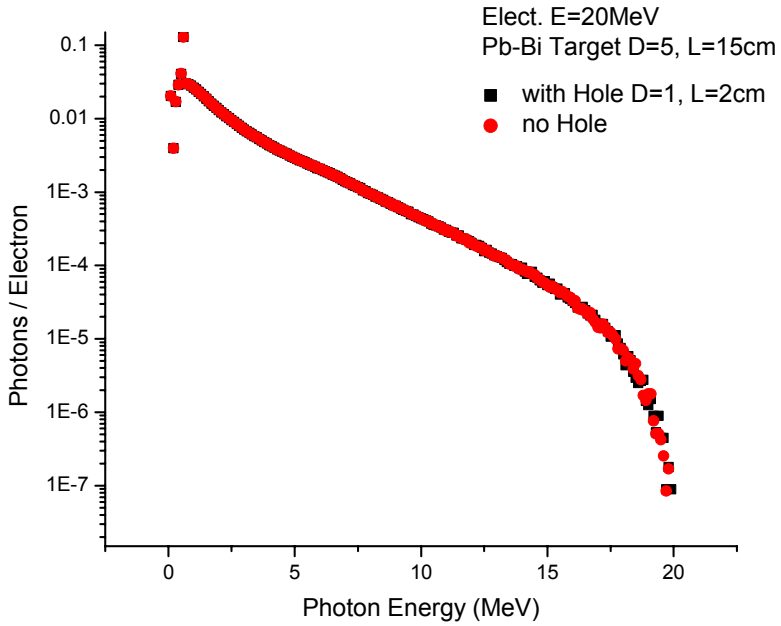

Fig. 5.1.5. Calculation of photon energy distribution in LBE target for estimation of photon dose with and without irradiation cavity

Other activities. Completed upgrade and testing of beam transport and electron injector on the DOE fast pulse linac. This work completes the FY'02 project.

6 UNIVERSITY OF NEVADA LAS VEGAS (UNLV)

UNLV Transmutation Research Program. The University of Nevada, Las Vegas supports the AFCI through research and development of technologies for economic and environmentally sound refinement of spent nuclear fuel. The UNLV program has four components: infrastructure, international collaborations, student-based research, and management support.

6.1 Infrastructure Augmentation

6.1.1 Infrastructure Augmentation Scope

The infrastructure augmentation component of the UNLV Transmutation Research Program enhances UNLV's research staff and facilities to increase the ability of the university to perform AFCI research.

6.1.2 Infrastructure Augmentation Highlights

- **Chemistry Professorship**. UNLV is near conclusion of a search for a Materials Chemist tenure-track associate professor. Selection and an offer will be made next quarter.
- **Facilities Progress Update**. Three facilities are in the laboratory remodeling stage. Architectural and engineering drawings have been completed for the remodeling. The bidding process for construction will be completed by next quarter for the Transmission Electron Microscope user facility and the Interim Lead-Bismuth Eutectic loop facility. The third facility is an inductively coupled plasma (ICP) Atomic Emission Spectrometer (AES) user facility that requires minimal improvements to the existing laboratory space. The ICP AES has been ordered and is expected to arrive and be installed next quarter.

6.2 International Collaboration

6.2.1 International Collaboration Scope

The international collaboration component of the UNLV Transmutation Research Program enhances UNLV's breadth of scientific and scholastic experience. University collaboration is also an efficient conduit for international collaboration that benefits the national AFCI. UNLV has ongoing relationships with the Khlopin Radium Institute (KRI) in St. Petersburg, Russia; the Institute for Physics and Power Engineering (IPPE) in Obninsk, Russia; and members of the International Molten Metal Advisory Group (from Sweden, Germany, Belgium, and Italy).

6.2.2 International Collaboration Highlights

- **International Science and Technology Center (ISTC)**. UNLV became an approved Partner Organization with the ISTC. The UNLV program directors reviewed and approved a new scope of work with the Institute for Physics and Power Engineering in Obninsk, Russia, to prolong the LANL contract to develop and conduct research on the ISTC Target Complex 1 located at UNLV.

- **Khlopin Radium Institute**. KRI completed construction and testing of a He-3 neutron detector. It will be shipped to UNLV next week for use in a graduate student research project investigating neutron multiplicity. UNLV has also finalized two new contracts with KRI that support two other graduate student projects: Iodine Sequestration and Fluorapatite Waste Forms.

6.3 Student Research

6.3.1 Student Research Scope

The Student Research component is the core of the UNLV Transmutation Research Program with steadily increasing funds as the program evolves and capability expands. The milestones, schedules, and deliverables of the student research projects are detailed in the individual research proposals. UNLV currently has 16 student research tasks that include 37 graduate students and involve 33 faculty members. The tasks are divided below in terms of their research area: fuels, separations, and transmutation sciences.

6.3.2 Student Research Highlights

Metallic Fuel Pins Highlights.

- The computational meshes for the metallic fuel pins model were refined to get better numerical results.
- A few different mold materials associated with the different initial and boundary conditions (such as filling velocities and mold and melt temperatures) have been used for the solidification process.
- Modeling results for constant pressure casting, which is more realistic, have been obtained and produce physically realistic results for flow that starts, flows, and then eventually stops as it enters the mold.
- Potential mass transfer modeling features (Lammuir's law for example) are being studied to enhance the capabilities of a mass transfer in a detailed system model.
- Different parameters are being varied as part of a parametric study to evaluate factors that impact the flow of the melt into the molds.
- The ability to include the induction heating governing equations as part of an overall system model is being studied and preliminary efforts to include this complex phenomenon as part of a more detailed model are underway.

Remote Fuel Fabrication Highlights.Development continued on a 3-D process simulation model with a Waelischmiller hot cell robot.

- Worked on concepts and methods for vision-based hot cell supervision and control.

Systems Engineering Model Highlights.

- Development of the Visual Basic (VB) Interface for AMUSE code was completed.
- Trade-off techniques for optimizing the system model were examined. Development of the design matrix was initiated.

- A successful meeting was held March 6 and 7 with Argonne National Laboratory (ANL) researchers to discuss project details and provide feedback and support.
- Five specific objects are being implemented for the graphical user interface as a result of the meetings with ANL researchers: flow sheet, section, streams, stages and concentrations.
- Work continues on the development of flow sheet objects that allow the user to select flow sheet name, reports location, type of process, and other required input.
- A Separations area called "Tools" is being developed to allow the user to develop process blocks within the software environment to build a specific process flow sheet, which includes the ability to generate process streams, sections, stages, and input data for each of them.
- Development of an overall process model continues using MATLAB with SIMULINK that will eventually allow the top five most influential factors to the process to be automatically selected; those factors will be used for the design variables for the optimization.

Criticality and Heat Transfer Analyses of Separations Process Highlights

- Completion of plutonium and americium mixture criticality and heat transfer analysis.
- Research began on criteria for use of commercial dry casks for the storage of strontium and cesium.

Immobilization of Fission Iodine Highlights

- The iodine vapor generator assembly was completed.
- Several tests of iodine sequestration/adsorption were conducted with a commercial peat moss (Natural Organic Matter, NOM). The results indicate extremely low breakthrough at iodine vapor concentrations close to saturation.
- We have tested and used the ion selective electrode to monitor iodine vapor breakthrough (after bisulfite reduction) in the iodine generator experiments. Also, the ion chromatography method for separation of various iodine species was tested.
- We have examined the kinetics of iodine oxidation by chlorine sulfonamide resins. These resins may be used with NOM to promote iodine binding.
- We have begun assembling an apparatus for simulating nuclear fuel dissolution. Several additional glass items were ordered and we are awaiting delivery.
- The ion chromatography method for separation of various iodine species was tested with NOM samples. Serious interference was discovered and a new column has been ordered.
- The transfer of iodide to organic matter, as facilitated by the by the chlorine sulfonamide resins, was examined. Using NOM analogs, iodine was shown to become associated with organic matter in the presence of the active chlorine resins.

Fluorapatite Waste Forms Highlights

- Baseline Raman spectra have been obtained for hydroxyapatite and fluorapatite.
- Natural fluorapatite crystals have been obtained commercially and will be examined spectroscopically to determine what contaminants occur naturally.

- Plans were developed for chemically preparing samples in which some of the calcium in apatite materials is substituted by nonradioactive actinide surrogates or elements produced by decay of actinides.

Niobium Cavity Fabrication Optimization Highlights

- Niobium cavities design optimization code appears to be working but is converging to undesired geometries having same constraints. Modified niobium cavity optimization code and created a random seed cavity generator.
- Flow visualization system was modified with new back-lighting system and camera deployment. Flow visualization system has completed testing phase and is ready for experimental use. Tuning camera for fluid flow studies.
- Two new optimized geometries based on resonant frequency and mode were found.

LBE Corrosion of Steel Highlights

- Complete maintenance of the X-ray Photoelectron Spectroscopy (XPS) system.
- Completed experimental design for benchtop LBE corrosion experiments at UNLV.
- Completed characterization of steel samples of HT9 using XPS.
- Enlarged the bibliography of LBE-related and associated publications.

Environment-induced Degradation of Materials Highlights

- Stress corrosion cracking (SCC) tests using constant-load and slow-strain-rate (SSR) techniques are ongoing in aqueous solutions at ambient and elevated temperatures.
- SCC tests under controlled cathodic potentials (with respect to the corrosion potential) are ongoing to evaluate the effect of hydrogen charging on cracking.
- Localized corrosion (pitting and crevice) behavior of all three alloys is being evaluated by cyclic potentiodynamic polarization (CPP) method.
- Smooth and notched tensile specimens of Alloys EP-823, HT-9 and 422 are being used for SCC testing.
- Metallographic evaluations of failed samples by optical microscopy are ongoing.
- Fractographic evaluations of failed samples by scanning electron microscopy are in progress.

LBE Corrosion Modeling Highlights

- Modeling and simulation of the DELTA Loop geometry is being benchmarked against observations at LANL.
- Modeling of sudden expansion geometry work simulation is proceeding and is now able to predict some already existing 3-D experimental work.
- Computer simulation results for Task 5 have been obtained for several geometries (i.e., 2-D sudden expansion flow, torroidal loop with momentum source simulation, and straight pipe flow simulation). Wall temperature and concentrations were prescribed. Objectives are to estimate concentration wall mass flux to predict the areas on the wall that depict

corrosion rates and those that predict precipitation rates and to locate maxima for each corrosion site and precipitation site.

Neutron Multiplicity Highlights

- Nuclear Transport Code Models (MCNP 4B, MCNPX) needed to finalize the ^{6}Li glass fiber neutron multiplicity detector prototype design were completed. Detector design was finalized subsequent to completion and analysis of modeling results.
- Production of detector material (^{6}Li glass fiber) for the prototype sensor was begun and is nearing completion. Neutron Multiplicity detector prototype (^{6}Li glass fiber detector) is ~70% complete for all hardware and electronic card production (for optoelectronic interfaces, light guides, signal train, firmware). Communication output hardware and software are about 80% completed. Prompt signal circuitry needed for the detector to communicate with the cyclotron signals is ~60% completed.
- ^{3}He Neutron Multiplicity detector prototype (64-element) is nearing 90% completion and will be shipped to UNLV from Russia in April or May.
- Testing of the ^{6}Li glass fiber detector system prototype scheduled at the Crocker Nuclear Laboratory, University of California, Davis for May.

Dose Conversion Coefficients (DCC) Highlights

- International DCC consortium met at UNLV to:
  - Provide updates from consortium members on progress,
  - Develop a new timeline for completion of dose coefficient calculations,
  - Compare and contrast results of DCs from different institutions, and
  - Finalize the methodology for calculation of the DCs.
- Modifications to the computer codes used to calculated dose were completed with the assistance of Dr. K. Eckerman, ORNL.
- Completed the dose coefficients calculations for the QA radionuclides.
- Implemented the new EDISTR computer code.

Properties of Alloy EP-823 Highlights

- High-temperature tensile testing using new specimen grips on the Materials Testing System has been initiated.
- The ambient temperature tensile testing of Alloy EP-823 is ongoing.
- Additional tensile specimens of Alloy EP-823 are being machined from the heat-treated bars.

Oxygen Sensing in LBE Highlights

- A 2-dimensional model of the oxygen-sensor/LBE experimental setup was completed using FEMLAB. After a few simulations, it was recognized that FEMLAB is not suitable for the simulation of the oxygen concentration and dissolving rate in LBE.

- Most of the parts for the Task 13 apparatus have been received and moved into TBE B310.
- LabView module for the control of our apparatus has been designed and is under testing and improvement.

Positron Annihilation Spectroscopy Highlights

- Cold-worked, bent, and welded specimens of heat-treated Alloy EP-823 and Type 304L stainless steel are being evaluated for residual stress measurements using positron annihilation spectroscopy at Idaho State University (ISU) and X-ray and Ring-Core methods at the Lambda Research Laboratory (LRL).
- All three types of specimens are being evaluated for residual stress measurements by positron annihilation spectroscopy at ISU.
- Residual stress measurements in bent and welded specimens are in progress at the LRL using X-ray and Ring-Core methods.

6.3.3 Student Research Technical Summary

FUELS TECHNOLOGY

Metallic Fuel Pins (Task 1). An important aspect of the AFCI is the development of a casting process by which a volatile actinide element (i.e., americium) can be incorporated into metallic alloy fuel pins. The traditional metal fuel casting process uses an inductively heated crucible. The process involves evacuation of the furnace, which also evacuates quartz rods used as fuel pin molds. Once evacuated, the open ends of the molds are lowered into the melt; the casting furnace is then rapidly pressurized, forcing the molten metal up into the evacuated molds where solidification occurs.

This process works well for the fabrication of metal fuel pins traditionally composed of alloys of uranium and plutonium, but does not work well when highly volatile actinides are included in the melt. The problem occurs both during the extended time period required to superheat the alloy melt as well as when the chamber must be evacuated. The low vapor-pressure actinides, particularly americium, are susceptible to rapid vaporization and transport throughout the casting furnace, resulting in only a fraction of the charge being incorporated into the fuel pins as desired. This is undesirable both from a materials accountability standpoint and from the failure to achieve the objective of including these actinides in the fuel for transmutation.

Candidate design concepts are being evaluated for their potential to successfully cast alloys containing volatile actinides. The selection of design concepts has been conducted in close cooperation with ANL staff. The research centers on the development of advanced numerical models to assess conditions that significantly impact the transport of volatile actinides during the melt casting process. The work includes the collection and documentation of volatile actinide properties, development of several conceptual designs for melt casting furnaces, modeling and analysis of these concepts, development of sophisticated numerical models to assess furnace operations, and analysis of these operations to determine which furnace concept has the greatest potential for success. Research efforts focus on the development of complex heat transfer, mass transfer, and inductive heating models.

Remote Fuel Fabrication (Task 9). The objective of this project is the design and evaluation of manufacturing processes for AFCI fuel fabrication. The large-scale deployment of remote fabrication and refabrication processes will be required for all transmutation scenarios. The evaluation of the fabrication processes will create a decision support database to document design, operations, and costs. Fabrication processes required for different fuel types differ in terms of equipment types, throughput, and cost. Differential cost implications of various fuel choices will be assessed. Another aspect is the assessment of robotic technology and robot supervision and control, and the simulation of material handling operations using 3-D simulation tools with view toward the development of a fully-automated and reliable autonomous manufacturing process. Such development has the potential to decrease the cost of remote fuel fabrication and to make transmutation a more economically viable process. An added benefit would be the potential for large reductions in dose to workers. This project is being conducted in close cooperation with the fabrication development group at ANL.

Manufacturing processes will be simulated as robotic operations supervised by remote operators. Both normal operations as well as failure scenarios will be investigated, analyzed, and simulated. The results of the simulations will be used by AFCI program personnel to perform sensitivity studies on the impact of different fuel types on system operation. Conceptual designs for plant designs and the accompanying supervision and control systems will be developed. Impacts on transmutation system capital cost, economics of operation, estimates of process loss, and environmental and safety issues will be estimated.

SEPARATIONS TECHNOLOGY

Systems Engineering Model (Task 8). The objectives of this task are the development of a systems engineering model and the refinement of the Argonne code AMUSE (Argonne Model for Universal Solvent Extraction). The detailed systems engineering model is the start of an integrated approach to the analysis of the materials separations associated with the AFCI Program. A second portion of the project is to streamline and improve an integral part of the overall systems model, which is the software package AMUSE. AMUSE analyzes the UREX process and other related solvent extraction processes and defines many of the process streams that are integral to the systems engineering model.

Combining these two tasks is important to ensuring that calculations made in AMUSE are accurately transferred to the overall systems model. Additional modules will be developed to model pyrochemical process operations not treated by AMUSE. These modules will be refined as experiments are conducted and as more knowledge is gained in process steps.

Integrating all aspects of the proposed separations processes will allow for detailed process analyses, trade-off studies or the evaluation of proposed process steps, complete material balances that include all potential waste streams, the impact of changes in feed streams, studies detailing the importance of process control and instrumentation, and the ultimate optimization of the process.

Criticality and Heat Transfer Analyses of Separations Processes (Task 11). The success of the AFCI will rely upon the ability of radiochemists to separate spent nuclear fuel. The Chemical Technology Division at ANL is actively involved in the development of pyrochemical separation technology that minimizes the usage of strong acids with the subsequent problems involved in disposing of the acidic residue.

Small-scale experiments are being validated at ANL to separate spent nuclear fuel, but they must be scaled up to accommodate the large amount of commercial spent fuel that must be treated. As the volume of waste to be treated is increased, there is a higher probability that fissionable isotopes of plutonium, americium, and curium can accumulate and form a critical mass. Criticality events can be avoided by ensuring that the effective neutron multiplication factor, k_{eff}, remains below a safe level. NRC regulations normally allow an upper value of 0.95 for k_{eff}. This parameter can be computed for any combination of fuel and geometry using Monte Carlo neutron transport codes. Scale 4.4a from the Oak Ridge National Laboratory and MCNP4C2 from the Los Alamos National Laboratory are two codes that are regularly used to assess criticality.

Immobilization of Fission Iodine (Task 15). The recovery of iodine released during the processing of used nuclear fuel poses a significant challenge to the transmutation of radioactive iodine. This task will develop and examine the use of Fullerene Containing Carbon (FCC) compounds as potential sorbents for iodine release from the reprocessing of nuclear fuel. This work will also include the development of bench-scale testing capabilities at UNLV to allow the testing of the FCC material in a simulated process off-gas environment. This experimental capability will also be used to test other potential sorbtion materials and processes, such as natural organic matter (NOM) and other promising alternatives. This work also examines the development of a process to convert the sorbed iodine into a ceramic material with the potential for use as either a transmutation target or as a waste form in a partitioning and sequestration strategy.

Bench scale experimental apparatus and methodologies to simulate iodine entrainment in the vapor phase released from the head end of the PUREX process (the 4M nitric acid dissolution of spent nuclear fuel) will be developed, along with procedures to test the sequestration of iodine from the vapor mixture. Long term performance/suitability of FCC and NOM will be tested for sequestration of iodine released by nuclear fuel reprocessing. FCC-bearing materials will be prepared and evaluated under laboratory conditions by collaborators at the Khlopin Radium Institute (KRI-KIRSI). Simulated process evaluations will be done on the FCC-bearing materials, NOM, and other matrices suggested by the collaborators at UNLV. Conversion of the sequestered iodine to a ceramic-like material will be examined by the KRI-KIRSI team. Recovery of the iodine from the sequestering matrices will also be examined by both teams.

Fluorapatite Waste Forms (Task 16). Fluorapatite, fluorinated calcium phosphate, has been identified as a potential matrix for the entombment of the zirconium fluoride fission product waste stream from the proposed FLEX process. If the efficacy of fluorapatite-based waste storage can be demonstrated, then new and potentially more efficient options for handling and separating high-level wastes, based on fluoride-salt extraction, will become feasible. This task is a dual-path research project to develop a process to fabricate a synthetic fluorapatite waste form for the ZrF_4, FP waste stream, characterize the waste form, examine its performance under environmental conditions, and correlate the behavior of the waste form with natural analogs. Characterization of the material will be accomplished through probing the molecular-scale electronic and geometric structure of the materials in order to relate them to macroscopic properties, with the goal of developing techniques to evaluate and predict the performance of different waste-form materials. Time and funding permitting, other waste forms for the zirconium fluoride, fission-product salt waste stream will be examined and benchmarked against the fluorapatite matrix baseline.

TRANSMUTATION SCIENCES

Niobium Cavity Fabrication Optimization (Task 2). Multipacting is one of the major loss mechanisms in rf superconductivity cavities for accelerators. This loss mechanism limits the maximum amount of energy/power supported by the cavities. Optimal designs have been identified in others' studies. In practice, these designs are not easily manufactured. Chemical etching processes used to polish the cavity walls result in a nonuniform surface etch. A nonuniform surface etch will leave some unclean areas with contaminants and micron-size particles. These significantly affect mutipacting. Further, a nonuniform etch will leave areas with damaged grain structure, which is not good for superconducting properties. Typically, the depth of chemical polishing etch ranges between 10 to 150 microns.

It is the purpose of this study to experimentally model the fluid flow resulting in the chemical etching of niobium cavities with the aid of a baffle. The current etching process with baffles does not uniformly etch the cavity surface. Multiple cavity cell geometries are being investigated. Optimization techniques will be applied in search of the chemical etching processes that will lead to cavity walls with near ideal properties.

The optimization procedure is intended to be fully automated among a variety of existing codes. Codes are to be modified to provide a statistical study of impacting in the multicavity geometry. Optimization techniques will be developed based on the desired resonant frequency of the geometry and/or on the multipacting condition. An existing vacuum system is, in part, to be modified for multipacting experiments to be conducted in this effort.

LBE Corrosion of Steel (Task 3). The goal of this task is to achieve a basic understanding of corrosion of steels by lead-bismuth eutectic (LBE). There have been previous studies of LBE, especially by the Russians, who have over 80 reactor-years experience with LBE coolant in their Alpha-class submarine reactors. The Russians found that the presence of small amounts (ppm) of oxygen in the LBE significantly reduced corrosion. However, a fundamental understanding and verification of its role in the corrosion of steels is still very incomplete. We are carrying out a program of post-experiment testing and analysis on steel samples that have been in intimate contact with LBE. We have employed surface analysis techniques, including Scanning Electron Microscopy (SEM), Energy Dispersive X-Ray (EDAX) spectroscopy, and X-ray Photoelectron Spectrometry (XPS), and laser Raman. These techniques, applied to the steel surface, have probed the surface morphology, elemental analysis and oxidation states as a function of position. The measurements were made using the facilities at UNLV. Chemical alterations and resulting chemical species are studied at the steel surface. We plan to use powder X-ray diffraction in the near future. In addition to these well-established laboratory-based instrumentation approaches at UNLV, we have begun to use a state-of-the-art synchrotron-based spectroscopy and microscopy technique, the X-ray fluorescence microprobe at the Advanced Light Source, at Lawrence Berkeley National Laboratory. We are characterizing spectroscopically the stainless steel samplesbefore and after interaction with LBE to determine their composition, including minor components such as chromium and nickel. The research moves toward establishing a rigorous experimental database of experimental measurements of LBE and its reactions with steels. Such a database can be used by DOE scientists and engineers in engineering efforts to control, avoid, and/or minimize the effect of corrosion of steels by LBE.

Environment-induced Degradation of Materials (Task 4). During the past two years of this project, the primary effort was focused on evaluating the effect of hydrogen on the cracking

behavior of candidate target materials, namely Alloys EP-823, HT-9, and 422, in aqueous environments of different pH values at ambient and elevated temperatures. More recently, emphasis is being placed to evaluate the cracking behavior of these materials in a molten lead-bismuth eutectic (LBE) environment at much higher testing temperatures in order to compare the cracking susceptibility in environments containing molten metals and aqueous solutions, respectively. The most recent tests to evaluate the cracking susceptibility were primarily based on two state-of-the-art techniques known as constant-load and slow-strain-rate (SSR) methods. Simultaneously, efforts were made to determine the localized corrosion (pitting and crevice corrosion) behavior in similar aqueous environments at ambient and elevated temperatures using electrochemical polarization techniques. However, these techniques can not be applied to a LBE environment. Therefore, the work scope described in the original proposal has been modified to include additional testing methods to suit the high-temperature LBE environment. Although testing will be continued to complete the original matrix involving all three alloys in aqueous environments using constant-load, SSR, and polarization techniques, future testing will be performed in both aqueous and LBE environments using self-loaded specimens such as C-Ring and U-Bend stress-corrosion-cracking (SCC) test specimens. In addition to this corrosion testing, significant efforts will be made to evaluate the crack-growth behavior of radiation-hardened target materials using sub-size compact tension (CT) specimens. The test materials will undergo appropriate thermal treatments prior to their testing. All tested specimens will be examined metallographically. Further, the scanning electron microscope (SEM) will be used to determine the extent and nature of cracking in the tested specimens. The thrust of this overall testing program is to evaluate the environmental and radiation effects on the cracking behavior of candidate target materials.

LBE Corrosion Modeling (Task 5). This project combines chemical kinetics and hydrodynamics in target and test-loop lead-bismuth eutectic (LBE) systems to model system corrosion effects. The goal is to produce a predictive tool that can be validated with corrosion test data, used to systematically design tests and interpret the results, and provide guidance for optimization in LBE system designs. The task includes two subtasks. The first subtask is to try to develop the necessary predictive tools to be able to predict the levels of oxygen and corrosion products close to the boundary layer through the use of Computational Fluid Dynamics (CFD) modeling. The second subtask is to predict the kinetics in the corrosion process between the LBE and structural materials by incorporating pertinent information from the first subtask.

In many cases a component fails because of the combined effect of mechanical or hydraulic factors and corrosion. Such cases are of three types: stress corrosion, corrosion fatigue, and liquid-velocity effects (corrosion erosion and cavitations). The compatibility issues arising from the interaction of liquid metals, corrosion/dissolution, with structural materials at temperatures of interest are important so long as lead alloy is used as a coolant for a fast breeder type nuclear reactor. The second subtask focuses on the kinetics of the dissolution/deposition process as a function of temperatures, flow velocities, dissolved metal concentrations and the oxygen potentials of the system, the kinetics of film formations in the presence of oxygen, and the kinetics of transports of metal through the oxidized surface film. Both mass transfer controlled and the diffusion coefficient of dissolved species will be parametrically studied for the corrosion process.

Neutron Multiplicity (Task 6). The goals of this task are to measure the neutron leakage from 15, 20 and 40-cm diameter Pb-Bi / Pb targets and to compare these empirical measurements with

MCNPX results. These measurements are essential in validating and benchmarking MCNPX modeling results of target materials. The neutron leakage measurements should provide a systematic set of precision data that will enable direct comparison with code calculations. Two detector systems that employ independent technologies are in fabrication. Comparisons of results obtained from both should remove many uncertainties and permit the derivation of relative measurements in the few percent range at the 95% confidence level (CL). A 60-detector element ^{3}He-tube-based system and a prototype neutron-sensitive glass fiber-based system were designed during Yr-1 of this study. The glass fiber detector prototype is complete and ready to test in upcoming target experiments at LANCSE. The 60 element ^{3}He-based target monitoring system is in final design and initial fabrication stages. MCNPX models of the ^{3}He system have been developed and will be integrated with target models. Models of the glass fiber detectors have been developed and were used for developing July 2002 LANSCE target experiments.

Dose Conversion Coefficients (Task 7). A research consortium comprised of representatives from several universities and national laboratories has been established as part of this task to generate internal and external dose conversion coefficients (DCC) for radionuclides produced in spallation neutron sources. Information obtained from this study will be used to support the siting and licensing of future accelerator-driven nuclear initiatives within the U.S. Department of Energy complex, including the Spallation Neutron Source (SNS) project. Determination of these coefficients will also fill data gaps for several hundred radionuclides that exist in Federal Guide Report No. 11 and in Publications 68 and 72 of the International Commission on Radiological Protection (ICRP).

Properties of Alloy EP-823 (Task 10). The purpose of this project is to evaluate the elevated temperature tensile properties of Alloy EP-823, a leading candidate material for transmutation applications. This alloy has been proven to be an excellent structural material to contain the lead-bismuth-eutectic (LBE) nuclear coolant needed for fast-spectrum operations. However, very little data exist in the open literature on the tensile properties of this alloy. The selection of Alloy EP-823 as the test material in the proposed task is based on the recommendation of our collaborator at the LANL. The test material will be thermally treated prior to the evaluation of its tensile properties at temperatures relevant to the transmutation applications. The deformation characteristics of tensile specimens, upon completion of testing, will be evaluated by surface analytical techniques using scanning electron microscopy (SEM) and transmission electron microscopy (TEM). The overall results will lead to the development of a mechanistic understanding of the elevated-temperature deformation processes in this alloy as a function of thermal treatment. Understanding deformation mechanisms of Alloy EP-823 may also help the development of suitable target materials possessing enhanced LBE corrosion resistance and acceptable radiation damage in the United States.

Oxygen Sensing in LBE (Task 13). Although liquid LBE is a good candidate as a coolant in fast nuclear systems, it is known to be very corrosive to stainless steel, the material of the carrying tubes and containers. Such a corrosion problem can be prevented by producing and maintaining a protective oxide layer on the exposed surface of stainless steel. The proper formation of this oxide layer critically depends on the accurate measurement and control of the oxygen concentration in liquid LBE. YSZ (Yttria Stabilized Zirconia) oxygen sensors, using molten bismuth saturated with oxygen as the reference, have been utilized to accurately measure the concentration of oxygen dissolved in LBE.

A new experimental apparatus with several important improvements to an older version at LANL is under development at UNLV. The proposed specific aims of the task are: 1) to complete and fully test the new oxygen control and measurement apparatus; 2) to continue the sensor calibration by using our new set-up in UNLV at higher temperature ranges (350 ^{0}C to 700 ^{0}C); 3) to employ a more precise and easier H_2/H_2O steam injection strategy for oxygen control instead of previous method of direct injection of O_2; 4) to simulate the dissolved oxygen concentration distribution in the liquid LBE of our system by using FEMLAB or other software (ABAQUS/FLUENT). The results obtained from the simulations will be used to cross-check and cross-validate with the experimental data; 5) to determine oxygen dissolving rates under various conditions, including changing temperatures and inlet O_2 supply; and, 6) to determine the diffusion coefficient of O_2 in liquid LBE under different temperatures through theoretical modeling and experimental measurement.

Positron Annihilation Spectroscopy (Task 14). The purpose of this collaborative research project involving UNLV and Idaho State University (ISU) is to evaluate the feasibility of determining residual stresses of welded, bent (three-point-bend), and cold-worked engineering materials using a new nondestructive technique based on positron annihilation spectroscopy. The technique uses x-rays from a small MeV electron Linac to generate positrons inside the sample via pair production. This method can be used for materials characterization and investigation of defects in thick samples that could not be accomplished by conventional positron technique or other nondestructive methods. The data generated will be compared to those obtained by other nondestructive methods, such as neutron diffraction and x-ray diffraction and a destructive method known as ring-core technique. Materials to be tested in the initial phase will be unirradiated austenitic (Type 304L) and martensitic (EP-823) stainless steels that will be welded, bent, and cold-worked prior to the evaluation of their residual stresses. Metallurgical microstructures will also be evaluated. In addition, deformation characteristics in terms of dislocations and their movements resulting from welding and plastic deformation will be analyzed by transmission electron microscope (TEM). Later, irradiated Alloy EP-823, HT-9, and austenitic materials (Type 316L stainless steel and Alloy 718) will be included in this program.

7 UNIVERSITY RESEARCH ALLIANCE – FELLOWSHIP PROGRAM

7.1.1 University Research Alliance Scope

Managing the on-going fellowship program

University Research Alliance continues the ongoing detailed management of the fellowship program, including ensuring that fellows receive their stipends in a prompt manner, ensuring that special needs are addressed and accommodated appropriately, and ensuring that students stay on track for completing their fellowships in a timely manner. In addition to these tasks, University Research Alliance worked with each of the active fellows and their universities to ensure that the financial aspects of enrollment, tuition, and stipends went well and to ensure prompt reimbursement to the students for appropriate and allowable expenses.

7.1.2 University Research Alliance Highlights

- FY ’01 fellow Jim Platte constructed a model of the July 2002 LANSCE irradiation on a 50 cm long, 40 cm diameter lead-bismuth eutectic target using the high energy physics code MCNPX. The neutron spectrum calculated by the MCNPX model was used as an initial guess neutron spectrum in the input of the spectral unfolding code STAYSL, which recalculated the neutron spectrum based on foil activation data. The two spectra, STAYSL and MCNPX, were then compared to gauge the accuracy of the MCNPX calculation. Jim graduated in December and is working on his thesis.
- Thomas Roddey, FY’01 Fellow, UC-Berkeley, is working as a Nuclear Licensing Engineer for Exelon Nuclear Corporation, Mid-West Regional Operating Group. His job entails acting as a corresponding liaison between Exelon and the NRC. Thomas expects to finish writing his project report by the end of March and give his final presentation during the week of May 5, 2003. These steps will complete Thomas’ master’s degree requirements.
- AFCI ’01 Fellow Kamilah Turner graduated in April from the University of Michigan with a master’s degree in Chemical Engineering. Her thesis is entitled “Development Processes to Deposit Refractory Metal Coatings on Transuranic Nitride Fuel Particles.” Kamilah has accepted a position with Dupont in their Field Engineering Program.
- FY ’01 Fellow Ben Milliron graduated in December from Ohio State University. Ben writes: “Life is good. I was recently hired as a reactor engineer for the Davis-Besse Nuclear Power Station in Oak Harbor, OH. It's a pretty interesting and challenging job. I hope all is well with you and the program. Thank you to everyone once again! I wouldn't be here if I hadn't had your help! I'm interested in working on the nuclear/hydrogen cogeneration project if it ever gets funding. I think I could handle Idaho for a while. Regardless, The National Lab scene will probably be right up my alley post-Italy *(Ben is marrying shortly and hopes to move to Italy for 1-2 years with his wife who is studying art)*. At least I hope so! How about giving me a hand with that in a couple of years?”
- Seven Fellows provided posters for the AFCI Quarterly Meeting. FY02 Fellows presenting posters were: Jennifer Ladd, Tom Carter, Frank Szakaly, and Michael

Gregson. FY01 Fellows were Jim Platte (University of Michigan), Alan Bolind (University of Illinois at Urbana-Champaign, and Leigh Outten (MIT).

- Four FY02 Fellows attended the AFCI Quarterly Meeting: Jennifer Ladd (UT-Knoxville), Tom Carter (University of Florida), Frank Szakaly (Texas A&M), and Michael Gregson (University of Texas).
- AFCI '02 Fellow Shafaq Amdani withdrew from school citing personal problems. She has been granted a leave of absence from the AFCI fellowship program through September 1, 2003.
- AFCI '02 fellow Mike Gregson, UT, has been working on modeling an accelerator driven core within MCNP based upon research and AFCI designs. "The MCNP deck is being converted into an MCNPx deck such that simulation of GeV protons can take place." With the completion of the "decks and a successful run" he was able to evaluate and write about what was learned from the design. Mike says that the LANL Accelerators group is interested in the data from the project and a subsequent graduate student will continue the work. Mike was named an AFCI Fellow in the second year of his master's degree program and will graduate in May. He has accepted a position at Sandia National Laboratories.
- FY '02 Fellow Lee Van Duyn, Georgia Tech, has been studying the finite element computer code ABAQUS and trying to write a python scripting file that can generate the geometries that he would like to be able to form to effectively run parameter studies when the model for his research is complete. Lee has been successful in creating a basic model through the graphical user interface and solving for simple things like stress and strain and temperatures, but has a number of numerical and computational problems that he is trying to resolve. Lee has been in close contact with Steve Hayes and Mitch Meyer at ANL-W as he will be working with them for the summer starting on May 19.
- FY'02 fellow Frank Szakaly, Texas A&M University, is working on writing the code for the MOCUP modeling program. He is working on getting reference reactor design information from the national labs so that he can model the fuel pins for at least one of the Generation IV designs. He has written some input files and is presently testing them to see if they work. Frank is working with Los Alamos to secure a security clearance that will allow access to LANL's computer network. Frank presented a paper at the American Nuclear Society Student Conference in Berkeley.
- Lee Van Duyn, '02 Fellow, Georgia Tech, will spend the summer at Argonne West, furthering his research. He has been gathering material properties, and trying to characterize what he needs to construct a successful model. He is also learning how to use the computer code ANSYS so that it can do the modeling he needs in order to fully understand the aspects of his research topic.
- FY'02 fellow Lisa Cordova, University of New Mexico, is planning to complete her degree in December. Meanwhile, she is working part time at Sandia National Laboratories and is developing her computer/simulations skills. Lisa presented a paper at the American Nuclear Society Student Conference in Berkeley, April 2-3.

- AFCI ’02 Fellow Matthew Sowa, University of Michigan, was named a fellow in the second year of his master’s degree program. Matt graduated in April and is continuing his studies for a Ph.D.
- FY ‘02 Fellow Billy Rothstein, University of Illinois at Urbana-Champaign, has finished making his samples (thin Ni/Ti films on a silicon substrate) for his research on “The Effect of Radiation on Ni/Ti Super Mirrors.”
- AFCI ’02 Fellow Jennifer Ladd, UT Knoxville, is working at ORNL, where she is seeking all the necessary data to begin modeling. Jennifer will be at ORNL this summer in the Higher Education Research Experience (HERE) and will be working on her thesis research. She hopes to be finished modeling by the end of the summer and begin writing her thesis in September.
- The FY02 class of fellows has submitted its Final Research Plans and a timeline for completing their master’s degree programs:

FY ‘02 Fellow	**Research**	**Projected Grad Date**
Thomas Carter	Feasibility of Mixed Carbide Fuel for Use in Transmutation Systems	12/03
Lisa Cordova	An Investigation of the Angular and Spatial Spreading of a Relativistic Proton Beam in a High Z Material	12/03
Michael Gregson	Full Core Analysis of ATW Prototype for Nuclear Cross Section Data for Core Components	05/03
Jennifer Ladd	Separation of Fluoride Residue Arising from Fluoride Volatility Recovery of Uranium from Spent Nuclear Fuel	05/04
Billy Rothstein	The Effect of Radiation on Ni/Ti Super Mirrors	12/03
Matthew Sowa	Fluorite to Pyrochlore Transition in Yttrium Stabilized Zirconia	04/03
Frank Szakaly	Thorium-Based Nitride Fuels for Spent Fuel Transmutation	12/03

- In the past quarter, program management developed the AFCI Fellowship Program Announcement for master’s degree and Ph.D. degree students for FY03. The Program Announcement was not used during FY03 due to funding issues. The announcements will provide the program with a starting place that will facilitate developing the Program Announcement for the FY04 fellowship program.
- Program management verified and added to the Fellowship Program Announcement mailing list.
- Program management prepared the AFCI University Fellowship Program web site for the FY03 fellowship cycle.
- University Research Alliance is collaborating with UNLV, Idaho State University, and other schools on the “International Meeting on Accelerator Driven Transmutation System Technologies” on April 29.

8 TECHNICAL INTEGRATION

8.1.1 Technical Integration Objective and Scope

The Technical Integration program element serves as the mechanism for integrating the myriad of technical efforts into a single overarching cohesive program focused on resolving spent nuclear fuel issues. The scope of Technical Integration encompasses all technical program elements including systems analysis, separations, fuels, and transmutation, and abstracts the salient elements of each program element to perform a technical and programmatic synthesis to derive a consolidated overview of the advanced fuel cycle.

8.1.2 Technical Integration Highlights

- Held first AFCI Semi-Annual meeting in January. Technical presentations were given in all program elements and working groups met to discuss paths forward.
- Finalized the *Advanced Fuel Cycle Initiative Five-Year Program Plan* highlighting the program structure, technical work, schedules, and budget.
- Started development of the Reactor Process and Fuel Cycle Narrative Screening and Comparison Matrices.
- Finalized AFCI FY03 Budget on March 17th. Began work package development process.

8.1.3 Technical Integration Summary

The first Semi-Annual meeting of the Advanced Fuel Cycle Initiative was held January 21-24. National Technical Directors (NTDs) and their teams for each program element presented technical talks on current work tasks. On the last day of the meeting, the working groups and NTDs met to discuss the FY03 work scope, strategies, and schedules.

Due to the voluminous and often interconnected technical information regarding fuels, reactors, separations, transmutation technologies, as well as the overall integrated fuel cycles, a series of summary matrices comparing the salient characteristics of each competing technology were developed for the Advanced Fuel Cycle Initiative. The matrices were developed as a coupled pair of detailed narrative text and low/medium/high qualitatively valued screening summaries for the reactor systems concepts and fuel processing technologies, supporting a higher level comparison of the advanced integrated fuel cycles.

As a result of decreased budget levels appropriated by Congress, two full-day meetings were held with the AFCI NTDs at DOE/HQ in Germantown on Tuesday and Wednesday, April 8-9, in order to revise both current year activities and five-year plans. Working directly with the NTDs responsible for each technical element of the AFCI Program, revised budget allocations, activities schedules, and resource loadings were developed for updating the current fiscal year 2003, as well as out-year planning projections for FY04-FY09.